University of Stavanger

Faculty of Science and Technology

MASTER'S THESIS

Study program/ Specialization: Offshore Marine & Subsea Technology	Spring semester, 2014 Open / Restricted access
Writer: Mebrahtu Welderufael Weldeslassie	…… (Writer's signature)
Faculty supervisor: Sverre Haver External supervisor(s):	
Thesis title: Investigation of which sea state yield the dominating contribution to fatigue accumulation in offshore structures	
Credits (ECTS):	
Key words: Wave spectrum, Response spectrum & Response Amplitude Operator (RAO)	Pages: ……81…… + enclosure: ……48…… Stavanger, …23/06/2014…….. Date/year

ABSTRACT

Majority of the fatigue damage on offshore structures is generally assumed to be caused by relatively frequently occurring moderate sea states, i.e. sea states with significant wave height in the range of 4m – 8m.On the contrary, Økland [17] claims that the dominating fatigue damage is caused due to higher sever sea states. These two claims in regard to the major cause of fatigue damage are opposite to each other, therefore, this thesis aims to investigate the inter relationship between fatigue damage verses sea state severity. To perform this study, the thesis has identified the Kvitebjør Statoil jacket platform, in which 3-hour duration wave records are available from 1957 to 2013. These short term waves are assumed as a stationary Gaussian process in which the sea surface elevation process is completely described by Pierson-Moskowitz wave spectrum.

In this thesis, the analysis is performed using the spectral-based fatigue assessment method, which is frequency domain analysis and attempts to account for the random nature of sea states in a rational manner. The analysis is performed by developing uni-directional transfer function or Best fit RAO, which is generated from 21 Gaussian sea surface processes and their corresponding linear nature response processes using the Fast Fourier Transform method (FFT). Response spectrum for a given sea state is generated using the Best fit RAO and furthermore standard deviation and number of response cycles of this response process are determined assuming as a narrow band response process. The standard deviation is used to determine the scaling parameter of the Rayleigh-distribution, which represents the distribution of stress ranges for short term. The Rayleigh distribution and the number of response cycles of the process are combined to calculate the number of cycles for a constant stress range in a given stress block. The number of cycles to failure corresponding to the stress range in the given stress block are determined from "T" S-N curve. The effect of the accumulated fatigue damage on the structure is observed by analyzing the S-N curve with double and single slope. Finally, the linear damage calculation by "Miner-Palmgren" summation is used to evaluate the accumulated fatigue damage. Furthermore, the Best fit RAO is assumed to deviate at four different frequency ranges and the fatigue damage for each deviated RAO is calculated.

The fatigue analysis results have asserted the first claim that fatigue damage in the structure is observed to be caused due to the moderate sea states. 60% to 65% of the accumulated fatigue damage is induced in the structure by the moderate sea states. This is because; the moderate sea states are more than the higher sea states and have relatively higher stress ranges than the lower sea states. On the other hand, when straight S-N curve with slope $m = 3$ is used, the accumulated fatigue damage are observed to be overestimated, particularly due to the lower sea states, i.e. sea states with significant wave height 2m to 6m.

BACKGROUND

It is generally expected that the major contributions to fatigue damage come from sea states of moderate severity, i.e. sea states with a significant wave height in the range 4m – 8m. This is because these sea states occur relatively frequently. Based on about 1 year of good quality measurements of the Statoil jacket Kvitebjørn, however, it was experienced that the dominating fatigue accumulation during the period of measurements occurred during two rather severe storms. This seems not to agree with common expectation.

The purpose of this thesis is to investigate fatigue accumulation versus sea state severity. The investigation shall focus on a drag dominated jacket structure. For such a structure the hydrodynamic loading is given by the Morrison equation. The topics that shall be given special focus are:

- Relative importance of mass term versus drag term in the Morrison load equation.
- Relative importance of dynamics.

The necessary weather information will be given by the Norwegian hind cast data base, NORA10, giving weather characteristics every 3 hours from 1957 – 2013. The fatigue assessment is to be done by calculating the fatigue accumulation for every 3-hour period during 1957 – 2013.
Below a possible division into sub-tasks is given.

1. Introduce briefly typical properties of jackets and jack-ups.
2. Discuss briefly fatigue accumulation in welded structures. The discussion should also include a brief introduction of two common methods for fatigue assessments; i) S-N approach and ii) Crack growth approach.
3. Describe closed form approximation of the S-N approach. This is an important part of the investigation. If one shall be able to address properly the bullet points above, the fatigue assessment must be based on a closed form approach. In this part one should also select the S-N curve that will be used in the following. Discuss one slope versus two slope curves in view of the closed for approximation. Can we for the purpose adopt a one slope curve?
4. Estimate generic RAOs that qualitatively can represent the response the Kvitebjørn jacket. Show how RAOs can be estimated from available measurements.
5. In the fatigue analysis, all waves can be considered to come from same direction, but the effects of this simplification shall be discussed. Fatigue accumulation is to be calculated for all 3-hours period. Results shall be shown versus hs and versus storm events. Variability in fatigue accumulation from year to year shall also be indicated. Fatigue shall be estimated using a base case set of RAOs. Thereafter fatigue shall be calculated for:
    - Various levels of resonance induced dynamics.
    - Different RAOs regarding their shape in the major wave frequency regime. The variation shall reflect the effects increasing importance of drag term.

6. Summarize the investigation in conclusions pointing out major learnings of this investigation.

The candidate may of course select another scheme as the preferred approach for solving the requested problem. He may also other subjects than those mentioned above.

The work may show to be more extensive than anticipated. Some topics may therefore be left out after discussion with the supervisor without any negative influence on the grading.

The candidate should in his report give a personal contribution to the solution of the problem formulated in this text. All assumptions and conclusions must be supported by mathematical models and/or references to physical effects in a logical manner. The candidate should apply all available sources to find relevant literature and information on the actual problem.

The report should be well organised and give a clear presentation of the work and all conclusions. It is important that the text is well written and that tables and figures are used to support the verbal presentation. The report should be complete, but still as short as possible.

The final report must contain this text, an acknowledgement, summary, main body, conclusions, suggestions for further work, symbol list, references and appendices. All figures, tables and equations must be identified by numbers. References should be given by author and year in the text, and presented alphabetically in the reference list. The report must be submitted in two copies unless otherwise has been agreed with the supervisor.

The supervisor may require that the candidate should give a written plan that describes the progress of the work after having received this text. The plan may contain a table of content for the report and also assumed use of computer resources. As an indication such a plan should be available by early March.

From the report it should be possible to identify the work carried out by the candidate and what has been found in the available literature. It is important to give references to the original source for theories and experimental results.

The report must be signed by the candidate, include this text, appear as a paperback, and - if needed - have a separate enclosure (binder, diskette or CD-ROM) with additional material.
Supervisor: Sverre Haver, Statoil ASA.

ACKNOWLEDGEMENTS

This thesis is the final work to fulfil the requirement of Master of Science degree in Offshore Technology at the Department of Marine and Subsea Technology, University of Stavanger, Norway. I would like to express my gratitude to my supervisor, Professor Sverre Haver, who works at Statoil ASA, for proposing the topic of this project and his support and guidance which had been instrumental in making this project a success.

Finally, special gratitude and love to my family and friends for supporting me in finishing this thesis work.

Stavanger, 05/06/2014
Mebrahtu

Table of Contents

List of Figures

List of Tables

SYMBOLS

Latin Symbols

A – Cross sectional areas of a submerged member

$c(x, \dot{x})$ – Damping force

c – Damping coefficient

C_D – Drag coefficient

C_m- Inertia or mass coefficient

C_A - Added mass coefficient

D – Dynamic amplification factor, fatigue damage ratio

D_o – Cross sectional dimension of a submerged structure

E – Energy under a wave spectral curve

F(t) – Time varying load/force

F_o - Static loading

$f_{(x,z,t)}$ - Normal or total force on a submerged structure

f_D - Drag force

f_{D-max} - Maximum drag force

f_I - Inertia or mass force

f_{I-max} – Maximum inertia force

f_s – Frequency increment or resolution

f_N – Nyquist frequency

$f(\Delta\sigma)$ – Stress range distribution function

g – Gravitational acceleration

$H_{\Xi\Gamma}$ - Transfer function

H – Wave height

H_s – Significant wave height

$k(x, \dot{x})$ – Stiffness

k – Wave number

k_c – Kealegan- Carpenter number

K – Number of segment

m – Mass of system

m_a – Added mass per unit length

M – Number of sections in which the total sample is equally divided

$M_{n,}$ – Response spectral moments

$M_{n,\Xi\Xi}$ – Wave spectral moments

$n_{o,\Gamma\Gamma}$ – Number of response cycles in a given duration

$n_{o,\Xi\Xi}$ – Number of wave cycles in a given duration

n_i – Number of stress cycles within a given stress block i.

N_i – Number of cycles to failure at constant stress range $\Delta\sigma_i$.

N – Number of data points in each section, number of stress cycles to failure

RAO – Response Amplitude Operator

$S_{\Xi\Xi}(\omega)$ – Wave energy spectral density or wave spectrum

$S(\omega)$ – Response energy spectral density or response spectrum

$S_{PM,\Xi\Xi}(\omega)$ – The Pierson-Moskowitz spectrum

$S_{J,\Xi\Xi}(\omega)$ – The JONSWAP spectrum

$S_{\Gamma\Xi}(\omega)$ – Cross spectral density function

T – Wave period

T_p – Wave spectral peak period

Ts – Total data length

t_{ref} – Reference thickness

$T_{z,\Xi\Xi}$ – Zero-up-crossing wave period

$T_{z,}$ – Zero-up-crossing response period

$u_{(x,z,t)}$ – Horizontal particle velocity at distance x, z depth below SWL and at time t.

$\dot{u}_{(x,z,t)}$ – Acceleration at distance x, z depth below SWL and at time t.

x – Transitional or rotational motion

x_o – Maximum displacement or amplitude

x_h – Homogeneous solution

x_p - Particular solution

$\dot{x}(t)$ - Rate change of response

Chapter 1

INTRODUCTION

1.1 Background and Motivation

The Kvitebjørn jacket platform is installed at a water depth of 190m in the North Sea. The jacket has bottom dimension of 50m X 50m and top dimension of 25m X 20m. It is a relatively slender structure and has a natural or Eigen period about 4 seconds [16]. Based on the measured responses in the diagonal bracings of the tubular joints of the jacket at elevation 108 m below still water level (SWL), the accumulated fatigue damage for one year was estimated and it was found that two large storms contributed to a relatively large part of the accumulated damage as shown in Figure 1-1 [17]. However, it has been assumed that major part of fatigue damage in offshore structures to be caused by moderate sea states, i.e. sea states with significant wave height in the range of 4m – 8m. The reason for this assumption is that these sea states occur relatively frequently than higher sea states and they have severe fatigue effect than the lower sea states. Therefore, this thesis aims to investigate the inter relationship between fatigue damage verses sea state severity for the available 3 hour duration from 1953 to 2013 at the jacket's installation site.

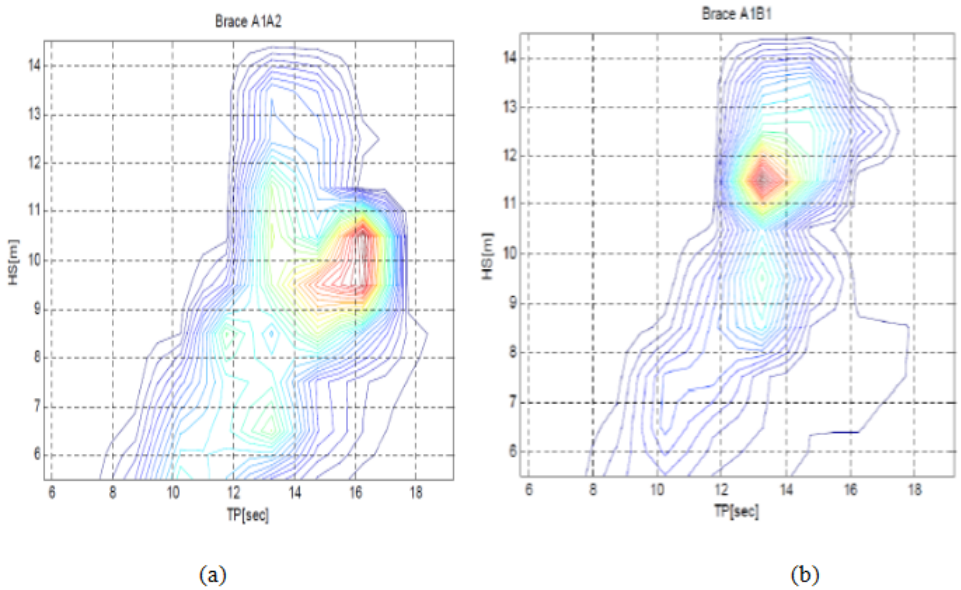

Figure 1.1: Contribution to fatigue life for brace A1A2 (a) and A1B1 (b). [17]

Figure 1.1 illustrates sea states contribution to fatigue life for A1A2 and A1B1 braces of the Kvitebjørn jacket platform and it shows that large part of the accumulated fatigue damage was from sea states with significant wave height in the range of 11m – 12m in Brace A1B1 and 9m – 11m in Brace A1A2. The damage on these bracing was estimated based on the Rain flow counting method which is designed to count reversals in accordance the material's stress-strain response [1].

1.2 Objective

The main objective of this master thesis is to investigate which sea states yield the dominating contribution to fatigue damage accumulation in offshore structures based on short term wave records.

1.3 Scope of Work

The scopes of this project include:

- An introduction to the dynamic behavior of offshore structures mainly on typical properties of jackets and jack-ups.
- Determination of wave induced loads on slender members (Jackets and Jack-ups) using Morison's equation in order to see the relative importance of mass term versus drag term.
- Estimation of the generic Response Amplitude Operator (RAO) that can qualitatively represents the Kvitebjørn jacket platform. This task includes, estimation of wave spectrum and response spectrum from the time series wave and response records respectively using the Fast Fourier Transform method (FFT).
- A brief discussion of fatigue assessment by crack propagation method and fatigue assessment based on S-N curve and an introduction about tubular joints and members and stresses in their joints.
- Derivation of the fatigue damage ratio based on the closed form approach, which is derived from the stress range distribution function and from S-N curve of the considered tubular joint.
- Determination of fatigue damage accumulated in the tubular joints using base case set of RAO (Best fit ROA) and double segment S-N curve for all 3-hours duration sea states from 1957 to 2013. Then the result will be presented as a function of significant wave height (Hs) and storm events. Farther fatigue damage are estimated for the following cases:
  - Deviated or shifted RAOs in the beginning and in the major wave frequency regime.
  - Deviated or shifted RAOs around the natural or Eigen frequency of the jacket.
  - With single straight S-N curve with slope m=3 and m=5.
- Finally, in conclusion section a review of the whole process of the investigation will be presented and the major finding will be concluded.

Chapter 2

OFFSHORE STRUCTURES

2.1 Introduction

For exploration and production the natural source of energy, oil and gas, number of offshore structures have been installed in different depth of water throughout the world. These structures can be categorized on different groups based on their support condition, rigidity, material of construction, response to excitation force etc. some typical offshore structures are given in Figure 2.1. In this thesis, the structures are categorized based on some important structural parameters such as:

- Based on the stiffness and dampness coefficient behavior of the structure as linear mechanical system and non-linear mechanical system, see section 2.2.
- Generally based on cross sectional dimensions: as linear response problem and non-linear response problems, see section 2.2 and 3.4.

Figure 2.1 shows typical floating and bottom supported offshore platforms. All these platforms are made of steel, except the one in Figure 2.1a, which is made of concrete platform with a steel deck.

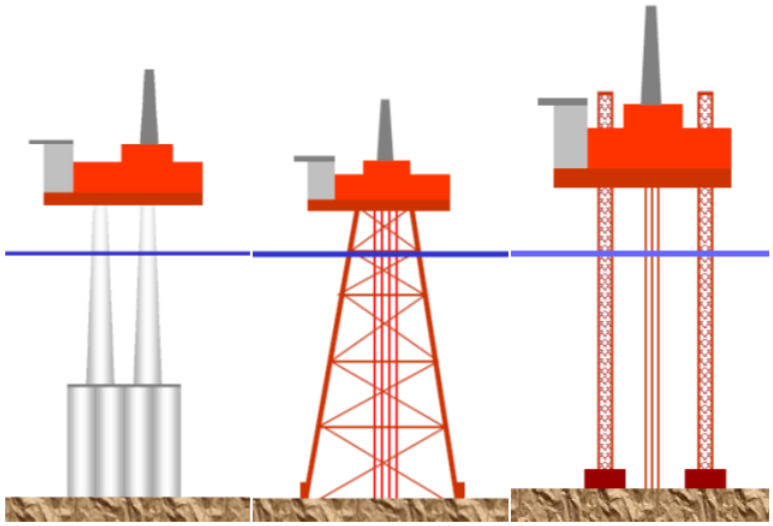

(a) *Gravity platform* (b) *Jacket platform* (c) *Jack-up platform*

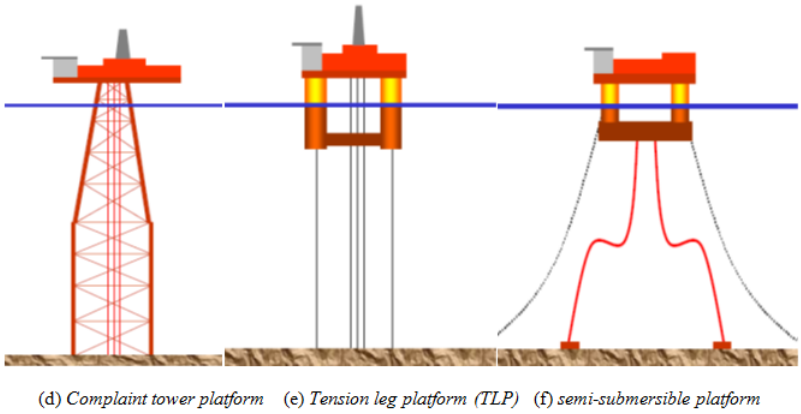

(d) *Complaint tower platform* (e) *Tension leg platform (TLP)* (f) *semi-submersible platform*

Figure 2.1: Selected offshore structures [12] .

2.2 Types of offshore Structures

When an offshore structure is exposed to time variable excitation load such as wave load, current load and wind load, the structure can react to the applied load differently based on the stiffness and dampness characteristics or state of the structure. According to the structural stiffness and dumping coefficient behavior, the response to the time varying load can be found by solving the general equation of motion for a single degree of freedom given below.

$$m * \ddot{x}(t) + c(x, \dot{x}) * \dot{x}(t) + k(x, \dot{x}) * x(t) = F(t) \tag{2.1}$$

This dynamic equation of motion includes mass force or inertial force, $m * \ddot{x}(t)$, damping force, $c(x, \dot{x})$, stiffness, $k(x, \dot{x})$ and the time varying force, F(t) .
where,

- x is translational or rotational motion.
- $\dot{x} = \frac{dx}{dt}$ is the rate change of response.
- m is mass of the system plus added mass if the system is moving.
- c(x, $\dot{x}$) is damping coefficient associated with the motion degree of freedom.
- k(x, $\dot{x}$) is stiffness coefficient associated with the motion degree of freedom.
- F(t) is external load acting on the mass in the direction of the selected degree of freedom.

Generally damping coefficient and stiffness coefficient are of nonlinear in nature, however, for a wide number of response problems, results of sufficient accuracy can be obtained by considering damping force as a linear function of the rate change of response, $\dot{x}$, and stiffness as a linear function of response, x, [8]. Hence, according to the characteristics of the damping and stiffness coefficient relative to the rate change of response and deformation respectively, an offshore structure can be categorized as:

- Linear mechanical system
- Non-linear mechanical system

2.2.1 Linear Mechanical system

As described above, dumping and stiffness coefficients are non-linear in nature. However, when a structure is within the elastic state, for example if we consider the stresses due to wave forces, it can be modeled with a sufficient accuracy as a linear mechanical system. In elastic state, dumping and stiffness coefficients do not depend on the rate change of response, $\dot{x}$, and deformation, x , respectively. This means that the dumping and stiffness coefficients remain constant as far as the structures are within this region or Hook's low is valid [1]. As a result, damping force will be considered as a linear function of the rate change of response, $\dot{x}$, and stiffness force as a linear function of deformation, x. Consequently, the general equation of motion for these structures is given as:

$$m * \ddot{x}(t) + c * \dot{x}(t) + k * x(t) = F(t) \tag{2.2}$$

The solution for equation 2.2 is given by the sum of homogeneous solution, x_h, and particular solution, x_p, as:

$$x = x_h + x_p \tag{2.3}$$

The homogeneous solution, x_h, may have larger value at the initial time and damped out with time and it is computed as:

$$x_h = e^{-\lambda\omega_0 t} * (Asin\omega_d t + Bcos\omega_d t) \tag{2.4}$$

where A and B are constants and they are determined from the initial or boundary conditions; λ is relative damping; ω_0 is natural frequency of the system and ω_d is damping frequency of oscillation given by:

$$\omega_d = \omega_0\sqrt{1-\lambda^2} \tag{2.5}$$

The particular solution, x_p, in equation 2.3 lasts as far as the external loading,F(t), exists. This solution depends on the behavior of the external load applied. The external loads can be either harmonic loading or arbitrary type of loading. If the external load is arbitrary type, the particular solution, x_p, can be determined using the impulse-response method or the frequency-response method, for detail see [10]. In this thesis only for harmonic loading is presented.

For Harmonic loading

If the load on a linear structure is harmonic type of loading, the external load, F(t), given in equation 2.2 will be given as:

$$F(t) = F_0 sin(\omega t) \tag{2.6}$$

Where F_0 is the static loading; ω is loading frequency. Then, the particular solution for the harmonic loading can be determined as:

$$x_p = x_0 sin(\omega t - \theta) \tag{2.7}$$

where: x_o is amplitude and and θ is phase angle which are determined as follows:

$$x_0 = \frac{F_0}{m\omega_0^2} D \tag{2.8}$$

and,

$$\theta = arctg\frac{2\lambda\beta}{(1-\beta^2)} \tag{2.9}$$

where: D is the Dynamic amplification number. which is given by:

$$D = \frac{1}{((1-\beta^2)^2 + (2\lambda\beta)^2)^{\frac{1}{2}}} \tag{2.10}$$

Where β is the relative frequency relation between the frequency of the loading ,ω and the natural frequency of the system, ω_0, given in the form:

$$\beta = \frac{\omega}{\omega_0} \tag{2.11}$$

The phase angle, θ , given in equation 2.9 describes the phase angle between the external loading, F(t), and the response, x(t), while the amplification factor, D, in equation 2.10 describes how much the dynamic response of the system is relative to its response due to the static loading, F_0.

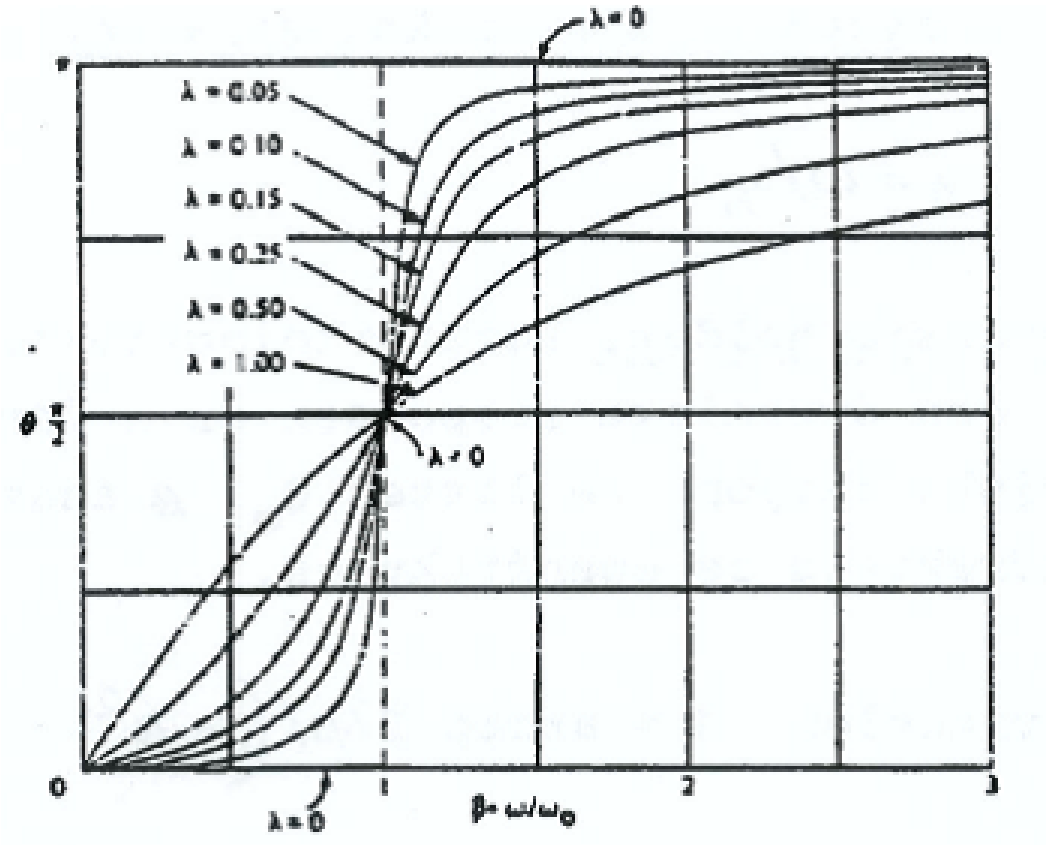

Figure 2.2: Phase angle as a function of relative frequency [10]

Figure 2-2 shows the phase angle, θ, as a function of relative frequency, β, based on equation 2.9.From this figure , we can see that:

- At relative frequency, $\beta, = 1$, the phase angle, $\theta, = 90^0$ for all values of the relative damping, λ.

- For relative frequency, $\beta, <1$, the phase angle, $\theta, \approx 0$ when the relative dumping, $\lambda, \rightarrow 0$.

- For relative frequency, $\beta, >1$, the phase angle, $\theta, \approx 180^0$ when the relative damping, $\lambda \rightarrow 0$ again.

Figure 2-3 shows dynamic amplification factor, D, as a function of relative frequency, β, based on equation 2.10.

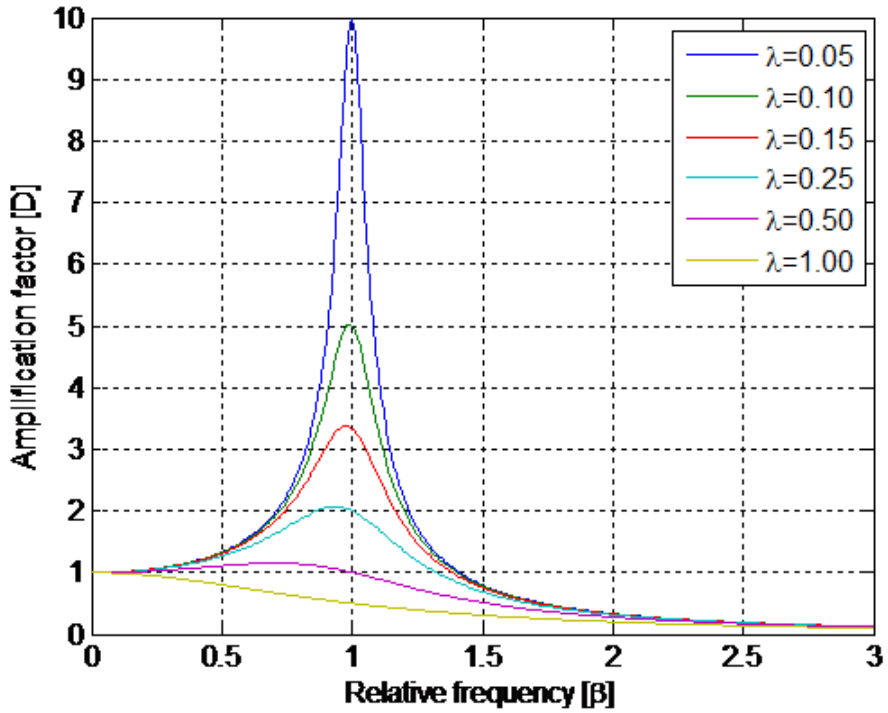

Figure 2.3: Dynamic amplification as a function of the relative frequency

From Figure 2-3, it can be noticed that at a relative frequency, $\beta, = 1$, i.e. when the loading frequency, ω, is equal to the natural frequency of the system, ω_0, the dynamic amplification factor reaches its maximum value and the system gets its resonance. Furthermore, it can be observed that the damping reduces the dynamic amplification factor and for higher damping values, the resonance top is for relative frequency, β, less than one.

From the above observations i.e. equation 2.9 or Figure 2-2 and equation 2.10 or Figure 2-3, the dynamics can be divided in to three cases:

1. $\beta \ll 1$: Where the dynamics is controlled by the stiffness of the system in phase with the loading. In this case there is small or no dynamic effect and such systems are termed as Quasi-statically behaving structures.

2. $\beta \approx 1$: When the system is at resonance or where there is large dynamic effect, the dynamics is controlled by the damping in the system by 90^0 out of phase with the loading.

3. $\beta \gg 1$: Mass controlled motion and it is out of phase to the loading by 180^0, i.e. the mass or inertia force acts in opposite direction to the external loading and tries to reduce the response of the system.

Generally linear mechanical systems can be grouped in two classes based on their response to the external loading as:

- Quasi-statically behaving structures
- Dynamically behaving structures

Quasi-statically Behaving Structures

Off shore structures such as jacket platforms installed up to water depth of around 150m have low natural period or larger natural frequency. As a result, the relative frequency for such structures are much less than one, $\beta \ll 1$, as case 1 in section 2.2.1. In such offshore structures, the dynamics is controlled by the stiffness of the structures and the energy lost due to dumping and acceleration or mass force on their structural members can be neglected and such structures are termed as quasi-statically behaving structures. In this case the mass term, m, and dumping coefficients, c, in equation 2.2 are assumed be zero. As a result, equation for harmonic loading is reduced to:

$$k * x(t) = F_0 sin(\omega t) \tag{2.12}$$

Where: k is stiffness of the elastic/linear mechanical structure; F_0 is the static loading; ω is loading frequency. Then, the response of a quasi-statically behaving structure for harmonic type of loading can be determined as:

$$x(t) = \frac{F_0 sin(\omega t)}{k} \tag{2.13}$$

Based on Haver [8], the following offshore structures can be considered as quasi-static structures:

- For jacket platforms installed up to water depth 150m.
- For jack-ups installed in shallower water depth, less than 70m, in particular if the support or foundation on the sea floor is close to fixed.
- Structures with natural period less than 2sec.

Dynamically Behaving Structures/Forced Linearly Damped Structure

As water depth increases the height of the offshore structure increase its natural period increases and as a result the structure behaves dynamically. In this case the energy lost due to dumping and the acceleration or mass force to control the dynamics cannot be ignored and this leads to dynamic effects that have to be accounted. The response of dynamically behaving linear structure in the direction of force can be determined by solving the linear equation of motion given in equation 2.2.

With reference to Haver [8], the following offshore structures can be considered as dynamically behaving structures:

- For jacket platforms installed in water depth greater than 150m.
- For jack-ups installed in water depth deeper than 70-80 m.
- Structures with natural period larger than 2s.

Linear response problem

In addition to the dependency of the stiffness coefficient and damping coefficient to the response and rate change of response discussed above, if the hydrodynamic load on an offshore structure can be modeled as a linear function of the surface elevation process, such structure is referred as a linear response problem [8]. Hydrodynamic loads can be reasonably modeled as a linear function of the surface elevation process, when the inertia or mass force dominates to the drag force as described in section 3.4.

For linear response problems, their response quantity —is conveniently characterized by a transfer function, $H_{\Xi\Gamma}(\omega)$, [8]. As is further discussed in chapter 6, transfer function is the ratio between the complex response amplitude, $\Gamma(t)$, and wave amplitude, $\Xi(t)$, and it is given in the form:

$$\Gamma(t) = (RAO) * \Xi(t) \tag{2.14}$$

where: RAO is the absolute value of the transfer function, $|H_{\Xi\Gamma}(\omega)|$, referred as the Response Amplitude Operator (RAO).
Based on Haver [8], for a short period of time if a sea surface process can be well described as Gaussian process, it can be well represented by a wave energy spectral density or wave spectrum, $S_{\Xi\Xi}(\omega)$. This means for linear systems, the response process is also Gaussian process which can be characterized by the response energy spectral density or response spectrum, $S_{\Gamma\Gamma}(\omega)$, which is given in the form:

$$S_{\Gamma\Gamma}(\omega/h, t) = |H_{\Xi\Gamma}|^2 * S_{\Xi\Xi}(\omega/h, t) \tag{2.15}$$

2.2.2 Non-linear Mechanical System and Non Linear Response Problems

As mentioned in section 2.2.1, when a structure is within its elastic behavior or the Hook's low is valid, the structure can be treated as a linear system. But for example, if the structure is subjected to higher load that the structure can reach within its plastic limit, then, in this state the stiffness coefficient, k, and damping coefficients, c, can't be assumed as constant. Instead the coefficients have to be updated at each time step when the structure is beyond its elastic limit and such systems are considered as non-linear systems.

When the hydrodynamic load on an offshore structure is dominated by its non linear component, the drag force, the right hand side of equation 2.1 can't be modeled as a linear function of the surface elevation process, and such structures are referred as non-linear response problems. The response of a non-linear mechanical system can be found by solving the general equation of motion given in equation 2.1.

Chapter 3

HYDRODYNAMIC LOADS ON OFFSHORE STRUCTURES

3.1 Introduction

A structure installed in an ocean can be subjected to different types of loads; generally these loads can be categorized as: permanent actions, variable actions, environmental actions, deformation actions and accidental actions [14]. As shown in Figure 3.1, environmental loads include wave load, current load, wind loads earthquake etc. One of the major sources of environmental forces on offshore structures is the wave loads, such loads are irregular in shape, variable in magnitude and may approach the structure from one or more directions which will cause stress variation in the structure and may lead to fatigue. For these reasons and economic and safe design of a platform good estimation of wave loads are essential.

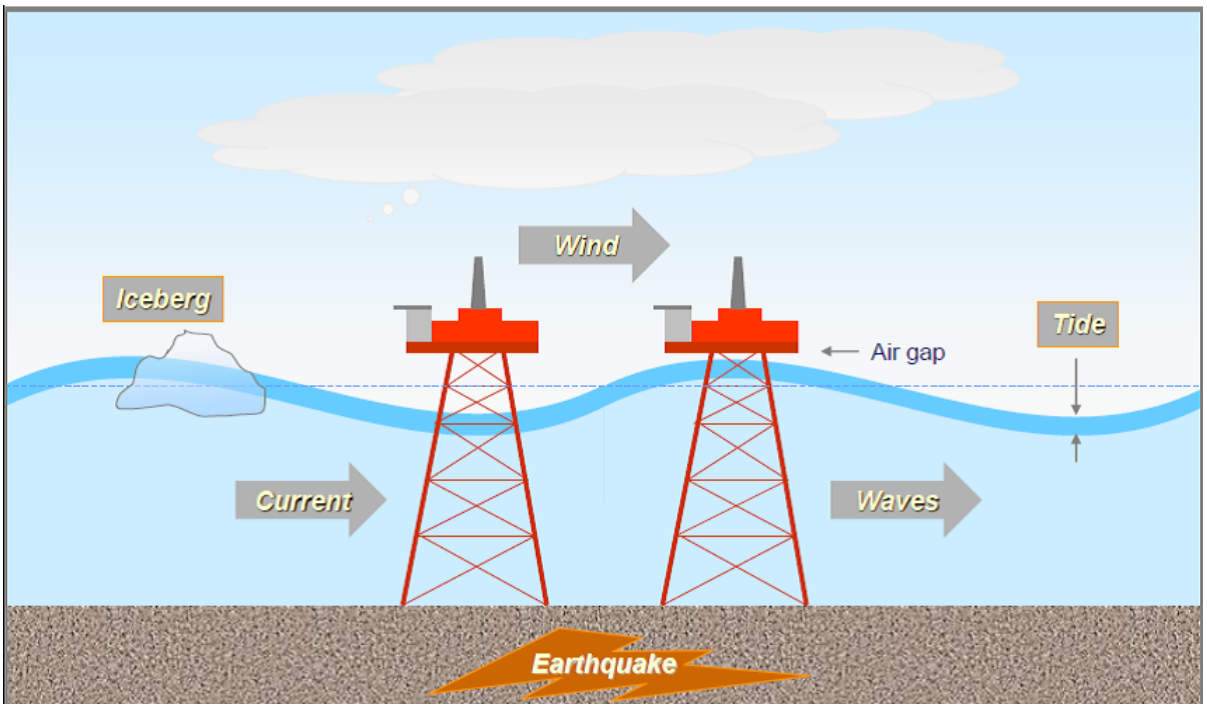

Figure 3.1: Environmental loads on offshore structures [12].

Based up on the flow regime in the vicinity of a submerged structure, which depends on the relative cross sectional dimension of the structural to the water wave length, the wave loads can be calculated using the following three different methods [3]:

1. Morison equation: Morison equation assumes that the hydrodynamic load is a linear composition of mass or inertia proportional to acceleration and drag force being proportional to the square of velocity. It is applicable when the structural member has a cross sectional dimension significantly small, slender members, relative to the water wave length, so that the fluid kinematics around the structural member is not affected by the presence of the member, i.e. to assuming as if the structural member is not there. Structural members of jacket platforms and jack-up platform are good examples slender members. Based on DNV-RP-C205[6], structural members are classified as slender members and Morison equation is applied when the equation below is satisfied:

$$\lambda > 5 * D_0 \tag{3.1}$$

   where: λ is the water wave length and D_0 is the diameter or other projected cross-sectional dimension of the member.

2. Froude-Krylov theory: The Froude-Krylov theory is applicable when the submerged structure has not too small or not too large cross sectional dimension relative to the water wave length. Similar to the Morison equation, the effect of the structural member to the wave field around it is ignored and assumed as if the structure is not there. Due to the above assumption, this method has limited practical application but good exercise in understanding the problem of wave forces on a structure and the force coefficients are easier to determine, for detailed information refer [3].

3. Diffraction theory: For larger volume structure, where the cross sectional dimension or size of the submerged member is comparable to the water wave length, the diffraction theory is used to determine the wave loads on the members. In this theory, the radiation or diffraction effect of the large volume structure to the wave fluid kinematics in the vicinity has to be taken in to account when calculating the wave load on it, for detailed information refer [3].

3.2 Wave kinematics

Fluid particle velocity and acceleration around a submerged structure can be calculated using numerous water wave theories. These theories assumes that the waves are periodic and uniform with a period T and height H. Note that the wave period is the time interval between successive crests or troughs passing a particular point, and the wave height is the vertical distance from a trough to the adjacent crest. The common wave theories which are described in [3] and [6] are:

- Linear Airy wave theory
- Stokes wave theory
- Cnoidal wave theory

- Steam function wave theory
- Solitary wave theory
- Standing wave theory

Selection of a specific wave theory from the common theories listed above depends up on the specific environmental parameters, such as wave height, wave period and water depth. The validity of the selected wave theory can be tested on Figure 3-2 given bellow, in which the horizontal axis measures the shallowness while the vertical is a measure of steepness.[6]

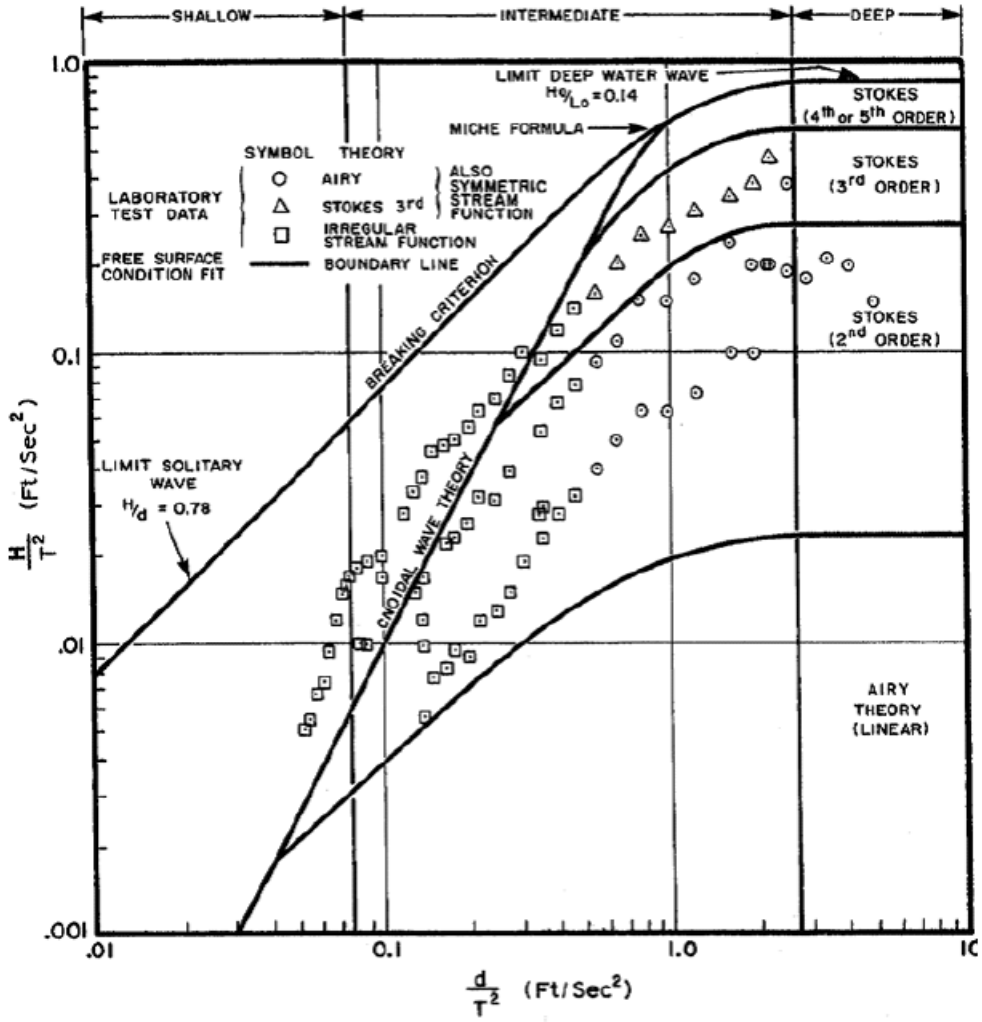

Figure 3.2: Ranges of validity of the various wave theories [6].

3.2.1 Linear Airy Wave Theory

This theory is based on the assumption that the wave height is small compared to the wave length and water depth, which allows the free surface boundary conditions to be linearized and the free surface conditions to be satisfied at the mean water level, rather than at the oscillating free surface [3]. Based on this theory the surface profile is given as:

$$\eta(x, y, t) = \frac{H}{2} cos\theta \tag{3.2}$$

where: H is the wave height; $\theta = k(xcos\beta + ysin\beta) - \omega t$ is the phase and β is the direction of propagation.

3.2.2 Horizontal particle velocity and Acceleration

For a given wave parameters and water depth, the horizontal particle velocity can be determined as a function time, t, and distance of propagation, x, at a specified depth below still water level as given bellow [15]:

$$u_{(x,y,z)} = \frac{\pi * H}{T} * \frac{cosh[k(z+d)]}{sinh(kd)} * cos(\omega t - kx) \tag{3.3}$$

By direct differentiation of the horizontal particle velocity equation (3.3), we get the acceleration of the water particles as:

$$_{(x,y,z)} = -\frac{2\pi^2 * H}{T^2} * \frac{cosh[k(z+d)]}{sinh(kd)} * sin(\omega t - kx) \tag{3.4}$$

In equations 3.3 & 3.4, H is trough to crest wave height; T is wave period; $k = \frac{2\pi}{\lambda}$ = wave number; λ is wave length; d is mean water depth; t = time; x is distance of propagation; z is distance from still water level (SWL) positive upward and $\omega = \frac{2\pi}{T}$ = angular wave frequency.

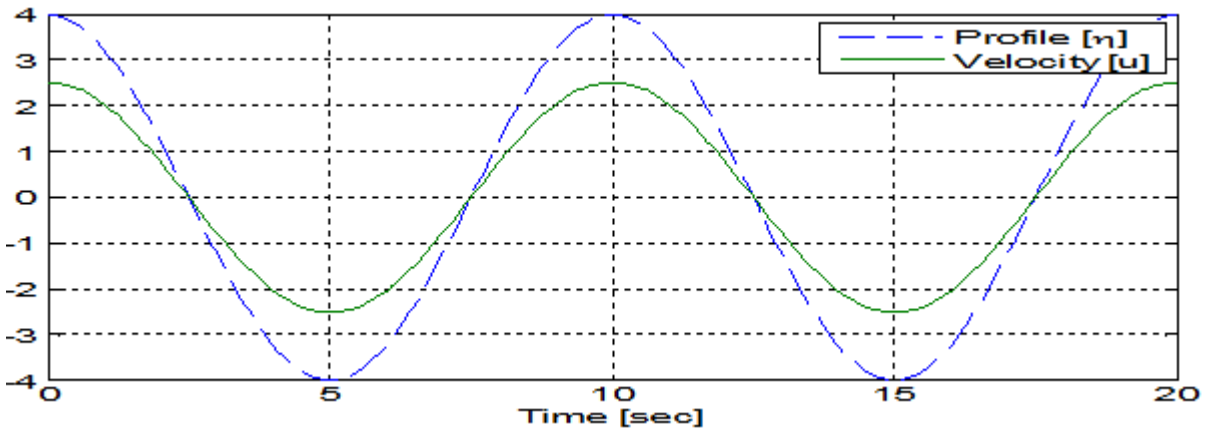

Figure 3.3: Surface profile and Horizontal particle velocity

Figure 3-3 and 3-4 show the horizontal water particle velocity and acceleration for a wave height 8m and period of 10 second in a mean water depth of 190m. The quantities, velocity, acceleration and profile, are calculated at the still water level (SWL) at a station given by x=0. From Figure 3-3, it can be seen that the horizontal velocity and the surface profile are in phase and the velocities are maximum at crests, minimum at troughs and zero at SWL. Also from Figure 3-4, it can be observed that the acceleration and the profile are out of phase by 90^0 and the acceleration is maximum at SWL and zero at trough and crest. Note that the velocity and the acceleration are out of phase by 90^0.

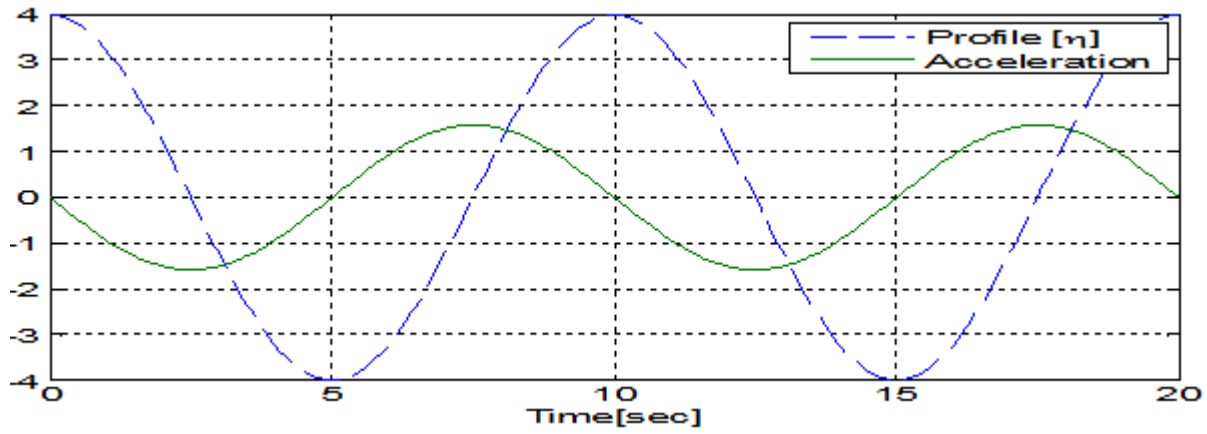

Figure 3.4: Surface profile and acceleration of water particles

3.3 Wave Induced Loads on Slender Members Using Morison Equation

As shown in Figure 3-5, the Morison equation was developed by Morison, O'Brien, Johnson, and Shaaf (1950) in describing the horizontal wave forces (f) acting on a vertical pile which extends from bottom through the free surface [3]. Morison's equation is composed of drag term, $f_{D(x,z,t)}$, and inertia term, $f_{I(x,z,t)}$, as in equation 3.4. The drag term is proportional to the square of the horizontal particle velocity, $u_{(x,z,t)}$, given in equation 3.3 and the inertia term being proportional to the horizontal acceleration, $_{(x,z,t)}$, given in equation 3.4. Normal wave force per a unit length on a submerged structural member can be calculated using the Morison's equation given in equation 3.5 [6]:

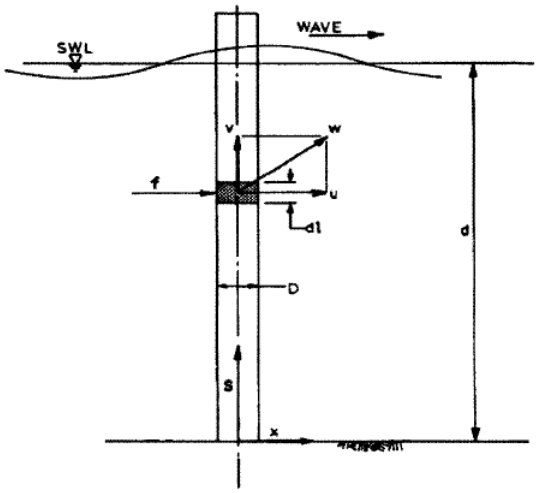

Figure 3.5: Morison force on a vertical pile [15]

$$f_{(x,z,t)} = f_{D(x,z,t)} + f_{I(x,z,t)} = \frac{1}{2}1/2 * \rho_w * C_D * D_0 * u * |u| + \frac{\pi}{4} * D_0^2 * \rho_w * C_m * u \quad (3.5)$$

where

- $f_{(x,z,t)}$: Normal wave load at a distance x and depth z

- $f_{D(x,z,t)}$: Drag force at a distance x, depth z and time t.
- $f_{I(x,z,t)}$: Mass or inertia force at a distance x, depth z and time t.
- ρ_w : Density of sea water
- $u = u_{(x,z,t)}$: Undisturbed horizontal particle velocity at the center of the member at a given depth z
- $=_{(x,z,t)}$: Fluid particle acceleration at a given depth and time.
- D_0 = Diameter or typical cross-section dimension.
- A: Cross sectional area.
- C_D : drag coefficient [-]
- $C_m = (1 + C_A)$: Inertia coefficient
- $C_A = \frac{m_a}{(\rho_w)} A$:added mass coefficient
- m_a : Added mass per unit length that can be determined based on [7].

As shown in the Figure 3-5, x is zero at the center of the submerged vertical pile and z is distance from still water level positive upward, i.e. it is zero at the mean free surface and –d at the mean water depth.
When using the Morison's equation to determine the hydrodynamic loads on a submerged structure, one should take in to account the variation of the hydrodynamic coefficients. These coefficients depend on different parameters such as the flow characteristics around the structure, cross sectional dimension and roughness of the submerged structure, see [6]. Based on laboratory experiments and field measurements, various certifying agencies such as American Petroleum Institute, British standard Institute and Det Norske Veritas etc have made specific drag and inertia coefficients, see [15].

An example of the drag force, inertia force and total/normal force is shown in Figure 3-6. These forces are on a 5m diameter submerged cylindrical structure of a wave height 8m and period of 10 second in a mean water depth of 190m. The quantities are calculated at the depth of 108m bellow the still water level at the center of the cylinder, i.e. at a fixed point.

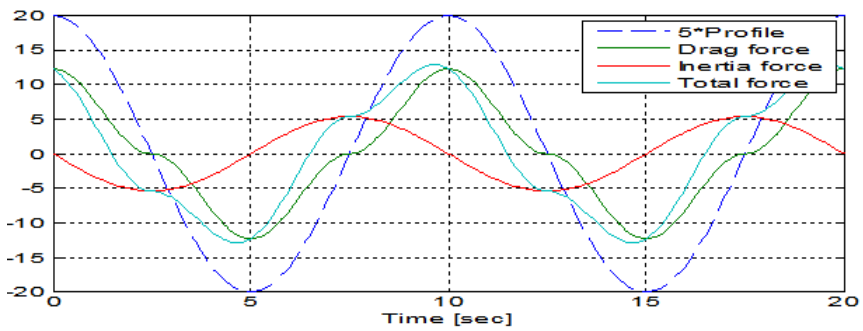

Figure 3.6: Drag, Inertia and normal forces on a submerged cylinder.

In Figure 3.6 it can be observed that similar to the velocity in Figure 3-3, the drag force reaches minimum at crests, maximum at troughs and zero at the SWL. The inertia or mass force has maximum value at the SWL and zero at crests and troughs as the acceleration does, see Figure 3.4. It can be noticed that when the inertia force is zero, the drag force reaches maximum and the vise verse is true.

3.4 Mass or Inertia Term Versus Drag Term on Slender Members:

As described in section 3.3, the Morison's equation is composed of drag term and inertia term. As the drag term is proportional to the square of the horizontal particle velocity, it is not linearly related to the incident wave amplitude or wave process while the inertia term being proportional to the acceleration and it is linearly related to the incoming wave amplitudes. Based on DNV-RP-C205 [6], the relative importance of maximum drag force $f_{D,max}$ and maximum inertia force $f_{I,max}$ for a circular cylinder can be determined using the equation given bellow.

$$\frac{f_{(D,max)}}{f_{(I,max)}} = \frac{C_D}{\pi^2 * C_m} * K_c \tag{3.6}$$

where C_D and C_M are drag and mass coefficients respectively which can be determined from laboratory experiments and field measurements and K_c is the Keulegan-Carpenter number that can be written as a function of wave height, H, and the structural cross sectional dimension, D_0, as below:

$$K_c = \frac{\pi * H}{D_0} \tag{3.7}$$

Substituting equation 3.7 in equation 3.6 gives as:

$$\frac{f_{(D,max)}}{f_{(I,max)}} = C * \frac{H}{D_0} \tag{3.8}$$

where: C=$\frac{C_D}{\pi C_M}$ is constant.

Figure 3.7 to 3.9 shows drag forces Vs inertia or mass force for slender structures of various wave heights and cross sectional diameter of the submerged structure based on the Morison's equation given in equation 3.5. Note that the wave period is kept constant, T=10sec, for each case that means the wave length is kept to be 317 m, which is determined by the dispersion relation given in the form [15]:

$$\omega^2 = g * k * tanh(kd) \tag{3.9}$$

where: ω is wave frequency; $k = \frac{2\pi}{\lambda}$ is wave number; λ is wave length; d is mean water depth and g is gravitational acceleration taken as $9.81 m/sec^2$.

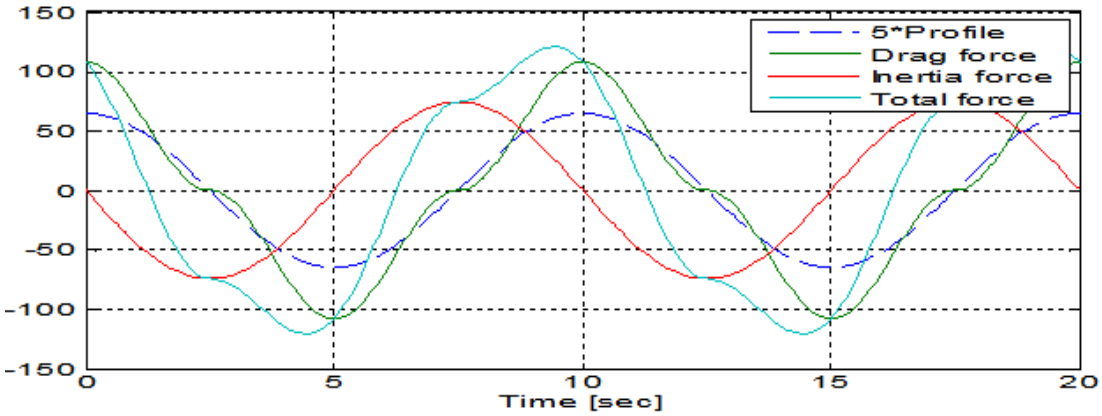

Figure 3.7: Drag term dominant for H= 26m, T= 10 sec and Do= 3m

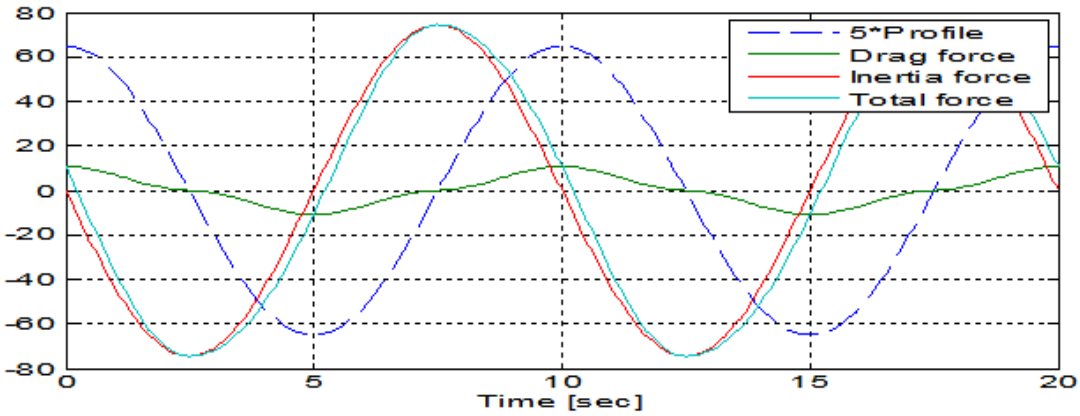

Figure 3.8: Inertia term dominant for H= 26m, T= 10 sec and Do= 30m

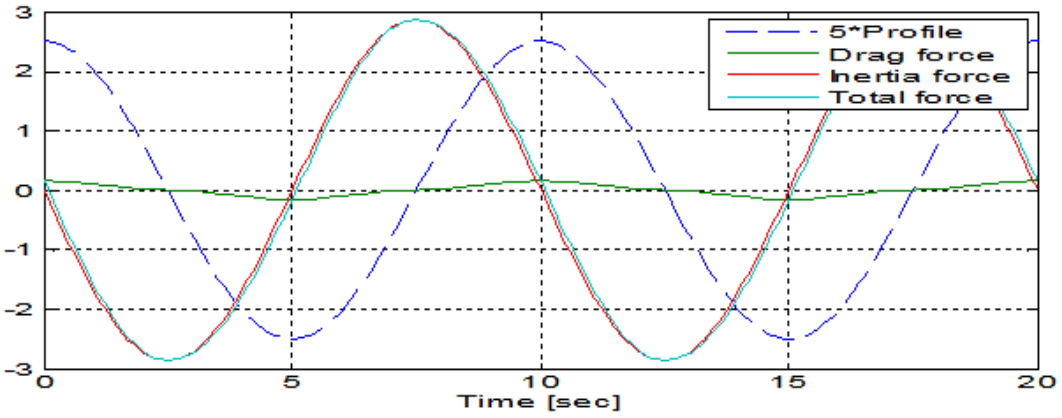

Figure 3.9: Drag term dominant H=1m, T=10 sec and Do= 3m

From equation 3.8 and Figures 3-7 to 3-9, it can be seen that the magnitude of the maximum drag force depends on the ratio between the wave height, H, and the structural cross sectional dimension, Do, and it dominates when the wave height is much larger than the structural cross sectional dimension. Thus, if the wave height is much larger than the structural diameter, the system may be treated as nonlinear system or non-linear response problem as the drag term is non-linearly related to the wave process.

As in Figure 3-8, if the structural diameter is larger relative to the wave height such as floating platforms or Semi-submersible platforms and Tension leg platforms (TLP) etc.., the inertia force dominates. Also as in Figure 3-9 inertia force may dominate as in the case of jacket and jack-up platforms on small wave height provided that equation 3.1 is satisfied or the Morison equation is valid. Therefore, for large volume and for more slender offshore structures, the hydrodynamic load applied on them can be reasonably well modeled as linear function of the surface elevation process, provided that the inertia force is dominant to the drag force on the Morison's equation (3.5) and such systems are called linear response systems or problems while a linearization method may be adopted to the drag force, for detail see [3].

Chapter 4

ESTIMATION OF WAVE ENERGY SPECTRAL DENSITY

4.1 Introduction

Based on Haver [8], for short period of times, within time interval of three to six hours, observed sea surface at a fixed location can be modeled as a stationary stochastic process, $\Xi(t)$. Stationary stochastic process is a process in which its statistical properties (such as mean value, standard deviation etc.) do not change with time and such process are often assumed to be a Gaussian process. For real sea surface, the Gaussian surface process may not describe in a sufficient accuracy and this inaccuracy can create some deviation in modeling detailed structures. In order to minimize this inaccuracy of the Gaussian process, a new process called a second order process can be used. However, for this study case, the stationary stochastic process is assumed of a sufficient accuracy. Under this process, the zero mean sea surface process can be represented with higher accuracy by the wave energy spectral density function, $S_{\Xi\Xi}(\omega; h, t)$. A wave energy spectrum is a power spectral density function which describes the vertical displacement of the sea surface and how energy of harmonic wave components is distributed on various frequency bands. Energy of a harmonic wave is proportional to the square of its amplitude. A wave process can be either a broad band, a process with many local maxima and minima, or narrow band process, process with no local maxima), which can affect the shape of the wave spectra.

4.2 Screening of Model Test Conditions

The available data includes 21 time series wave records of 20 minute duration given in table 4-1. Note that the name convention used as a file name in the table 4.1 for each event is based on the start time for each 20 minute record (e.g. 200312311900 is for the 20 minute record from 19:00 to 19:20 on 31/12/2003).

4.3 Estimation of wave Energy Spectral Density

As mentioned in section 4.1, a wave energy spectral density, $S_{\Xi\Xi}(\omega|h, t)$, is a power spectral density function which describes the vertical displacement of the sea surface and shows how energy of harmonic wave components is distributed on various frequency bands. As

Table 4.1: Time series wave records test conditions.

Test condition (test.con)	*File name*	*Wave recorded*
1	200312140700	On 14/12/2003 from 07:00 to 07:20
2	200312142100	On 14/12/2003 from 21:00 to 21:20
3	200312150820	On 15/12/2003 from 08:20 to 08:40
4	200312150900	On 15/12/2003 from 09:00 to 09:20
5	200312311900	On 31/12/2003 from 19:00 to 19:20
6	200312311920	On 31/12/2003 from 19:20 to 19:40
7	200312311940	On 31/12/2003 from 19:40 to 20:00
8	200312312000	On 31/12/2003 from 20:00 to 20:20
9	200312312020	On 31/12/2003 from 20:20 to 20:40
10	200312312040	On 31/12/2003 from 20:40 to 21:00
11	200312312100	On 31/12/2003 from 21:00 to 21:20
12	200312312120	On 31/12/2003 from 21:20 to 21:40
13	200312312140	On 31/12/2003 from 21:40 to 22:00
14	200312312200	On 31/12/2003 from 22:00 to 22:20
15	200312312220	On 31/12/2003 from 22:20 to 22:40
16	200312312240	On 31/12/2003 from 22:40 to 23:00
17	200312312300	On 31/12/2003 from 23:00 to 23:20
18	200312312320	On 31/12/2003 from 23:20 to 23:40
19	200312312340	On 31/12/2003 from 23:40 to 24:00
20	2004010112000	On 01/01/2004 from 12:00 to 12:20
21	200401011400	On 01/01/2004 from 14:00 to 14:20

described in S.K. Chakrabarti[3], the time series records of an ocean can be transformed in to the frequency domain wave energy spectrum by two commonly used methods, namely Autocorrelation and Fast Fourier Transform method (FFT). In this study, for estimation of the wave spectrum the MATLAB's built in FFT function is used. A brief introduction of the FFT method is presented in section 4.3.1 and for more detail and derivation of equation 4.11 see [9]. Estimation of wave spectral density for the 21 time series records given in Table 4-1 have done and the first four are presented in section 4.3.2 while the others are presented in Appendix A-1.

4.3.1 Fast Fourier Transfer Method

In FFT technique, the transformation is taken directly from the time domain to frequency domain and then the result is squared to convert to the energy unit. If $\Xi(t)$ is the wave elevation as a function of time for a total data length T_s and Δt is a constant time increment, then the energy spectrum by FFT can be estimated as [3]:

$$S_{\Xi\Xi}(\omega) = \frac{1}{T_s}[\sum_{n=1}^{N} \Xi(n\Delta t) * e^{i2\pi * f(n\Delta t)} * \Delta t]^2 \tag{4.1}$$

General parameters that involved in the estimation of a wave spectrum using the above equation from a time series wave records are:

- Number of sections, M, in which the total data length is equally divided.
- Number of data points in each section, N.
- Number of segment,$K = \frac{M}{N}$.
- Time increment or sampling rate, Δt.
- Frequency increment or resolution, $f_s = \frac{1}{\Delta t}$.
- Nyquist frequency, $f_N = \frac{1}{2*\Delta t}$.

In this process, for each test condition the total data length ,T_s, is divided in to numbers of segments and each segment is divided in to N data pints. The wave spectrum is evaluated with the equation given in equation 4.11 at all data pints within a given segment and then, the final wave spectrum result is averaged over the number of segments. Note that for a given record T_s and Δt are fixed, and $T_s = N * K * \Delta t$.

As shown in equation 4.1, the estimated wave spectrum depends on the magnitude of the data points, N. As result, the shape of the spectral curve as well as the wave parameters for a given test condition change as the magnitude of the data point changes. Figure 4.1 "a" to "d" and Table 4.2 show the estimated wave spectral curves and wave parameter values for different value of number of data point for test.con 1 given in Table 4.1.

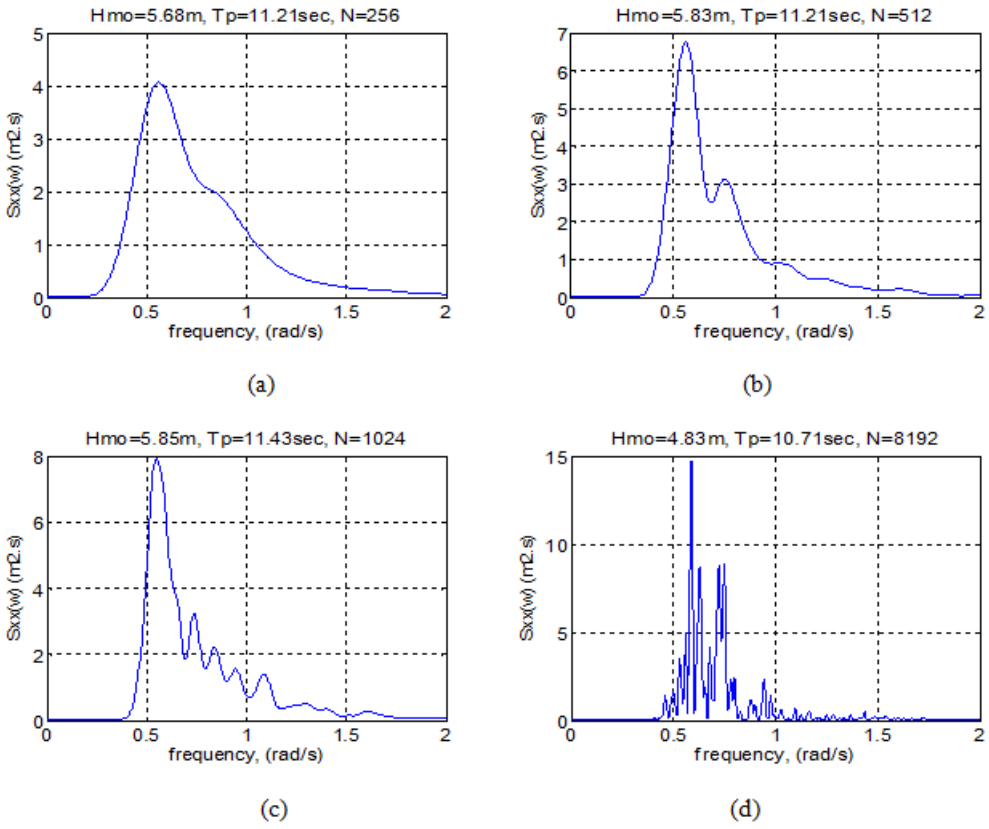

Figure 4.1: Variation of wave spectrum curve with variation of N for Ts=1200 sec.

From Figure 4-1 "a" to "d" one can notice that the estimated wave spectrum of a given wave record is not unique. The shape of the curve or relative distribution of energy

changes slightly as the value of data point, N, changes and the larger the values of N the sharper is the spectrum with an increase number of peaks, the smaller the data point the smoother the spectral curve is. Similarly table 4.2 shows that the significant wave height, H_s, and spectral peak period, T_p, vary slightly as the value of data point, N, changes.

Table 4.2: Wave parameters for test.con1with varying of number of data points

Figure 1	*Number of data point (N)*	H_s	T_p	*Remark*
a	256	5.68	11.21	Smoother curve
b	512	5.83	11.21	Smooth curve
c	1024	5.85	11.43	Sharp curve
d	8192	4.83	10.71	Noisy curve

4.3.2 Estimation of Wave Energy Spectral Density from test conditions

In this section, each time series wave record listed in table 4.1 are transformed in to frequency domain using the FFT-Matlab built in function. In this process, the total data length of a given time series record ,$T_s = 1200$ sec, is divided in to nine numbers of segments each one having 1024 data points and time increment of 0.1302 seconds. Here, as shown in Figure 4-2 to 4-9 only the first four test conditions, test.con 1-4, from table 4-1 are presented, while the remaining are attached in appendix A.1.

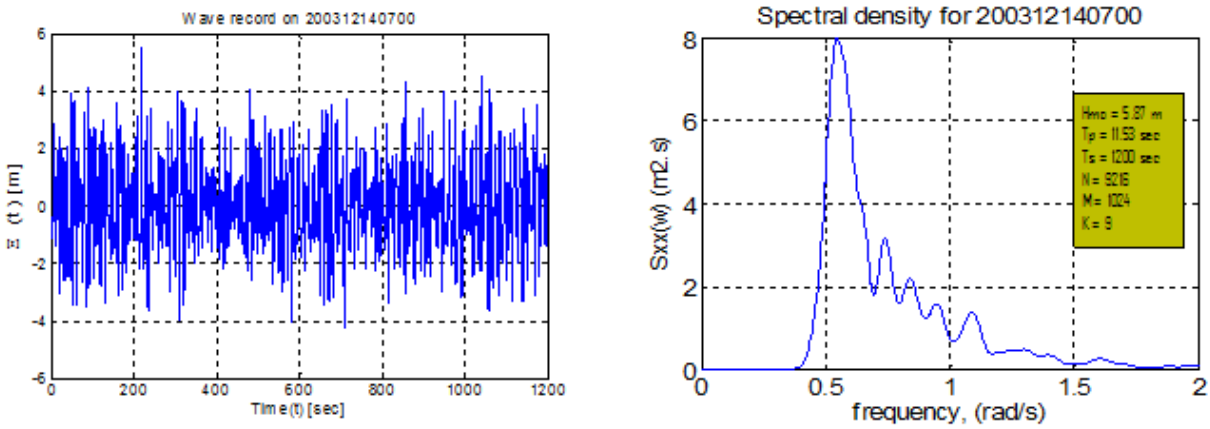

Figure 4.2: Time series wave records (a) & estimated wave spectrum (b) for test.con 1.

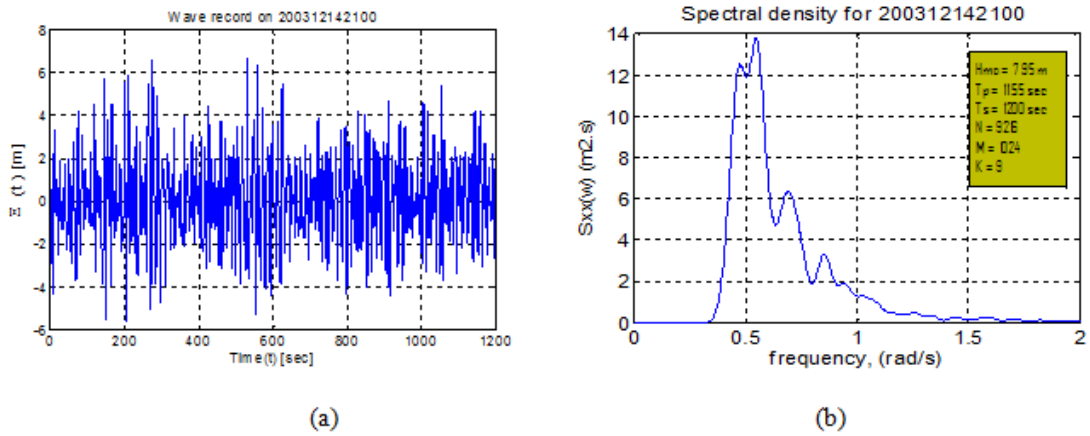

Figure 4.3: Time series wave records (a) & estimated wave spectrum (b) for test.con 2.

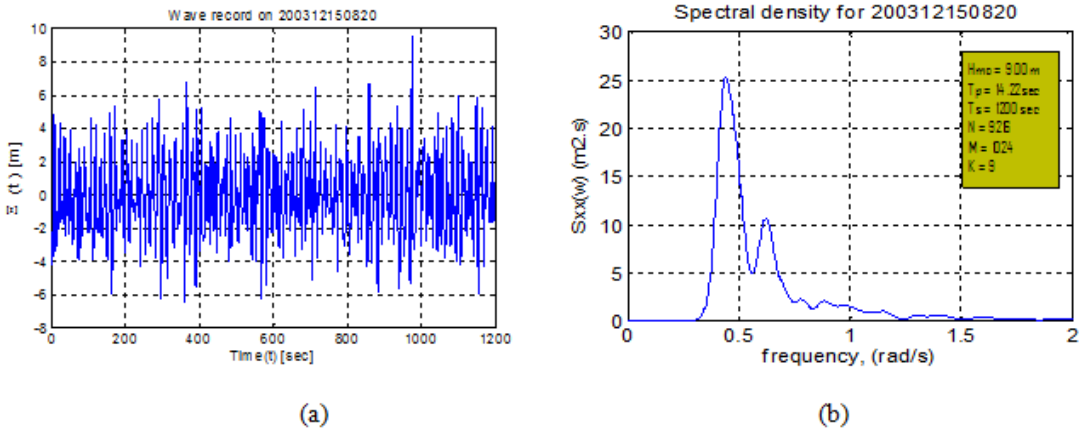

Figure 4.4: Time series wave records (a) & estimated wave spectrum (b) for test.con 3.

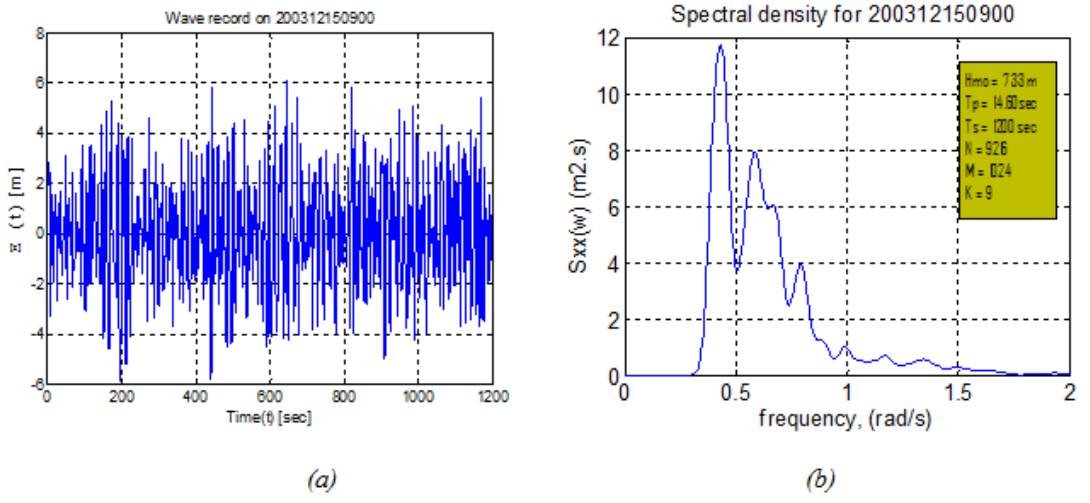

Figure 4.5: Time series wave records (a) & estimated wave spectrum (b) for test.con 4.

For each test conditions in Table 4-1, significant wave heights, H_s, and peak spectral periods, T_p, are determined as shown in Figure 4.6. The significant wave heights, H_s, are estimated using equation 4.5 which is derived as follows:

$$H_s = 4 * \sqrt{M_{(0,\Xi\Xi)}} \tag{4.2}$$

where: $M_{(0,\Xi\Xi)}$ is zero order spectral moment of a given sea state which is equal to the area under the estimated spectral curve and it represents the total energy of the process. This can be computed as:

$$M_{0,\Xi\Xi} = \int_0^\infty S_{\Xi\Xi}(\omega) * d\omega \tag{4.3}$$

Substituting equation 4.13 in to equation 4.12 gives as:

$$H_s = 4 * [\int_0^\infty S_{\Xi\Xi}(\omega) * d\omega]^{\frac{1}{2}} \tag{4.4}$$

As the frequency resolution goes closer to zero, i.e. as $d\omega \to 0$, the integration, $\int$, can be approximated in to summation, $\sum$, as a result equation 4.14 becomes as:

$$H_s \approx 4 * [\sum_0^\infty S_{\Xi\Xi}(\omega) * \Delta\omega]^{\frac{1}{2}} \tag{4.5}$$

The spectral peak periods, T_p, are estimated from the wave spectra which are determined by the inverse of the frequencies at which the estimated wave energy spectra reach their maximum values, i.e.$T_p = \frac{2\pi}{\omega_p}$, where ω_p is peak frequency determined from each spectral density.
As shown in Figure 4-6, for each test condition the significant wave heights, H_s and spectral peak periods, T_p, are estimated by writing a script in MATLAB as shown below, this scrip is an example for the first test condition, test.con1, given in Table 4.1.

```
%% Significant wave heights and spectral peak period
% significant wave height from equation 4.15
 Hs_14_07=4*sqrt(sum(Sxx_14_07*fs*2*pi/(2*length(fw_14_07))));
 fprintf('Hs_14_07 is %d\n',Hs_14_07)
 % Spectral period
   maxi_14_07=0;
for i=1:length(Sxx_14_07);
   if Sxx_14_07(i) > maxi_14_07
      maxi_14_07= Sxx_14_07(i);
      fp_14_07 = fw_14_07(i);
   end
end
Tp_14_07=(2*pi/fp_14_07);
fprintf('Tp_14_07 is %d\n',Tp_14_07)
```

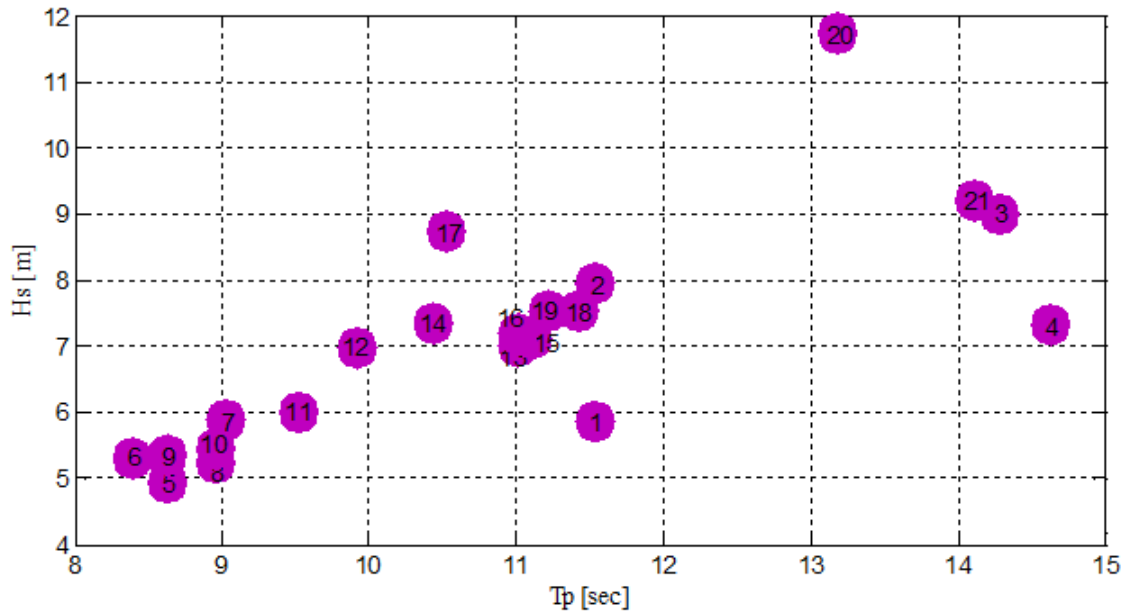

Figure 4.6: Estimated Hs and Tp for test conditions

4.4 Standard Wave Spectra

4.4.1 Introduction

Based on the geographical area with local bathymetry and sea state severity, wave energy spectra can be developed as single peak applied for wind or swell seas or double peak spectrum applied for a combined sea (wind and swell seas) using mathematical spectral models. As described in S.K. Chakrabarti [3], there are several mathematical spectral models, However, in this thesis only the Pierson –Moskowitz and JONSWAP spectra are introduced in Appendix A.2 and compared with the estimated wave spectra in section 4.3.2.

4.4.2 Comparison between the Estimated Wave Spectra Vs Standard Wave Spectra

Based on the estimated significant wave heights, H_s, and spectral peak periods, T_p, in section 4.3.2, the standard mathematical spectral models are plotted in the same graph in order to compare the area/energy under these spectral curve relative to their corresponding estimated spectral curve. For the first four test conditions, test.con 1-4, listed in table 4.1, are shown in Figure 4-7 and the standard deviations for these four test conditions are given in Table 4-3.

Figure 4-7 is presented to compare which mathematical wave spectra fits best to the estimated wave spectra and their standard deviation are computed as in Table 4-3. The standard deviation of each test condition is estimated as the square root of the zero order wave spectral moment, $M_{0,\Xi\Xi}$. The zero spectral moment is the area under the given spectral curve which is equal to tha variance of the sea surface process. In Table 4-3 it can be seen that the area under the Pierson-Moskowitz has almost identical to the area under the estimated spectrum, but there is slight difference to the JONSWAP spectrum.

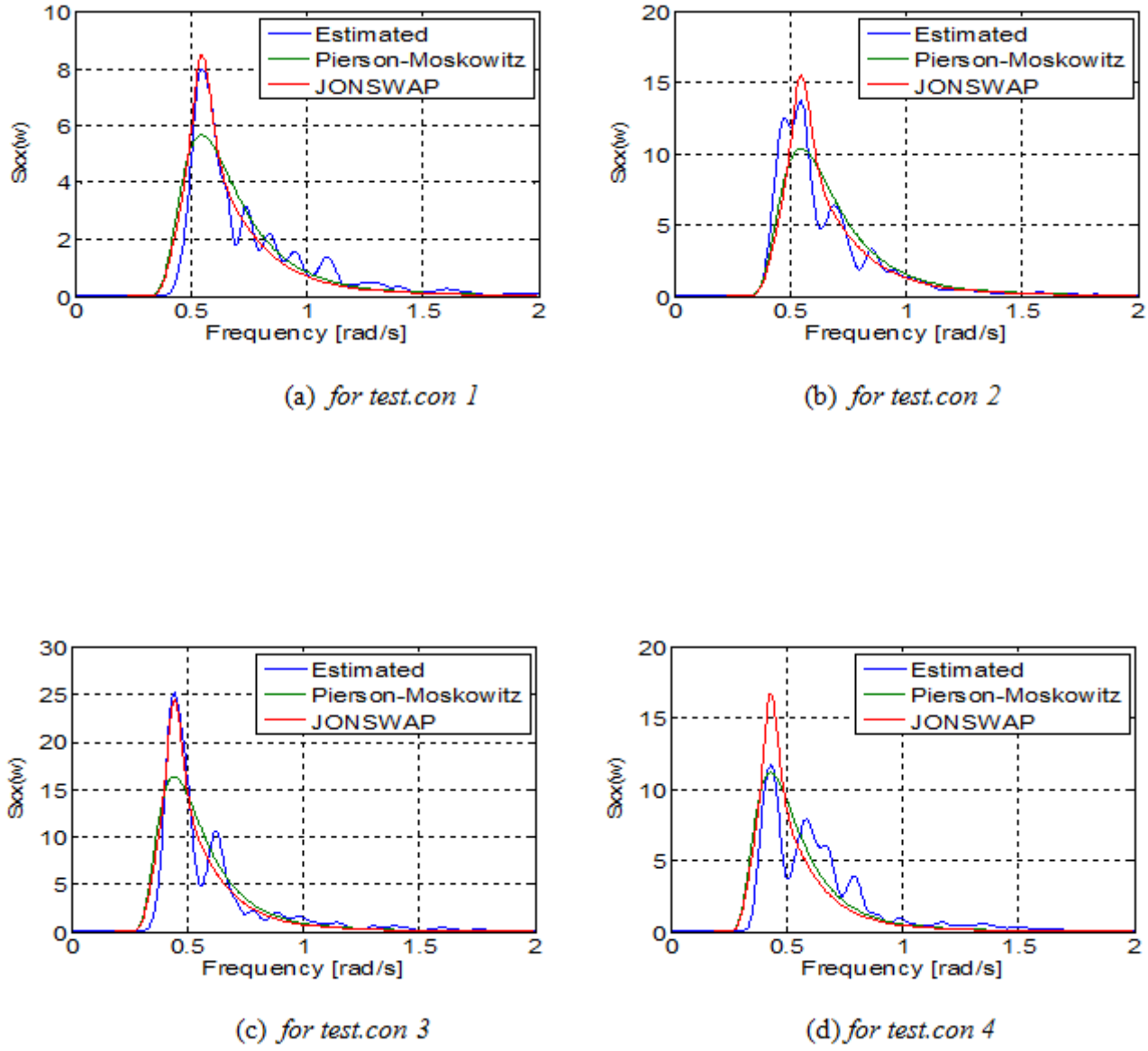

Figure 4.7: Estimated, Pierson-Moskowitz and JONSWAP spectra

Table 4.3: Standard deviation from estimated and standard wave spectra for test.con 1-4

Test condition	*Estimated spectrum*	*Pierson-Moskowitz*	*JONSWAP*	*Remark*
test.con 1	1.468	1.463	1.462	
test.con 2	1.987	1.981	1.979	
test.con 3	2.249	2.246	2.243	
test.con 4	1.832	1.829	1.827	

Chapter 5

ESTIMATION OF RESPONSE ENERGY SPECTRAL DENSITY

5.1 Introduction

As described in Chapter 2, for more slender structural members such as jacket and jack ups the inertia term of the Morison equation is dominant and then the hydrodynamic load on such structures can be treated as a linear function of the surface elevation process, Gaussian process, and their response as a linear response problem.

For the time series wave records listed in the screening of model test conditions Table 4.1, their corresponding time series responses, $\Gamma(t)$, of the Kvitebjørn jacket platform are also recorded. In this study, axial force responses of leg A1 and leg A2 of the platform at a water depth of 108m below the still water level are considered. Natural period of the jacket platform is around 4 seconds [16]. Figure 5-1 shows the orientation of the jacket with reference to the geographical north. North of the platform is assumed along the y-axis.

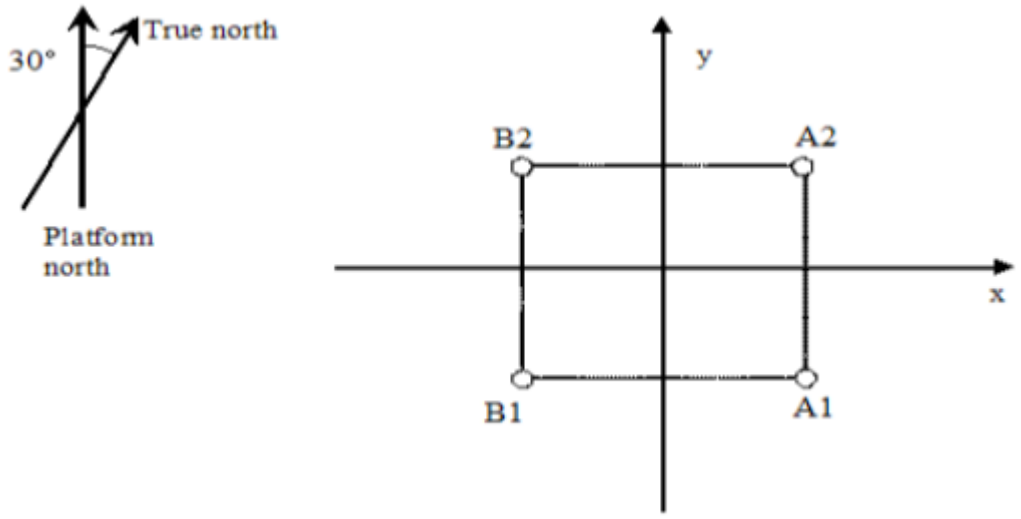

Figure 5.1: Orientation of Kvitebjørn jacket relative to geographical north and location of Leg A1 and A2.[16]

5.2 Estimation of Response Spectrum From Time Series Records

For estimation of the response spectrum, $S_{\Gamma\Gamma}(\omega)$, the MATLAB's built in Fast Fourier Transform (FFT) function is used, see section 4.3.1. Do keep in mind that in equation 4.1, the time series sea surface elevation, $\Xi(t)$, has to be replaced by the time series response, $\Gamma(t)$. For leg A1 four time series response records were taken, i.e. responses to the first four wave record listed in table 4.1 while for leg A2, 21 response records were taken, i.e. responses to the 21 time series wave records listed on table 4.1. In this sub chapter, response spectrum from the first four time series test conditions (test.con 1-4) of both legs are presented while the others are attached in Appendix B.1. A table showing the period, $T_{s,peak}$, where the response spectrum reaches its maximum around the wave spectral peak, resonance period, $T_{r,peak}$, where response spectrum reaches maximum around the natural period of the jacket, and their corresponding wave spectral peak, T_p, for all test conditions is presented in Table 5.1. The period $T_{s,peak}$ is estimated by the relation in equation 5.1.

$$T_{s,peak} = \frac{2\pi}{\omega_{s,peak}} \tag{5.1}$$

where: $\omega_{s,peak}$ [rad/sec] is the frequency where the response spectrum reaches its maximum around the wave spectral peak.
And the resonance period is determined by:

$$T_{r,peak} = \frac{2\pi}{\omega_{r,peak}} \tag{5.2}$$

where: $\omega_{r,peak}$ [rad/sec] is the frequency where the response spectrum reaches its maximum around the natural frequency of the jacket.

5.2.1 Estimated Response Spectrum from Leg A1

Figures 5-2 to 5-5 parts "a" and "b" show 20 minute of time series axial load records on the Kvitebjørn platform leg A1 and estimated response spectrum on 14/12/03 from 07:00, during test.con1, on 14/12/03 from 21:00, during test.con2, on 15/12/03 from 08:20, during test.con3, and on 15/12/03 from 09:00, during test.con4, respectively. Where as Figures 5-2 to 5-5 part "c" are plotted to show the estimated response spectrum of the leg relative to their corresponding wave spectrum estimated in section 4.3.2. Note that the vertical values of $S_{\Gamma\Gamma}(\omega)$ are multiplied by factor four in Figures 5-2 to 5-5 part "c".

Figure 5-2 and 5-3 part "b" and "c" shows that the response spectra of leg A1 increased when the wave spectra reached around their spectral peak periods of 11.53 and 11.55 second on 14/12/03 from 07:00 to 07:20 and on 14/12/03 from 21:00 to 21:20 respectively, this is the region where the wave energy concentrated. As discussed in section 2.2.1, when the forcing frequency is equal to the natural frequency of the structure, the dynamic amplification factor reaches at its maximum value. Consequently the response energies lost to control the amplified dynamics reached at their maximum value at the frequency 1.56, which is close to the natural frequency of the jacket platform.

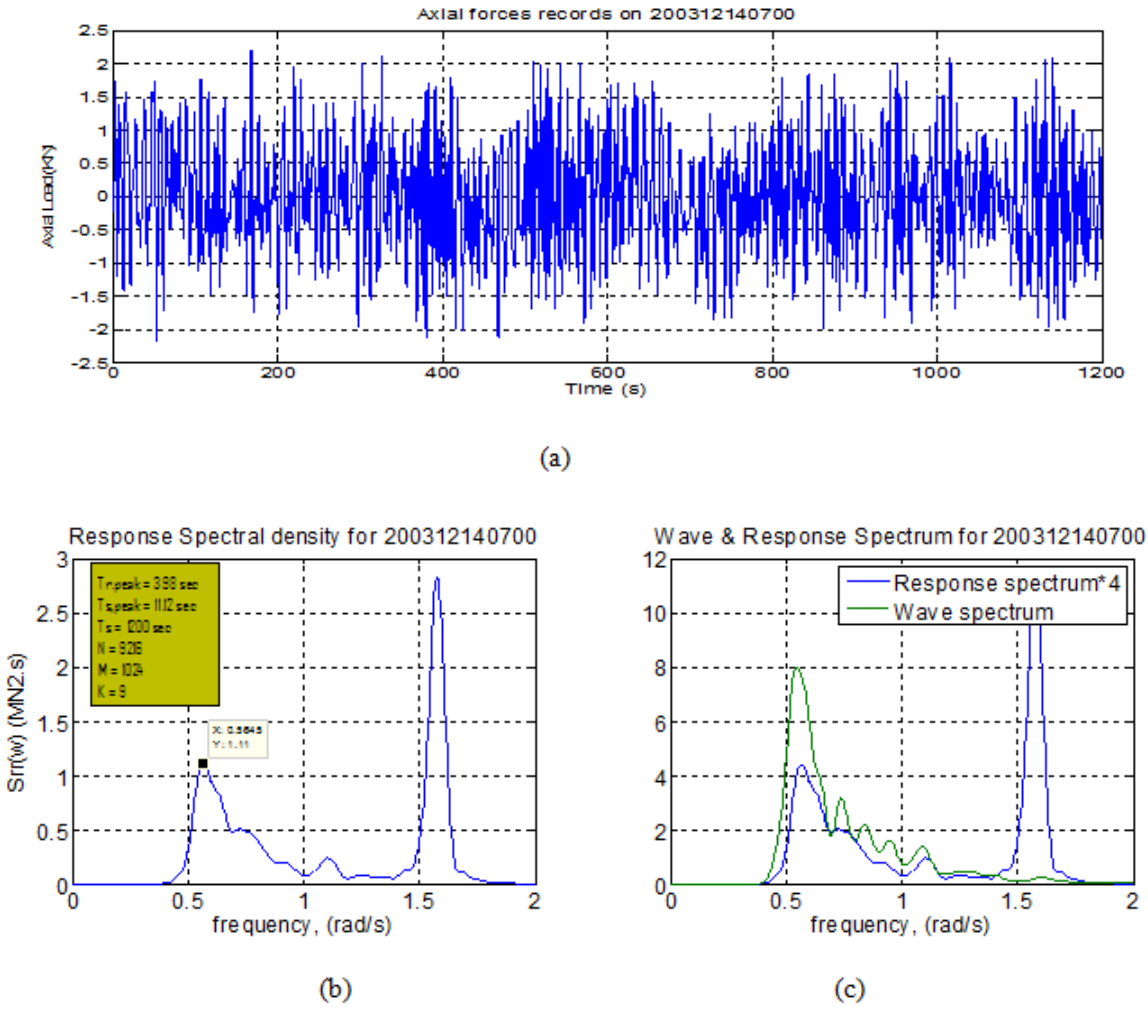

Figure 5.2: A1 time series response records (a), A1 response spectrum (b) and A1 response & Wave spectrum (c) during test.con1

From Figure 5-4 and 5-5 part "b" and "c", it can be seen that the response spectra reach their maximum value away from the wave spectral peak and this might be there were additional secondary forces such as wind, current or others during the recording time, that is on 15/12/03 from 08:20 and on 15/12/03 from 09:00. The response spectra reached their maximum value when the wave frequency reached around the natural frequency of the jacket platform.

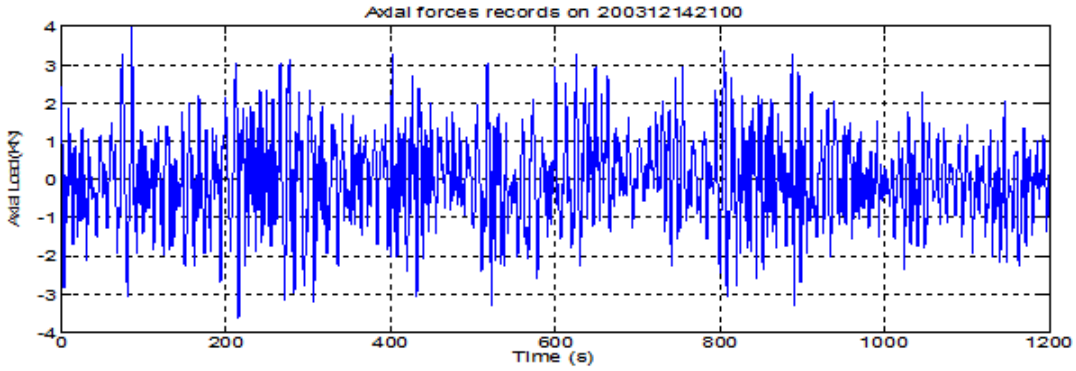

(a)

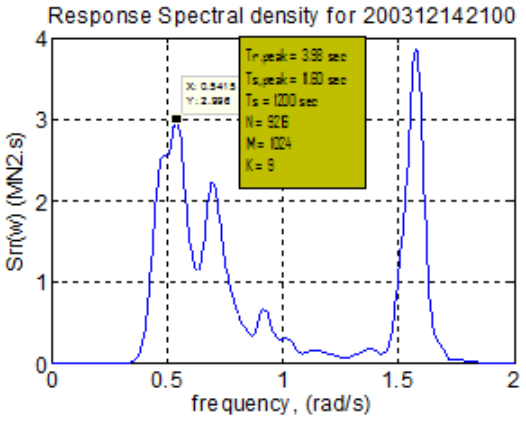

(b)

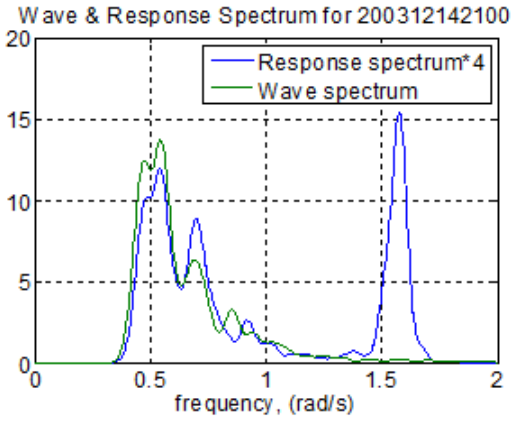

(c)

Figure 5.3: A1 time series response records (a), A1response spectrum (b) and A1 response & Wave spectrum (c) during test.con2

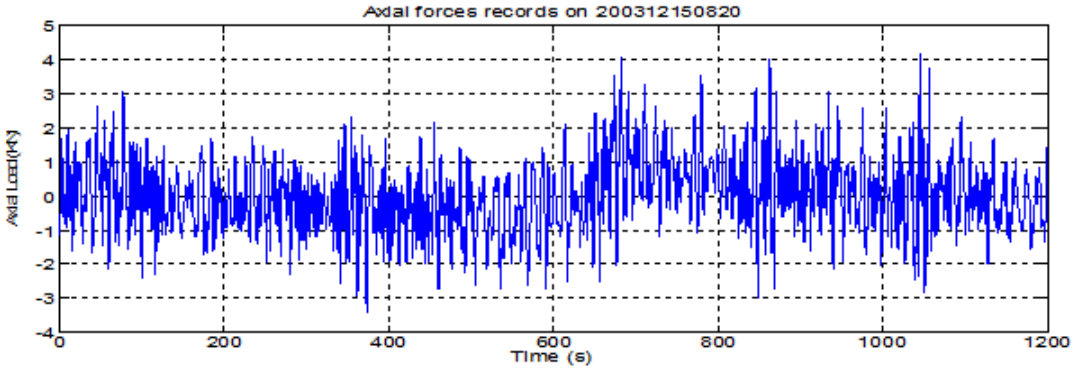

(a)

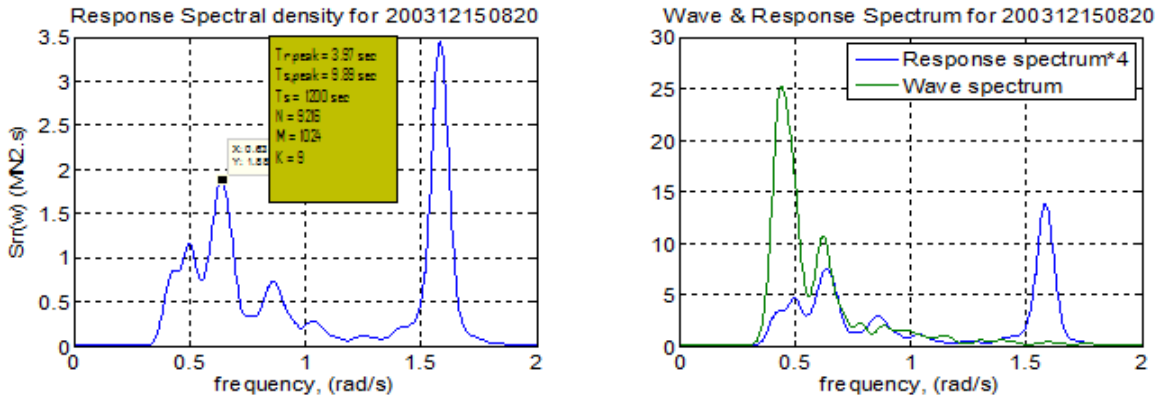

(b) (c)

Figure 5.4: A1 time series response records (a), A1 response spectrum (b) and A1 response & Wave spectrum (c) during test.con3

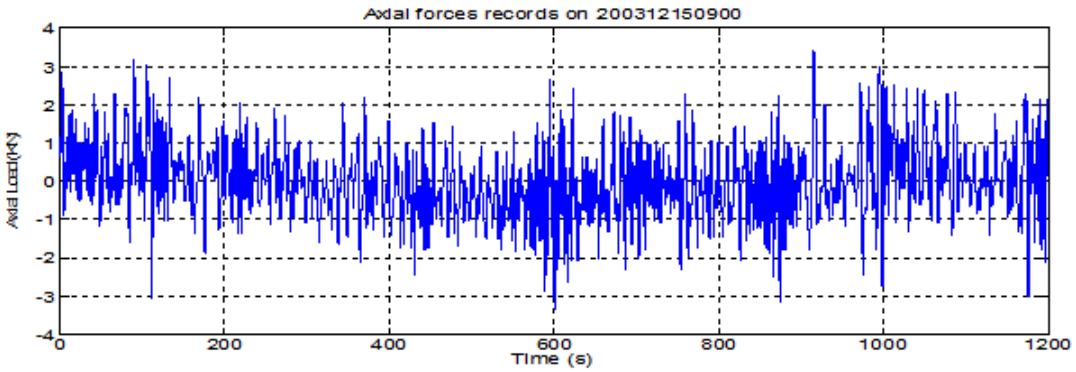

(a)

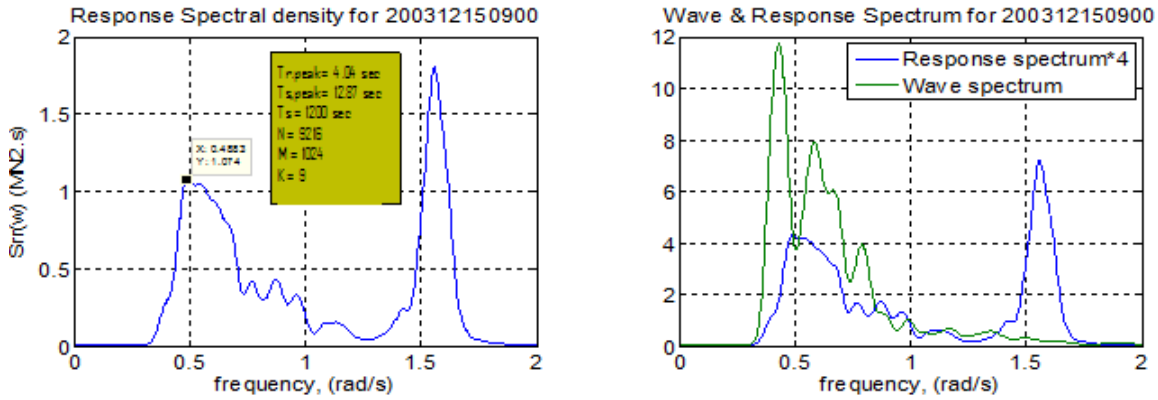

(b) (c)

Figure 5.5: A1 time series response records (a), A1 response spectrum (b) and A1 response & Wave spectrum (c) during test.con4

5.2.2 Estimated response spectrum from Leg A2

Figures 5-6 to 5-9 part "a" and "b" show 20 minute of time series response or axial load records on the Kvitebjørn platform leg A2 and estimated response spectrum on 14/12/03 from 07:00, during test.con1, on 14/12/03 from 21:00, during test.con2, on 15/12/03 from 08:20, during test.con3, and on 15/12/03 from 09:00, during test.con1, respectively. Where as Figures 5-6 to 5-9 part "c" are plotted to show the estimated response spectrum of the leg relative to their corresponding estimated wave spectrum described in section 4.3.2.

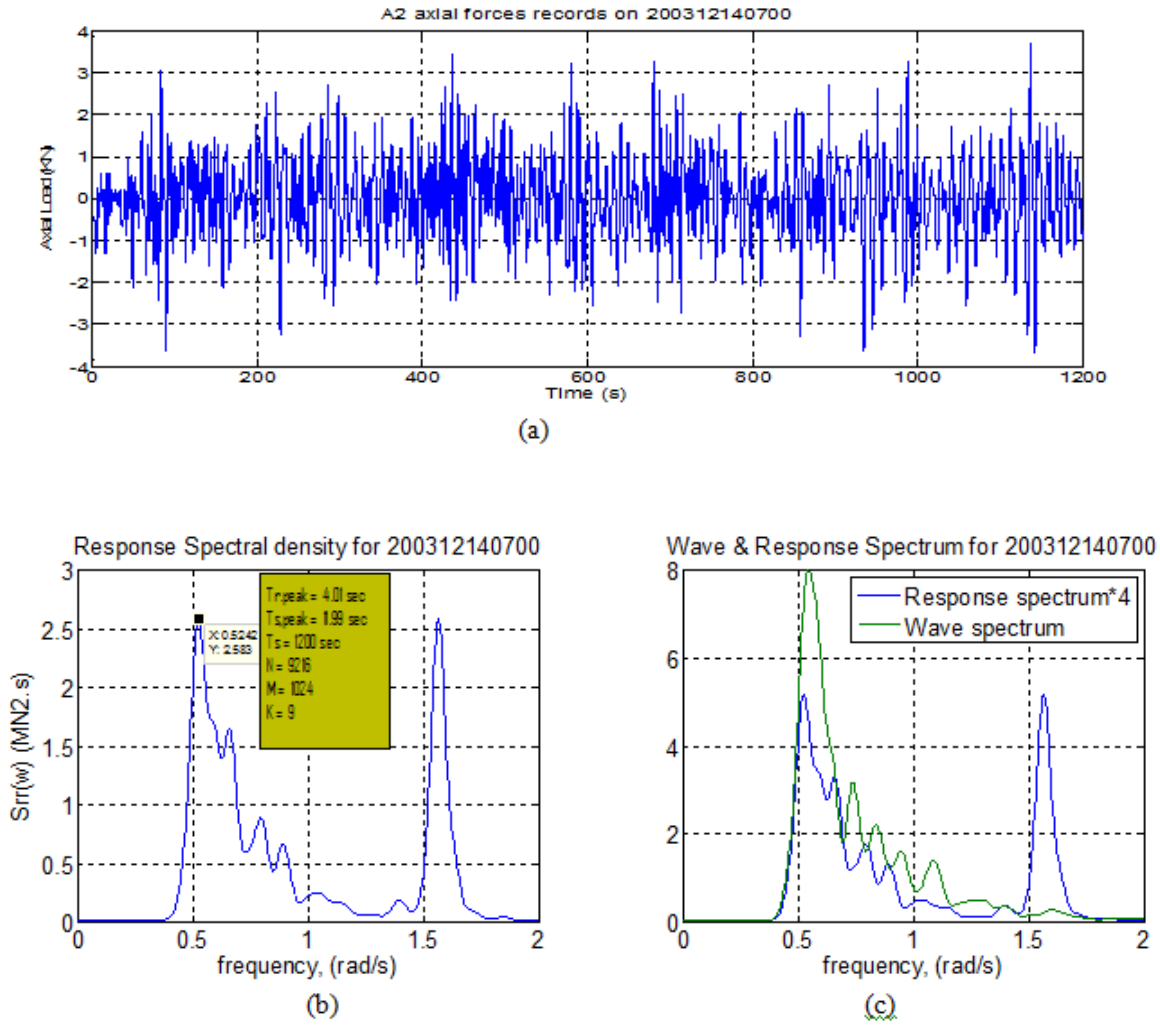

Figure 5.6: A2 time series response records (a), A2 response spectrum (b) and A2 response & Wave spectrum (c) during test.con1

From Figure 5-6 to 5-9 part "b" and "c" one can notice that the response spectra reach their maximum at their corresponding wave spectral peak period, where the wave energy is concentrated. At around the natural period of the jacket platform, the response spectrum reached at its peak, this is the energy lost to resist to the amplified dynamics of the jacket.

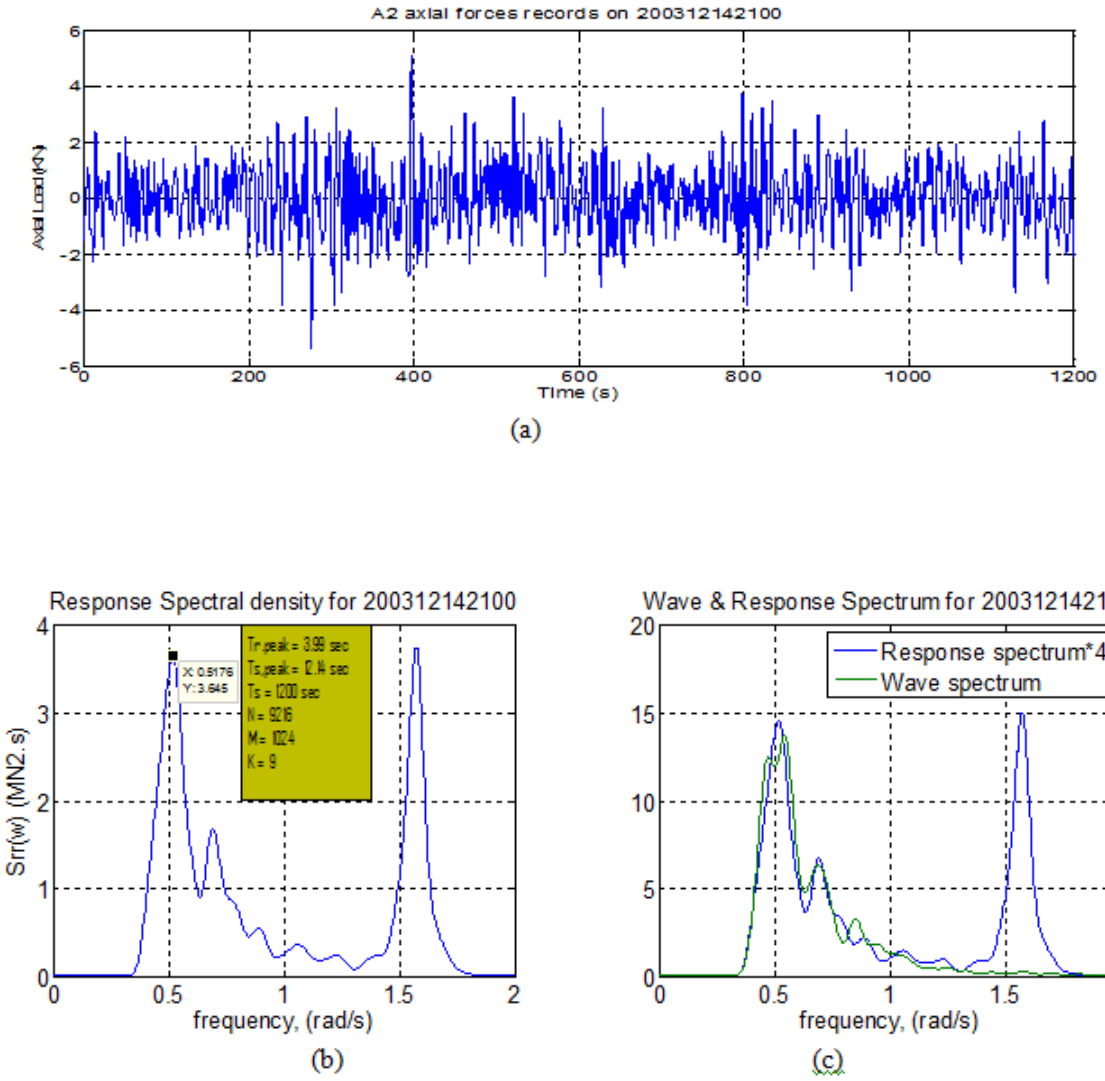

Figure 5.7: A2 time series response records (a), A2 response spectrum (b) and A2 response & Wave spectrum (c) during test.con2

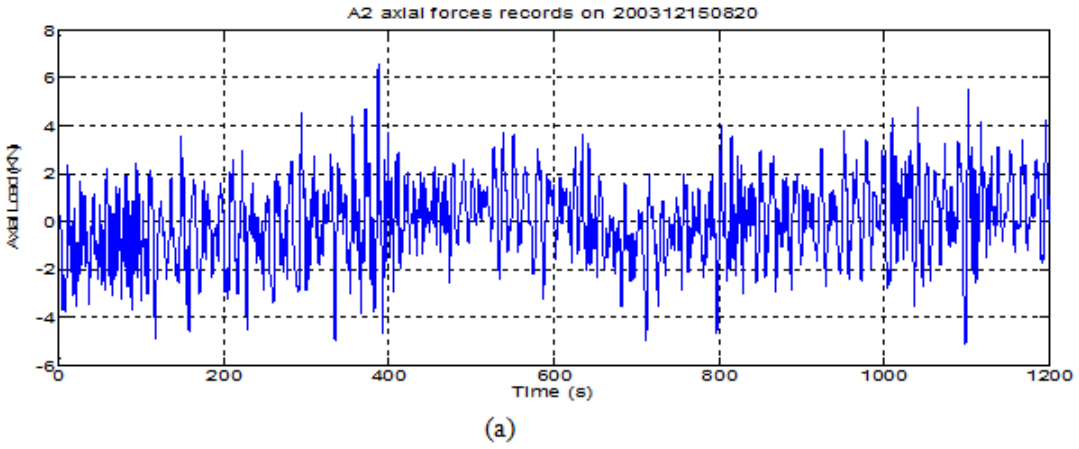

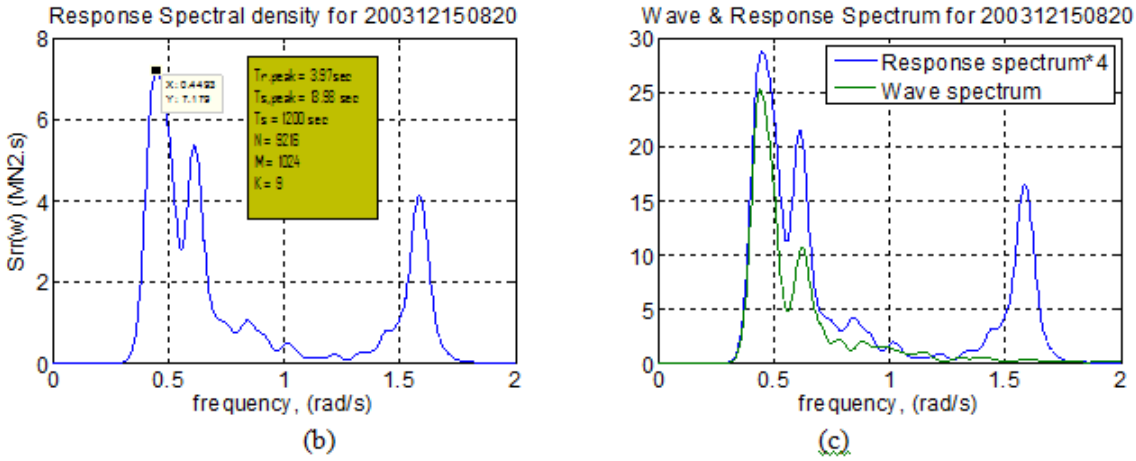

Figure 5.8: A2 time series response records (a), A2 response spectrum (b) and A2 response & Wave spectrum (c) during test.con3

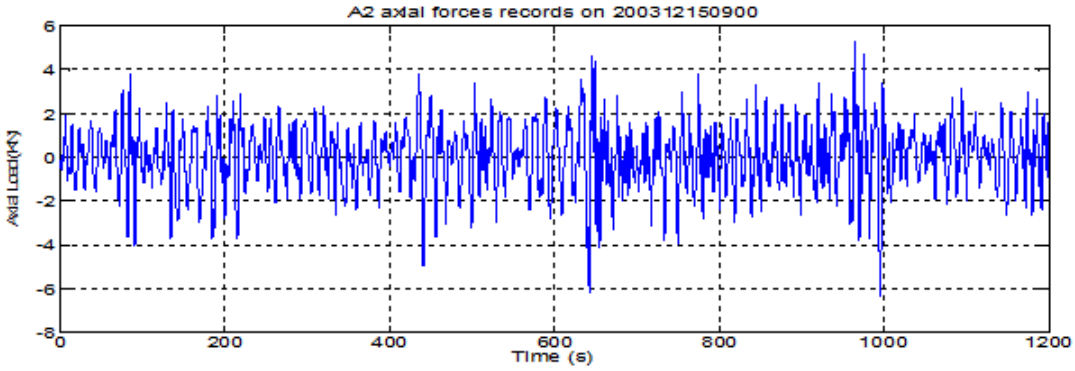

(a)

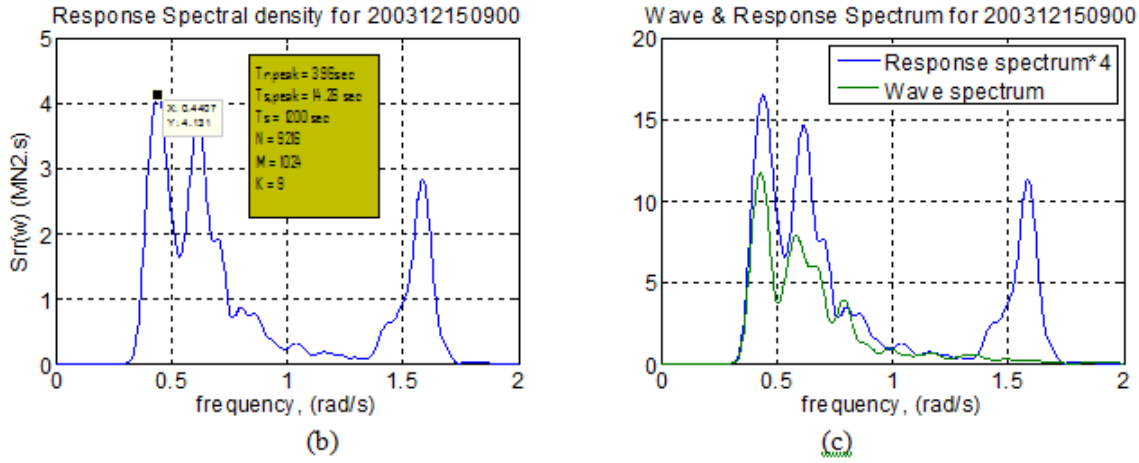

Figure 5.9: A2 time series response records (a), A2 response spectrum (b) and A2 response & Wave spectrum (c) during test.con 4

Table 5.1: T_p for all test conditions and their corresponding $T_{r,peak}$ and $T_{s,peak}$ for leg A1 and A2.

test.con	T_p	Leg A1		Leg A2	
		$T_{s.peak}$	$T_{r.peak}$	$T_{s.peak}$	$T_{r.peak}$
1	11.53	11.12	3.98	11.99	4.01
2	11.55	11.60	3.98	12.14	3.99
3	14.22	9.89	3.97	13.98	3.97
4	14.60	12.87	4.04	14.26	3.96
5	8.63	-	-	8.76	4.03
6	8.39	-	-	9.02	4.03
7	9.02	-	-	8.89	4.03
8	8.95	-	-	8.45	3.93
9	8.63	-	-	8.95	4.03
10	8.95	-	-	9.52	4.00
11	9.52	-	-	9.60	4.04
12	9.92	-	-	9.30	4.00
13	11.01	-	-	10.52	4.03
14	10.43	-	-	10.17	4.00
15	11.11	-	-	10.17	4.03
16	11.01	-	-	10.62	4.03
17	10.53	-	-	11.11	3.99
18	11.43	-	-	10.17	3.99
19	11.21	-	-	11.21	3.96
20	13.19	-	-	13.79	4.03
21	14.12	-	-	13.79	4.03

From Table 5.1 it can be noticed that;

- The wave spectral peak periods, T_p, are close to $T_{s,peak}$ for both legs, which show that the response energy was more at the wave spectral peak period where the wave energy is concentrated. The small difference may be due to the presence of secondary additional forces, i.e. in addition to wave load, such as wind loads, current load etc during the recording time.

- $T_{r,peak}$ are also close to the natural period of the jacket platform that show there was high energy lost to control amplified dynamics at resonance. As discussed in section 2.2.1, when relative frequency is close to unity, its dynamic amplification factor reaches at its peak as a result the response/particular solution in section 2.2.1 gets its maximum value.

Chapter 6

ESTIMATION OF TRANSFER FUNCTION

6.1 Introduction

Transfer function $H_{\Xi\Gamma}(\omega/\theta)$, can be defined as the response of a linear offshore structure to a sinusoidal wave with unit amplitude for sufficient number of frequencies, ω, and different wave heading directions, θ, where in this study only unidirectional is considered. As explained in chapter 2, by linear offshore structure means that the structure response amplitude $\Gamma(t)$, e.g., the axial forces on legA1 and leg A2, and the excitation amplitude,$\Xi(t)$, e.g., wave elevation given on test conditions, has linear relation. Transfer function gives amplitude scaling and phase shift of response relative to the excitation component. The absolute or scaling value of a transfer function, $H_{\Xi\Gamma}(\omega/\theta)$, is known as the response amplitude operator, $RAO(\omega)$. Transfer function can be written either as a function of angular frequency in radian per second or frequency in hertz. RAO of a structure can be estimated using the following two methods.

6.1.1 RAO Using Spectral Relation

From the time series wave records of each test condition listed in Table 4.1 and their corresponding axial responses on leg A1 and A2, the wave energy spectra and response energy spectra are estimated in chapter 4 and 5 respectively. Furthermore, RAO of the system can be evaluated using the spectral relation given in the form:

$$|H_{\Xi\Gamma}(\omega)| = [\frac{S_{\Gamma\Gamma}(\omega)}{S_{\Xi\Xi}(\omega)}]^{\frac{1}{2}} \tag{6.1}$$

In which, $S_{\Gamma\Gamma}(\omega)$ is the energy density spectrum of the measured response on leg A1 and A2 from chapter 5 and $S_{\Xi\Xi}(\omega)$ is the corresponding energy density spectrum of the incoming wave record from chapter 4. Estimation of RAO using this method, equation 6.1, produces uncorrelated signal noises especially at the beginning and at the tail end of the spectrum as shown in Figure 6-1. These unwanted frequency components that appear as noises can be minimized by applying a filtering routine to the original time series wave and/or response record. An example of a band pass filtered with a cut off lower frequency, $\omega_1 = 0.02$, and higher frequency, $\omega_2 = 0.4$ is shown in Figure 6-2. However, it should be noted that there may still leakage of neighboring frequencies in the filtering process.

In the spectral relation method, the phase relationship between the wave amplitude and response amplitude cannot be determined.

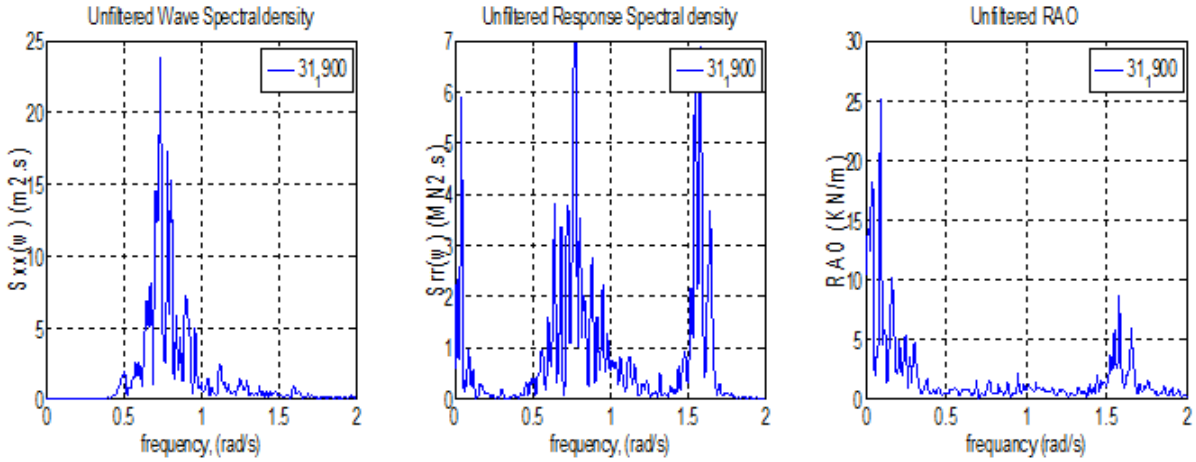

Figure 6.1: Unfiltered Wave spectral density, Response spectral density, and RAO

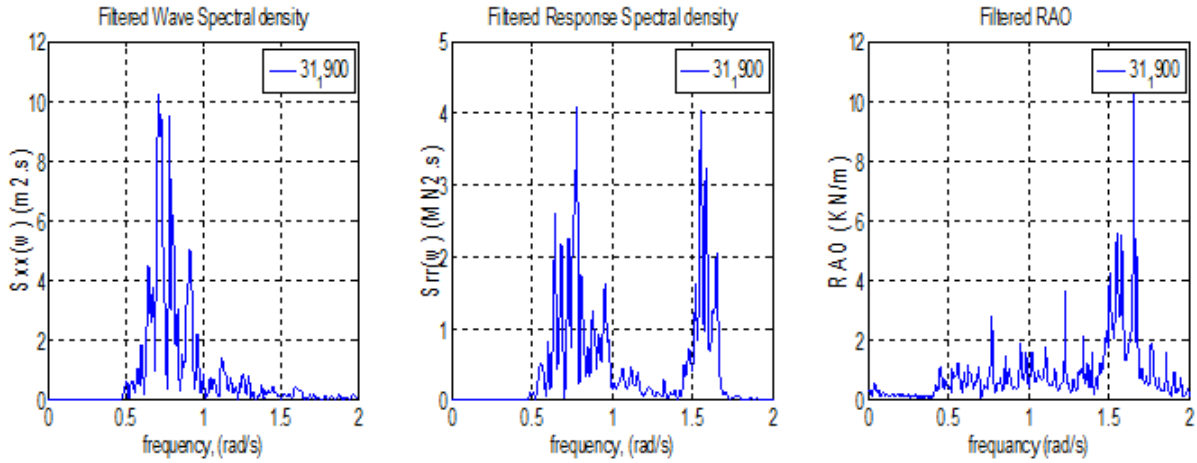

Figure 6.2: Filtered Wave spectral density, Response spectral density and RAO

6.1.2 RAO Using Cross Spectral Density

In order to avoid the uncorrelated signal noise at the tail beginning and end of a spectrum and to determine the information of the phase relationship between the response and forcing amplitudes a cross spectral density analysis method may be used. To apply this method, the cross spectral density function $S_{\Xi\Gamma}(\omega)$, between the wave and the response under consideration has to be determined. Thenafter, the transfer function can be determined by the relation given below [4]:

$$C(\omega) + iQ(\omega) = \frac{S_{\Xi\Gamma}(\omega)}{S_{\Gamma\Gamma}(\omega)} \tag{6.2}$$

where: C and Q are the coincident and quadrature spectra as a function of frequency, ω, and i is the imaginary quantity. The RAO is computed as the scaling amplitude of the

transfer function:

$$|H_{\Xi\Gamma}(\omega)| = [C^2(\omega) + Q^2(\omega)]^{\frac{1}{2}} \tag{6.3}$$

And the corresponding phase angle is determined from:

$$\epsilon(\omega) = tan^{-1}(\frac{Q(\omega)}{C(\omega)}) \tag{6.4}$$

6.2 Estimation of RAO Using the Spectral Relation

Using the spectral relation described in section 6.1.1, equation 6.1, RAOs during the 21 test condition listed in Table 4.1 for both legs are determined. In this case, the wave spectra $S_{\Xi\Xi}(\omega)$, and response spectra $S_{\Gamma\Gamma}(\omega)$, for both legs are estimated in Chapter 4 and 5 respectively. In section 6.2.1 and section 6.2.2, RAOs during the first four test condition (test.con 1-4) for leg A1 and leg A2 respectively are presented while the remaining are attached on Appendix C.1.

6.2.1 Estimated RAO from Leg A1

Figure 6-3 to 6-6 show that the wave spectral density, response spectral density and their respective RAO during the first four test conditions from leg A1.

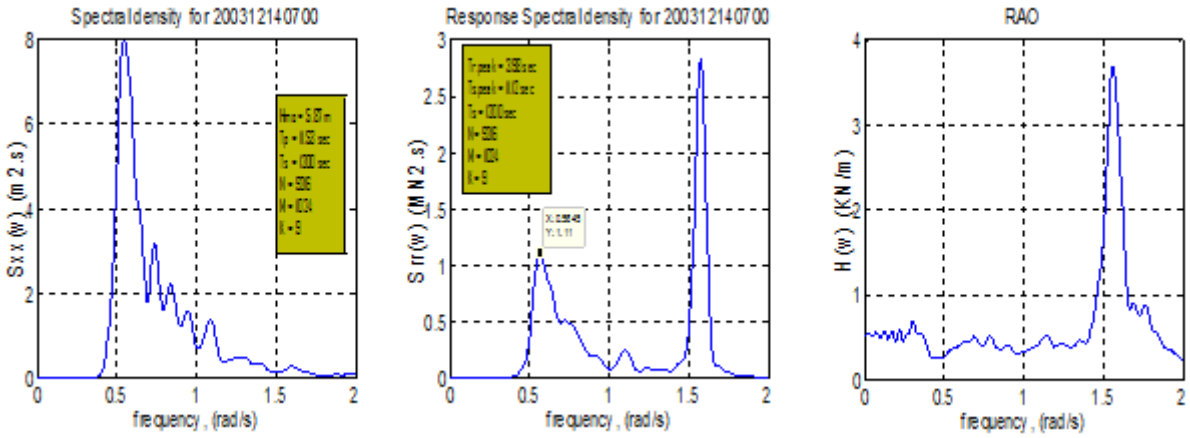

Figure 6.3: Wave spectrum, response spectrum and RAO from Leg A1 during test.con 1.

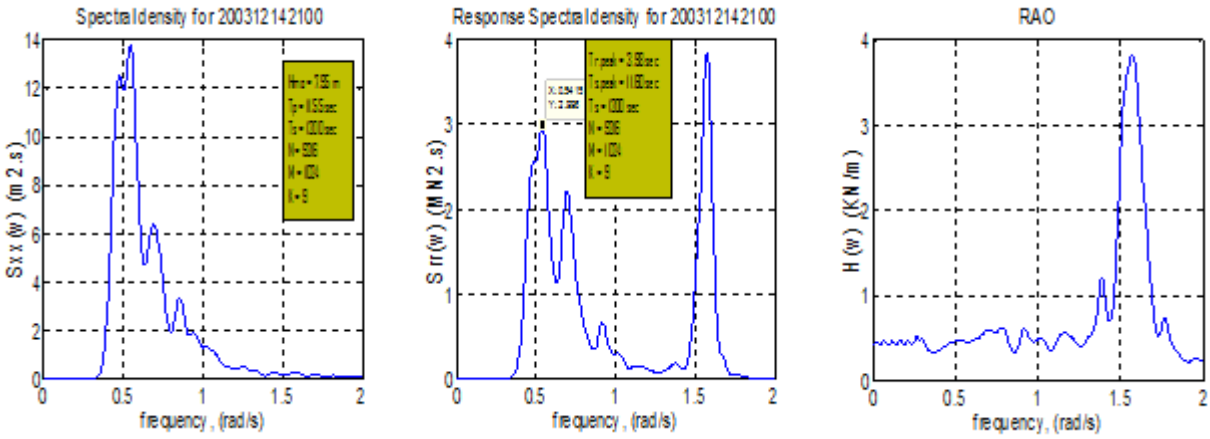

Figure 6.4: Wave spectrum, response spectrum and RAO from Leg A1 during test.con 2.

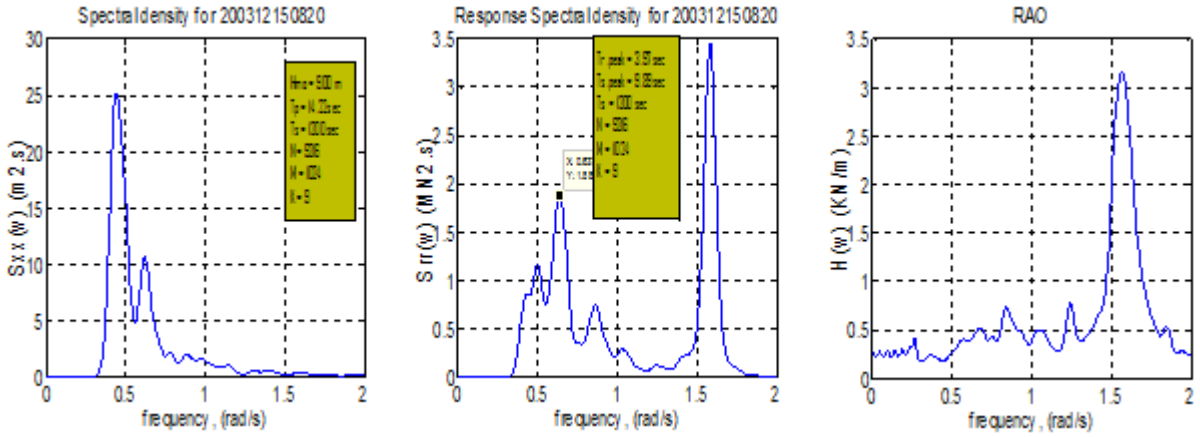

Figure 6.5: Wave spectrum, response spectrum and RAO from Leg A1 during test.con 3

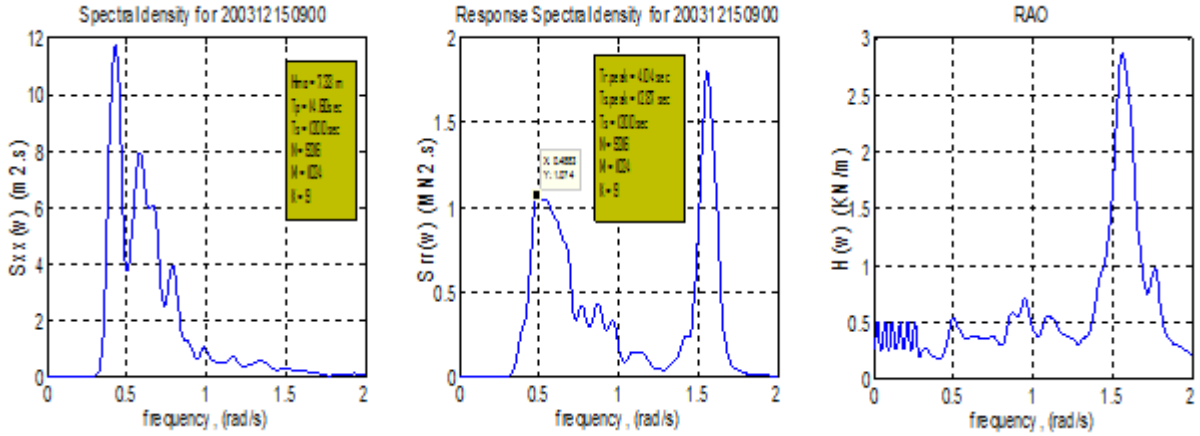

Figure 6.6: Wave spectrum, response spectrum and RAO from Leg A1 during test.con 4

6.2.2 Estimated RAO from Leg A2

Figure 6-3 to 6-6 below shows that the wave spectral density, response spectral density and their respective RAO for the first four test conditions and their corresponding response on leg A2 respectively.

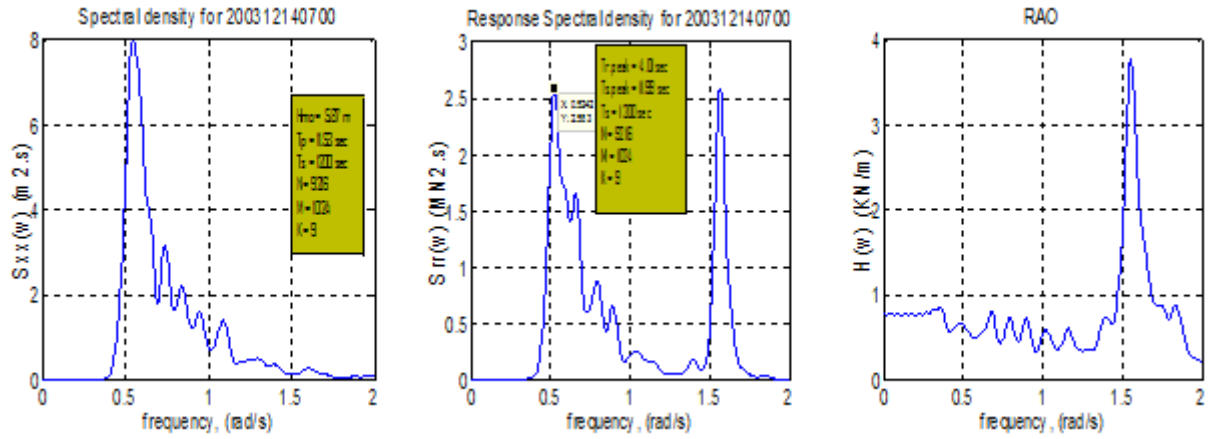

Figure 6.7: Wave spectrum, response spectrum and RAO from Leg A2 during test.con 1

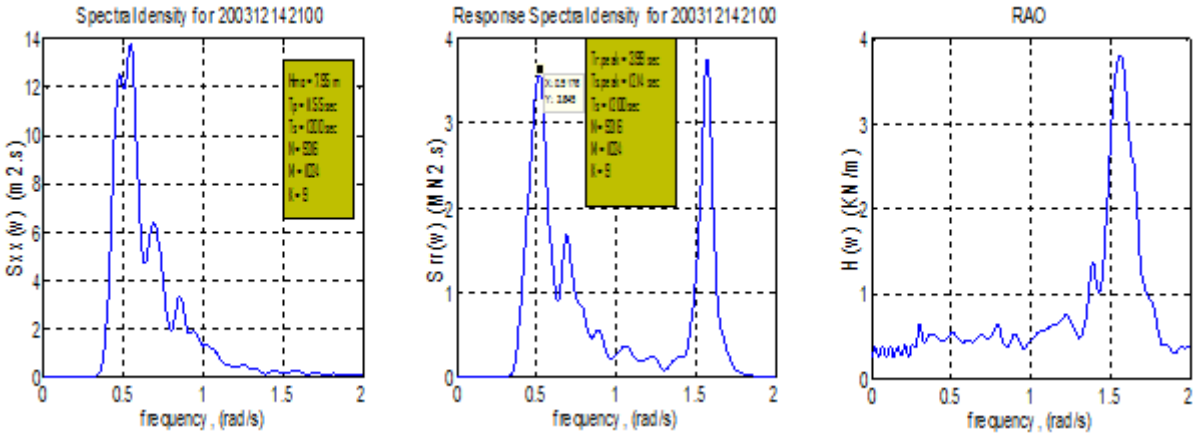

Figure 6.8: Wave spectrum, response spectrum and RAO from Leg A2 during test.con 2

From the estimated RAOs, Figures presented in section 6.2.1 and 6.2.2 and Appendix C.1, one can notice the following:

- The RAO value reaches at its maximum within the natural frequency of the system, but with different values.
- Leakage of Signal noise particularly at the beginning.
- Most of the RAOs die for higher frequencies, but some RAOs do not, see Appendix C.1.

These observations might be due to the following reasons:

- Due to the non-linear proporty of the structure

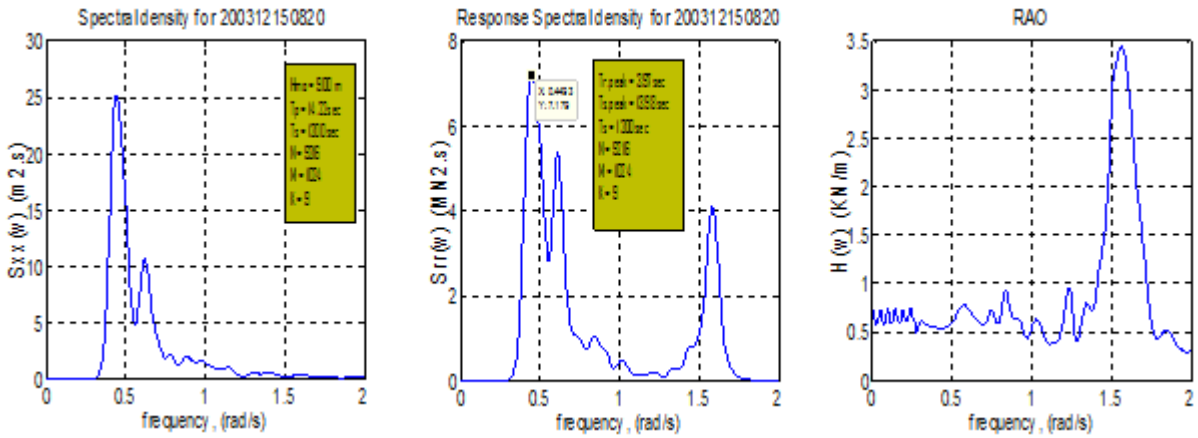

Figure 6.9: Wave spectrum, response spectrum and RAO from Leg A2 during test.con 3

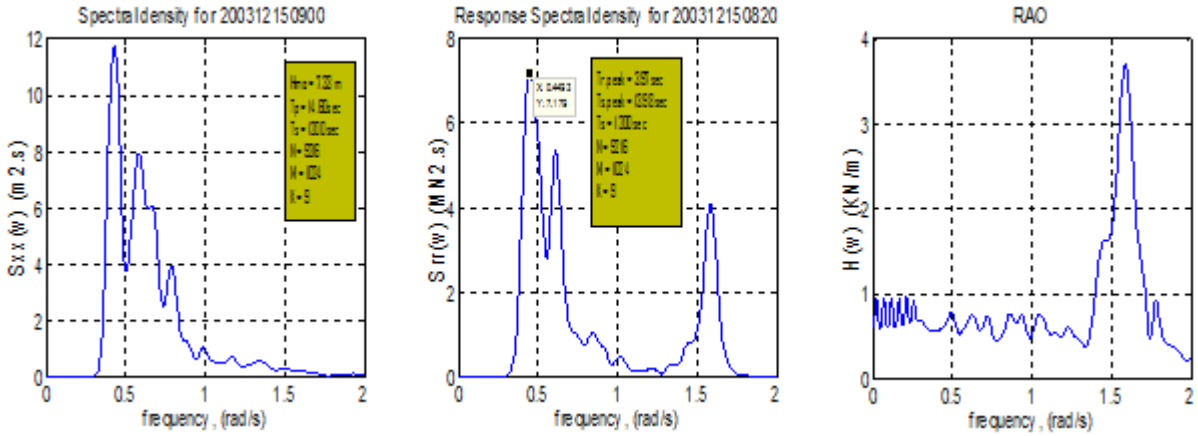

Figure 6.10: Wave spectrum, response spectrum and RAO from Leg A2 during test.con 4

- There might be additional secondary forces such as wind load, current load etc.., during recording of the time series data, which could reduce the correlation between the incident wave amplitude and their corresponding response on the structure.
- Due to leakage of neighboring frequencies in the filtering process.
- Due to the unidirectional assumption of the incoming waves.

Hence, in order to analyze the degree of linear correlation between an incident wave and its corresponding response on leg A1 and A2 and to determine where the RAOs can be relatively trusted, the coherence analysis has been done in section 6.3 below.

6.3 The Coherence Function

6.3.1 Introduction

A coherence function states the degree of linear correlation between an incident wave/input and its corresponding response of a structural member. In this case, the linear dependency between the 21 test condition and their corresponding response on leg A1 and A2

at 108 m bellow still water level are performed. By measuring the correlation between the incident waves and their corresponding output or responses, the frequency ranges where the RAOs can be relatively trusted can be determined. As shown in Figures 6-11 to 6-14 and in Appendix C.2, the relatively trusted frequencies are highlighted with dashed rectangle while noises caused by secondary driving forces, i.e. in additional environmental forces other than wave loads are neglected.

Value of a correlation function, $\eta_{\Xi\Gamma}$, ranges between zero and one. The correlation or degree of linear dependency between an incident wave and its corresponding response is good as the correlation value, $\eta_{\Xi\Gamma}$, approaches unity while it is a poor correlation as the value approaches to zero.

The coherence function between the incident wave, $\Xi(t)$, and response, $\Gamma(t)$, at a given frequency, ω_f, can be determined by using the following relations[11]:

$$\eta^2_{\Xi\Gamma}(\omega_k) = \frac{S_{\Xi\Gamma}(\omega_k) * S_{\Xi\Gamma}(\omega_k)}{S_{\Xi\Xi}(\omega_k) * S_{\Gamma\Gamma}(\omega_k)} \tag{6.5}$$

Since $S_{\Xi\Gamma}(\omega_k) = S^*_{\Xi\Gamma}(\omega_k)$, $S_{\Xi\Gamma}(\omega_k) * S_{\Xi\Gamma}(\omega_k) = S_{\Xi\Gamma}(\omega_k) * S^*_{\Xi\Gamma}(\omega_k) = |S_{\Xi\Gamma}(\omega_k)|^2$, then equation 6.5 can be rewritten as:

$$\eta_{\Xi\Gamma}(\omega_k) = \frac{|S_{\Xi\Gamma}(\omega_k)|}{\sqrt{S_{\Xi\Xi}(\omega_k) * S_{\Gamma\Gamma}(\omega_k)}} \tag{6.6}$$

where: $S_{\Xi\Gamma}(\omega_k)$ is the cross-spectrum between the incident wave and its corresponding response on both legs; $S_{\Xi\Xi}(\omega_k)$ is estimated wave spectrum and $S_{\Gamma\Gamma}(\omega_k)$ is estimated response spectrum.

6.3.2 The Coherence Analysis of the Estimated RAOs

By using equation 6.6, the correlation relation between the incident wave amplitudes and their corresponding response amplitudes are analyzed. These analyses include for the 21 test conditions listed in Table 4.1 to their corresponding responses on leg A1 and A2 at 108m below still water level. In this section, only during the first four test conditions, test.con1-4, for both legs are presented as shown in Figures 6-11 to 6-14 and the others are presented in Appendix C.2. In this case, correlation value greater or equal to 0.62 is assumed to be trusted and as shown in Figures below the trusted frequency ranges are highlighted with dashed rectangular box.

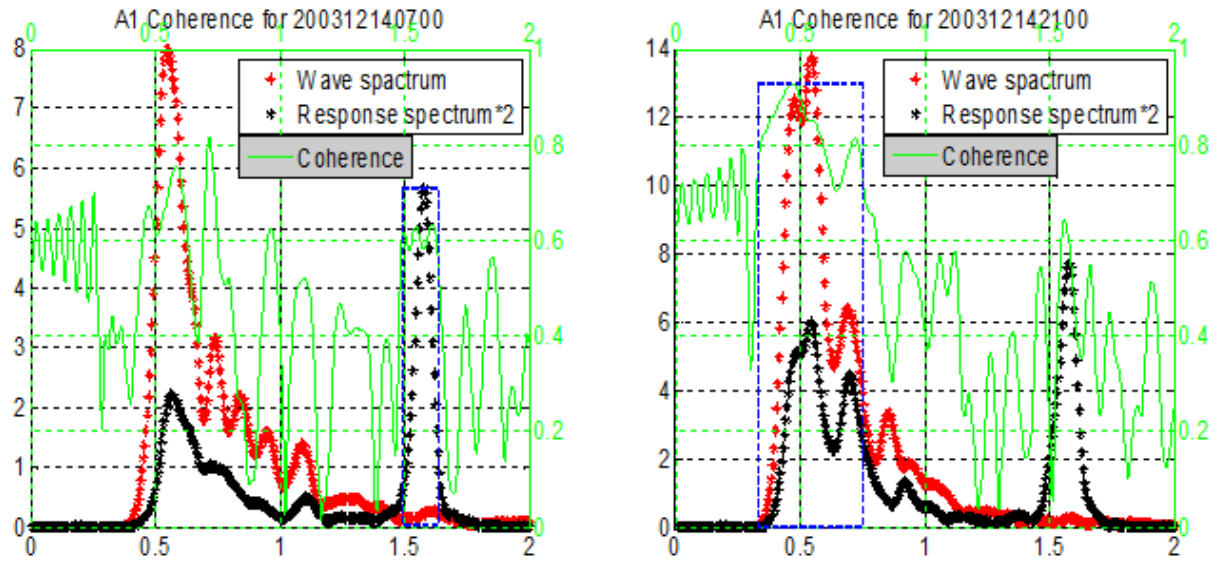

Figure 6.11: Coherence analysis during test.con1 & 2 on leg A1.

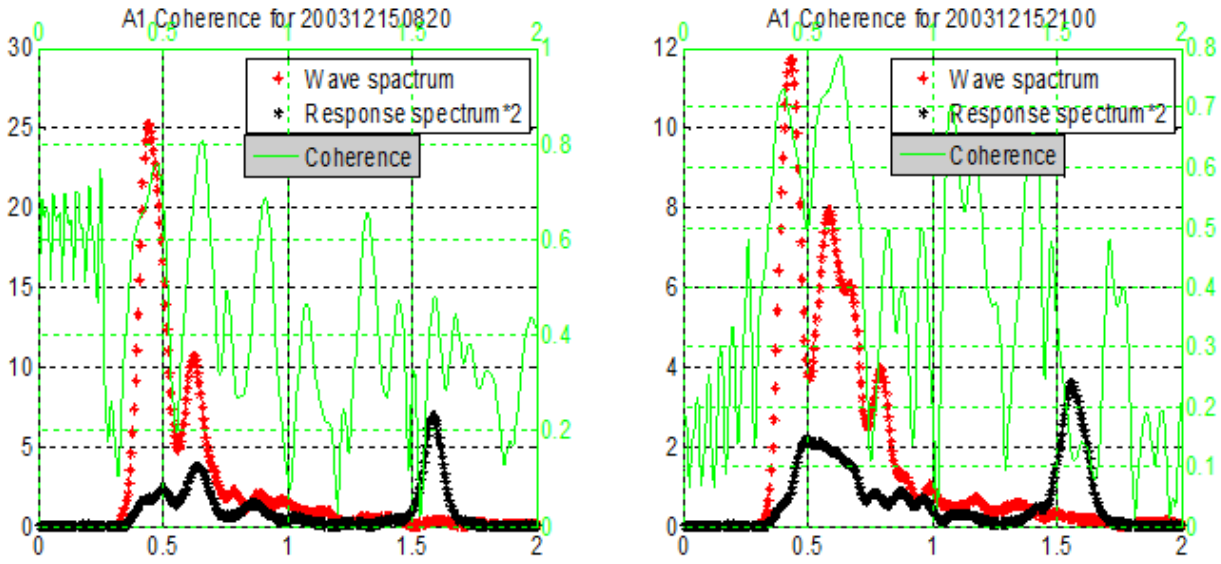

Figure 6.12: Coherence analysis during test.con 3 & 4 on leg A1.

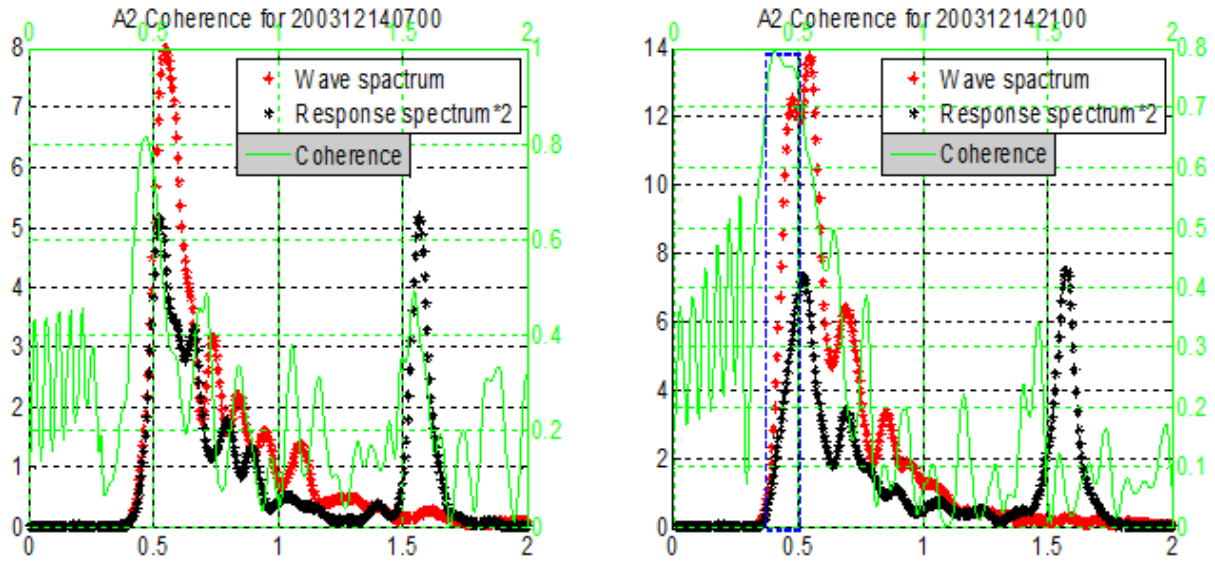

Figure 6.13: Coherence analysis during test.con 1 & 2 on leg A2.

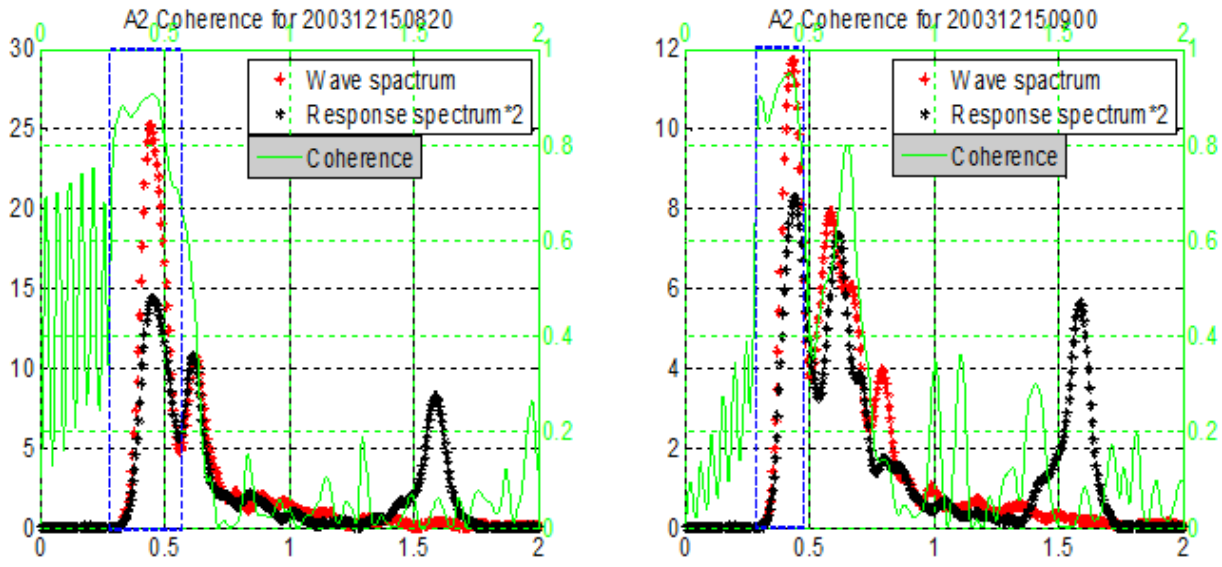

Figure 6.14: Coherence analysis during test.con 3 & 4 on leg A2.

6.4 Relatively Trusted Part of RAOs From the Trusted Frequency Ranges

After the coherence analysis is performed and the relatively trusted frequency ranges are determined, highlighted with dashed rectangular box, in section 6.3, the RAOs corresponding to these relatively trusted frequency ranges for each case are also determined. Figure 6-15 shows RAOs corresponding to the frequency ranges highlighted with dashed rectangular box, i.e. relatively trusted frequency ranges, in Figure 6-11 to 6-14 and Figures in appendix C.2. Note that by trusted frequency ranges means frequency ranges where the incident wave and the axial response are assumed to have good linear correlation or in the frequency ranges where the coherence, $\eta_{(\Xi\Gamma)}$, approaches to unity.

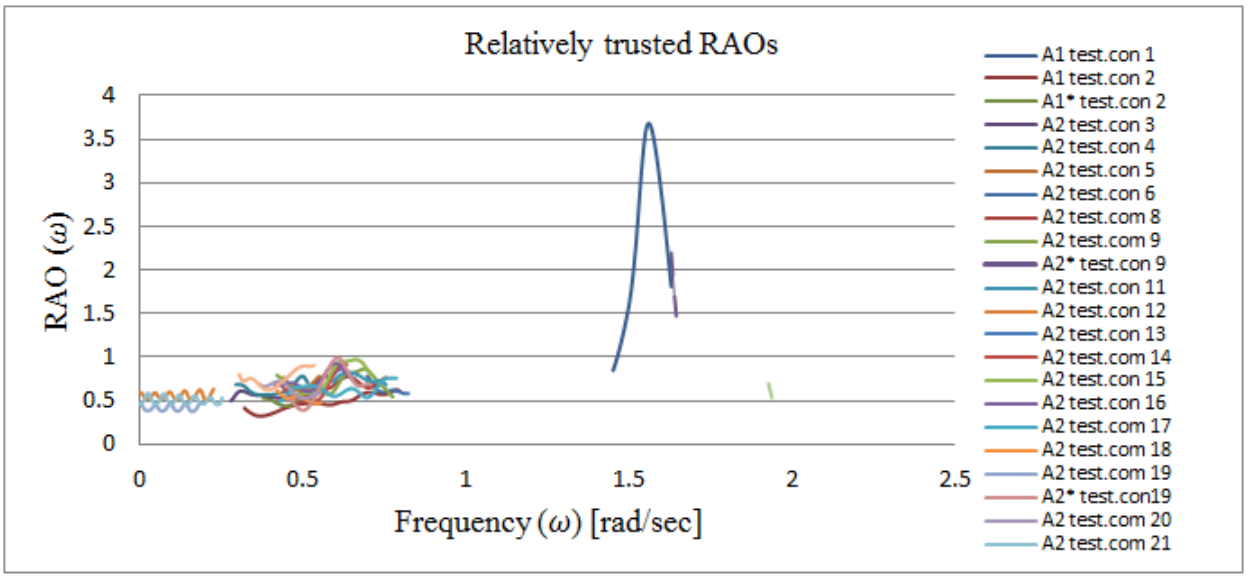

Figure 6.15: Relatively trusted RAOs during all test conditions

From the relatively trusted RAOs in Figure 6-15, one can see that the trusted RAOs are approximately 0.5 in the frequency range of [0-0.3], and they diverge in the frequency range of [0.3 – 0.85], which is around the wave spectral peak periods or in the regime where the wave energy is concentrated. Around the natural frequency of the jacket, i.e. around 1.57 radian per second, the correlation between the incident waves and the axial responses on both legs were found relatively poor during all test conditions. This might be due to the presence of secondary environmental loads in addition to the wave load during the data recording time. In addition, in the frequency range of around [0.7-1.5] the correlation is very low, which leads for further uncertainties in this area.

6.4.1 Mean of Trusted RAOs and Best Fit RAO

From the relatively trusted RAOs that have been evaluated in section 6.4, a mean value of the RAOs is determined as shown in Figure 6-16. The mean value is further approximated to a combination of linear, quadratic and exponential best fit equation given in equation 6.7, Best fit RAO. However, as it has been mentioned above, there is poor correlation between the incoming waves and thier corresponding responses, divergence of the relatively trusted RAOs in some frequency ranges and generation of unwanted noises particularly

at the beginning. This means that there is some uncertainty on the Best fit RAO and to cover this uncertainty, the Best fit RAO is decided to deviate at various frequency ranges as in section 6.4.2.

$$RAO(\omega) = \begin{cases} 0.50, & \text{for } 0 \leq \omega \leq 0.39 \\ -5.34\omega^2 + 6.65\omega - 1.28, & \text{for } 0.39 \leq \omega \leq 0.85 \\ 0.50, & \text{for } 0.85 \leq \omega \leq 1.39 \\ 123.39\omega^2 - 345.50\omega + 242.35, & \text{for } 1.39 \leq \omega \leq 1.56 \\ 9181.18 * exp(-5.04\omega) & \text{for } \omega > 1.56 \end{cases} \tag{6.7}$$

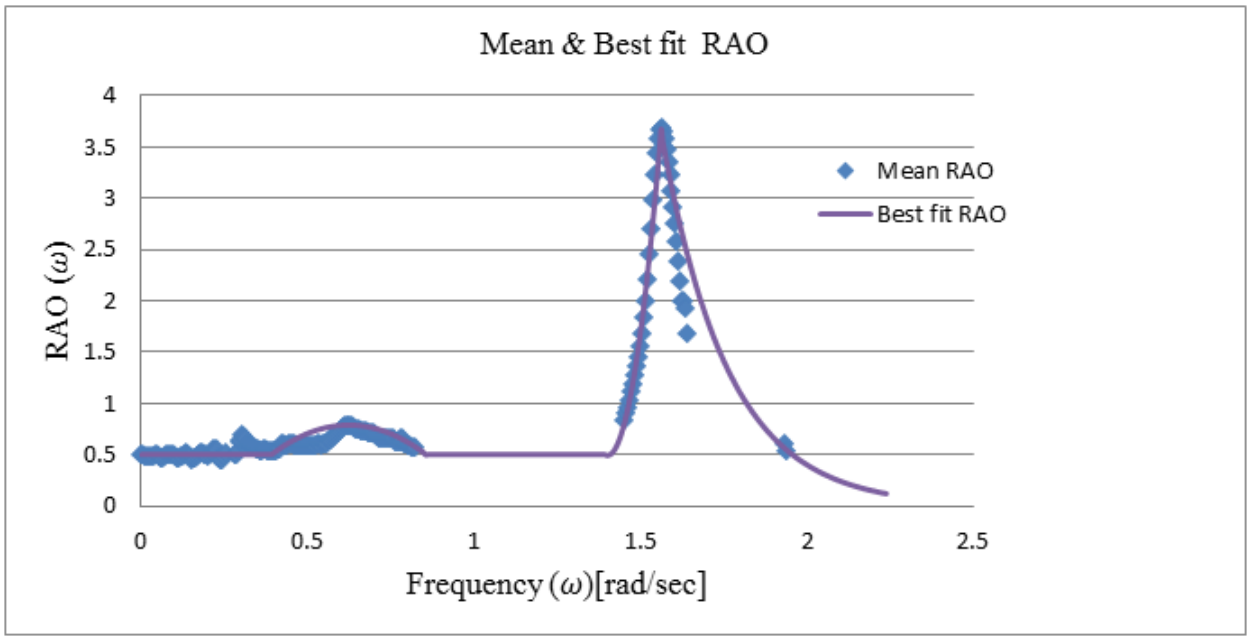

Figure 6.16: Mean of the trusted RAOs and best fit RAO

6.4.2 Possible Deviations of the Best Fit RAO at different Frequency Ranges

Due to number of reasons mentioned in section 6.4.1, the Best fit RAO has a possibility to deviate at different frequency ranges. In order to include these possibilities and to investigate their effect in fatigue damage accumulation on a structural detail, the following possible deviations in different frequency ranges are considered.

At the Beginning of the Best fit RAO [0 - 0.39]

Even though there may be high correlation at the lower frequencies between the incident waves and their corresponding axial forces on both legs, but as mentioned in section 6.1.1 there is a probability of generating uncorrelated signal noise at this frequency range. To

cover this uncertainty, the Best fit RAO is assumed to start from zero as given in Appendix C.3, Figure C-61 and equation 4.

In the major wave frequency regime [0.39-0.85]

In Figure 6-15 it has been observed that the relatively trusted RAOs diverge in the frequency range of [0.39-0.85] and to include this divergence, the Best fit RAO is shifted in the specified frequency range:

- ***a.*** 50% deviation above the best fit RAO in the frequency range [0.39-0.85]: see Figure 62 and equation 5 in Appendix C.2.
- ***b.*** 50% below the estimated RAO in the frequency range [0.39-0.85]: see Figure 63 and equation 6 in Appendix C.2.

Between the Major Wave Frequency Regime and Natural Frequency of the Structure [0.85-1.39]

During the coherence analysis in section 6.3, it has been found that the correlation between the incident waves and their corresponding response on the jacket was very low in the frequency range [0.85-1.39]. Therefore, due to this uncertainty some deviation is considered as shown in Appendix C.2, Figure 64 and equation 7.

Around the natural frequency of the jacket [1.56]]

To cover the various levels of resonance induced dynamics, the Best fit RAO is also shifted by 50% above and below its resonance peak. The equations of these RAOs are given in:

- ***a.*** For 50% deviation above the Best fit RAO around the natural frequency [1.56]: See Figure 65 and equation 8.
- ***b.*** For 50% deviation below the Best fit RAO around the natural frequency [1.56]: see Figure 66 and equation 9.

Chapter 7

INTRODUCTION ON FATIGUE

7.1 What Is Fatigue?

Fatigue is the main source of structural degradation. When a structure is subjected to a fluctuating stress or strain, time varying load, the structure can be subjected to fatigue failure mainly steel structures. For offshore structures the main source of fatigue inducing stress ranges are ocean waves and to ensure that the structures have an adequate fatigue life, a fatigue assessment should be carried out for each and individual members of the structure. Generally, any element or member of a structure, every welded joint and attachments or other sources of stress concentration, under a time varying load are potentially source of fatigue failure and should be individually assessed for their fatigue capacities. Fatigue capacity of a structural detail can be assessed using two common methods; namely crack growth propagation and S-N curve approach.

7.2 Fatigue Assessment by Crack Propagation

In this method, the fatigue life of a given structural detail can be subdivided in a crack initiation period or stage 1 and crack propagation period or stage 2, N_p, as in Figure 7-1. The crack initiation period normally contributes a small part of the total life of the structural detail under consideration and it is often ignored. During the crack propagation period in stage 2, the crack growth can be determined using the Paris' equation (7.1). This equation gives good description behavior for the mid-range of the growth rate. Based on this equation, the fatigue crack propagation rate, $\frac{da}{dN}$, is determined as:

$$\frac{da}{dN} = \begin{cases} 0.00, & \text{for } 0 \leq \Delta K < \Delta K_{th} \\ C_0 * \Delta K^m, & \text{for } \Delta K_{th} \leq \Delta K \leq \Delta K_c \\ \infty, & \text{for } \Delta K > \Delta K_c \end{cases} \tag{7.1}$$

where: a is crack size [m]; N is number of stress cycles [cycle]; ΔK is stress intensity factor range [MPa$\sqrt{m}$]; ΔK_{th} is threshold of the stress intensity factor range below which crack propagation is ignored; K_c is critical value where fast fracture triggers and C_o & m are constants, which depend on a particular material and particular testing conditions.

As shown in Figure 7.1, fatigue process goes through three general stages, from the initial state of the material to the final fracture, each stage characterized by the nature of the

fatigue process, for more detail see [1].

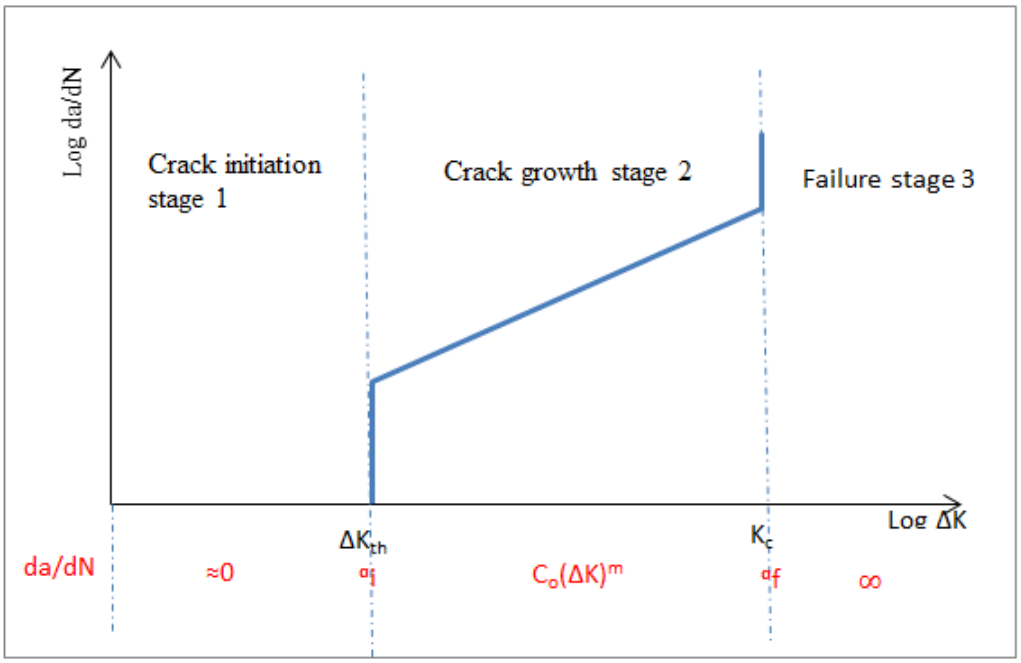

Figure 7.1: Crack growth rate curve and stages of crack growth

The crack propagation period, N_p, of a structural detail under consideration is determined by integrating the curve under stage 2 in Figure 7.1 starting from initial crack length (depth), a_i, to a final (critical) crack length (depth), a_f, as given below:

$$N_p = \int_{a_i}^{a_f} \frac{da}{C_0 * \Delta K^m} \tag{7.2}$$

By substituting the relevant parameters of crack growth rate and stress intensity in equation 7.2, one is able to obtain an estimate of crack propagation period.

7.3 Fatigue Analysis Based on S-N Curve

7.3.1 Basic S-N Curve Design

In this method, the fatigue design is based on use of S-N curves which is derived by fatigue testing of small specimens in test laboratories [5] . Typical S-N curve has two-segment with different slopes m_1 and m_2 as shown in Figure 7.2. When the predicted number of cycles to failure, N, is less than N_Q, equation of the S-N curve of the upper segment is given as:

$$N = a_1 * \Delta\sigma^{-m_1} \tag{7.3}$$

where: N is the number of cycles to failure; $\Delta\sigma = \sigma_{max} - \sigma_{min}$: is stress range; m_1 is the negative inverse slope of the upper S-N curve and a_1 is constant which depends on a particular material and particular testing conditions.

When the predicted number of cycles, N, to failure for a stress range, $\Delta\sigma$, is greater than N_Q, then the equation for the lower segment of S-N curve is given as:

$$N = a_2 * \Delta\sigma^{-m_2} \tag{7.4}$$

Where: m_2 is the negative inverse slope of the lower S-N curve and a_2 is constant which depends on a particular material and particular testing conditions.

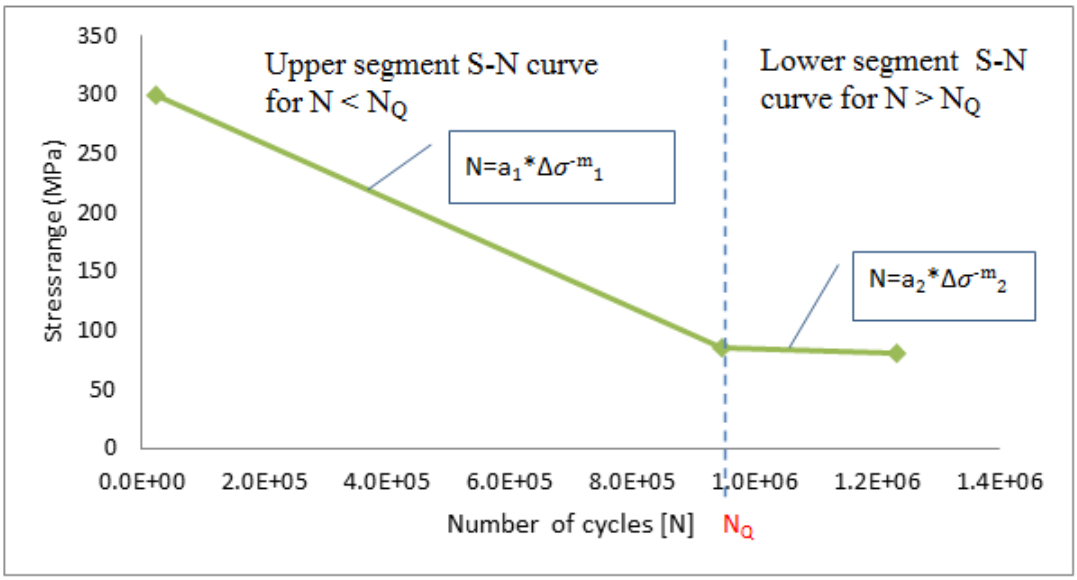

Figure 7.2: Basic upper and lower segments S-N curve

NB: N_Q is number of stress cycle where the two segments meet. It depends on the on a particular material and particular testing conditions.

7.3.2 Adjustment of the S-N Curve

Adjusting S-N curves for Environment

As mentioned above, the basic S-N curve is derived by fatigue testing of small specimens in test laboratories which means that the S-N constant parameters or coefficients, a_1 and a_2, are determined under the laboratory test conditions that may represent a specified environmental and surface protections. However, these coefficients may vary with the environmental conditions and surface protection type. Thus, to account these variations, the classification of a detail needs appropriately matching it to the applicable environmental condition. Based on the environmental conditions and corrosion protection of a tubular or non-tubular detail, as shown in Figure 7.5, S-N curves are be categorized as follows:

a. S-N curves in air conditions

b. S-N curves in seawater with cathodic protection

c. S-N curve in seawater for free corrosion/without corrosion protection.

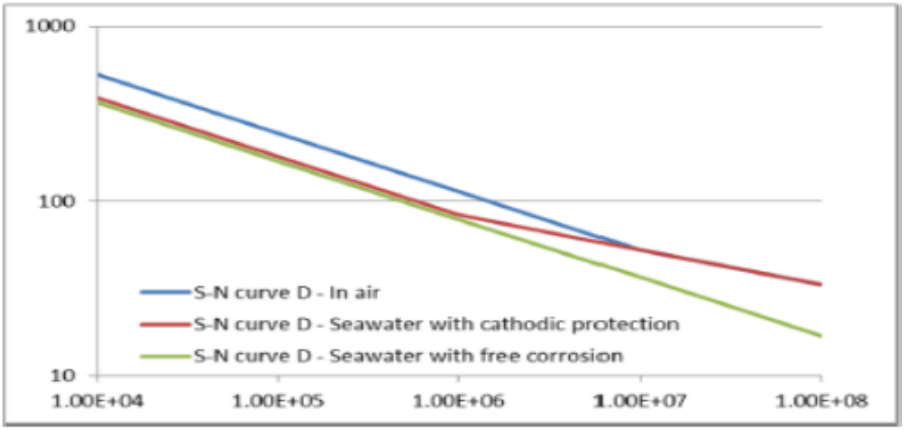

Figure 7.3: Basic S-N curve for a detail based on the environmental and surface protection. [5]

Adjusting S-N curves for the Effect of plate Thickness

The S-N curve equations given above are applicable only for thicknesses that are less than the reference thickness, t_ref, which varies with standards – for example in DNV-RP-C203 [5] the reference thickness starts form 25 mm while 22 mm in Plaza [13]. However, to account the effect of the local geometry of weld toe in relation to the thickness of the adjoining plates and the stress gradient over the thickness, the basic S-N curves in section 7.3.1 should be modified for thickness greater than the reference thickness, t_{ref}, as:[5]

$$logN = loga - m * log(\Delta\sigma(\frac{t}{t_{ref}})^k \tag{7.5}$$

where: m is negative inverse slope of the S-N curve; $loga$ = intercept of log N axis; t_{ref} is reference thickness; t is thickness through which crack most likely to grow and k is thickness exponent depend on fatigue detail type and stress concentration factors (SCF).

7.3.3 Types of S-N Stress Curves

1. Nominal stress S-N curve

Nominal fatigue S-N curves are derived for classified structural details. The fatigue test data for these structural details are determined mainly from samples subjected to axial and bending loads with consideration to the effects of stress concentration due to sudden geometrical changes and weld profiles on the samples. The design stress for this type S-N curve can be regarded as nominal stress which can be calculated based upon:

1. The cross sectional area of the structural detail under consideration including effect of local stress raising due to concentrated loads and macro geometric features such as access holes or in way of cut-outs as shown in Figure 7.4 b. That means an additional stress concentration factor (SCF) should be introduced in order to include the local stress, σ_{local}, as given in shown in Figure 7.4.

$$\sigma_{local} = SCF * \sigma_{nominal} \tag{7.6}$$

2. Ignoring the effect of stress raise due to weld joints as shown in Figure 7-4 a, because their effect are already included in the nominal S-N curve.

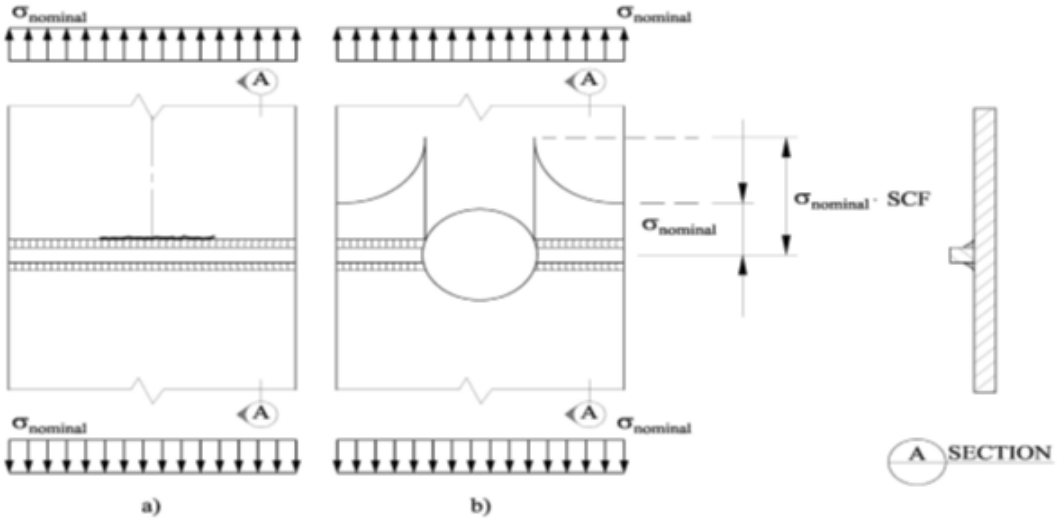

Figure 7.4: Effects of micro geometric features and welds on nominal stress.[5]

3. By applying of an additional stress modification factor, $K_{m.eff}$, if the angular misalignment or eccentricity of the structural detail is greater than that it has been already covered by the S-N curve for the structural detail under consideration. Figure 7.5 presents the variation of nominal stress on structural joints due to excessive misalignment or eccentricity.

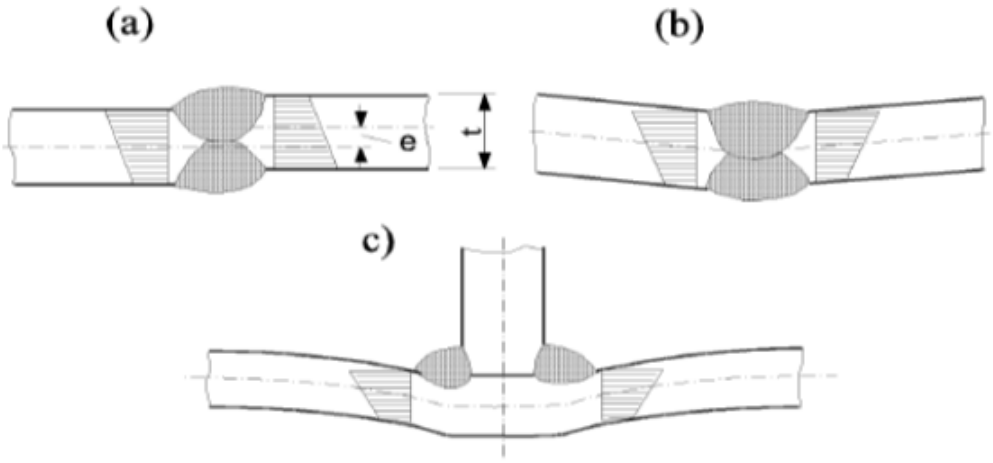

Figure 7.5: Effects of eccentricity or angular misalignment on nominal stresses.[5]

2. Hot spot stress S-N curve

The hot spot stress S-N curves is categorized for non-tubular, i.e. plated structures and tubular joints which include brace to chord connections. According A.Hobbacher [2], hot spot stress is applied in a situation where there is no clearly defined nominal stress due to complicated geometrical effects, or where the structural discontinuity is not comparable

to a classified structural detail in section 7.3.4. Even though this method can be used for analysis of sites where there is a potential for fatigue crack initiation such as weld root, mostly it is used for assessment of a weld toe - for example at the toe weld of a structural attachment and on both chord and brace sides of a tubular welds, see section 7.4. It should be noted that the stress change due to concentrated loads or shape is not included in the hot spot stress, as it is in the nominal stress.

Hot spot stresses are usually obtained by analyzing the structural detail in structural computer software that employs finite element analysis. It can be determined as well from nominal stress by applying stress concentration factor (SCF) to include the stress changes due to weld profile and macro geometrical features as given as below:

$$\sigma_{hotspot} = SCF * \sigma_{nominal} \tag{7.7}$$

3. Notch stress S-N curve:
According to DNV-RP-C203 [5], effective notch stress is the total stress at the root of a notch, which includes the hot spot stress and the stress due to the presence of weld. Effective notch stress is obtained under the assumption of linear-elastic material behavior. To account the non-linear material behavior and the statistical nature and scatter of a weld shape parameter the real weld is replaced as effective one [5]. Do keep in mind that for fatigue design the calculated notch stress should be linked to notch stress S-N curve.The Figure 7.3 shows how notch and hot spot stress can be extrapolated.

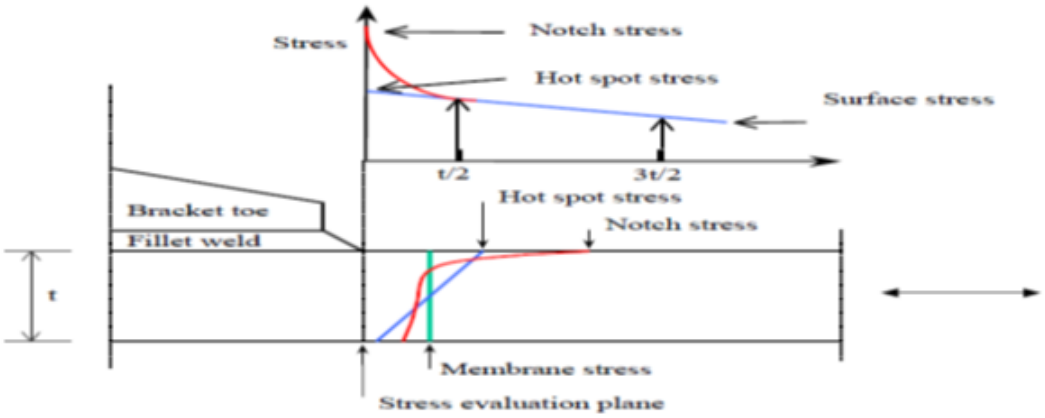

Figure 7.6: Hot and Notch stresses on a given plane.[5]

7.3.4 S-N curves and joint classification

As per DNV-RP-C203 [5] and Plaza [13], for practical fatigue design, the S-N curves of structural details are classified in to nominal classes: donated as B, C, D, E, F, G, W and T. For example all tubular joints are assumed to be categorized on class "T" S-N curve. S-N curves for tubular and non tubular structural details are classified based upon:

7.4 Tubular Joints and Members

7.4.1 Classification of tubular joints

Based on the axial force in a brace of a joint, tubular joints can be classified in to three classes as K, X and Y joints. A joint can be classified as K-joint, if the axial force carried by a brace can be balanced to within 10% by another brace, which is on the same side and in the same plane of the joint as in Figure 7.7. But if the axial force on a brace at a joint is not shared or balanced by other brace in the same joint and if it reacted as beam shear in the chord, it is classified as Y-joint as in Figure 7.8. The X-joint classification, for an axial force in a brace is balanced by a brace in the opposite direction, see Figure 7.8.

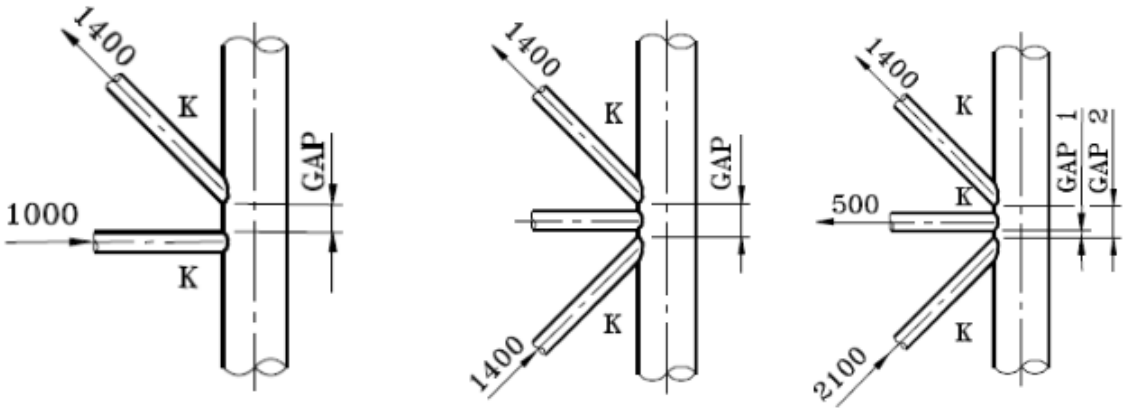

Figure 7.7: Tubular K-joint classification. [5]

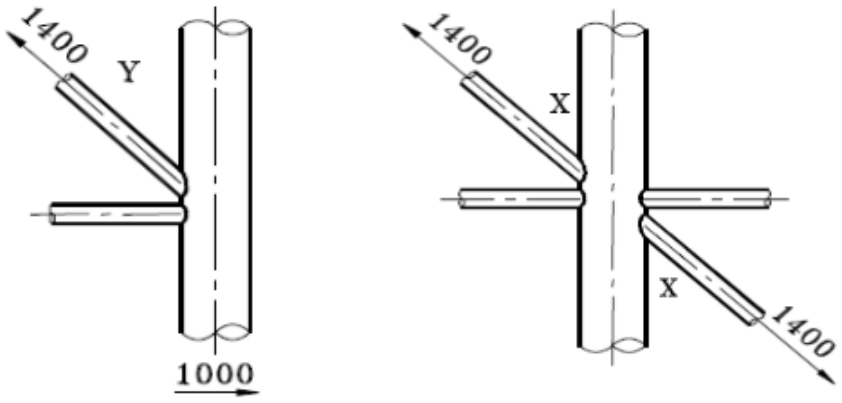

Figure 7.8: Figure: Tubular Y and X-joint classification. [5]

7.4.2 Stresses in Tubular Joints

For fatigue analysis of tubular joints, the hot spot stresses around the circumference of the joint have to be determined. These stresses are obtained by the summation of the stress components due to an axial loading, in-plane loading and out of plane loading on the tubular member or brace as shown in Figure 7.9.

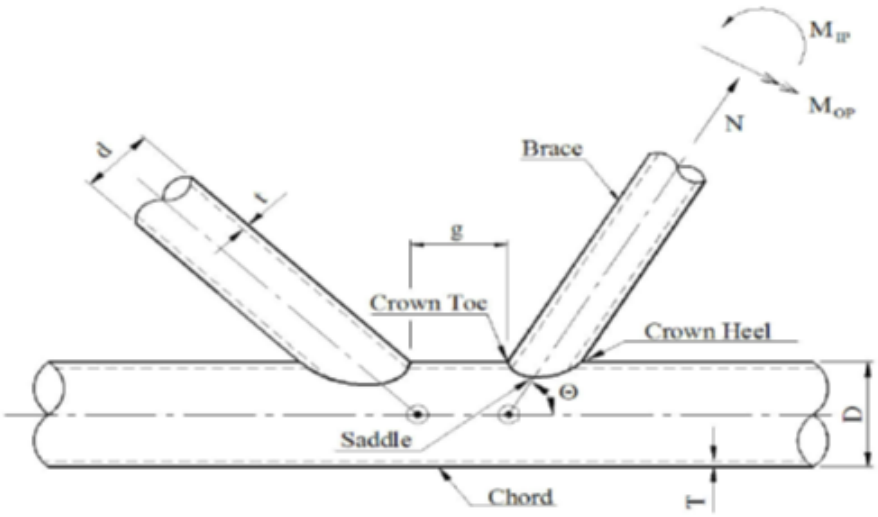

Figure 7.9: Geometrical definition & Loading on tubular members. [5]

where: N is axial loading of the brace; M_{IP} is in-plane bending of the brace and M_{OP} is out of plane bending of the brace.

The stresses due to the above load cases are calculated at 8 locations, i.e. around the circumference of the joint between the brace and chord as in Figure 7-10. These stresses are determined based on equations 7.8 - 7.15 given below. [5]

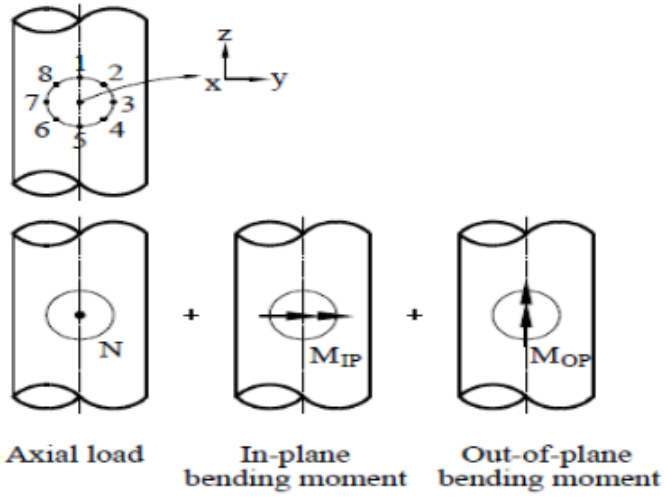

Figure 7.10: Superposition of stresses around a tubular joint. [5]

$$\sigma_1 = SCF_{AC} * \sigma_X + SCF_{MIP} * \sigma_{my} \tag{7.8}$$

$$\sigma_2 = \frac{1}{2}(SCF_{AC} + SCF_{AS})\sigma_X + \frac{1}{2}\sqrt{2}SCF_{MIP} * \sigma_{my} - \frac{1}{2}\sqrt{2}SCF_{MOP}\sigma_{mz} \tag{7.9}$$

$$\sigma_3 = SCF_{AS} * \sigma_X - SCF_{MOP} * \sigma_{mz} \tag{7.10}$$

$$\sigma_4 = \frac{1}{2}(SCF_{AC} + SCF_{AS})\sigma_X - \frac{1}{2}\sqrt{2}SCF_{MIP} * \sigma_{my} - \frac{1}{2}\sqrt{2}SCF_{MOP}\sigma_{mz} \tag{7.11}$$

$$\sigma_5 = SCF_{AC} * \sigma_X - SCF_{MIP} * \sigma_{my} \tag{7.12}$$

$$\sigma_6 = \frac{1}{2}(SCF_{AC} + SCF_{AS})\sigma_X - \frac{1}{2}\sqrt{2}SCF_{MIP} * \sigma_{my} + \frac{1}{2}\sqrt{2}SCF_{MOP}\sigma_{mz} \tag{7.13}$$

$$\sigma_7 = SCF_{AS} * \sigma_X + SCF_{MOP} * \sigma_{mz} \tag{7.14}$$

$$\sigma_8 = \frac{1}{2}(SCF_{AC} + SCF_{AS})\sigma_X + \frac{1}{2}\sqrt{2}SCF_{MIP} * \sigma_{my} + \frac{1}{2}\sqrt{2}SCF_{MOP}\sigma_{mz} \tag{7.15}$$

Where σ_X, σ_{my}, and σ_{mz} are the maximum nominal stresses due to axial loading, bending in-plane and bending out of plane respectively. $SCFAS$ is the stress concentration factor at the saddle for the axial load and the $SCFAC$ is the stress concentration factor at the crown. $SCFMIP$ is the stress concentration factor for in plane bending moment and $SCFMOP$ is the stress concentration factor for out of plane bending moment.

Chapter 8

SHORT TERM-SPECTRAL-BASED FATIGUE ASSESSMENT

8.1 Screening of Model Test Data

As in table 8-1 and appendix D.2, Table 2, the available data for this assessment includes 163133 sea states of three hour duration from 1957 to 2013. In each year there are around 2920 sea states, but in 1957 and 2013 there are 974 and 1448 respectively.

Table 8.1: Sea state ranges and their frequency of occurrence from 1957 to 2007

No	H_s range[m]	Sea states in range	Frequency of Occurrence (%)
1	<= 1	14780	9.0601
2	1-2	54483	33.3979
3	2-3	41364	25.3560
4	3-4	24894	15.2599
5	4-5	14139	8.6672
6	5-6	7177	4.3995
7	6-7	3549	2.1755
8	7-8	1612	0.9882
9	8-9	714	0.4377
10	9-10	278	0.1704
11	10-11	101	0.0619
12	11-12	28	0.0172
13	12-13	7	0.0043
14	13-14	5	0.0031
15	14-15	1	0.0006
16	15-16	1	0.0006
17	>16	0	0.0000
Total		**163133**	**100**

8.2 Standard Wave Energy Spectral Density

As described in chapter 4, for short term period it can be assumed that the sea surface elevation at a fixed location can be accurately modeled by a zero-mean Gaussian process. This process can be completely characterized by the frequency spectrum of standard mathematical models, $S_{\Xi\Xi}(\omega|H_s,T_p)$, for a given average direction of wave propagation θ, which can be described by two parameters, namely by the significant wave height, H_s, and the spectral peak period, T_p. As in appendix A.2, the common standard wave spectral models are JONSWAP and Pierson-Moskowitz. For fatigue assessment, the Pierson-Moskowitz, $S_{(PM,\Xi\Xi)}(\omega|H_s,T_p)$ mathematical model, which is originally developed for fully-developed wind sea state, is adopted as a reasonable model of the sea surface. The mathematical equation for this spectral model is given as:

$$S_{PM,\Xi\Xi}(\omega|H_s,T_p)=\frac{5}{16}*H_s^2*\omega_p^4*\omega^{-5}*exp^{(-\frac{5}{4}*(\frac{\omega}{\omega_p})^{-4})} \tag{8.1}$$

where: H_s is the significant wave height in meter; $\omega_p=\frac{2\pi}{T_p}$ is angular spectral peak frequency in radian per second and T_P is the spectral peak period in seconds.

Wave Spectral Moments

The n order spectral moment, $M_{n,\Xi\Xi}$, for a given wave spectral density, $S_{PM,\Xi\Xi}(\omega|H_s,T_p)$, as a function of angular frequency, ω, is given as:

$$M_{n,\Xi\Xi}(H_s,T_p)=\int_0^\infty \omega^n*S_{PM,\Xi\Xi}(\omega|H_s,T_p)*d\omega \tag{8.2}$$

where: ω is angular frequency and $n=0,1,2,3,...$
When n is zero, the spectral moment it is called zero order moment ($M_{(0,\Xi\Xi)}$) which gives the area under the spectral curve and this represents the total energy of the process. Further, for a Gaussian process, the zero order spectral moment is equal to the variance, $\sigma^2_{\Xi\Xi}$, of the water surface elevation.

$$M_{0,\Xi\Xi}(H_s,T_p)=\sigma^2_{\Xi\Xi}=\int_0^\infty S_{PM,\Xi\Xi}(\omega|H_s,T_p)*d\omega \tag{8.3}$$

The Zero-Up-Crossing Wave Period

The zero-up-crossing wave period, $T_{z,\Xi\Xi}$, can be defined as the average time interval between two successive up-crossings of the mean sea level. The zero-up-crossing period can be estimated from the wave spectral moments and it can be estimated by:

$$T_{z,\Xi\Xi}(H_s,T_p)=2\pi\sqrt{\frac{M_{0,\Xi\Xi}(H_s,T_p)}{M_{2,\Xi\Xi}(H_s,T_p)}} \tag{8.4}$$

where: $M_{0,\Xi\Xi}(H_s,T_p)$ and $M_{2,\Xi\Xi}(H_s,T_p)$ are the zero and second order wave spectral moment respectively for a given sea state.

Number of Wave Cycles within a given short term duration

For a stationary Gaussian and narrow band process, where there are no local maxima or minima, the number of cycles, $n_{0,\Xi\Xi}$, and wave number can be assumed to be equal during the short term duration [hours]. Thus, the number of cycles for 3-hour duration can be estimated as:

$$n_{0,\Xi\Xi}(H_s, T_p) = \frac{3hr}{T_{z,\Xi\Xi}(H_s, T_p)} \tag{8.5}$$

Substituting the zero-up-crossing wave period, $T_{z,\Xi\Xi}(H_s, T_p)$, from equation 8.4 to equation 8.5 gives as:

$$n_{0,\Xi\Xi}(H_s, T_p) = \frac{5400}{\pi} * \sqrt{\frac{M_{2,\Xi\Xi}(H_s, T_p)}{M_{0,\Xi\Xi}(H_s, T_p)}} \tag{8.6}$$

8.3 Response Amplitude Operator (RAO) of the Jacket

As explained in chapter 6, Response Amplitude Operator (RAO) is the absolute value or the modulus part of the transfer function, which is the response of a linear offshore structure to a sinusoidal wave with unit amplitude for sufficient number of frequencies, ω, and different wave heading directions, Θ, where only from one direction is considered in this study.

Based on the analysis and linearity assumption considered in chapter 6 for the determination of the Response Amplitude Operator , RAO(ω), of the structure, the Best fit RAO equation developed in section 6.4.1 is assumed to be reasonably acceptable for the Kvitebjørn jacket platform, see equation 8.7. This equation will be used initially for the assessment of fatigue accumulation due to all the sea states given in Table 8.1. Furthermore, its possible deviations will be analyzed to investigate if these deviations will have an effect on the accumulated damages. Four possible deviations of the Best fit RAO have been discussed in section 6.4.2 and their equations are available in Appendix C.3.

$$RAO(\omega) = \begin{cases} 0.50, & \text{for } 0 \leq \omega \leq 0.39 \\ -5.34\omega^2 + 6.65\omega - 1.28, & \text{for } 0.39 \leq \omega \leq 0.85 \\ 0.50, & \text{for } 0.85 \leq \omega \leq 1.39 \\ 123.39\omega^2 - 345.50\omega + 242.35, & \text{for } 1.39 < \omega \leq 1.56 \\ 9181.18 * exp(-5.04\omega) & \text{for } \gamma > 1.56 \end{cases} \tag{8.7}$$

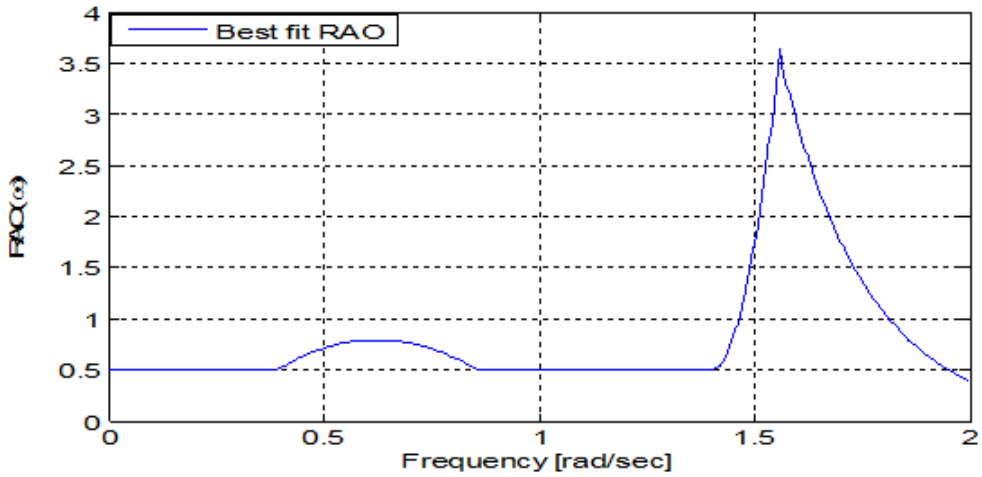

Figure 8.1: Best fit RAO for the jacket platform.

8.4 Linear response spectrum

Since the sea surface elevation process is described as a Gaussian process for the short term duration and the response process is also modeled as a Gaussian process due to the linearity assumption, for detail information see chapter 2. Once the response amplitude, Best fit RAO, of the structure is generated as given in section 8.3, the response spectrum, $S_{\gamma\gamma}(\omega|H_s, T_p)$, is evaluated for each sea state listed in Table 8.1 using the spectral relation given below.

$$S_{\gamma\gamma}(\omega|H_s, T_p) = |H_{\Xi\Gamma}|^2 * S_{\Xi\Xi}(\omega|H_s, T_p) \tag{8.8}$$

Figure 8-2 presents an example of wave spectrum, RAO and their corresponding response spectrum of the jacket platform for a sea state of 8 meter significant wave height and spectral peak period of 10 second.

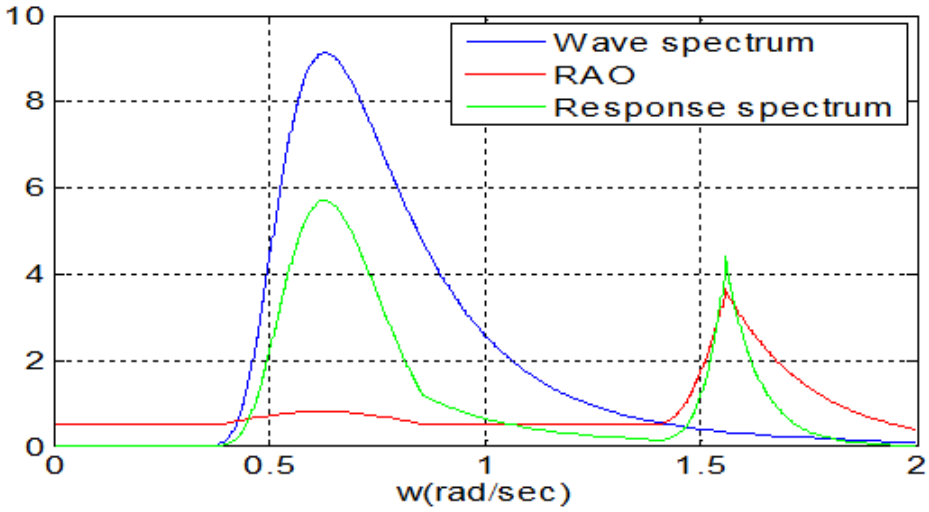

Figure 8.2: Wave spectrum, RAO and Response spectrum for a given sea state

Response Spectral Moments

Similar to the wave spectral moments,$M_{n,\Xi\Xi}$, in section 8.2, the spectral response moments, $M_{n,\Gamma\Gamma}$, are determined using the following equation:

$$M_{(n,\Gamma\Gamma)}(H_s, T_p) = \int_0^\infty \omega^n * S_{\Gamma\Gamma}(\omega|H_s, T_p) * d\omega \tag{8.9}$$

where: ω is angular frequency and $n = 0, 1, 2, 3.\ldots\ldots\ldots$
When n is zero, it is called zero order response moment, $M_{0,\Gamma\Gamma}$, which gives the area under the response spectral curve and this represents the total energy lost during of the process. The zero order spectral moment is also equal to the variance of the response process, $\sigma^2_{\Gamma\Gamma}$, which is determined as:

$$M_{0,\Gamma\Gamma}(H_s, T_p) = \sigma^2_{\Gamma\Gamma} = \int_0^\infty S_{\Gamma\Gamma}(\omega|H_s, T_p) * d\omega \tag{8.10}$$

Expected Zero-Up-Crossing Response Period

Similar to the zero-up crossing wave period,$T_{(z,\Xi\Xi)}$, in section 8.2, the zero-up-crossing response period, $T_{(z,\Gamma\Gamma)}$, is defined as the average time interval between two successive up-crossings of the mean sea level. It is calculated from the zero and second order response spectral moments using equation below:

$$T_{(z,\Gamma\Gamma)}(H_s, T_p) = 2\pi\sqrt{\frac{M_{0,\Gamma\Gamma}(H_s, T_p)}{M_{2,\Gamma\Gamma}(H_s, T_p)}} \tag{8.11}$$

where: $M_{0,\Gamma\Gamma}(H_s, T_p)$ and $M_{2,\Gamma\Gamma}(H_s, T_p)$ are the zero and second order wave spectral moment respectively for a given sea state.

Number of Response Cycles For The Given Duration

For Gaussian and narrow band response process, the number of response cycles of given duration can be determined from the expected zero-up crossing response period, $T_{z,\Gamma\Gamma}(H_s, T_p)$. The number of response cycles within the given duration,τ [hours], is given as:

$$n_{0,\Gamma\Gamma}(H_s, T_p) = \frac{\tau}{T_{z,\Gamma\Gamma}(H_s, T_p)} \tag{8.12}$$

By substituting equation 8.11 in to equation 8.12 for 3-hour duration gives as:

$$n_{0,\Gamma\Gamma}(H_s, T_p) = \frac{5400}{\pi} * \sqrt{\frac{M_{2,\Gamma\Gamma}(H_s, T_p)}{M_{0,\Gamma\Gamma}(H_s, T_p)}} \tag{8.13}$$

8.5 Closed Form Fatigue Damage Using S-N Curve

Cumulative fatigue damage is normally calculated based on the Miner-Palmgren's rule, which assumes that the cumulative fatigue damage (D) inflicted by a group of variable amplitude stress cycles is the sum of the damage inflicted by each stress range, $\Delta\sigma$, independent of the sequence in which the stress cycles occur [13]. The Miner-Palmgren formula for cumulative fatigue damage is given as:

$$D = \sum_{i=1}^{k} \frac{n_i}{N_i} \tag{8.14}$$

where: k is number of stress blocks; n_i is number of stress cycles in stress block i with constant stress range $\Delta\sigma_i$; N_i is number of cycles to failure at constant stress range $\Delta\sigma_i$.

Let's assum that a linear submerged structural detail is subjected to a total number stress cycles, $n_{0,\Gamma\Gamma}(H_s, T_p)$, of a given sea state. The total stress cycles are the number of response cycles for a given duration of time which are estimated from the spectral response moments given in equation 8.13. Further it can be assumed that these stress cycles are randomly distributed with a probability density function $f(\Delta\sigma)$ as shown in Figure 8-3.

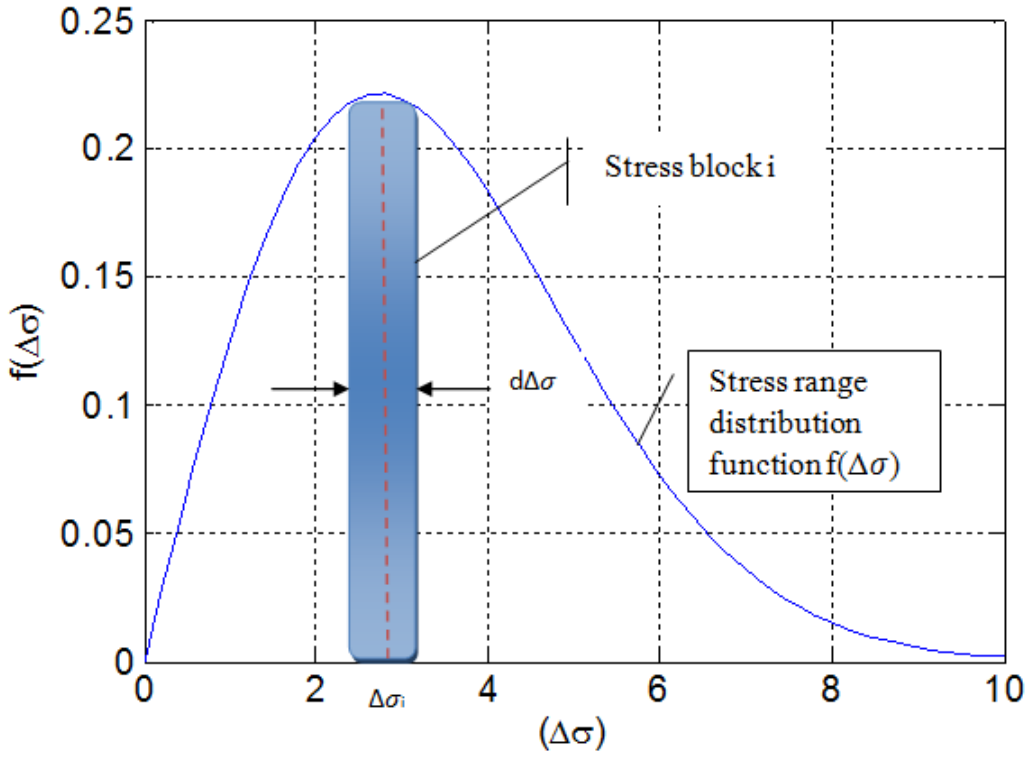

Figure 8.3: Typical stress range distribution function

In this case, the number of stress cycles, $n_{i,\Gamma\Gamma}(H_s, T_p)$, in a given stresses block i of width $d\Delta\sigma$, i.e. between $\Delta\sigma$ and $(\Delta\sigma + d\Delta\sigma)$, can be determined as:

$$n_{i,\Gamma\Gamma}(H_s, T_p) = n_{0,\Gamma\Gamma}(H_s, T_p) * f(\Delta\sigma) * d\Delta\sigma \tag{8.15}$$

As in section 7.3, the S-N curve is usually used to determine the number of cycles to failure, N_i, for a given structural detail at constant stress range $\Delta\sigma_i$ with the equation is given by:

$$N_i = a * \Delta\sigma_i^{-m} \tag{8.16}$$

where: m is slope of the S-N curve and a is coefficient which depends on the structural detail under consideration.
Substituting equations 8.15 and 8.16 in to equation 8.14 gives as:

$$D(H_s, T_p) = \frac{n_{0,\Gamma\Gamma}(H_s, T_p)}{a} * \sum_{0}^{\infty} \Delta\sigma^m * f(\Delta\sigma) * d\Delta\sigma \tag{8.17}$$

As the stress block width, $d\Delta\sigma$, is close to zero, the summation, $\sum$, can be approximated in to integration, $\int$. As a result equation 8.17 can be rewritten equivalently as:

$$D(H_s, T_p) = \frac{n_{0,\Gamma\Gamma}(H_s, T_p)}{a} * \int_0^{\infty} \Delta\sigma^m * f(\Delta\sigma) * d\Delta\sigma \tag{8.18}$$

For offshore structures, the stress range distribution function for short term duration is represented by a special type of Weibull distribution function called Rayleigh distribution, i.e. when the Weibull shape parameter,β, is assumed to be 2. The Weibull scale parameter,α, is approximated to $2\sqrt{2} * \sigma_{\Gamma\Gamma}(H_s, T_p)$, where $\sigma_{\Gamma\Gamma}(H_s, T_p)$ is standard deviation of the structural response process for a given sea state [13]. Note that standard deviation of response process is the square root of its variance as described in section 8.4.

The cumulative Weibull distribution functions as a function of stress range is given as:[3]

$$F(\Delta\sigma) = 1 - exp^{(-(\frac{\Delta\sigma}{\alpha})^{\beta})} \tag{8.19}$$

where: β is the shape parameter; α is the scale parameter.
Substituting the scale parameter, α, in equation 8.19, the cumulative stress distribution for a given sea state becomes as:

$$F(\Delta\sigma) = 1 - exp^{-(\frac{\Delta\sigma}{2\sqrt{2}*\sigma_{\Gamma\Gamma}(H_s,T_p)})^{\beta}} \tag{8.20}$$

By differentiating equation 8.20 with respect to the variable stress range, $\Delta\sigma$, it gives the Weibull probability density function as:

$$f(\Delta\sigma) = \frac{\beta}{2\sqrt{2} * \sigma_{\Gamma\Gamma}(H_s, T_p)} * (\frac{\Delta\sigma}{2\sqrt{2} * \sigma_{\Gamma\Gamma}(H_s, T_p)})^{\beta-1} * exp(-(\frac{\Delta\sigma}{2\sqrt{2} * \sigma_{\Gamma\Gamma}(H_s, T_p)})^{\beta}) \tag{8.21}$$

Figure 8-4 shows the stress range distribution for a given sea state based on the Weibull distribution function given in equation 8.21.
When the Weibull shape parameter, β, is assumed to be 2, equation 8.21 reduces to a Rayleigh- distribution function as:

$$f(\Delta\sigma) = \frac{\Delta\sigma}{4\sigma_{\Gamma\Gamma}^2(H_s, T_p)} * exp(-(\frac{\Delta\sigma}{2\sqrt{2} * \sigma_{\Gamma\Gamma}(H_s, T_p)})^2) \tag{8.22}$$

Figure 8-5 shows distribution of the stress ranges for different sea states based on the Rayleigh distribution equation 8.22.

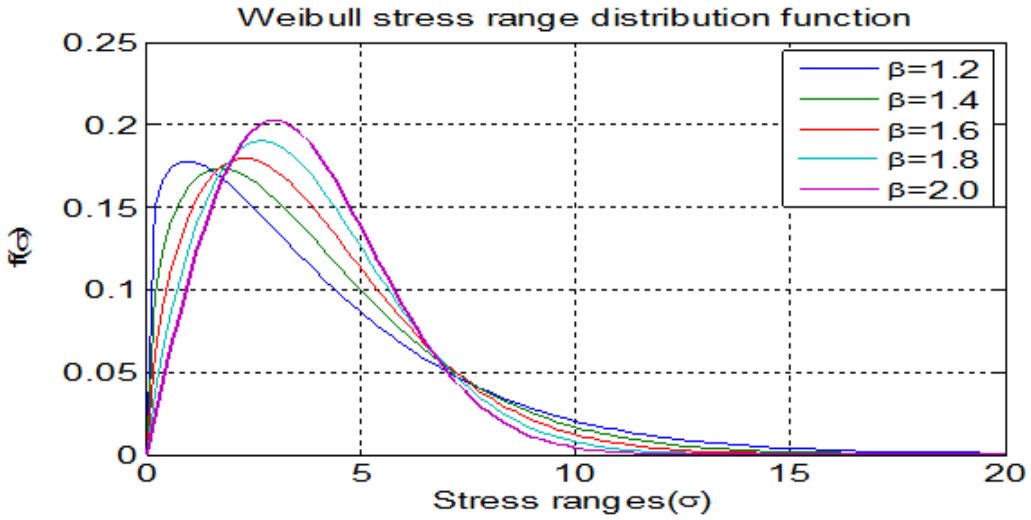

Figure 8.4: Weibull probability stress range density function for a given sea state.

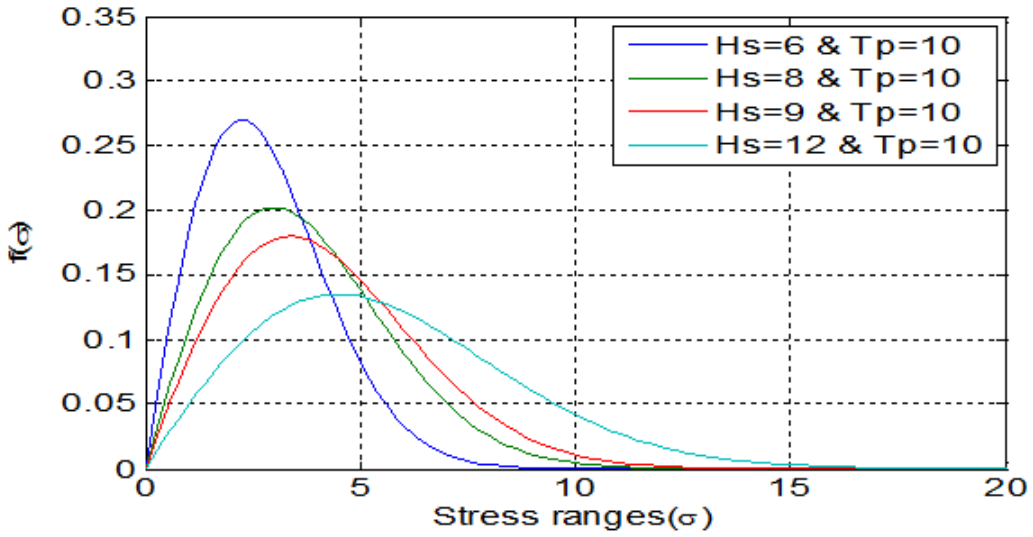

Figure 8.5: Rayleigh probability stress range density function for a given sea state.

In the Figure 8-5 one can notice that the stress ranges for lower sea states are concentrated in the lower values. In reference to the basic S-N curve design given in section 7.3.1, the number of stress cycles to failure is relatively higher for the lower stress range values. Thus, based on the "Miner-Palmgren" formula, lower sea states have lower fatigue damage effect compared to the higher sea states in which their stress ranges are relatively distributed over a wider range. Remember that the number of stress cycles to failure, N, is inversely proportional to the fatigue damage in "Miner-Palmgren" rule (equation 8.14).

By substituting the Rayleigh-distribution equation (8.22) in to equation 8.18, the damage ratio equation for a given sea state yields as:

$$D(H_s, T_p) = \frac{n_{0,\Gamma\Gamma}(H_s, T_p)}{a} * \int_0^{\infty} \frac{\Delta\sigma^{m+1}}{4\sigma_{\Gamma\Gamma}^2(H_s, T_p)} * exp(-(\frac{\Delta\sigma}{2\sqrt{2} * \sigma_{\Gamma\Gamma}(H_s, T_p)})^2) \qquad (8.23)$$

Therefore, for linear offshore structures under the assumptions of Gaussian process, their fatigue damage is evaluated using equation 8.23. This equation will be used for analysis of the fatigue accumulation on the Kvitebjørn jacket platform due to 163133 sea sates listed in Table 8.1. Similarly, by substituting the Weibull-distribution equation 8.21 in to equation 8.18, the fatigue damage can be estimated for different values of the Weibull shape parameter, β.

8.6 Procedures And Numerical Calculations

Assumption Taken For Base Case Analysis

In this short term closed form approach analysis, the Kvitebjørn platform will be taken as a case study. For the base/primary study case of the fatigue damage analysis, the assumptions taken are as follows:

- The sea state given in table 8.1are considered as a stationary Gaussian process of 3 hour duration.
- All waves are considered to come from the same direction.
- The wave spectra are assumed to be narrow band width.
- The variation of the stress ranges are assumed as a narrow band and random Gaussian process.
- The jacket is assumed as a linear mechanical system, i.e. the structural members of the jacket will remain in their elastic limit state under the applied hydrodynamic loads.
- The joint thickness is assumed to be less than the reference thickness; hence, further thickness correction for the S-N cure is ignored.
- The eccentricity effect is assumed to be within the effect embodied in the design S-N curve.
- The jacket is assumed to be in seawater with cathodic protection, i.e. corrosive environment adjustment is ignored.
- The jacket is assumed to have tubular joints and class "T" S-N curve as described in section 7.3.4. For this type of S-N curve, the constant parameters are given in Table 8-2, i.e. a and m in equation 7.3 and 7.4.

Table 8.2: S-N curve constants for tubular "T class" structural details. [5]

S-N curve	*N <= 10^6 cycles*		*N >10^6 cycles*	
	m_1	$\log a_1$	m_2	$\log a_2$
T	3.0	11.764	5.0	15.606

Figure 8-6 shows two segmented "T" S-N curve for tubular structural details based on the basic S-N curve design equations 7.3 and 7.4. The constant parameters of this type

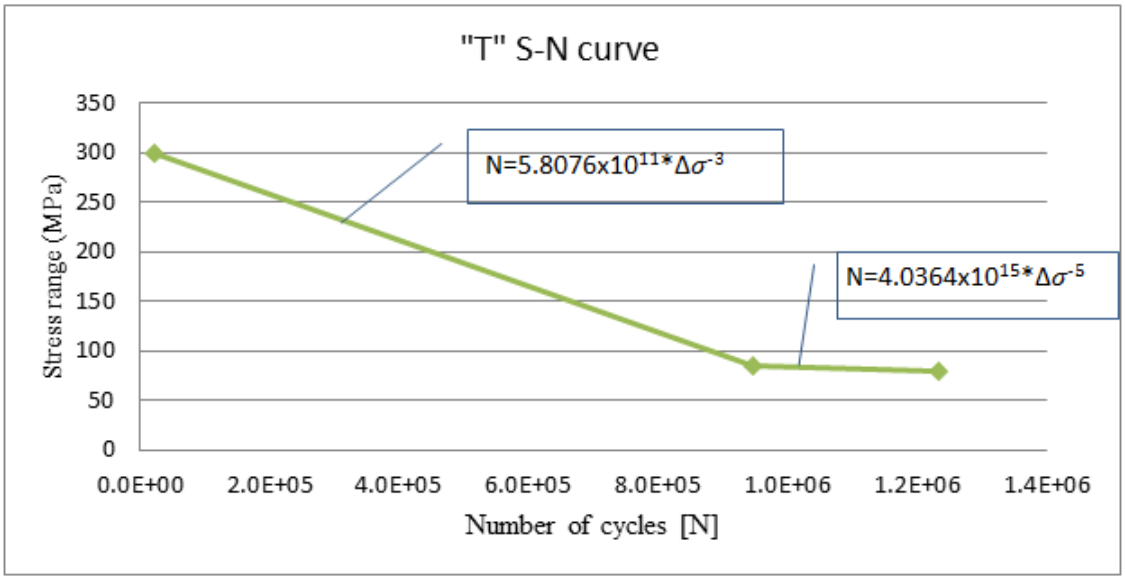

Figure 8.6: Two segment S-N curve for tubular "T class" structural details

of S-N curve are given in Table 8-2. The "T" S-N curve has a transition in slope from m=3.0 to m=5 at 10^6 cycles, which corresponds to a stress range 83.4 MPa.

General Procedures For The Primary/Base Case Study

The following procedures and flow chart diagram in Figure 8-6 illustrate the general steps for short term-spectral –based fatigue assessment on the structure:

1. Estimation of wave spectral density, $S_{\Xi\Xi}(\omega|h,t)$,from the standing Gaussian sea surface process,$\Xi(t)$. As in section 4.3.1, this is done by Fast Fourier Transfer Method (FFT) using equation 4.1.

2. Similar to step 1, estimate response spectral density, $S_{\Gamma\Gamma}(\omega|h,t)$, from the time series response process, $\Gamma(t)$.

3. From steps 1 and 2 estimate the stress transfer function, RAO(ω), or response amplitude operator, by using equation 6.1.

4. For correlation relation between the incident waves and their corresponding response of the structure, perform Coherence analysis, $\eta_{\Xi\Gamma}(\omega_k)$, using the relation in 6.6. Then, from the correlated or linearly dependent waves and responses, determine the Best fit RAO(ω), in this case equation 6.7 is taken to be the Best fit.

5. Develop wave spectra, $S_{(PM,\Xi\Xi)}(\omega|H_s,T_p)$ for a given sea state of H_s and T_p using Perison-Moskowitz formula (8.1).

6. From the RAO(ω) in step 4 and the wave spectra generated in step 5, $S_{(PM,\Xi\Xi)}(\omega|H_s,T_p)$, develop the response spectrum, $S_{\Gamma\Gamma}(\omega|H_s,T_p)$, using the relation given in equation 8.8.

7. Once we have the response spectrum, $S_{\Gamma\Gamma}(\omega|H_s,T_p)$, from step 6, calculate the response spectral moments, $M_{n,\Gamma\Gamma}(H_s,T_p)$, using equation 8.9, standard deviation or variance of the response process, $\sigma^2_{\Gamma\Gamma}(H_s,T_p)$, from equation 8.10 and number of response cycles, $n_{0,\Gamma\Gamma}(H_s,T_p)$, using equation 8.13.

8. Decide which probability density function describes best to the short term responses/ stress range distribution. For linear response problems, the Rayleigh distribution is assumed to be best as given in equation 8.22.

9. Using the probability function in step 8 and the number of response cycles found in step 7, determine the number of cycles $n_i(H_s, T_p)$, within in a given stress range block i of the distribution by equation 8.15.

10. Decide the structural detail type and based on its type determine the constant parameters of the S-N curve.

11. Determine the number of stress cycles to failure, N_i, at constant stress range $\Delta\sigma_i$ of the stress block considered in step 9 based on the S-N curve chosen in step 10.

12. Determine fatigue damage,$D_i(H_s, T_p)$, as the ratio of the number of cycles $n_i(H_s, T_p)$ and N_i in steps 9 and 11 respectively. Again back to step 9 and repeat this for all stress block in the distribution. Finally, fatigue damage due to the given sea state, $D(H_s, T_p)$, is linear summation of the damages due to each stress block as given in equation 8.14.

13. Back to step 5 and redo steps 5 to 12 for the next sea states.

Similarly the flow chart diagram given in Figure 8.7 shows the general procedures followed for the transformation of the time domain wave and response records in to frequency domain and for calculation of the fatigue damage accumulation on the tubular structural detail.
The procedures on how to determine the fatigue damage on the structural detail by the short term-spectral-based fatigue assessment illustrated above and in Figure 8.7 are generally followed. But to show these steps numerically, fatigue damage due to one sea state is presented in Appendix D.1. In this thesis, these procedures are written in the MATLAB script as in Appendex D-1 and fatigue damage for all the sea states given in Table 8.1 are analyzed and the results are presented in section 8.7. The procedures given are for one study case/base case study only, but by modifying steps 4, for deviate RAOs, and 11, Single slope S-N curves, the following further investigation about the fatigue damage on the tubular joints are performed.

Secondary Study Case (Possible Deviation of the Best Fit RAO)

In section 6.4.2, it has been discussed that there are four possible deviations of the Best fit RAO at different frequency ranges. By replacing the Best fit RAO in step 4 with these possible deviated RAOs, the fatigue damage on the structure are analyzed and the results are presented in section 8.7.

Third Study Case (Single Slope S-N Curves)

In the base case and secondary study cases, the S-N curve of the structural detail has been considered to have two slope segments as given in Figure 8-6. The effect of the accumulated fatigue damage on the structural detail is also observed by analyzing with a single slope "T" S-N curve in step 11. The single slope S-N curve is given as:

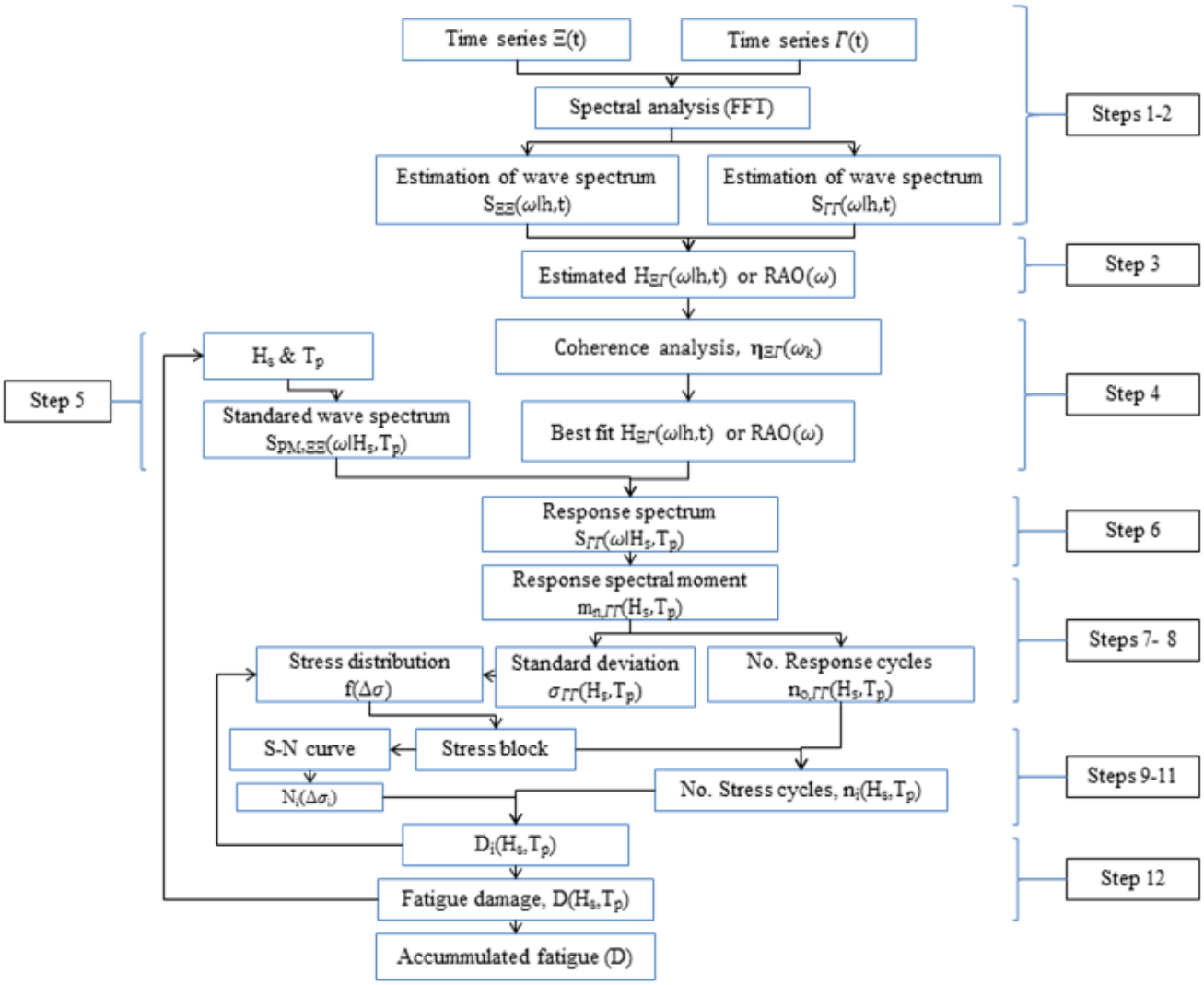

Figure 8.7: General procedures for estimating fatigue damage on a submerged structure detail by the short term-spectral – based fatigue assessment method

- ***Option 1:*** The upper segment of the "T" S-N curve to be continuous. In this case, the single slope "T" S-N curve equation for all stress ranges within the stress distribution function is by:

$$N = 5.8076 * 10^{1}1\Delta\sigma^{-3} \tag{8.24}$$

- ***Option 2:*** The lower segment of the "T" S-N curve to be continuous where "T" S-N curve equation for all stress ranges within the stress distribution function is given as:

$$N = 4.0364 * 10^{1}5\Delta\sigma^{-5} \tag{8.25}$$

8.7 Results Of The Closed Form-Based Fatigue Analysis

A - Fatigue Damage Result For The Base/Primary Study Case

In this subsection, the analysis is performed based on the assumptions and procedures described in section 8.6 and the fatigue damage accumulation is presented in two options.

- ***Option 1 -*** Fatigue damage accumulation versus significant wave heights, H_s.

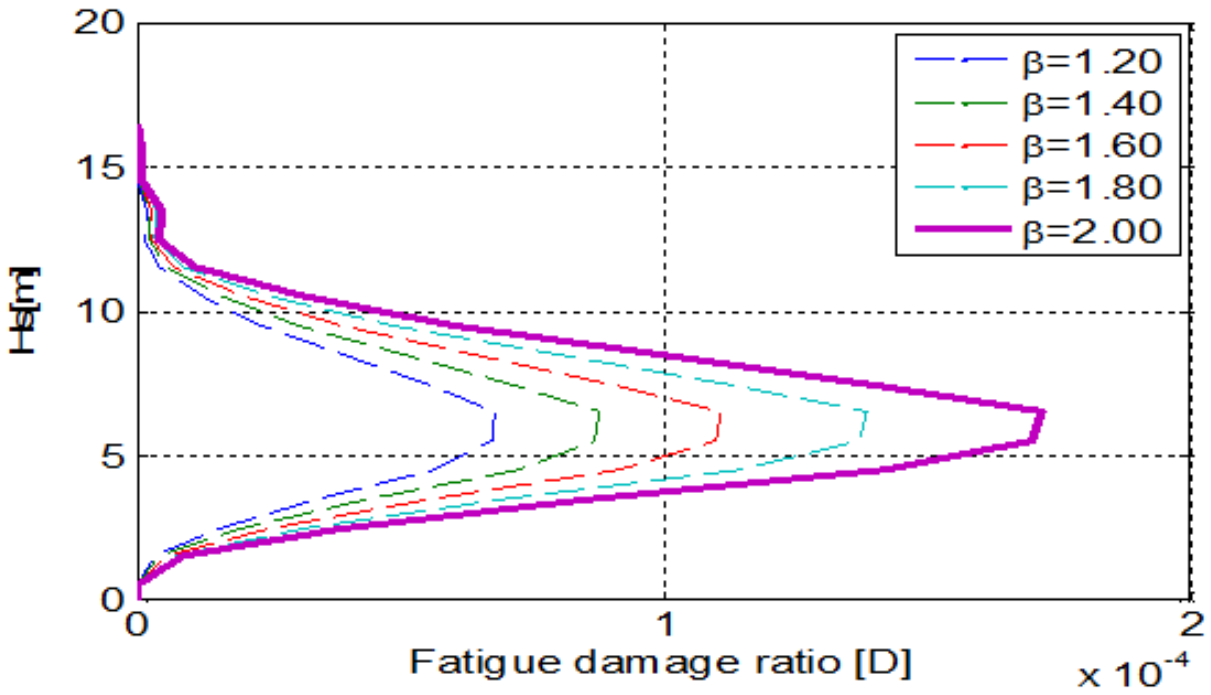

Figure 8.8: Fatigue accumulation vs. H_s for the base/primary study case

In the base case, i.e. when the double slope "T" S-N curve and the Best fit RAO are taken, around 60% of the fatigue damage are accumulated from the sea states within the range 4 to 8 significant wave height, particularly from sea states within the range of 6m to 7m as shown in Figure 8-8 and Table 1 in Appendix D.2. As in Figure 8-8, the fatigue damage accumulation is included for different values of the Weibull shape parameter, β. This is done to find out if these shape parameter values could have some effect on the fatigue damage - sea state severity relationships. The results have been found that the fatigue damage decreases as the shape parameter value decreases, but the shape parameter values have no role on the damage versus sea state severity.

- ***Option 2 -*** Fatigue damage accumulation versus storm events for the base case study

  Figure 8-9 shows yearly accumulated fatigue damage on the structure detail under consideration from the end of 1957 until the beginning of 2013. In this analysis, 974 and 1448 sea states were recorded in 1957 and 2013 respectively; while in the other

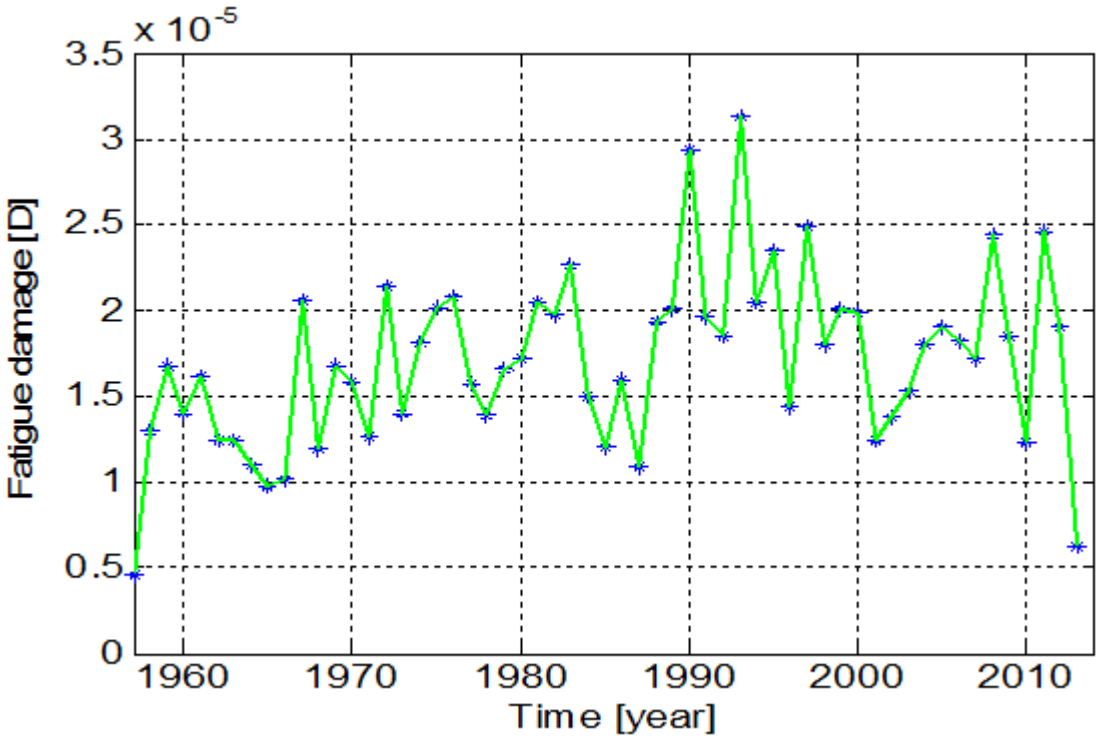

Figure 8.9: Fatigue accumulation vs. storm events for the base/primary study case

years around 2920 sea states were recorded, see Appendix D.2 in Table 2. Excluding in 1957 and 2013, the lowest fatigue accumulation was estimated in 1965, around 1% of the total damage. The reason for this might be that there were higher numbers of lower sea states during this year which have lower fatigue damage effect. In 1993 the highest fatigue damage accumulation was estimated around 3.23% of the total damage accumulated from 1957 to 2013, this might be there were higher number of higher and/or moderate sea states during this year.

B - Fatigue Damage Results For the Secondary Study Case (Possible Deviations Of The Best Fit RAO)

As mentioned in section 6.4.2, there is a doubt that the Best fit RAO equation can be different, if the uncorrelated signal noise could be minimized or if the correlation between the incoming waves and their corresponding response could be good enough. To take account of these possibilities, the Best fit RAO equation is customized in different frequency ranges, deviated RAOs, as given in section 6.4.2 and Appendix C-3. To investigate the effects of these deviated RAOs on the accumulated fatigue damage, the Best fit RAO in the base/primary study case is replaced by these deviated RAOs. Similar to the base case for various values of the Weibull shape parameter are also included in these cases.

1. Deviation of the Best fit RAO at the beginning [0-0.39]
   As in the Figure 8-10 and Appendix D.2 in Table 3, the fatigue damage distribution remain equivalent as in the base/primary case study. This shows that deviation of the Best fit RAO at the lower frequency does not have effect on the accumulated fatigue damage on the structural detail.

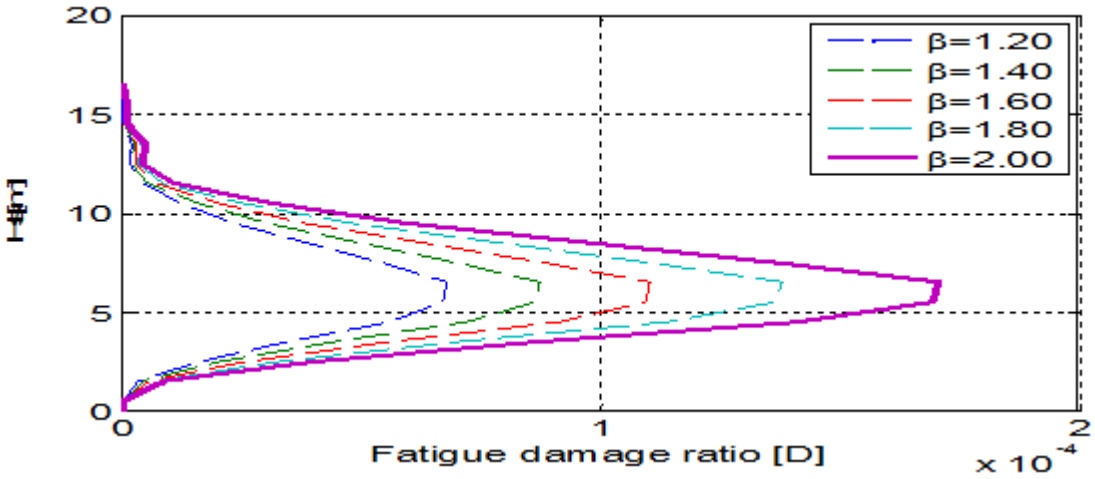

Figure 8.10: Fatigue accumulation for the secondary study case, where the Best fit RAO deviated at [0-0.39]

2. Deviation Of The Best Fit RAO in The Major Frequency Regime [0.39-0.85]

a. 50 % deviation above the Best fit RAO in the frequency range [0.39-0.85]

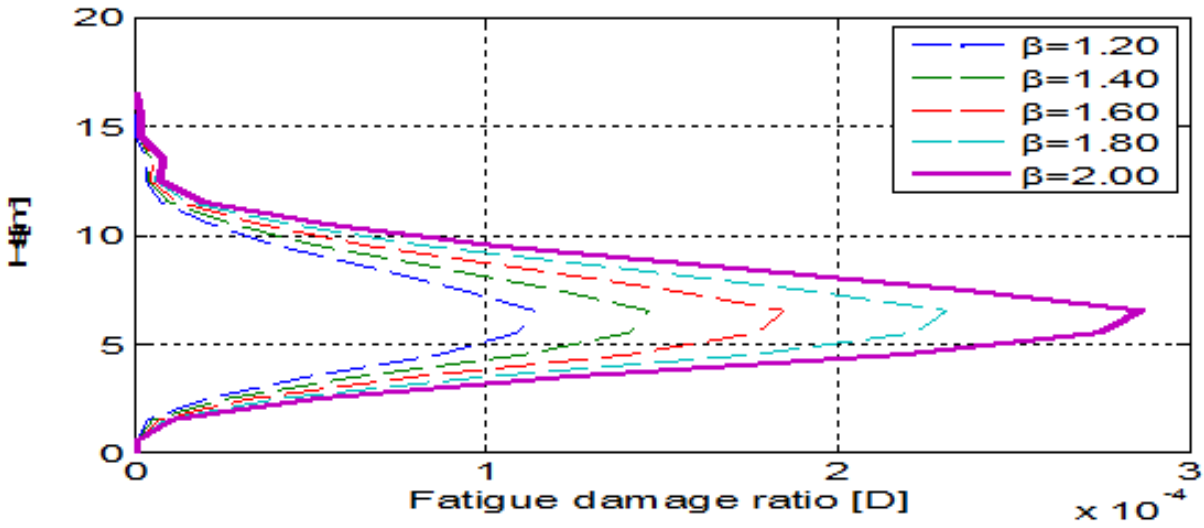

Figure 8.11: Fatigue accumulation for secondary study case, where the Best fit RAO deviated 50% up at [0.39-0.85].

In this analysis, similar to the base case study, it has been found that around 65% of the accumulated fatigue damage came from the moderate sea states. However, the fatigue damage due to each sea state ranges increased in some percentage of the base case study as presented in Appendix D.2, Table 4.

b. 50% deviation below the Best fit RAO in the frequency range [0.39-0.85]

As in the Figure 8-12, similar to base case study it has been found that large amount of the accumulated fatigue damage, around 62.5%, was from these

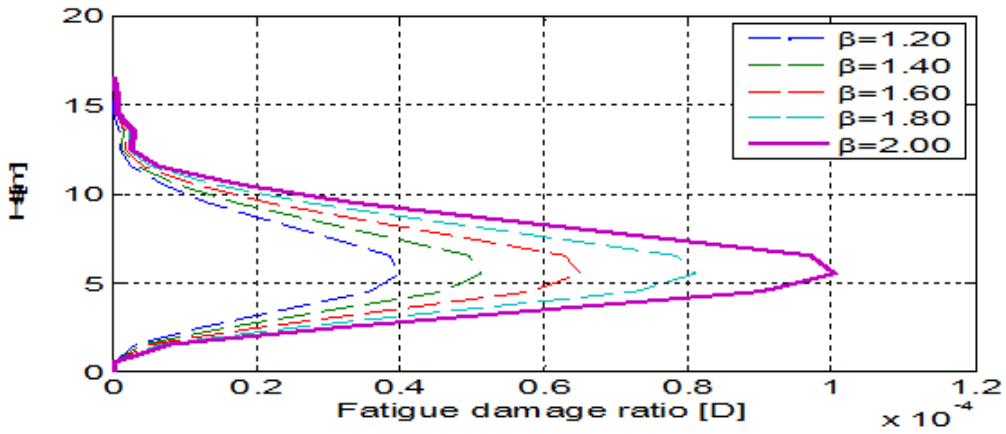

Figure 8.12: Fatigue accumulation for the secondary study case, where the Best fit RAO deviated 50% down at [0.39-0.85].

moderate sea states. But, the fatigue damage due to each sea state ranges decreased in some percentage of the base case study; see Appendix D.2 in Table 5.

3. Deviation between the major wave frequency regime and natural frequency of the Jacket [0.85-1.39]

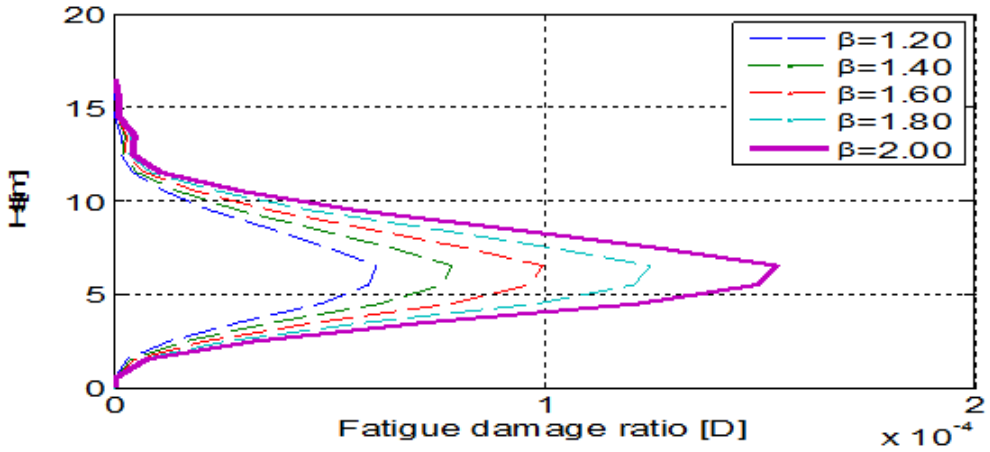

Figure 8.13: Result of fatigue accumulation for the secondary study case, where the Best fit RAO deviated at [0.85-1.39].

As in the Figure 8-13, still the fatigue damage accumulation is dominated by the moderate sea states as in the base case. The fatigue damage accumulation was found around 64% from the moderate sea states and only 23% from higher sea states, but generally it decreased due to all sea states in some percentage relative to the base case, see Appendix D.2 in Table 6.

4. Deviation around the natural frequency of the Jacket [1.57]
To investigate the effect of resonance induced dynamics to the fatigue damage accumulation on the structural detail, the Best fit RAO is shifted 50% below and above

around the natural frequency of the jacket, see section 6.4.2. The results for this analysis are found as in below.

a. When the Best fit RAO is deviated up by 50% around the natural frequency

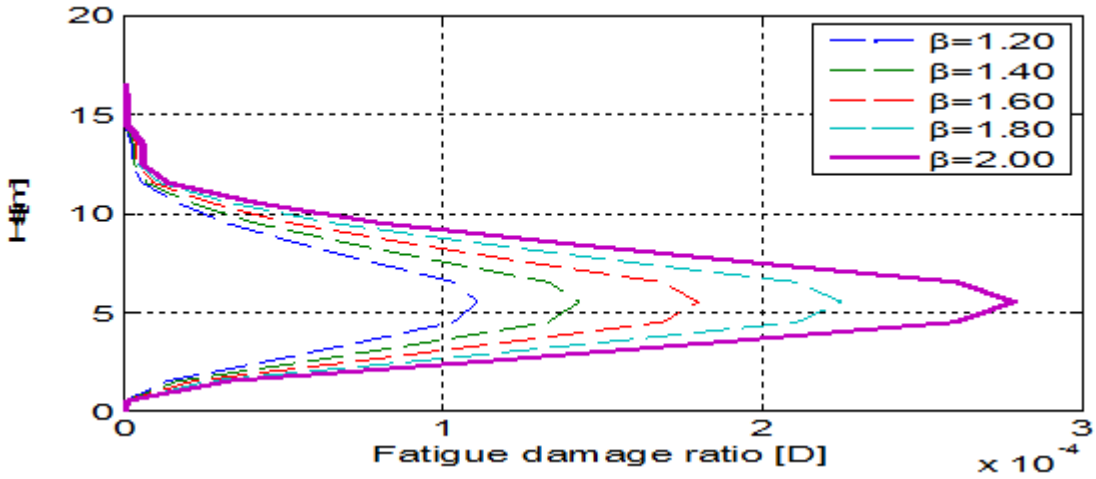

Figure 8.14: Fatigue accumulation for the secondary study case, where the Best fit RAO deviated 50% up at [1.56].

Even if when the Best fit ROA is assumed to be shifted by 50% around the Eigen frequency of the jacket, majority of the accumulated fatigue damage, around 62%, was found from the moderate sea states as in the base and only around 18% from the higher sea states, see Figure 8-14. However, the fatigue damage due to each sea state ranges increased in some percentage of the base case study as presented in Appendix D.2 in Table 7.

b. When the Best fit RAO is deviated down by 50% around the natural frequency From Figure 8-15, one can notice that the fatigue damage accumulation

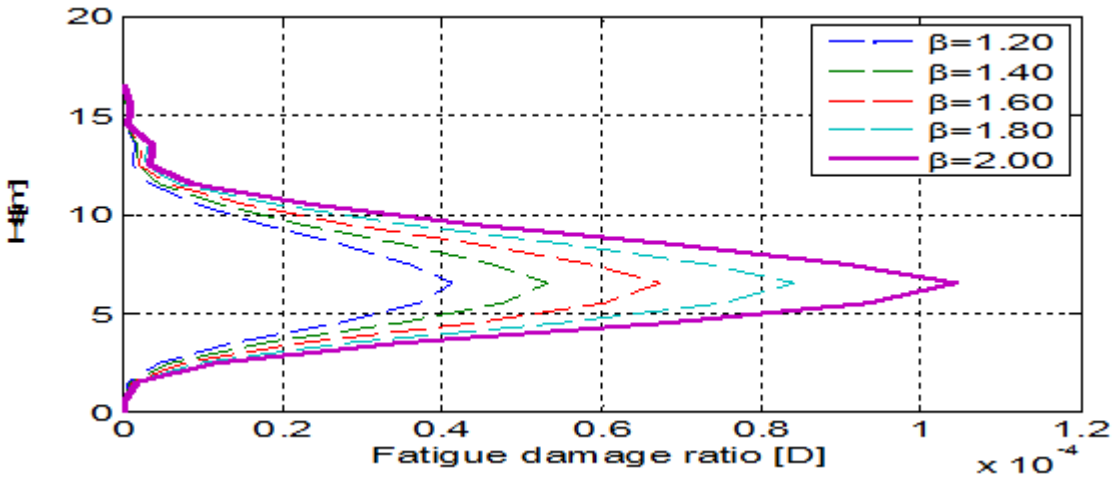

Figure 8.15: Fatigue accumulation for the secondary study case, where the Best fit RAO deviated 50% down at [1.56].

reached maximum for the sea states around 6.5 m significant wave height. In this case, around 64% of the accumulated fatigue damage was found from the moderate sea states and it decreased for all the sea state ranges in some amount relative to the base case study. The values for each sea state range is available in Appendix D.2 in Table 8.

C - Fatigue Damage Result For The Third Study Case (Single Segment S-N Curve)

As mentioned in section 8.6, the following parameters are taken in this study case

- The Best fit RAO determined in section 6.4.1 is assumed as a reasonable RAO of the system.
- The "T class" S-N curve in Figure 8-5 is modified as single slope curve, i.e. either equation 8.24 or 8.25.
- ***Option 1:*** With a straight "T" S-N curve with slope m=3.
  Figure 8-16 shows the fatigue damage on the structural detail assuming that the upper segment of "T class" S-N curve, equation 8.24, to be continuous.

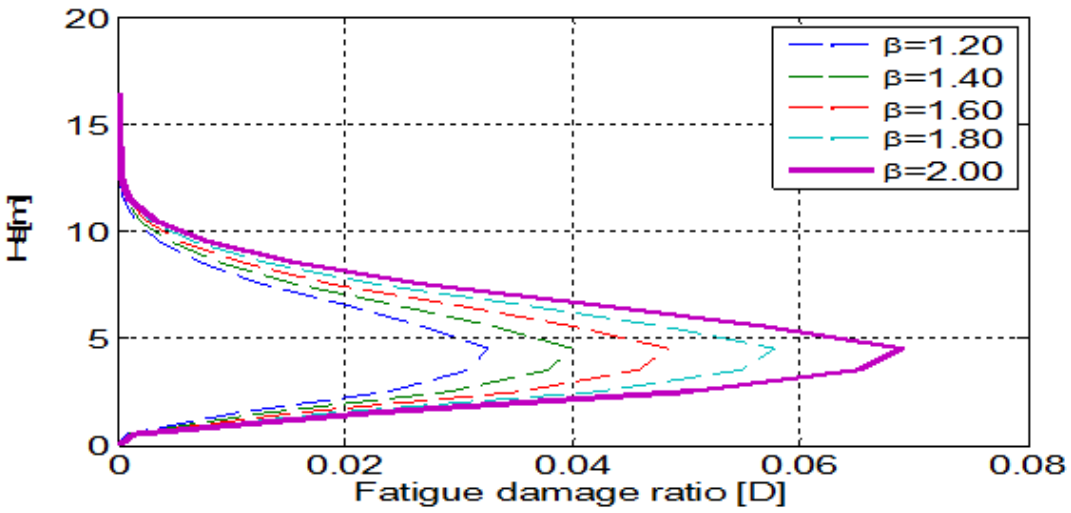

Figure 8.16: Fatigue accumulation for the third study case, with straight S-N curve with m=3

As in the Figure 8-16, it has been found that around 66% of the accumulated fatigue damage came from relatively lower sea states, sea states of significant wave height between 2m – 6m and the fatigue damage accumulation for each sea state range increased by large quantity relative to the base case, see Appendix D.2 in Table 9.

- ***Option 2:*** With a straight "T" S-N curve with slope m=5.

In this case the fatigue damage on the structural detail is determined assuming that "T" S-N curve to be continuous as a single slope as in equation 8.25. This means the lower segment is extended up-word with the same slope and number of cycles to failure, N, for all stress ranges within the stress distribution function are determined from this single

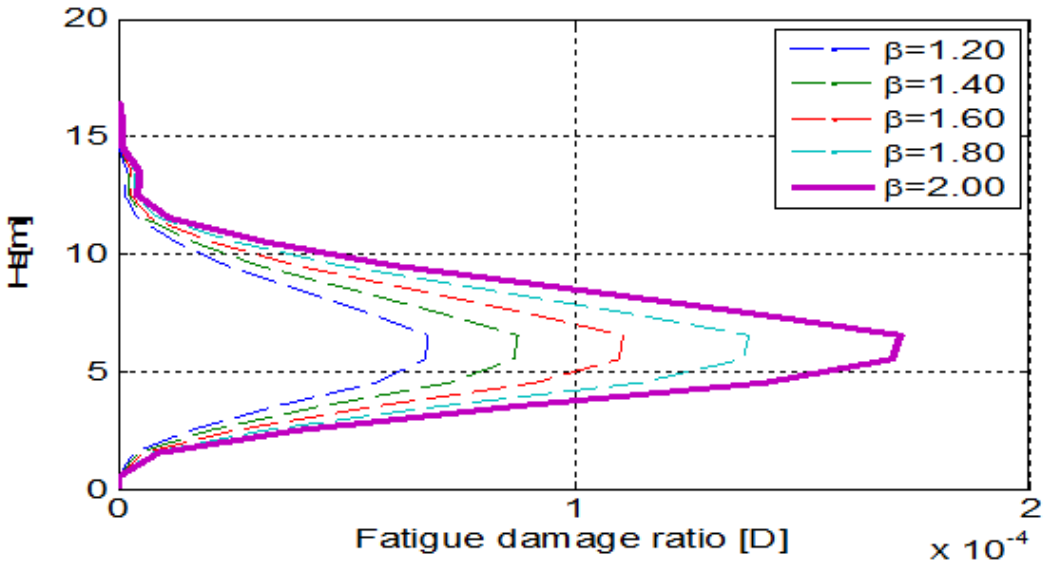

Figure 8.17: Fatigue accumulation for the third study case, with straight S-N curve with m=5

segment. As shown in the Figure 8-17 and Appendix D.2 in Table 10, the fatigue damage distributions versus significant wave heights and their magnitude is equivalent to the base case.

8.8 Discussion

In the previous sections, the fatigue damage accumulation on the structural detail under consideration was calculated in three study cases, namely base primary study case, secondary study case (deviated RAOs), and third case study (single slope S-N curve). In the base or primary study case the Best fit RAO and double slope "T" S-N curve are used for the damage analysis. The results for these three study cases are presented in the Figure 8-18. The figure is drawn as the fatigue damage accumulation in the horizontal axis Vs. significant wave height, H_s, in the vertical axis. It should be noted that the stress range distribution is represented by the Rayleigh probability density function in this part, i.e.$\beta = 2$.
Base on the Base case in Figure 8.18, the fatigue damage accumulation is concentrated in the sea states of moderate severity, i.e. sea states with significant wave height in the range of 4m – 8m. In this case, around 60% of the total accumulated fatigue was found from these sea states. This is because, these sea states are more than the higher sea states as in Table 8-1 and they have higher standard deviation consequently higher stress range distribution than the lower sea states. As discussed in section 8.5, higher sea states have higher stress ranges, $\Delta\sigma$, and higher stress ranges have less number of stress cycles to failure, N, which implies higher fatigue damage on the structural detail, see Miner-Palmgren formula (8.14). Thus, even though the moderate sea states are less than the lower sea states, they could cause higher fatigue damage due to their higher stress ranges.

In Figure 8.18, one can notice that the curves for the Base case, Deviated RAO at [0-0.39] and lower single S-N curve are overlapping. This shows that the fatigue damage for the

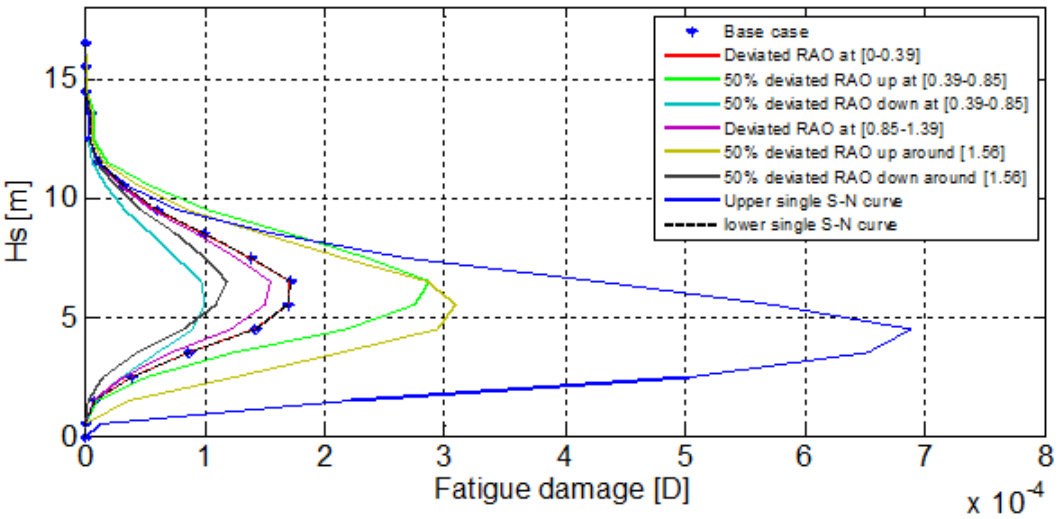

Figure 8.18: Fatigue damage on tubular structure joint vs. H_s

base case, for the secondary case when the Best fit RAO is deviated at the beginning [0-0.39] and for the third case where the "T" S-N curve is represented with the lower single slope $m = 5$ are equivalent. This is can be due to the following reasons:

- Deviating or shifting the Best fit RAO at lower frequencies [0-0.39] had no effect on the standard deviation of the response process, which could affect the stress range distribution function.
- The stress ranges, $\Delta\sigma$, on the structural detail under consideration were less than 83.4 MPa for all the sea states used for this analysis. This stress range value is the stress range at which the two segments of the "T" S-N curve meet and this stress range corresponds to 10^6 cycles, see Figure 8.18.

When the "T" S-N curve is assumed to be represented with a straight slope $m = 3$, the fatigue damage was increased by large quantity relative to the base case as shown in the Figure 8-18. In this case, it was found that around 66% of the total fatigue accumulated in the structural detail came from relatively lower sea states, i.e. sea states with significant wave height in the range of 2m – 6m.
When the upper segment of the "T" S-N curve was assumed to be extended as shown in Figure 8-19, the number of stress cycles to failure, N, for all stress ranges, $\Delta\sigma$, below 83.4 Mpa reduced. Based on the Miner-Palmgren formula, equation 8.14, it has been shown that the number of stress cycle to failure is inversely proportional to fatigue damage also. Thus, reducing the number of cycles to failure, N, means increasing the fatigue damage. Above it has been said that the stress ranges for all sea states in this analysis are below 83.4MPa which indicates that fatigue damage due to these sea states are over estimated.

In the Rayleigh stress range probability function, section 8.5, it has been observed that the stress ranges for lower sea states are concentrated on the lower value of the distribution. Consequently, for the double slope S-N curve, the fatigue damage due to the lower sea stats is very small compared to the moderate sea states. However, when the upper segment of the "T" S-N curve is assumed to be continuous as shown in Figure 8-19, the fatigue damage accumulation difference due to the stress range distribution between lower and

moderate sea states is relatively reduced. This is because the extended S-N curve has higher slope than the lower curve. Therefore, since the fatigue damage difference due to stress range distribution is minimized and there are higher number of lower sea states in the analysis, the fatigue damage due to these lower sea states could be higher than the moderate as shown in Figure 8-18.

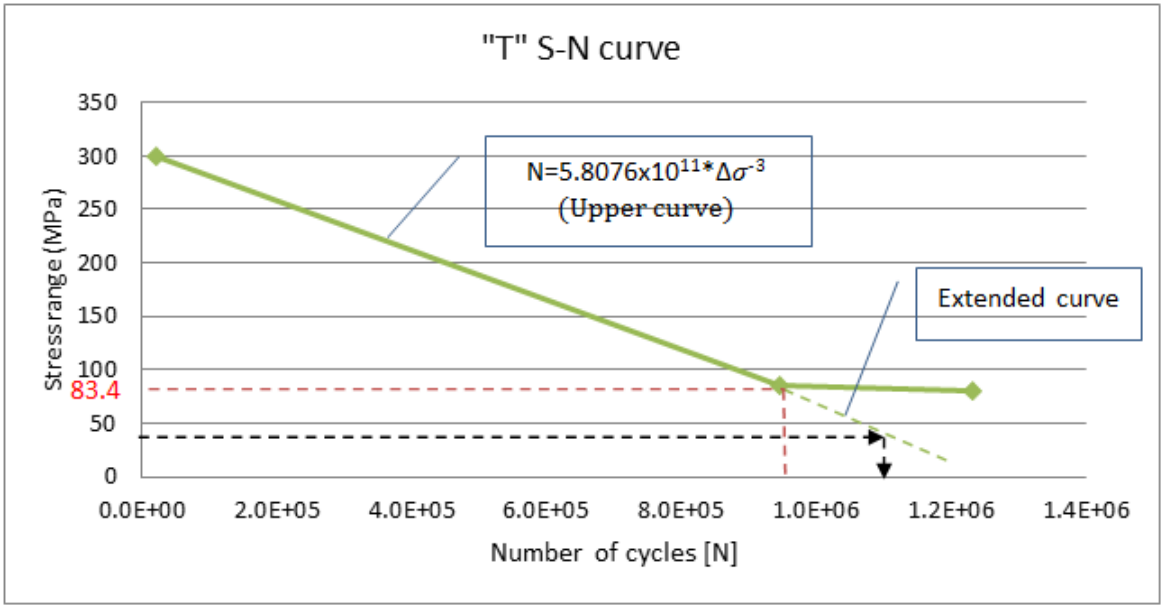

Figure 8.19: "T" S-N curve as a single slope segment

When the Best fit RAO is deviated at different frequency ranges, generally the fatigue damage increased if the RAO is shifted up and reduced if moved down, but the cumulative damage is still concentrated within the moderate sea states. The effect of the deviated RAOs for the fatigue damage is illustrated below by assuming 3-hour duration single sea state with 8m significant wave height, H_s, and 10sec spectral peak period, T_p.
As in section 8.4, response spectrum is determined from the RAO of the system and the wave spectrum of a given sea state. This indicates that for every deviated RAO, there may be different response spectrum, i.e. different standard deviation and different stress range distribution for the given sea state as shown in Table 8-3.

Table 8.3: Standard deviations and fatigue damage based on the Best fit RAO and the deviated RAOs for a given sea state.

	Base case	*Deviated RAO at [0-0.39]*	*50% deviated RAO up at [0.39-0.85]*	*50% deviated RAO down at [0.39-0.85]*	*Deviated RAO at [0.85-1.39]*	*50% deviated RAO up around [1.56]*	*50% deviated RAO down around [1.56]*
σ_{rr}	1.498	1.498	1.659	1.341	1.455	1.673	1.385
D(10^{-7})	2.9708	2.9708	3.8102	2.277	2.706	4.727	2.012

Stress range for short term duration is modeled by Rayleigh distribution function, equation 8.22. Using this distribution and standard deviation from Table 8-3, the stress range distribution of the six deviated RAOs and the base case, Best fit RAO, are given in Figure 8-20.

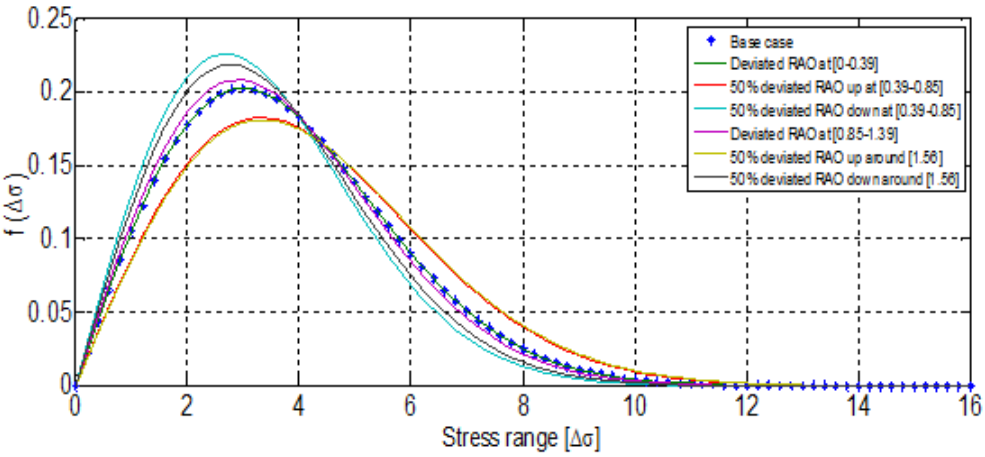

Figure 8.20: Variation of stress range distribution due to the deviated RAOs

In Figure 8-19, it can be noticed that when the Best fit RAO is deviated by 50% up in the major wave frequency regime, [0.39-0.85], and around the natural frequency of the jacket, [1.56], their corresponding distribution curves covers wider stress ranges than the base case, i.e. higher standard deviation as shown in Table 8-3. As mention above also larger stress ranges have less number of stress cycles to failure, N, and less number of cycles to failure means higher fatigue damage on the structural detail as shown in Figure 8-18 and table 8-3. Similarly, when the Best fit RAO is shifted by 50% down, their corresponding distribution curves covers smaller stress ranges than the base case, as a result low fatigue damage on the structural detail, see Figure 8-18 and Table 8-3.

Chapter 9

CONCLUSION AND RECOMMENDATIONS

9.1 Summary

In this section the main points of the project discussed in details in the previous chapters will be summarised.

First an introduction study has been done about offshore structures and their classification based on their dynamic behavior and cross sectional dimension relative to wave height, H. Offshore structures are classified as linear and non-linear mechanical systems as summarized below.

- Linear mechanical systems are structures where their damping and stiffness coefficients remain constant under the applied the time varying hydrodynamic loads. This means the structures are in elastic state or Hooke's law is valid under the whole process. Responses of these types of structures are determined by solving equation 2.2. Further, linear structures are also classified as:
  - Quasi-static structures: are structures where their relative frequency is much smaller than one $\beta \ll 1$. In this case the dynamics is controlled by the stiffness of the system in phase with the loading. For example structures with natural period less than 2 seconds (Haver, 2013).
  - Dynamically behaving structures: are structures where their relative frequency is close or much larger than one, $\beta \ll 1$. In this case the dynamics is controlled by the damping and mass of the system by 90^0 and 180^0 out of phase respectively. Examples of these type structures are structures with natural period larger than 2 seconds such as the Kvitebjørn platform (Haver, 2013).
  - Linear response problems: are linear structures where the hydrodynamic loads on them can be modeled as a linear function of the surface process and this can be applied when the inertia/mass term of the Morison's equation (3.5) dominated to the non-linear drag term. Inertia/mass term is dominant in large volume structures such as floating platforms, see Figure 3-8, and in more slender structures such as jacket and jack-up platforms as shown in Figure 3-9.
- Non-linear mechanical systems: are structures where their stiffness and damping coefficients change with time under the time varying hydrodynamic loading, which

means the structures are in their plastic regime and the Hooke's low is not valid. Responses of these structures are determined by solving the general equation of motion (2.1).

  - Non-linear response problems: are opposite to the linear response problems, in which the drag term of the Morison's equation dominates the inertia or mass term. As shown in equation 3.8 and Figure 3-7, drag term dominates when the wave height is much larger than the structural cross sectional dimension.

In order to determine good estimate of Best fit RAO of the Kvitebjørn platform, 21 time series wave records and their corresponding time series responses (axial loads) on leg A1 and A2 at 109m below SWL has been taken. These time series records have been transformed from time domain in to frequency domain by Fast Fourier Transfer (FFT) method. Findings during these transformations are described below.

- Estimation of wave spectrum or transforming time domain wave records in to frequency domain:
  - During the transformation process, it has been seen that wave spectrum for a given time series is not unique. The shape of the spectral curve, i.e. distribution of energy in the process, significant wave height, H_s, and spectral peak period, T_p, slightly changed as the value of data point, N, changed as in Figure 4-1 and Table 4-2. As shown in Figure 4-1, it has been found that as the number of data points, N, increases the sharper is the spectral curve and smoother is as the data point decreases
  - The first four estimated wave spectra are compared with the Pierson-Moskowitz (PM) and JONSWAP (J) spectrum as shown in Figure 4-7. As in Table 4-3, it has been observed that the Pierson-Moskowitz spectrum gave best approximation. This may imply that these waves were fully developed and windy generated waves.
- Estimation of response spectrum or transforming time domain response records in to frequency domain:
  - After transforming the time domain response records in to frequency domain, the wave spectra peak periods, T_p, with the response periods, $T_s.peak$, where the response reached maximum around T_p are compared, similarly the response peak period, $T_r.peak$, and the natural period of the jacket as shown in Table 5-1. Then, it has been observed that they have almost equal values with slight difference which indicates that the response energies were more around the spectral peak period, where the wave energies are concentrated, and there were high energies lost at resonance to control the resonance induced dynamics. The slight differences observed i.e. T_p vs. $T_s.peak$ and natural period Vs $T_r.peak$, may be there were secondary additional environmental loads, see Figure 3-1, during the recording time.

After having the estimated wave spectra and response spectra for the 21 time series records, the RAOs are estimated using the spectral relation equation (6.1). But to check the linear correlation between the incident waves and their corresponding responses on the jacket, the Coherence function analysis have been done. This

analysis has been performed in order to determine frequency ranges where the RAOs can be relatively trusted. During these processes the following remarks have been observed:

- When a RAO was estimating, uncorrelated signal noises were produced especially at the beginning and at the tail end of the RAO as shown in Figure 6-1. These were minimized by applying a band pass filtered with a cut off lower frequency, $\omega_1 = 0.02$, and higher frequency, $\omega_2 = 0.4$, as shown in Figure 6-2. However, still there were leakages of neighboring frequencies in the filtering process.
- Generally the linear correlation between the incident waves and their corresponding responses has been found low as shown in Figures 6-11 to 6-14 and Appendix C.2. Thus, due to the low correlations and leakages of unwanted frequencies during filtering process, possible deviations of the Best fit RAO at different frequency ranges has been done.

After the Best fit RAO of the jacket is estimated, the fatigue damage on the structural detail under consideration due to the short term sea states has been determined using the closed N-S approach. During this analysis the following findings have been observed:

- For the base/primary study case, Best fit RAO and double "T" S-N curve , around 60% of the fatigue damage was accumulated from the sea states within the range 4 to 8 significant wave height, mainly from sea states within the range of 6m – 7m significant wave heights as in Figure 8-8 or Table D-1. This was because these sea states were more than the higher sea states, see table 8-1, and had higher stress range values or higher standard deviation than the lower sea states. Similarly it has been found that the Weibull shape parameter, β had no effect on the damage versus sea state severity, however the damage decreased as the parameter value decreased, see Figure 8-8.
- When the best fit RAO was deviated at [0-0.39], the fatigue damage and its distribution versus H_s was equivalent to the base case, see Figure 8-18, which showed that this deviation had no effect on the stress range distributions or standard deviation of the response process, see table 8-3.
- When the Best fit is deviated by 50% in the major wave frequency regime [0.39-0.85] and around the natural frequency of the jacket [1.56], similar to the base case, majority of the fatigue damage were from the moderate sea states. However, the fatigue damage due to each sea state range increased when the Best fit RAO shifted up and reduced when it was shifted down. This was because, the standard deviations of the response process/stress ranges increased when the RAO shifted up and decreases when the RAO is shifted down see Table 8-3.
- When the lower segment of the "T" S-N curve was assumed to be continuous, straight S-N curve with slope m=5, the fatigue damage has been found equivalent to the base case, which showed that the stress ranges for all sea states included in the analysis had less or equal to 83.4 MPa.
- When the upper segment of the "T" S-N curve was assumed to be continuous, straight S-N curve with slope $m = 3$, the fatigue damage has been found to

be too high relative to the base case. The reason was that the extended curve reduces the number of cycles to failure, N, which is inversely proportional to fatigue damage, see Miner-Palmgren formula (8.14). In this case, it was observed also that major of the fatigue damage was accumulated from sea states of lower severity, i.e. sea states with significant wave height in the range 2m – 6m. This is because the extended curve over estimated the fatigue damage especially due to the lower sea states.

9.2 Conclusion

Based on the investigation that has done in this thesis, the major findings are listed below:

- As the general expectation, majority of the fatigue damage comes from sea states of moderate severity, i.e. sea states with significant wave heights between 4 and 8m.
- Straight S-N curve with slope m=3, upper segment to be continuous, can be adopted, but it over estimates the fatigue damage especially due to lower sea states.
- Straight S-N curve with slope m=5, lower segment to be continuous, can be adopted, but it can over estimate fatigue damage due to higher sea states, if their stress range is greater than 83.4MPa in case of tubular structural details.

9.3 Recommendation and Future Work

In chapter 8.6, numbers of assumptions have been considered to determine the fatigue damages on the tubular structural detail. But some of these assumptions might alter the results, if they could have been taken in to consideration. For example:

- The waves could have been considered to come from different directions.
- The variation of the stress ranges could be assumed as a broad band and random Gaussian process.
- The jacket could be assumed as a non-linear mechanical system, i.e. the structural members of the jacket will remain in their elastic limit state under the applied hydrodynamic loads.
- The jacket could be assumed as a non-linear mechanical system, i.e. the structural members of the jacket will remain in their elastic limit state under the applied hydrodynamic loads.

REFERENCES

[1] A.Almar-Næss. *Fatigue Handbook Offshore Steel Structures*. Tapir, Trondheim, 1985.

[2] A.Hobbacher. Recommendation for fatigue design of welded joints and components, December 2008.

[3] S. K. Chakrabarti. *Hydrodynamics of Offshore Structures*. Computational Mechanics Publication, Southampton Boston, 1987.

[4] Subrata Kumar Chakrabarti. *Offshore Structure Modeling*, volume Advanced Series on Ocean Engineering - Volume 9. World Scientific Publishing Co. Pte. Ltd., Plainfield,Illinois, 1994.

[5] DNV-RP-C203. Fatigue design of offshore steel structures, April 2010.

[6] DNV-RP-C205. Environmental conditions and environmental loads, October 2010.

[7] DNV-RP-H103. Modelling and analysis of marine operations, April 2011.

[8] Sverre K Haver. Prediction of characteristic response for design purposes, March 01 2013.

[9] Cheung Hun Kim. *Nonlinear waves and offshore structures*, volume 27. World Scientific publishing Co.Pte.Ltd., Texas A & M University, USA, 2008.

[10] Ivar Langen. *Dynamik analyse av konstruksjoner*. TAPIR, 1979.

[11] D.E. Newland. *An Introduction to Random Vibrations, Spectral and Wavelet Analysis*. Dover publication Inc., New york, third edition, 2005.

[12] Jonas Odland. Offshore field development, November 2012.

[13] American Bureau of Shipping ABS Plaza. Fatigue assessment of offshore structures, April 2003.

[14] NORSOK standard N-003. Action and action effects, September 2 2007.

[15] IB A. SVENDSEN and IVAR G. JONSSON. *Hydrodynamics Of Coastal Regions*. Den Private Ingeniørfond Technical University Denmark, Stougaard Jensen/København, 1980.

[16] Ole David Økland. Kvitebjørn jacket analysis. Report, SINTEF, 2006.

[17] Ole David Økland. Fatigue assessment for kvitebjørn jacket. Report, Norwegian Marine Technology Research Institute, 2010.

APPENDICES

Appendix A: Estimation of Wave Energy Spectral Density

A-1: Estimated Wave Energy Spectral Density from Test Conditions

As described in chapter 4.3.2, 21 wave spectra are estimated for each time series wave record listed in Table 4-1 using the FFT method. In this process, for each test condition of total data length ,$T_s = 1200$ sec, is divided in to nine numbers of segments, each one having 1024 data pints and time increment of 0.1302 second. Figure below show estimated wave spectra from test.con 5-21.

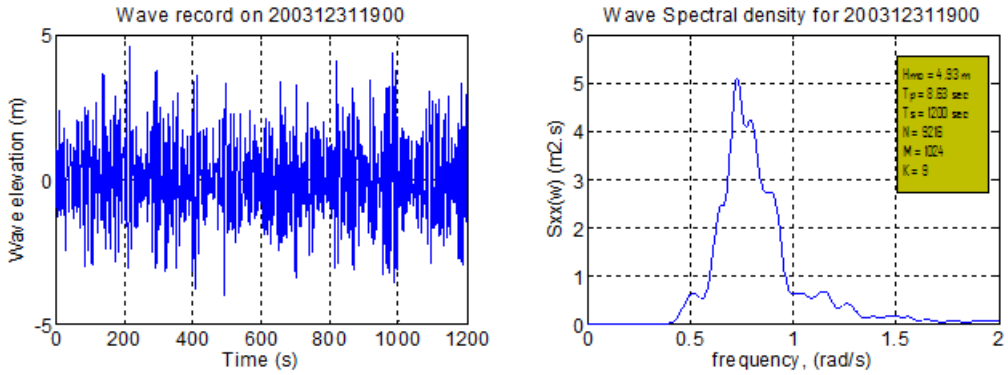

Figure 1: Time series wave records and estimated wave spectrum for test.con 5.

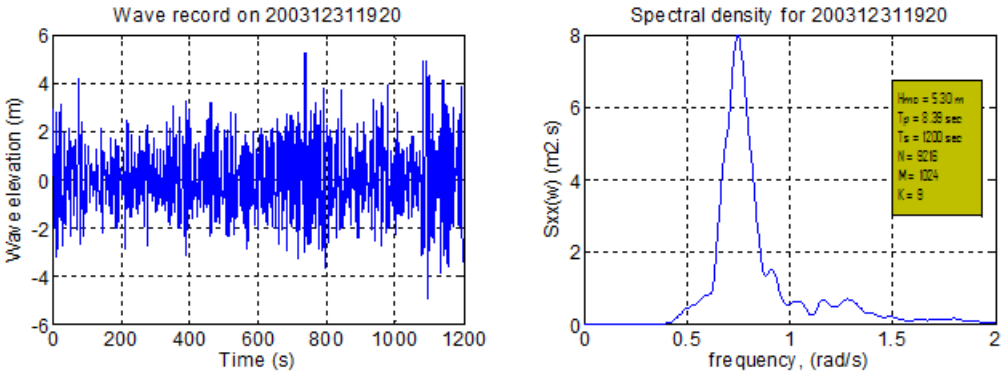

Figure 2: Time series wave records and estimated wave spectrum for test.con 6.

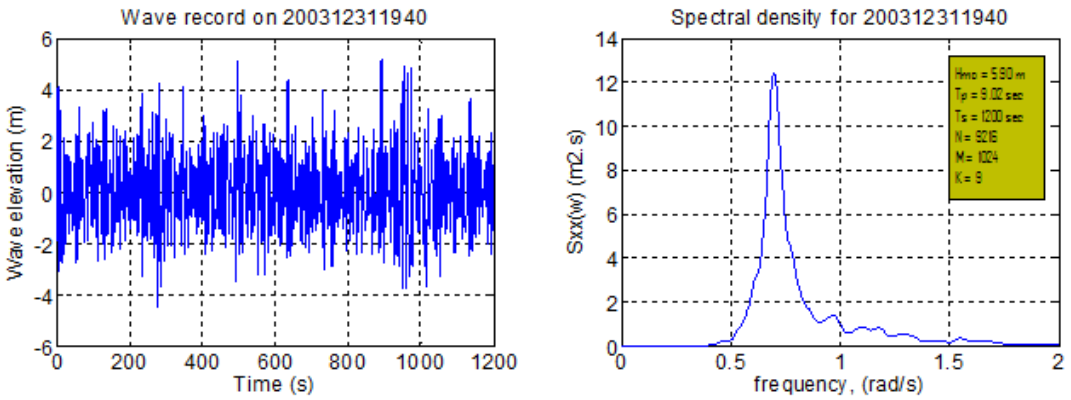

Figure 3: Time series wave records and estimated wave spectrum for test.con 7.

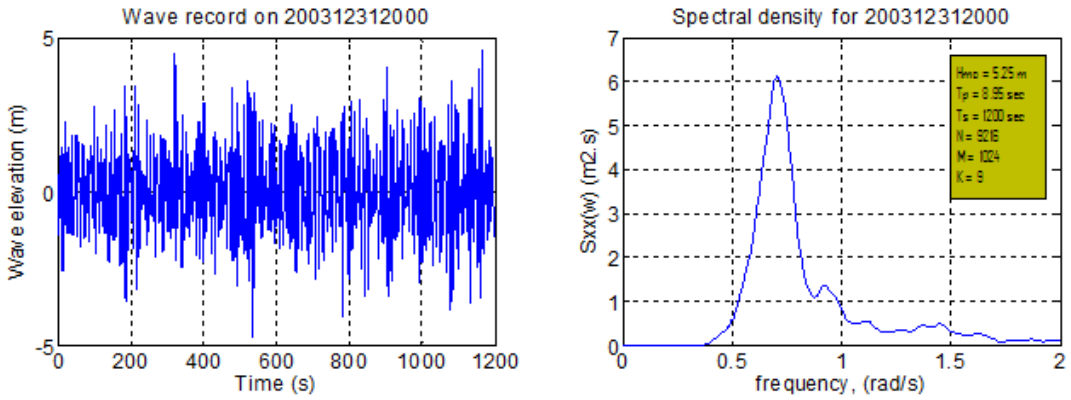

Figure 4: Time series wave records and estimated wave spectrum for test.con 8.

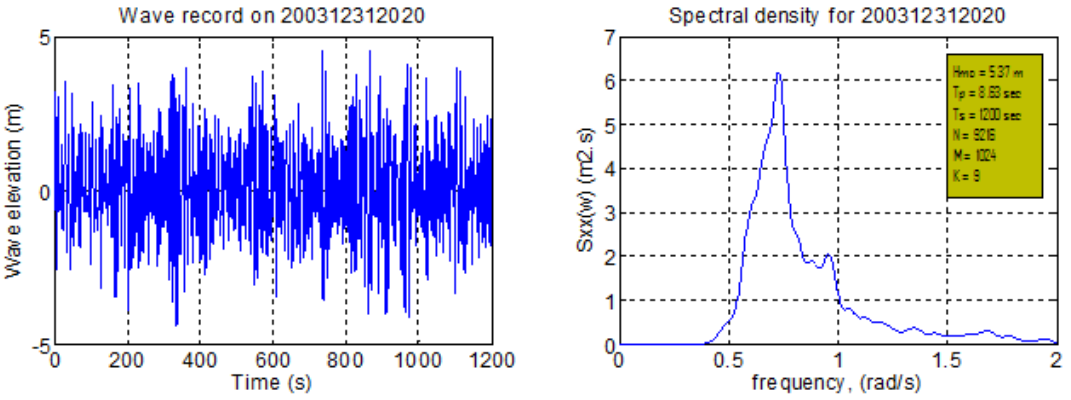

Figure 5: Time series wave records and estimated wave spectrum for test.con 9.

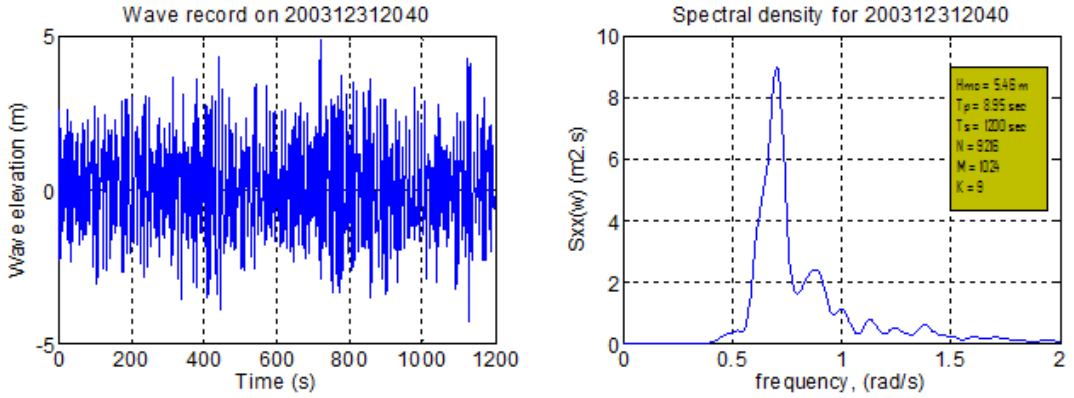

Figure 6: Time series wave records and estimated wave spectrum for test.con 10.

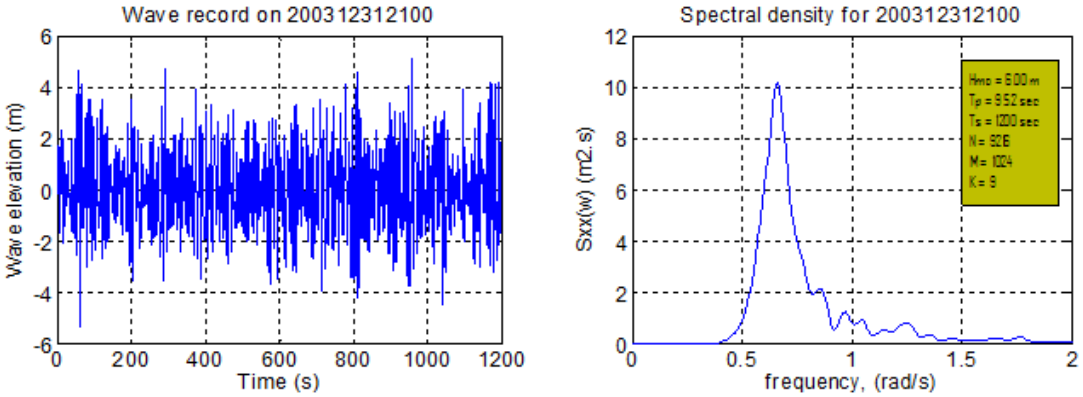

Figure 7: Time series wave records and estimated wave spectrum for test.con 11.

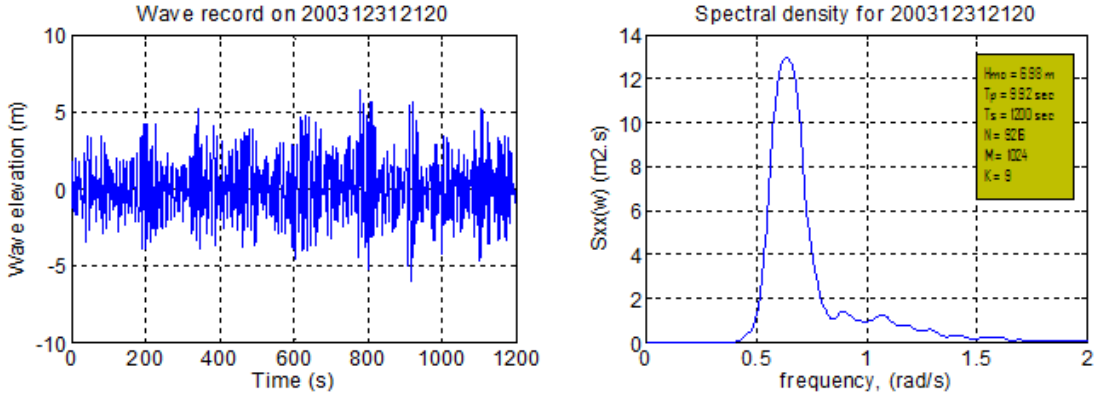

Figure 8: Time series wave records and estimated wave spectrum for test.con 12.

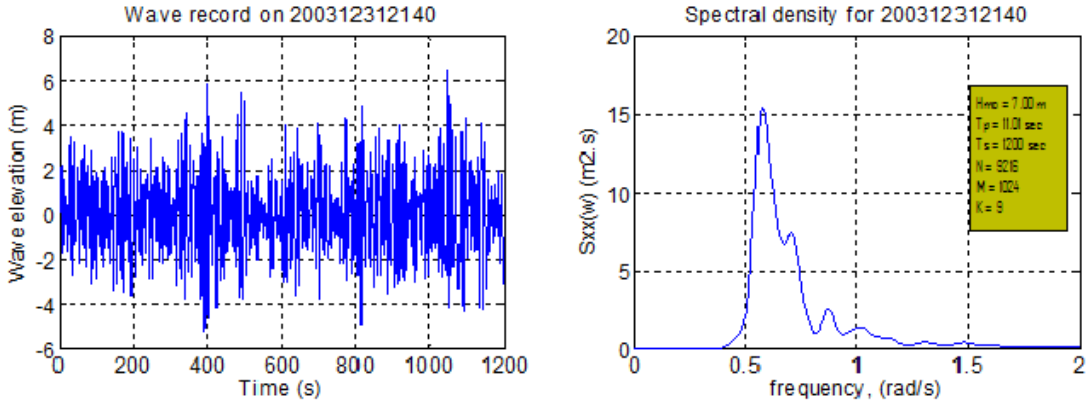

Figure 9: Time series wave records and estimated wave spectrum for test.con 13.

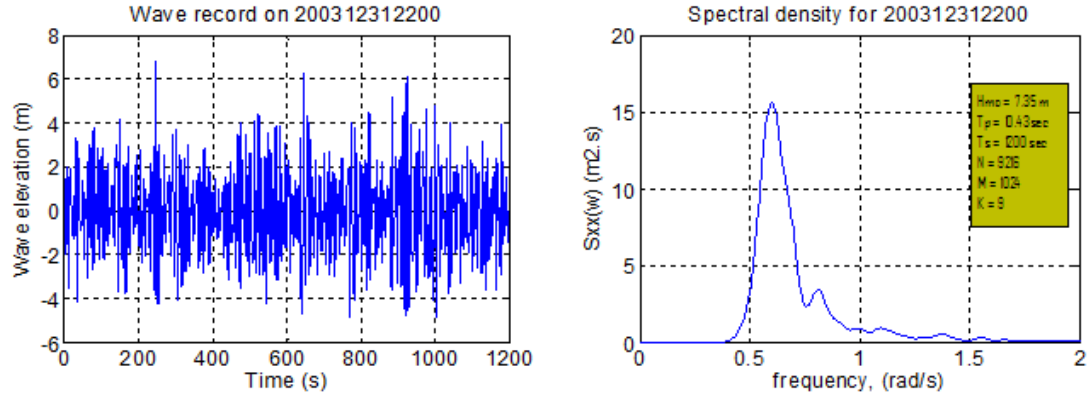

Figure 10: Time series wave records and estimated wave spectrum for test.con 14.

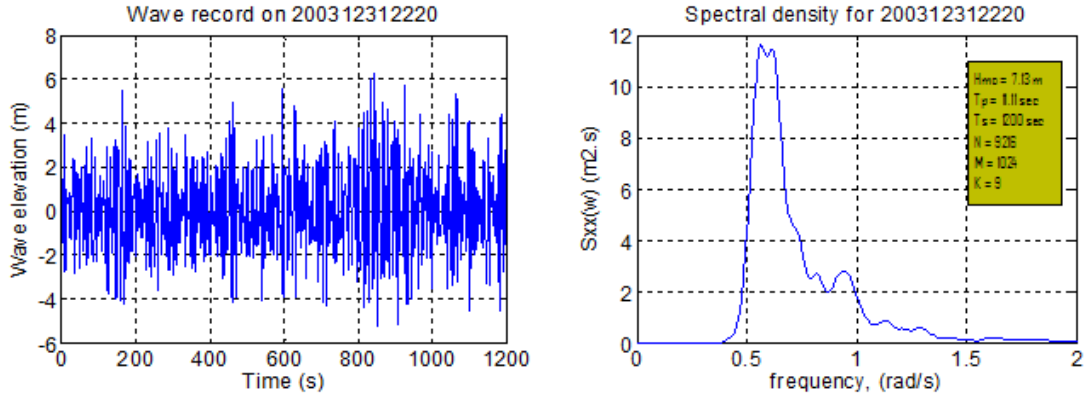

Figure 11: Time series wave records and estimated wave spectrum for test.con 15.

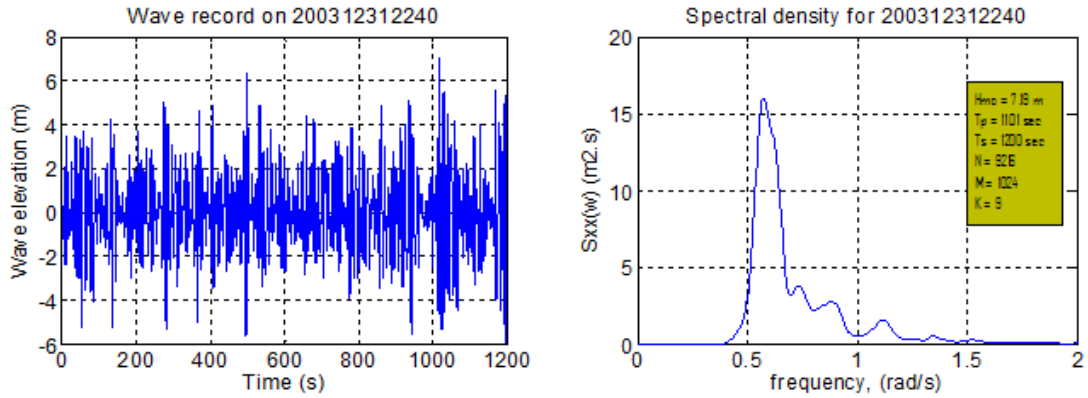

Figure 12: Time series wave records and estimated wave spectrum for test.con 16.

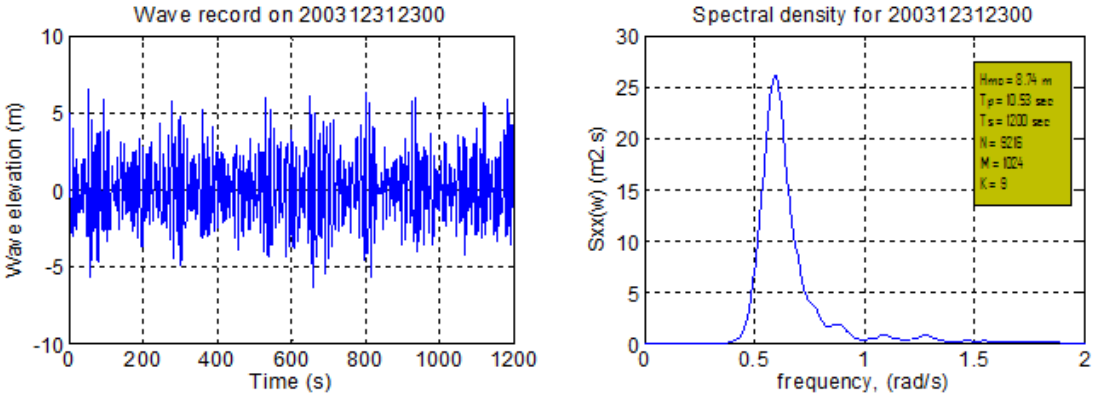

Figure 13: Time series wave records and estimated wave spectrum for test.con 17.

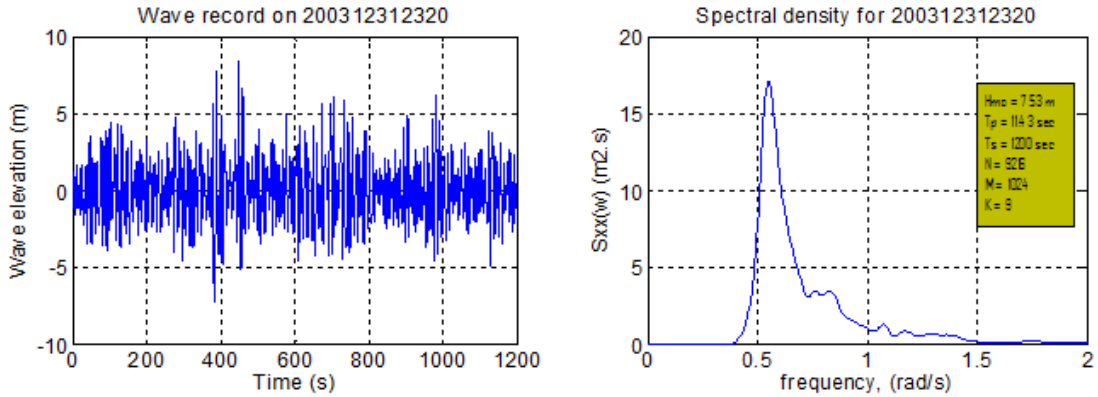

Figure 14: Time series wave records and estimated wave spectrum for test.con 18.

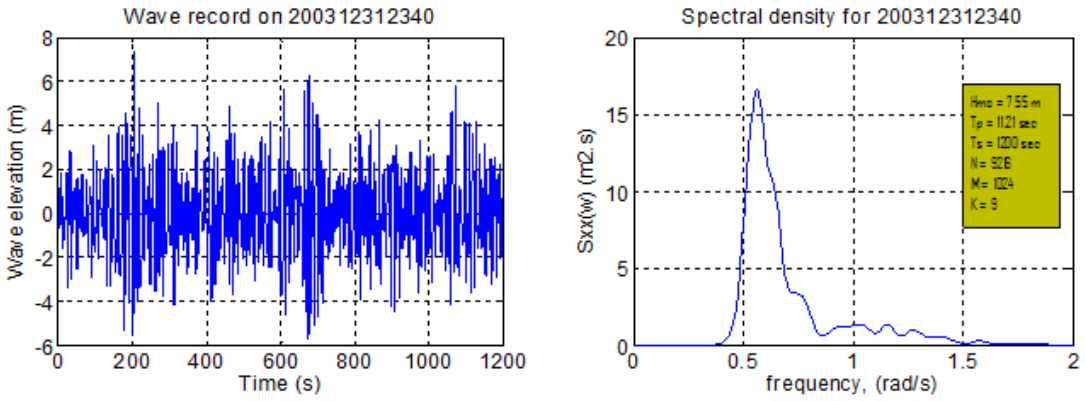

Figure 15: Time series wave records and estimated wave spectrum for test.con 19.

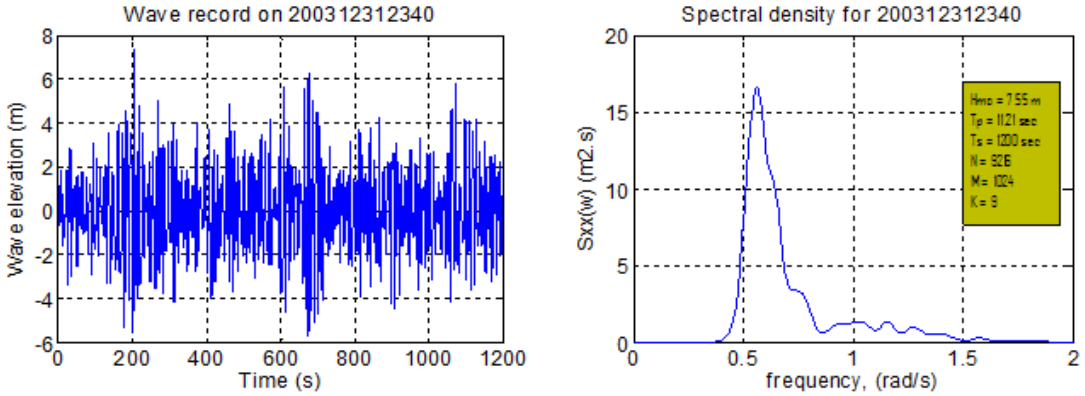

Figure 16: Time series wave records and estimated wave spectrum for test.con 20.

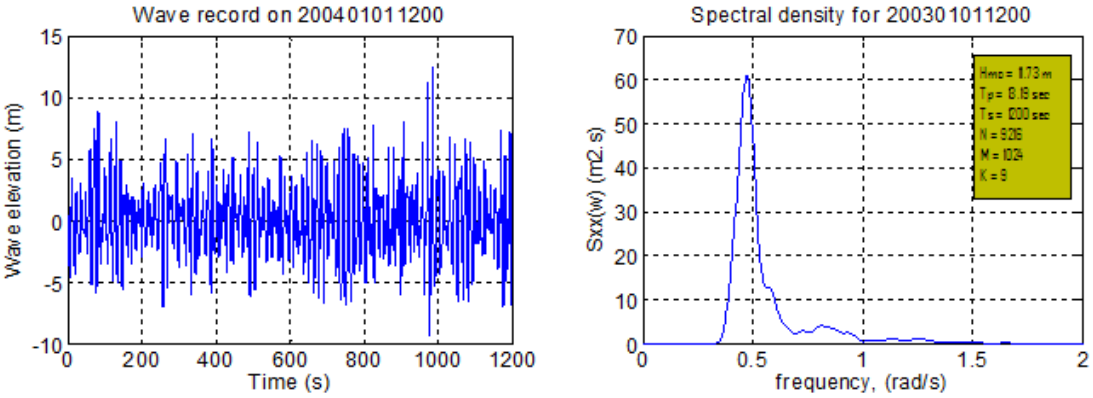

Figure 17: Time series wave records and estimated wave spectrum for test.con 21.

A-2: Standard Wave Spectrum

The Pierson-Moskowitz (PM) Wave Spectra)

The Pierson-Moskowitz spectrum was originally developed for fully-developed wind sea state, i.e. when the growth of the waves is not limited by the size of the generation area called fetch length. The PM spectrum is applicable for major part of the time in the North Sea and it may be used for most fatigue analysis, (A.Almar-Næss, 1985). Pierson-Moskowitz spectrum, $S_{PM,\Xi\Xi}(\omega|H_s,T_p)$, formula is given by:

$$S_{PM,\Xi\Xi}(\omega|H_s,T_p) = \frac{5}{16} * H_s^2 * \omega_p^4 * \omega^{-5} * exp^{(-\frac{5}{4}*(\frac{\omega}{\omega_p})^{-4})} \tag{1}$$

where: H_s is the significant wave height in meter; $\omega_p = \frac{2\pi}{T_p}$ is angular spectral peak frequency in radian per second and T_P is the spectral peak period in seconds.

The JONSWAP (J) Wave Spectra)

The JONSWAP spectrum is an extension of the PM spectrum to include limited size of wave generation area and to describe developing sea states. This method can be used for extreme wave conditions in the North Sea, (A.Almar-Næss, 1985). With reference to (DNV-RP-C205, 2010), this specral standard is expected to be a reasonable model when the relation given below is sutisfied.

$$3.6 < \frac{T_p}{\sqrt{H_s}} < 5 \tag{2}$$

The JONSWAP spectrum, $S_{J,\Xi\Xi}(\omega|H_s,T_p)$, formula is given as:

$$S_{J,\Xi\Xi}(\omega|H_s,T_p) = S_{PM,\Xi\Xi}(\omega|H_s,T_p) * A_\gamma * \gamma^{exp^{(-0.5*(\frac{\omega-\omega_p}{\sigma*\omega_p})^2)}} \tag{3}$$

where: γ is dimensionless peak shape parameter; σ is spectral width parameter given as:

- $\sigma = \sigma_a$ for $\omega \leq \omega_p$
- $\sigma = \sigma_b$ for $\omega \geq \omega_p$

$\sigma_a = 0.07$ and $\sigma_b = 0.09$ $A_\gamma = 1 - 0.287 * ln(\gamma)$ is normilizing factor. Note that the JONSWAP spectrum reduces to Pierson-Moskowtz spectrum if the peak shape parameter, γ is one.

B: Estimation of Response Energy Spectral Density

B-1: Estimated Response Energy Spectral Density from leg A2

The following Figures show the estimated response spectrum based on the time series axial load records on Leg A2.

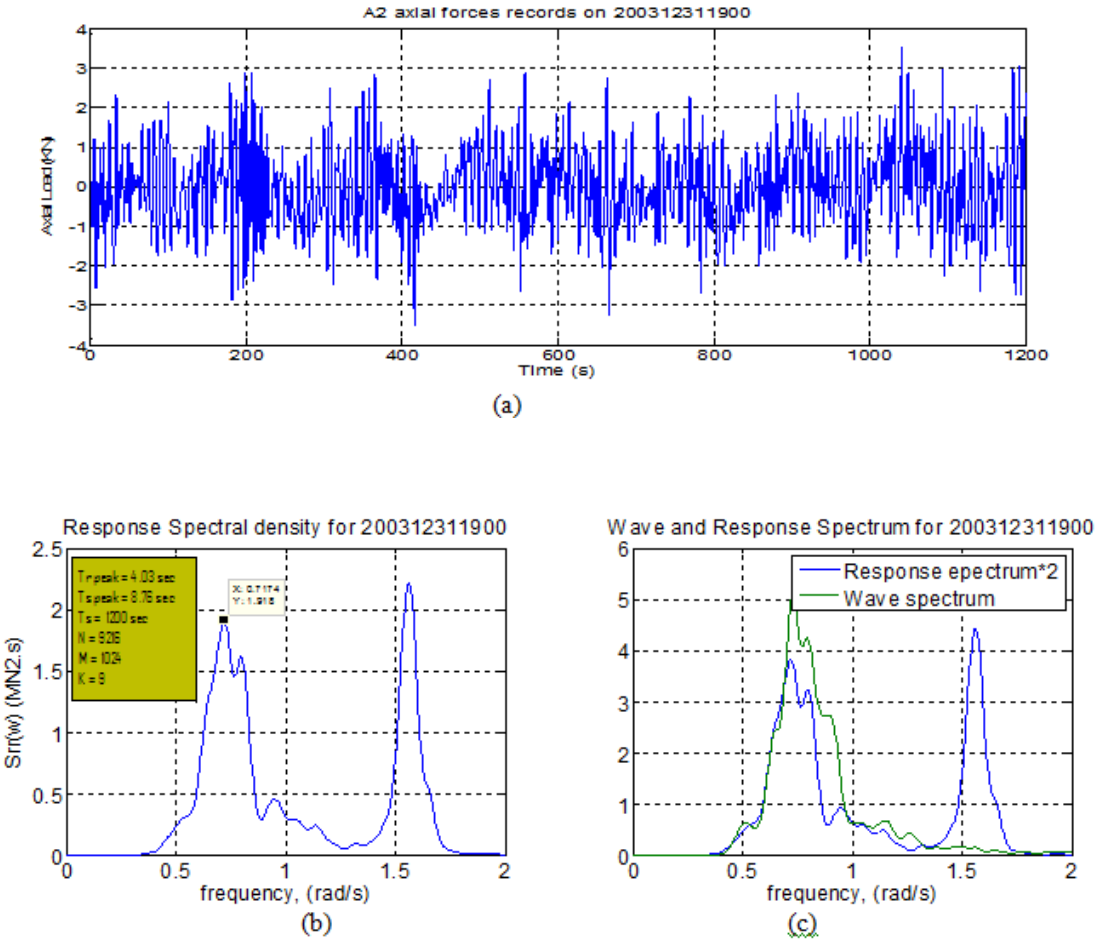

Figure 18: A2 time series response records (a), A2 response spectrum (b) and A2 response & Wave spectrum (c) during test.con5

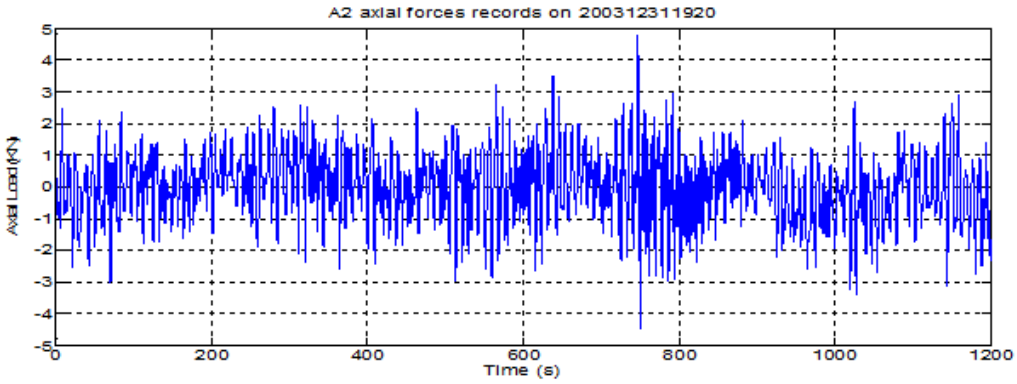

(a)

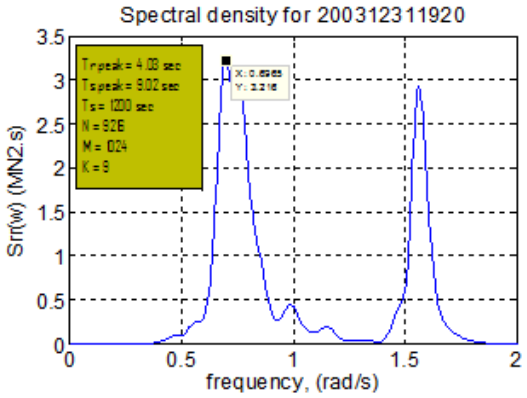

(b)

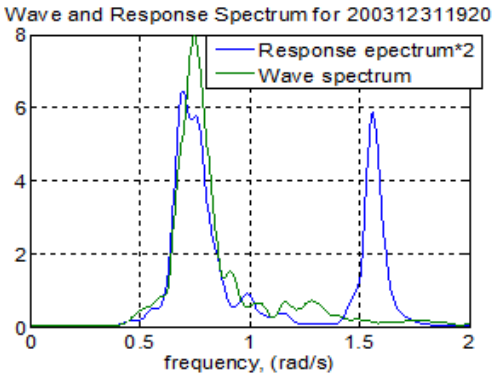

(c)

Figure 19: A2 time series response records (a), A2 response spectrum (b) and A2 response & Wave spectrum (c) during test.con6

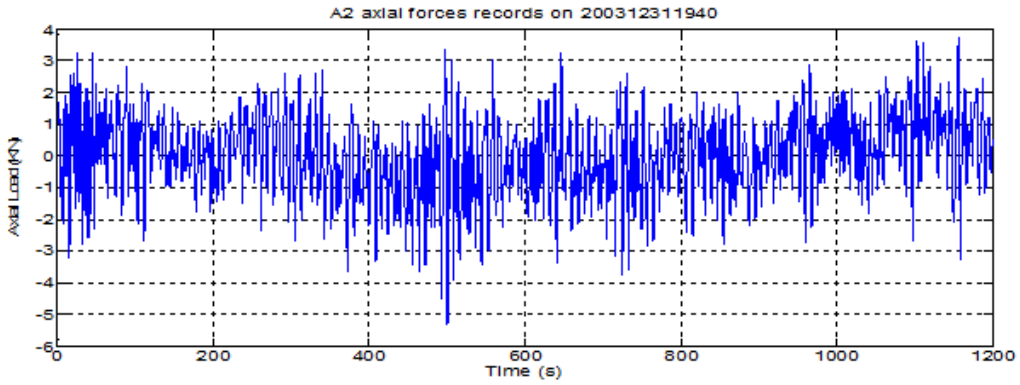

(a)

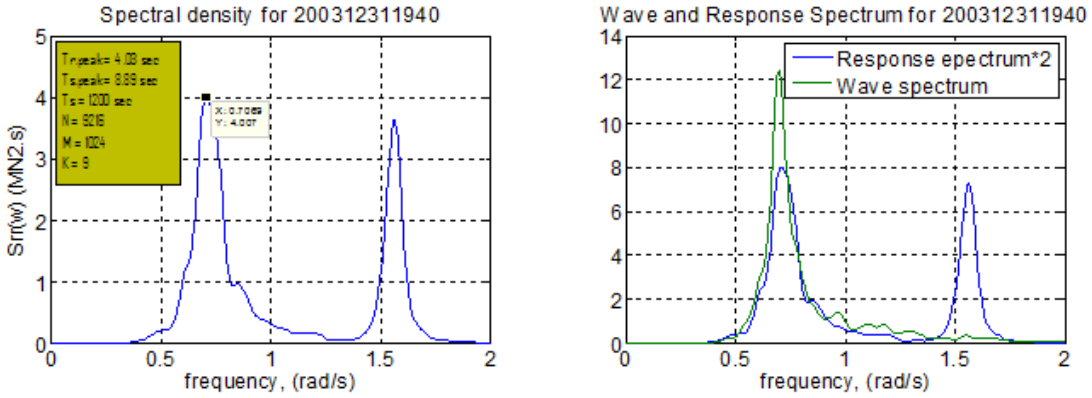

(b) (c)

Figure 20: A2 time series response records (a), A2 response spectrum (b) and A2 response & Wave spectrum (c) during test.con7

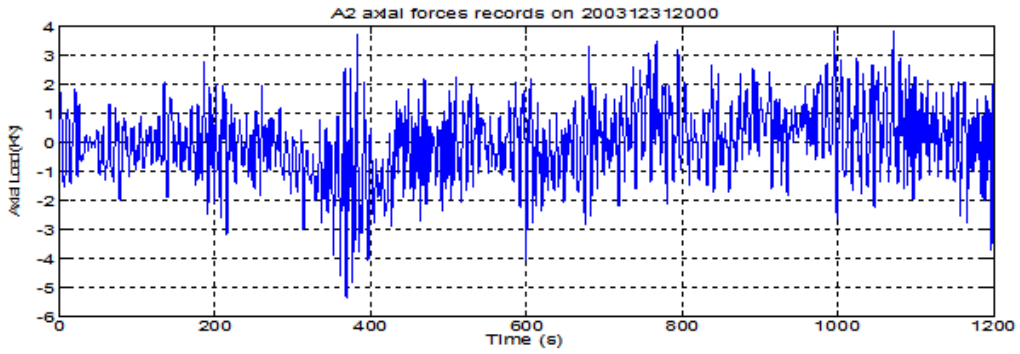

(a)

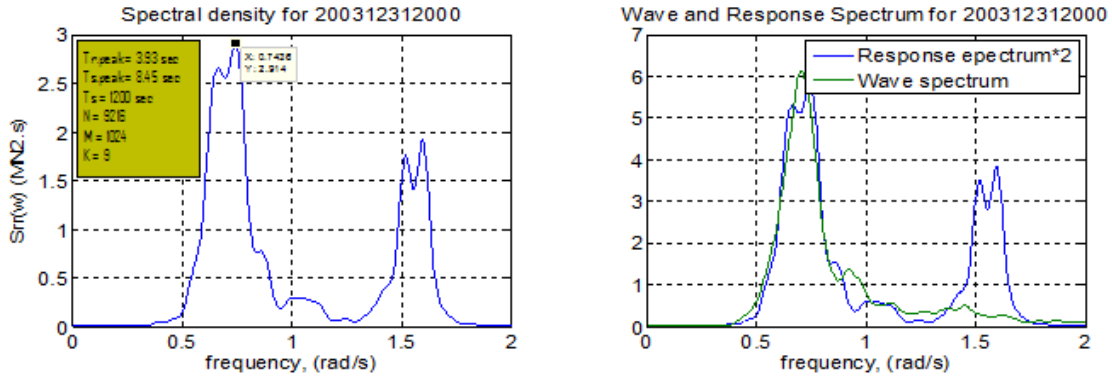

(b) (c)

Figure 21: A2 time series response records (a), A2 response spectrum (b) and A2 response & Wave spectrum (c) during test.con8

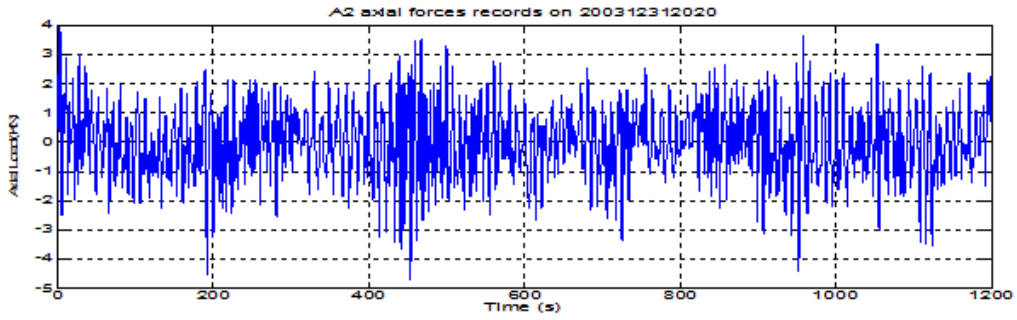

(a)

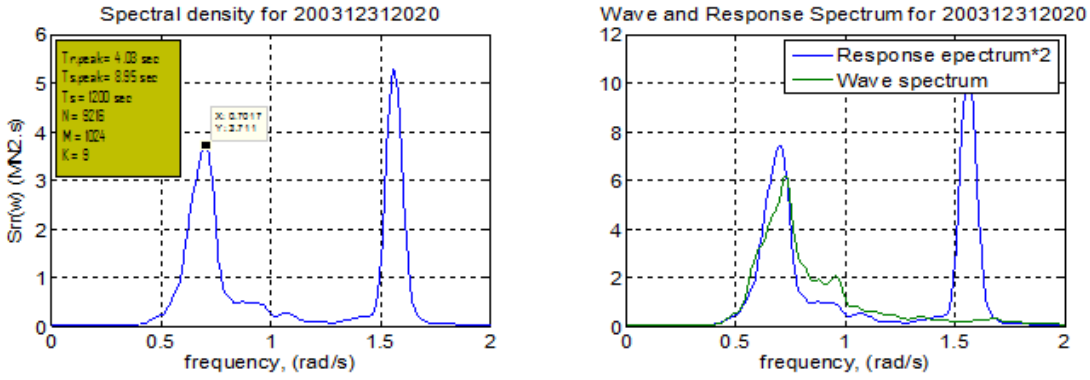

(b) (c)

Figure 22: A2 time series response records (a), A2 response spectrum (b) and A2 response & Wave spectrum (c) during test.con9

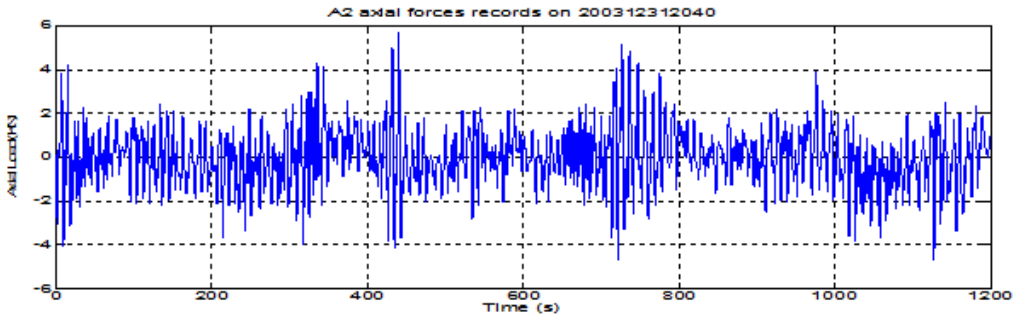

(a)

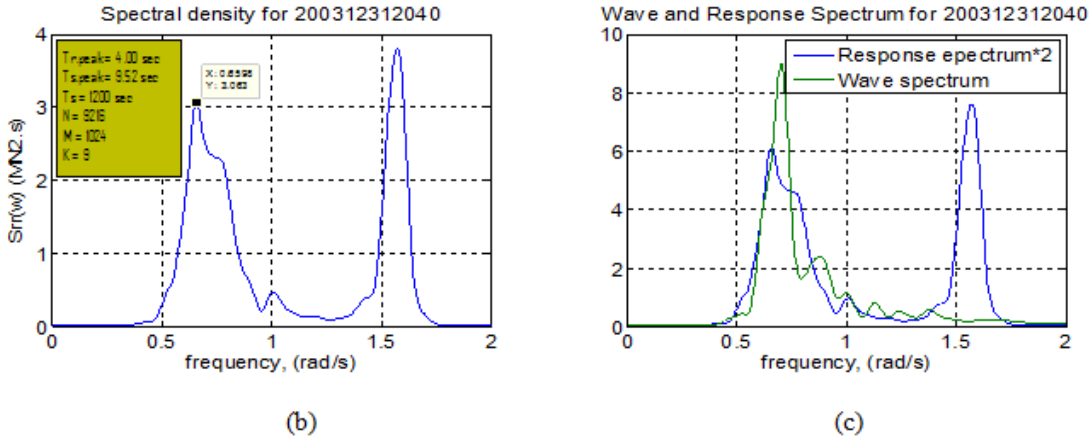

(b) (c)

Figure 23: A2 time series response records (a), A2 response spectrum (b) and A2 response & Wave spectrum (c) during test.con10

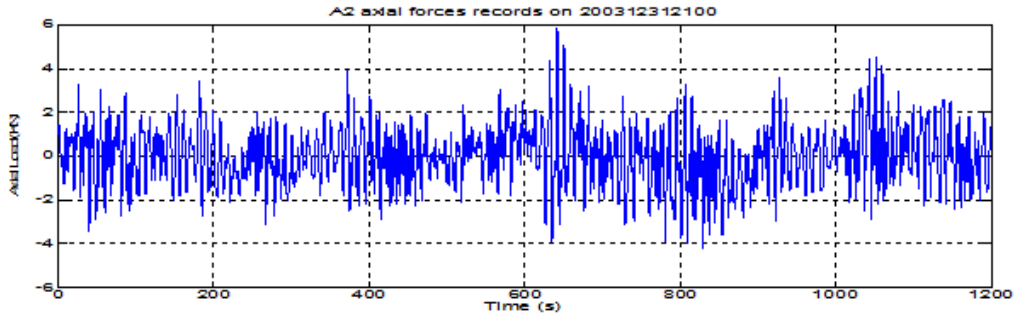

(a)

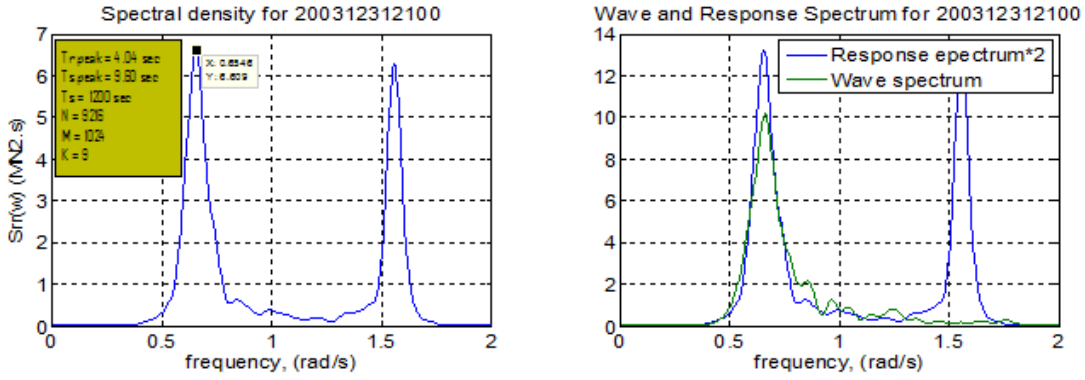

(b) (c)

Figure 24: A2 time series response records (a), A2 response spectrum (b) and A2 response & Wave spectrum (c) during test.con11

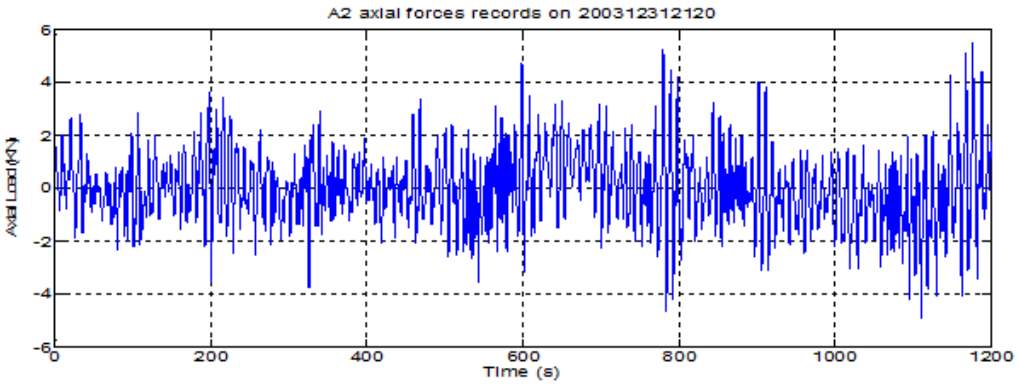

(a)

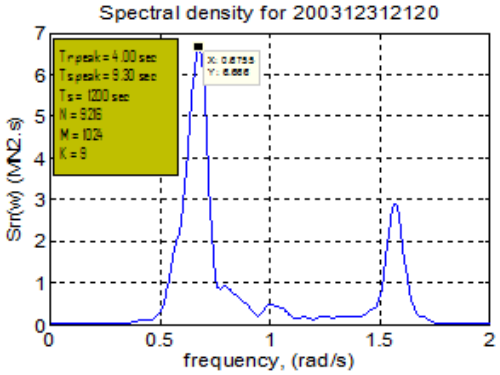

(b)

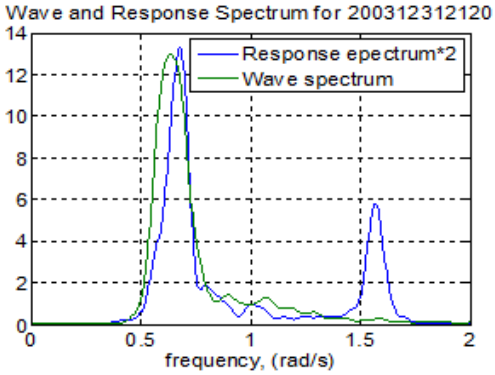

(c)

Figure 25: A2 time series response records (a), A2 response spectrum (b) and A2 response & Wave spectrum (c) during test.con12

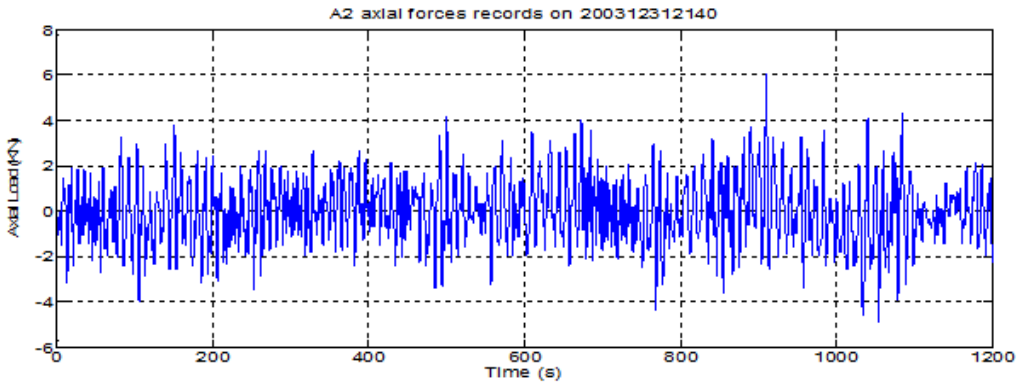

(a)

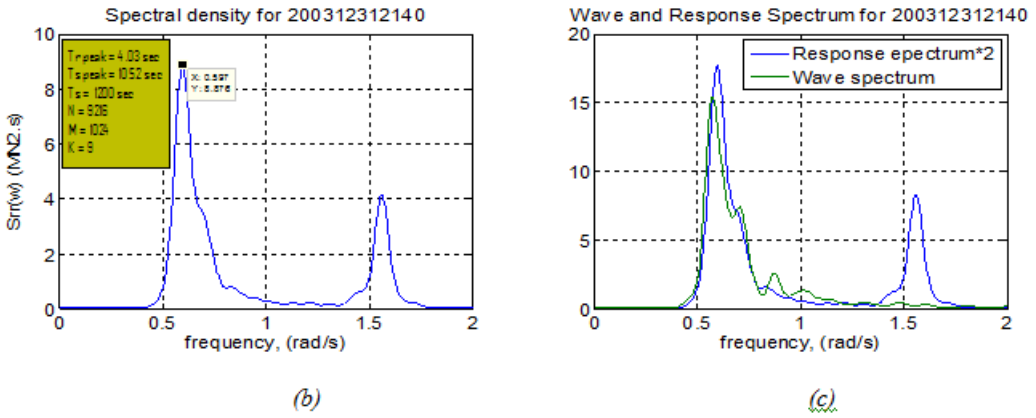

(b) (c)

Figure 26: A2 time series response records (a), A2 response spectrum (b) and A2 response & Wave spectrum (c) during test.con13

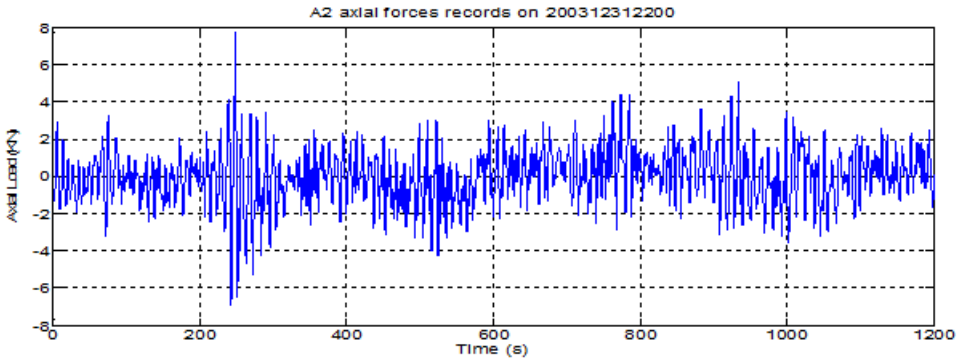

(a)

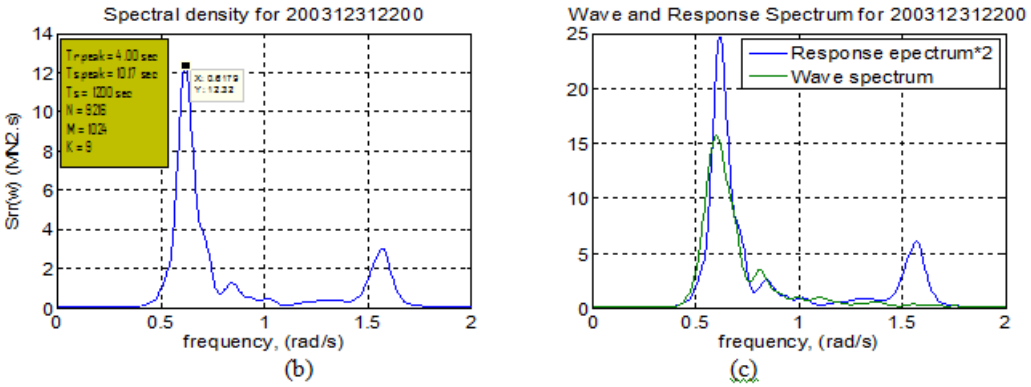

Figure 27: A2 time series response records (a), A2 response spectrum (b) and A2 response & Wave spectrum (c) during test.con14

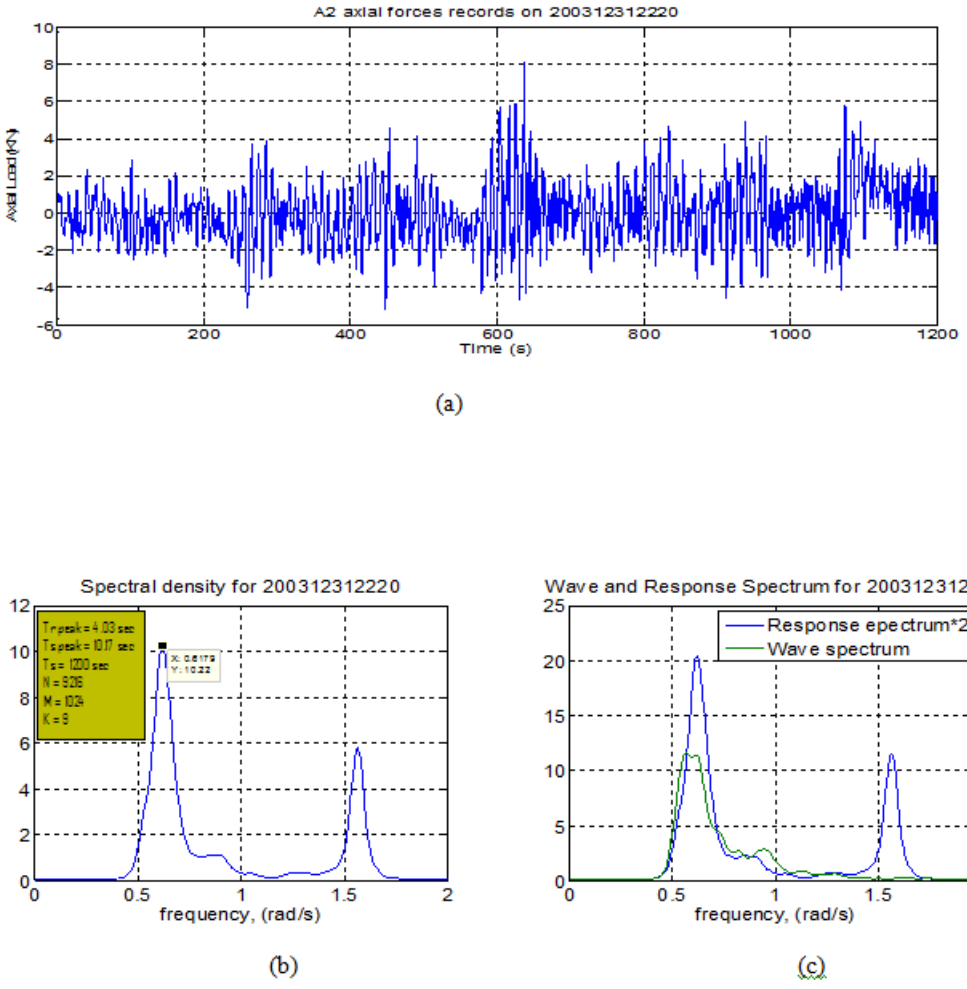

Figure 28: A2 time series response records (a), A2 response spectrum (b) and A2 response & Wave spectrum (c) during test.con15

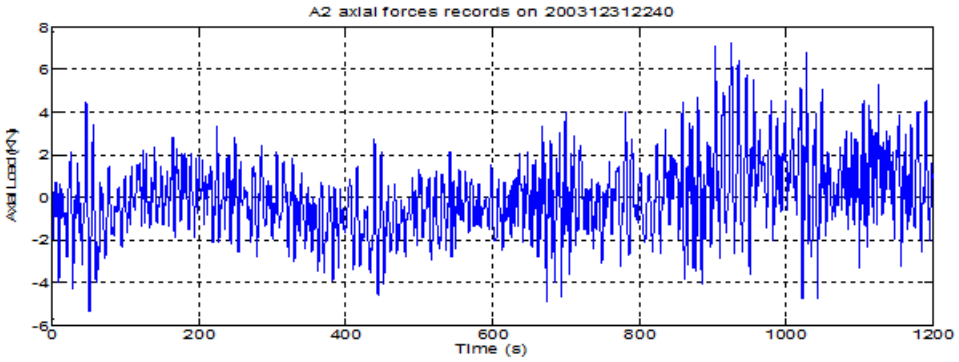

(a)

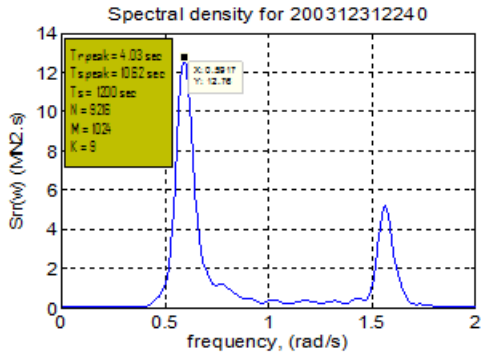

(b)

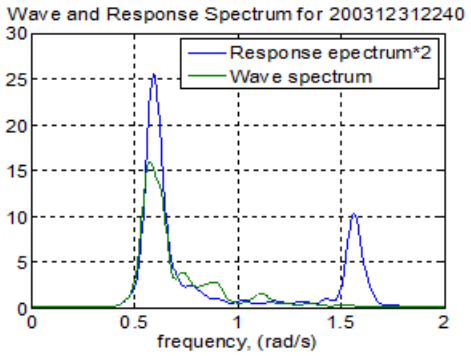

(c)

Figure 29: A2 time series response records (a), A2 response spectrum (b) and A2 response & Wave spectrum (c) during test.con16

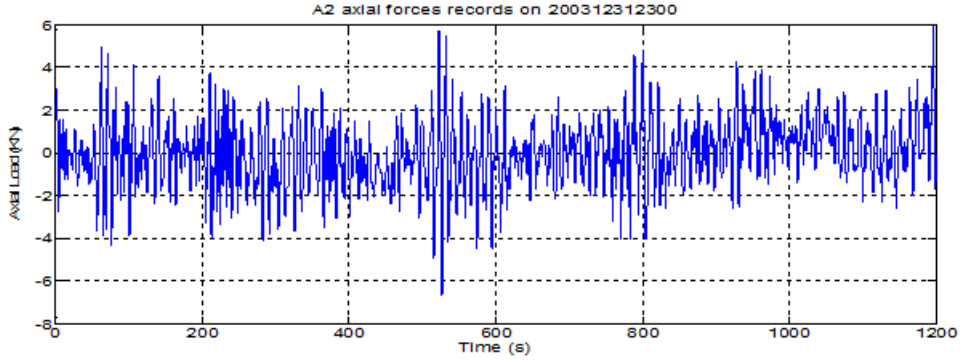

(a)

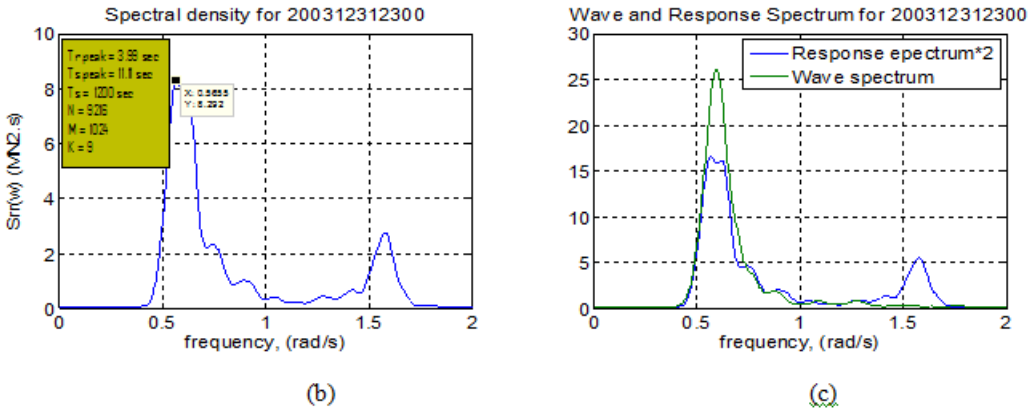

Figure 30: A2 time series response records (a), A2 response spectrum (b) and A2 response & Wave spectrum (c) during test.con17

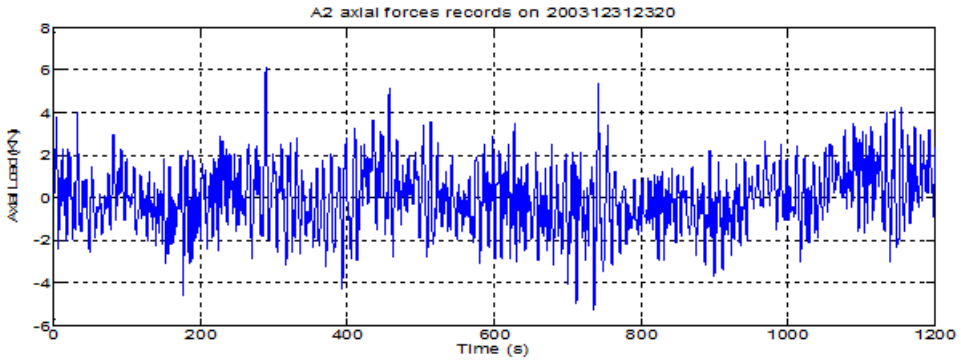

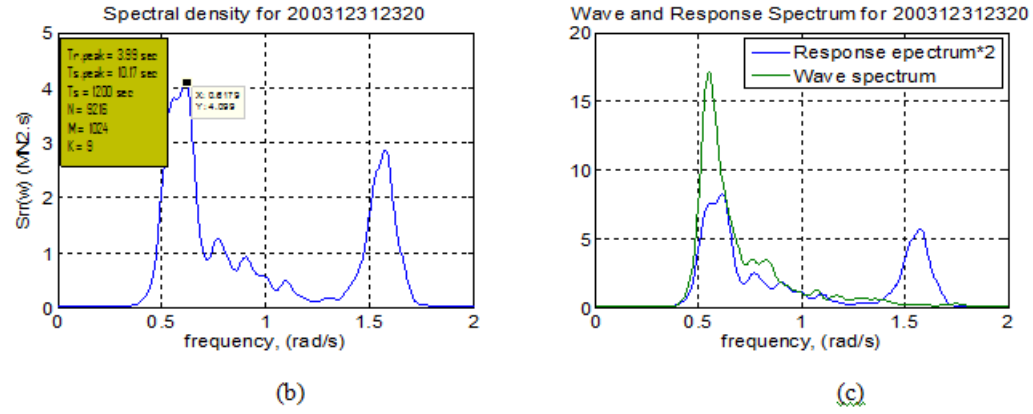

Figure 31: A2 time series response records (a), A2 response spectrum (b) and A2 response & Wave spectrum (c) during test.con18

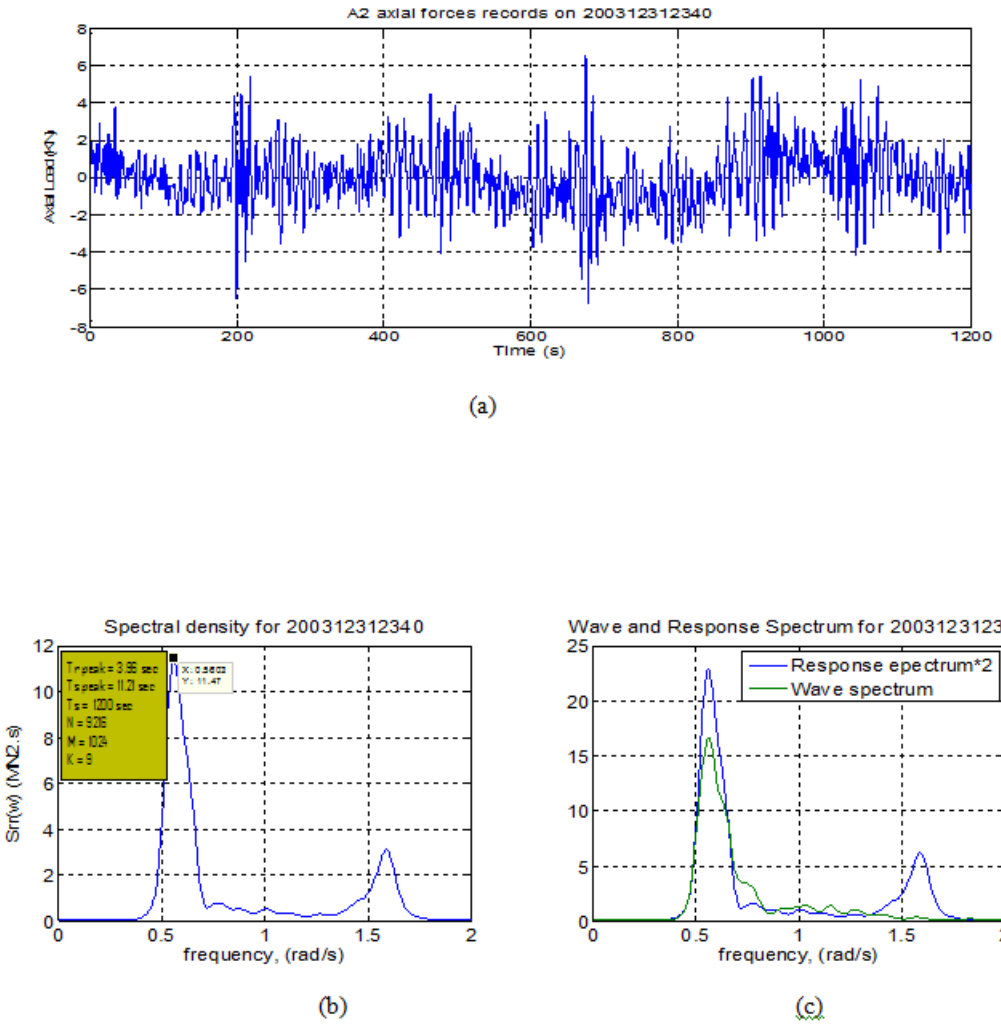

Figure 32: A2 time series response records (a), A2 response spectrum (b) and A2 response & Wave spectrum (c) during test.con19

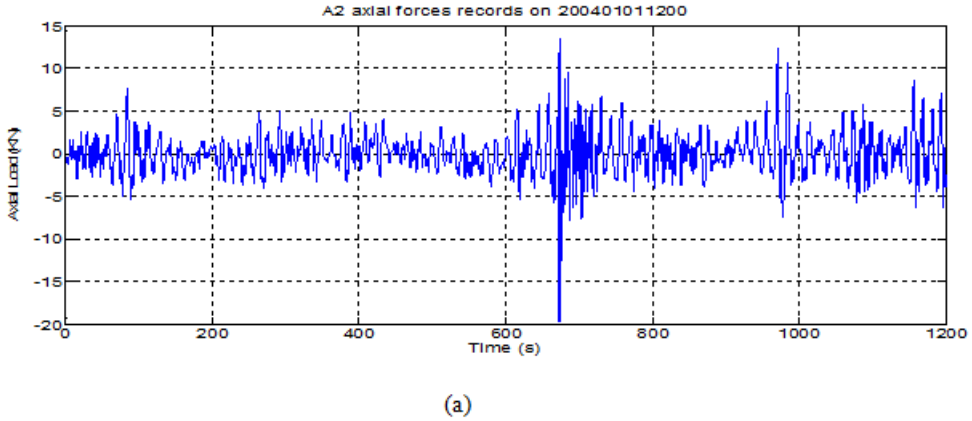

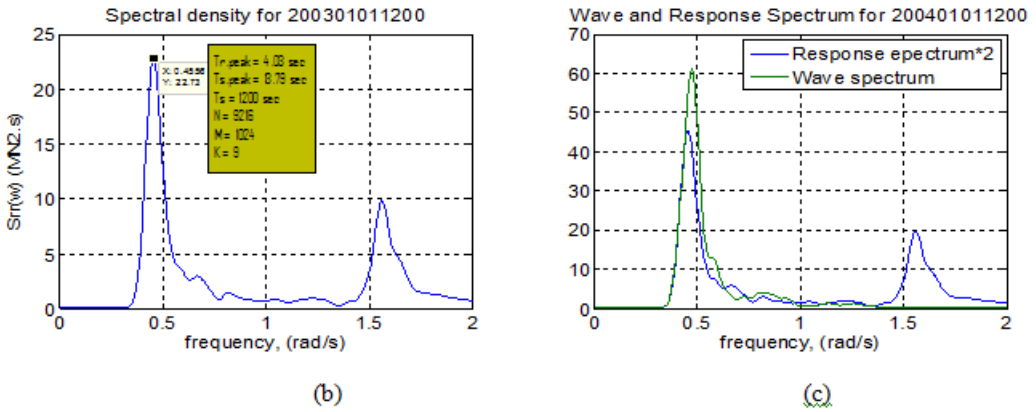

Figure 33: A2 time series response records (a), A2 response spectrum (b) and A2 response & Wave spectrum (c) during test.con20

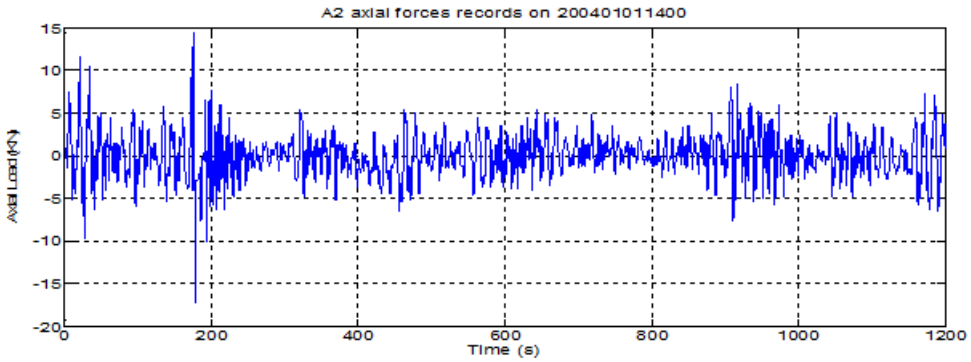

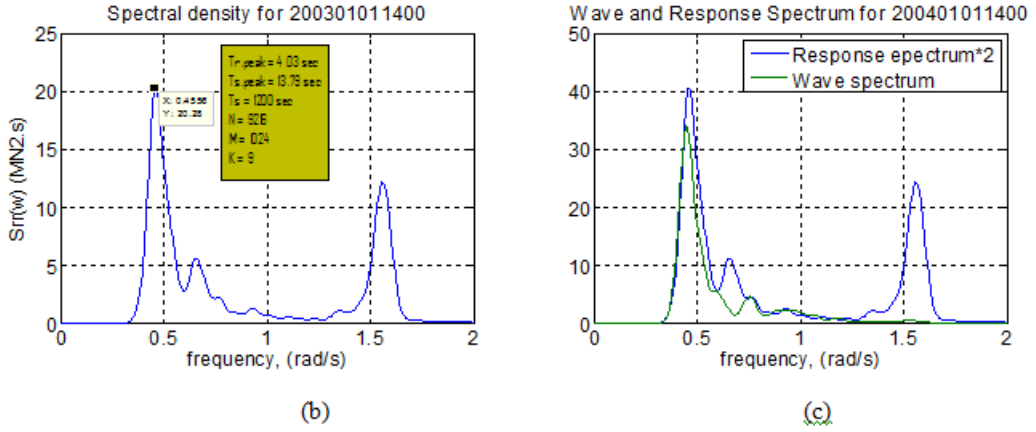

Figure 34: A2 time series response records (a), A2 response spectrum (b) and A2 response & Wave spectrum (c) during test.con21

C: Estimation of RAOs Using Spectral Relation

C-1: Estimated RAOs from Leg A2

Figures below shows estimated RAOs from leg A2 based on the spectral relation given in chapter 6.1.1, equation 6.1.

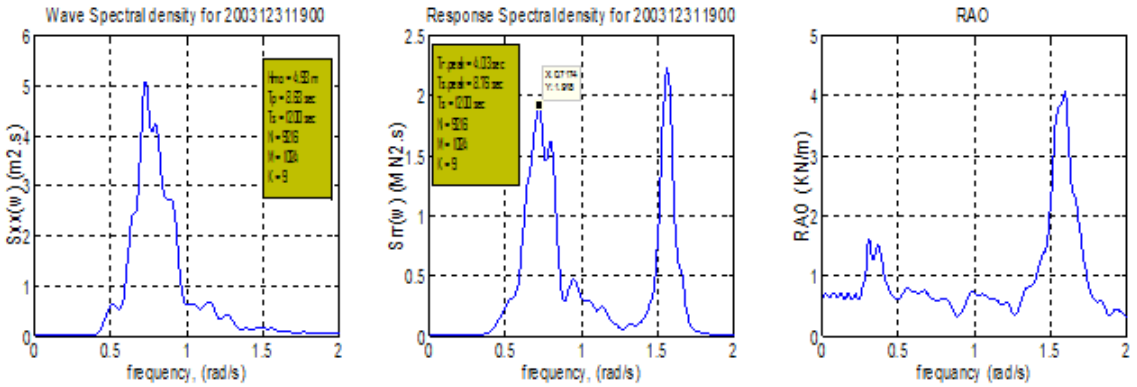

Figure 35: Wave spectrum, response spectrum, and RAO from Leg A2 during test.con 5.

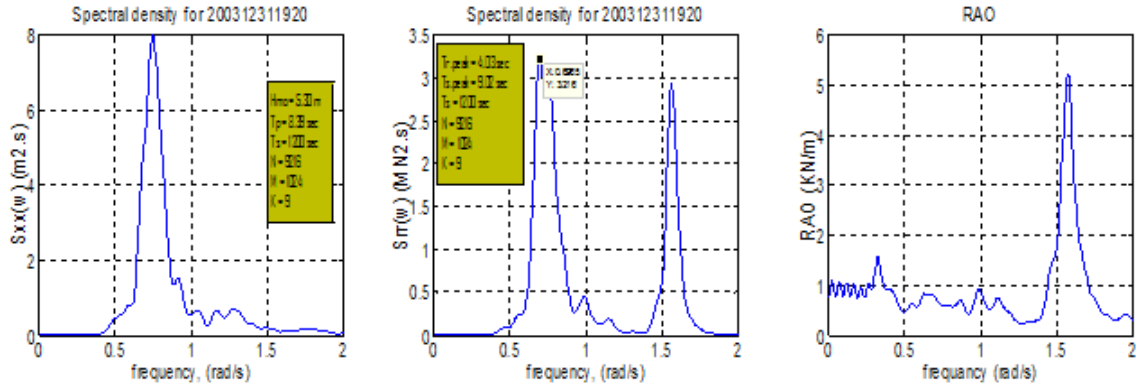

Figure 36: Wave spectrum, response spectrum, and RAO from Leg A2 during test.con 6.

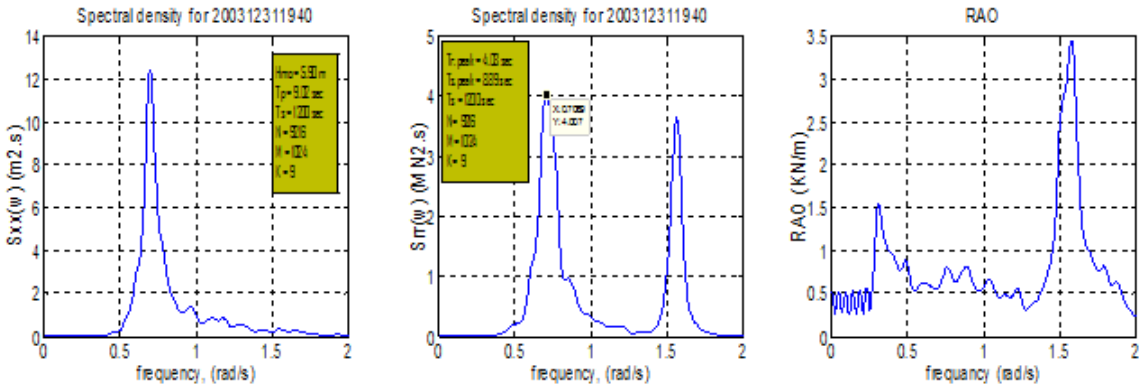

Figure 37: Wave spectrum, response spectrum, and RAO from Leg A2 during test.con 7.

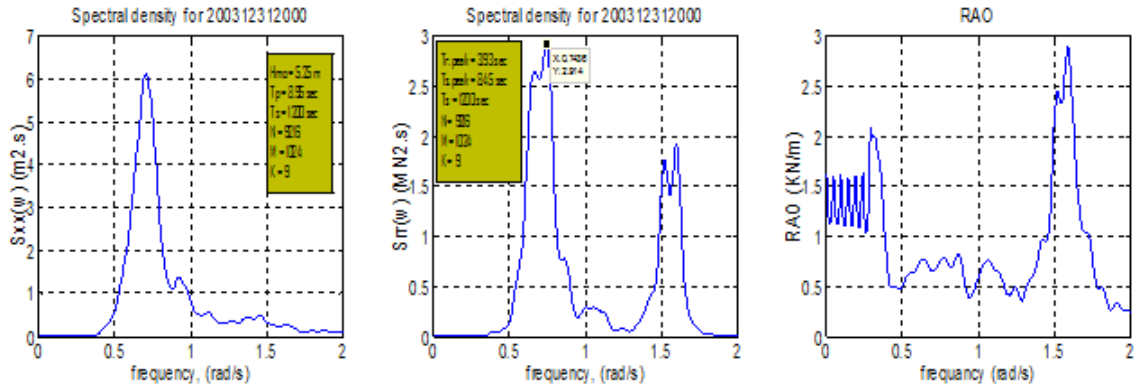

Figure 38: Wave spectrum, response spectrum, and RAO from Leg A2 during test.con 8.

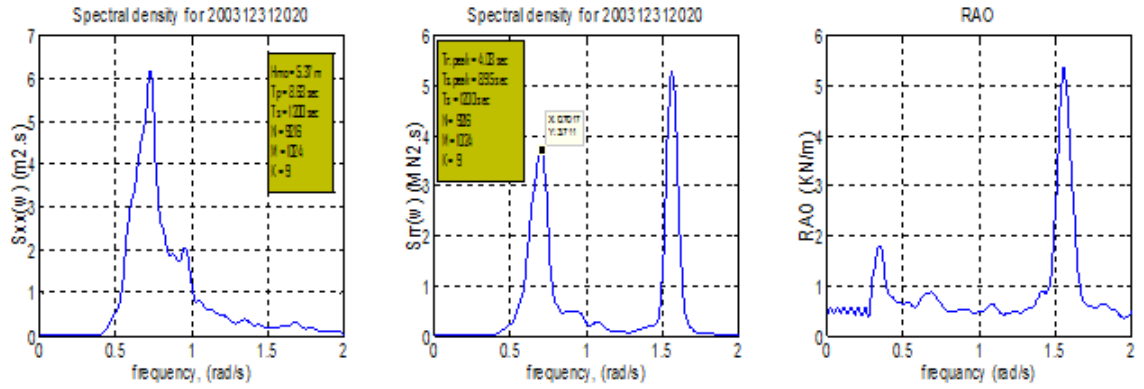

Figure 39: Wave spectrum, response spectrum, and RAO from Leg A2 during test.con 9.

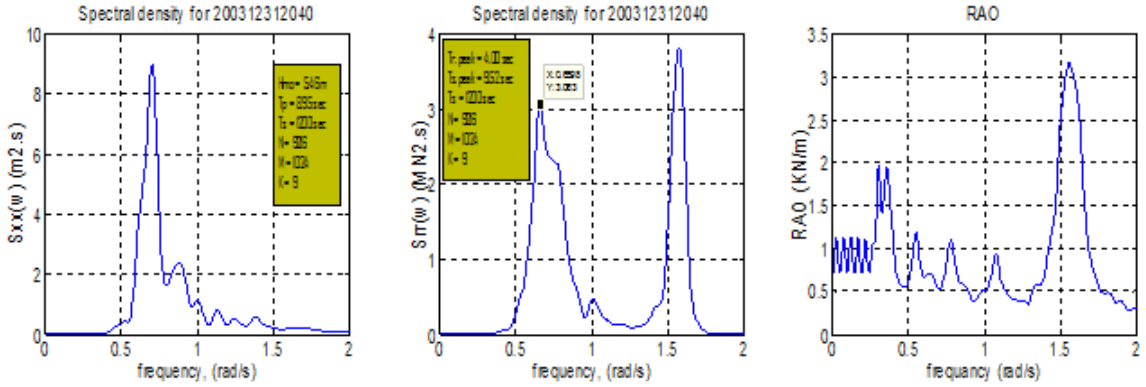

Figure 40: Wave spectrum, response spectrum, and RAO from Leg A2 during test.con 10.

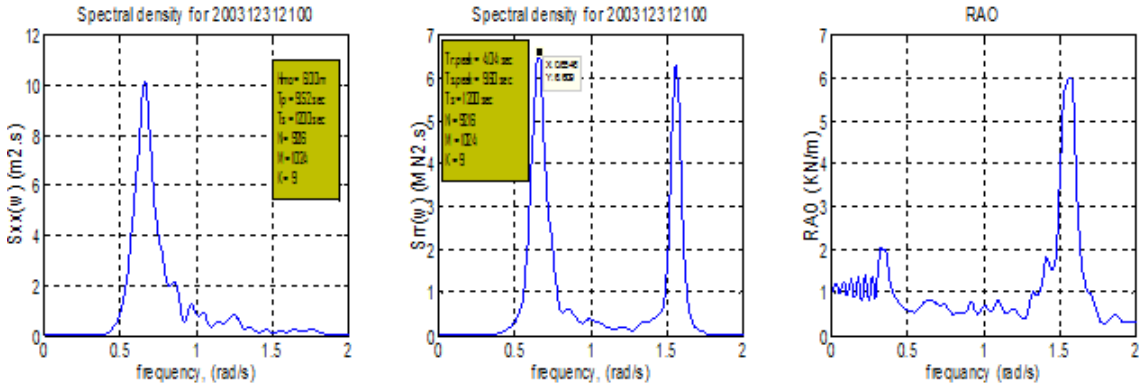

Figure 41: Wave spectrum, response spectrum, and RAO from Leg A2 during test.con 11.

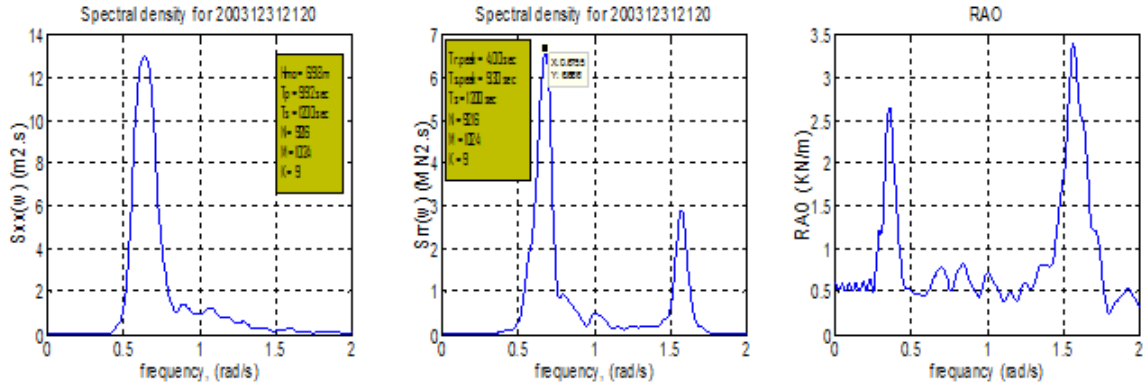

Figure 42: Wave spectrum, response spectrum, and RAO from Leg A2 during test.con 12.

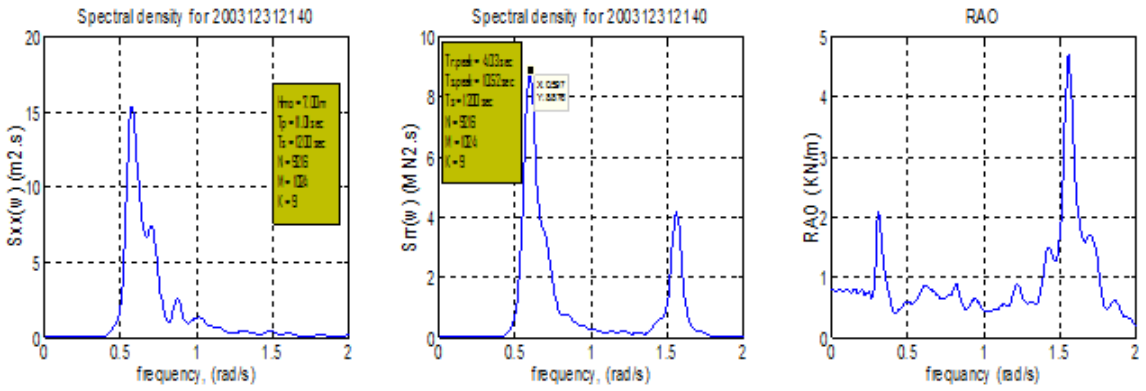

Figure 43: Wave spectrum, response spectrum, and RAO from Leg A2 during test.con 13.

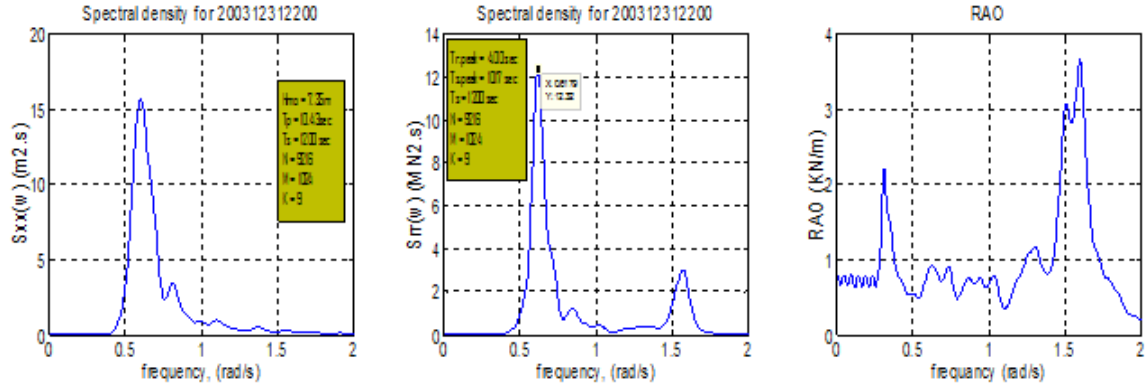

Figure 44: Wave spectrum, response spectrum, and RAO from Leg A2 during test.con 14.

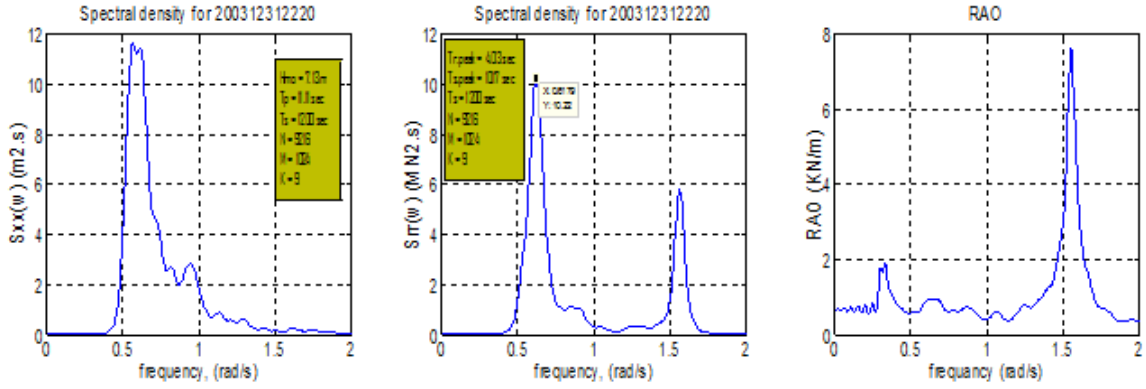

Figure 45: Wave spectrum, response spectrum, and RAO from Leg A2 during test.con 15.

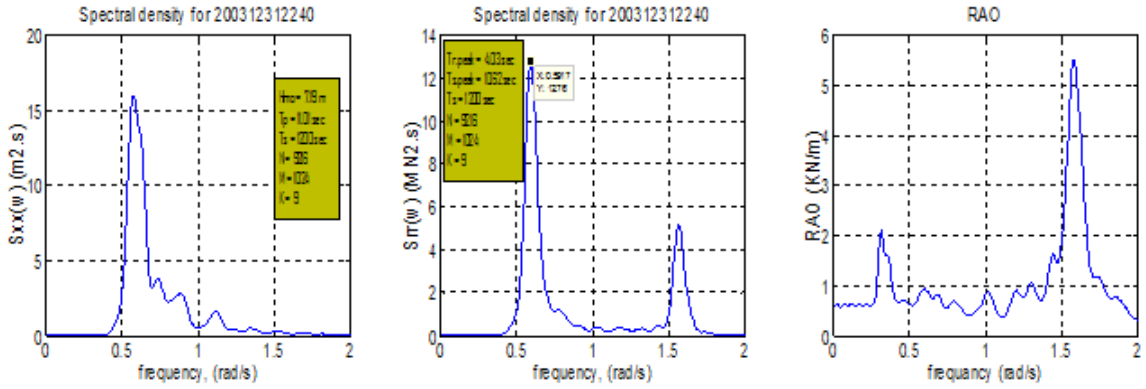

Figure 46: Wave spectrum, response spectrum, and RAO from Leg A2 during test.con 16.

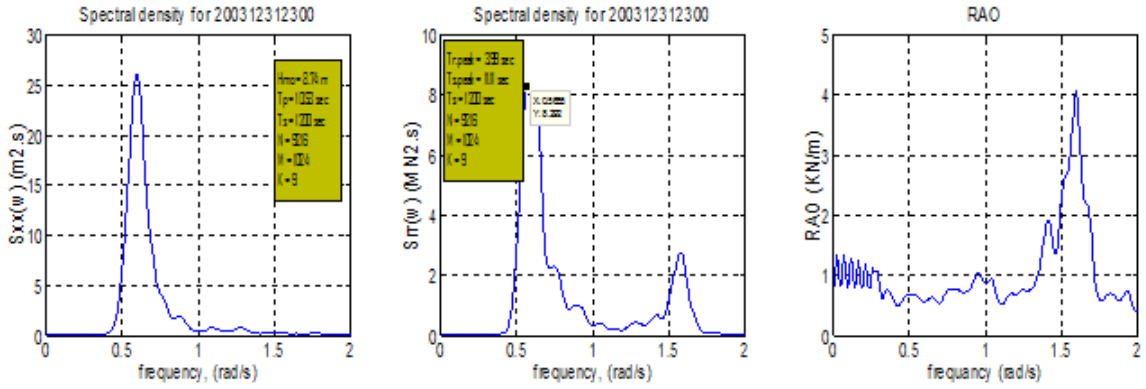

Figure 47: Wave spectrum, response spectrum, and RAO from Leg A2 during test.con 17.

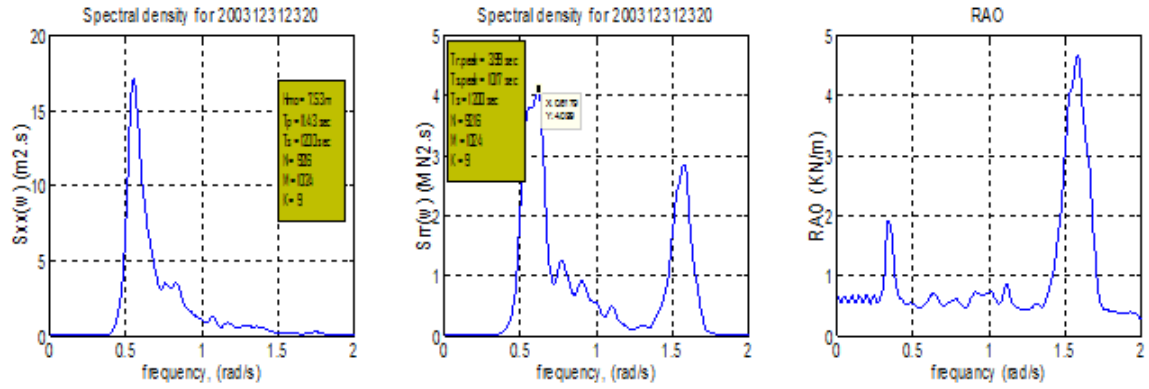

Figure 48: Wave spectrum, response spectrum, and RAO from Leg A2 during test.con 18.

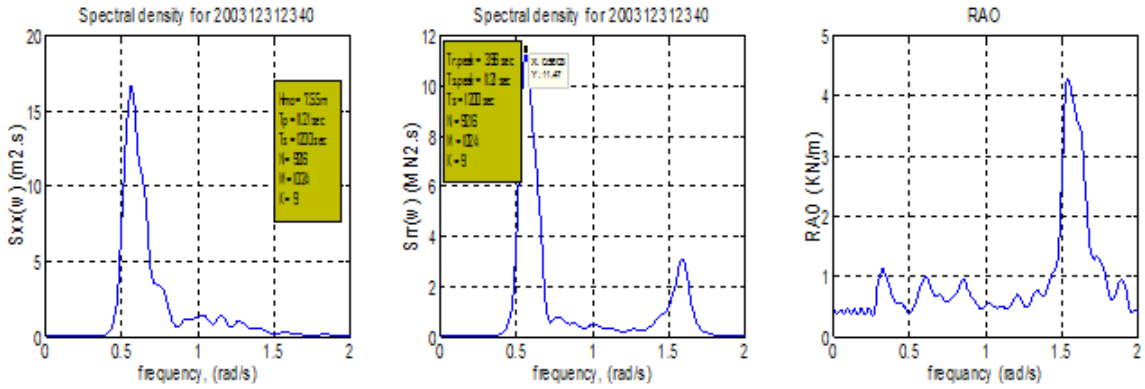

Figure 49: Wave spectrum, response spectrum, and RAO from Leg A2 during test.con 19.

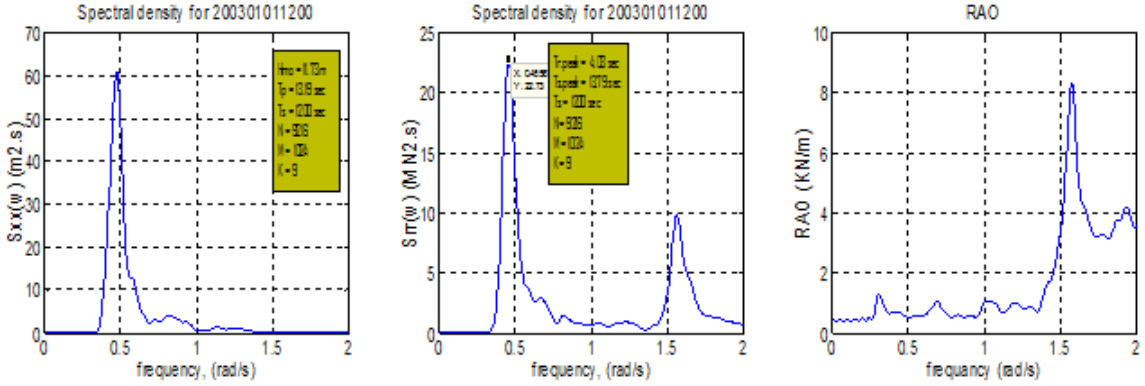

Figure 50: Wave spectrum, response spectrum, and RAO from Leg A2 during test.con 20.

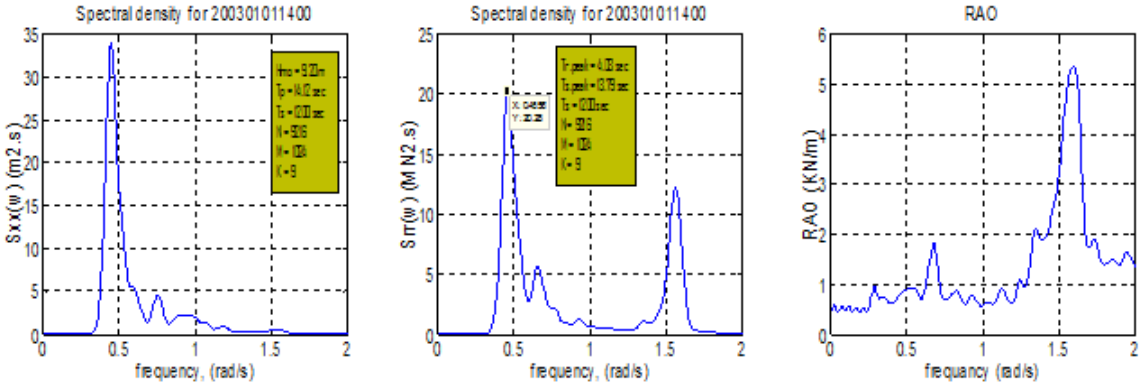

Figure 51: Wave spectrum, response spectrum, and RAO from Leg A2 during test.con 21.

C-2: Coherence Analysis of the Estimated RAOs from Leg A2

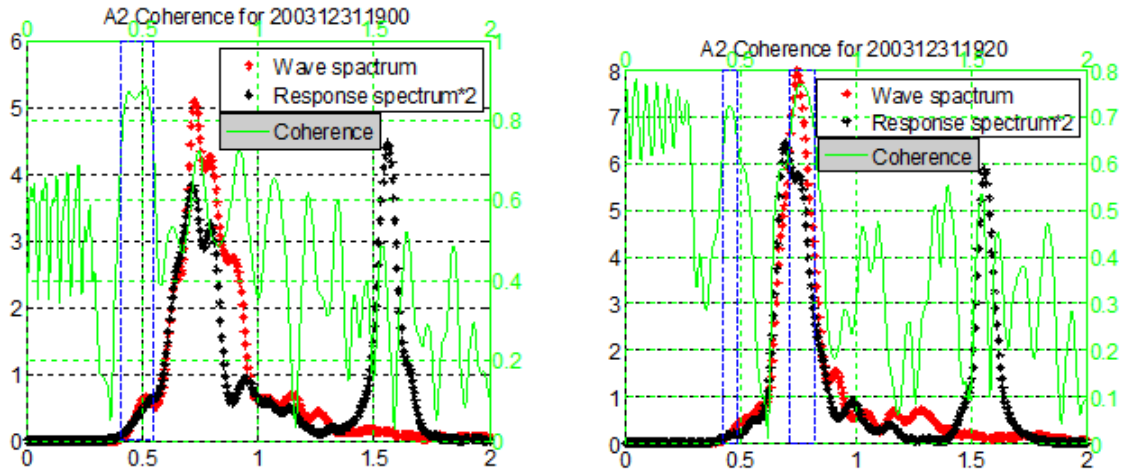

Figure 52: Coherence analysis during test.com 5 & 6 on leg A2

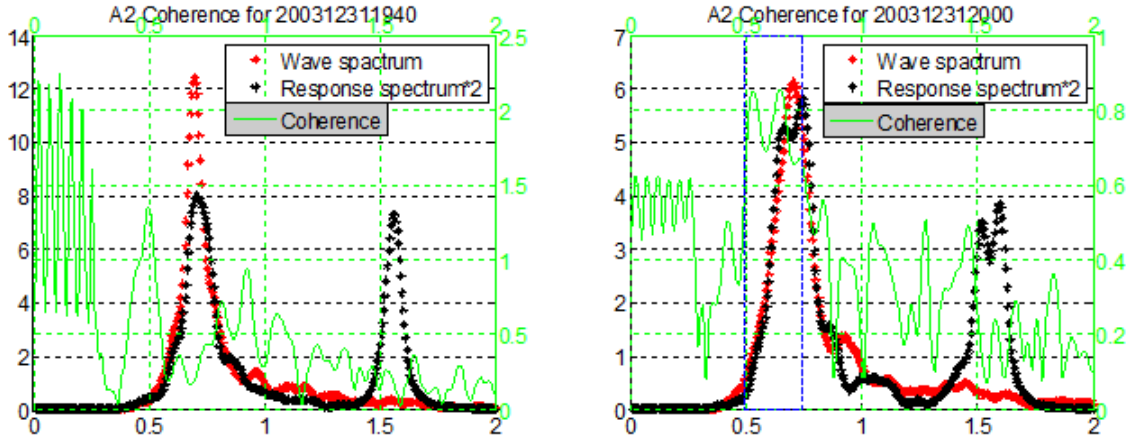

Figure 53: Coherence analysis during test.com 7 & 8 on leg A2

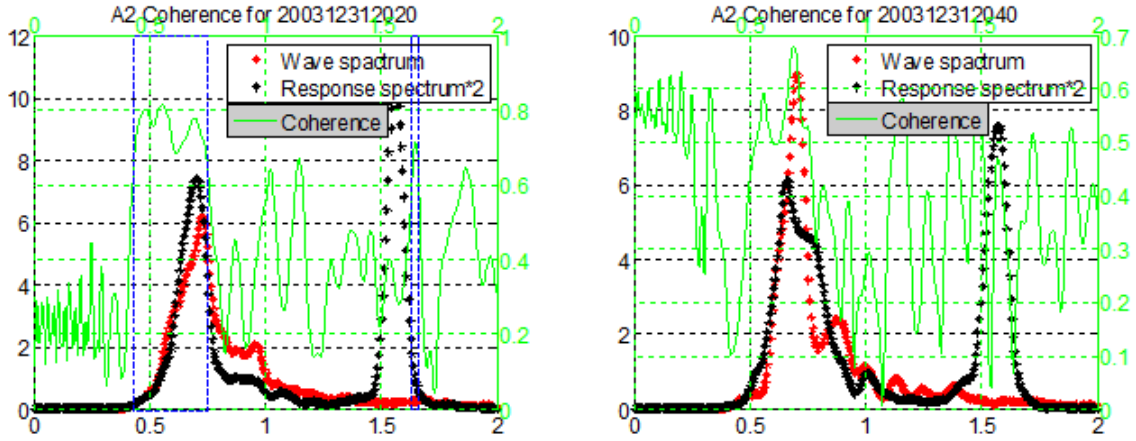

Figure 54: Coherence analysis during test.com 9 & 10 on leg A2

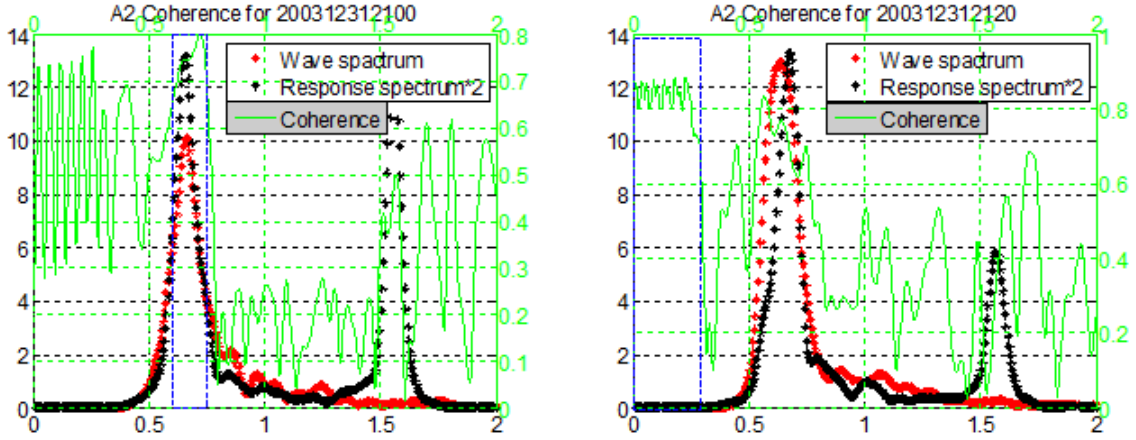

Figure 55: Coherence analysis during test.com 11 & 12 on leg A2

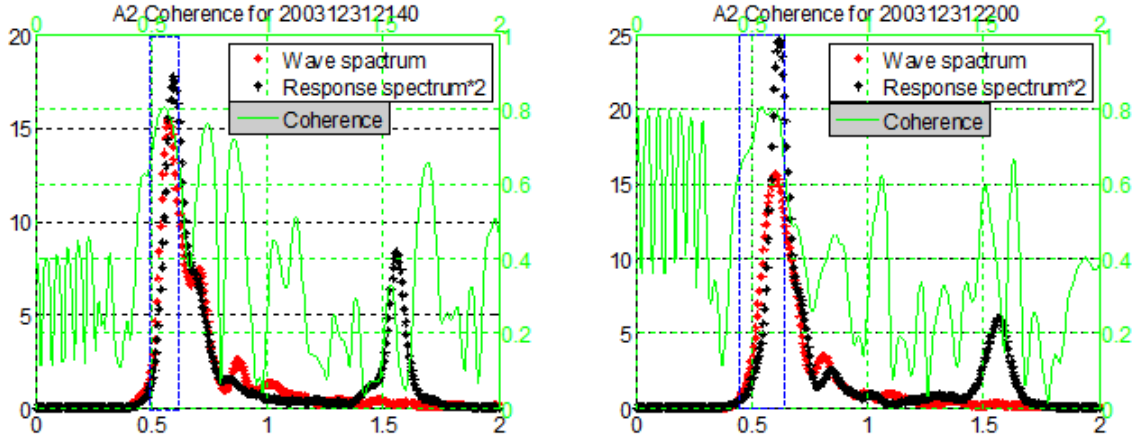

Figure 56: Coherence analysis during test.com 13 & 14 on leg A2

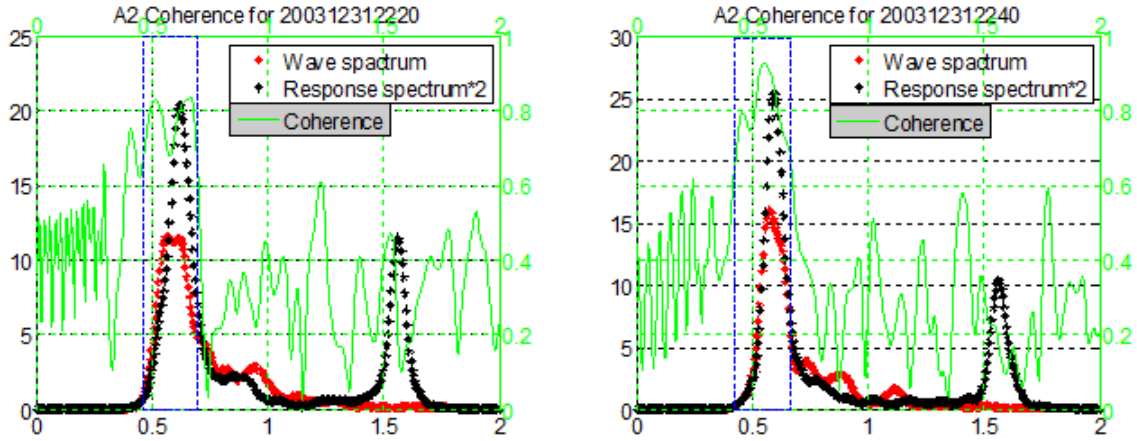

Figure 57: Coherence analysis during test.com 15 & 16 on leg A2

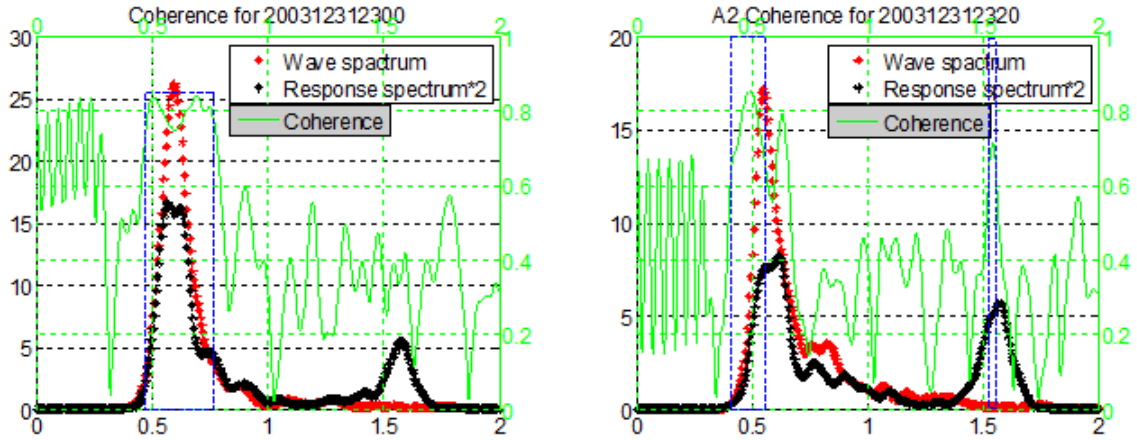

Figure 58: Coherence analysis during test.com 17 & 18 on leg A2

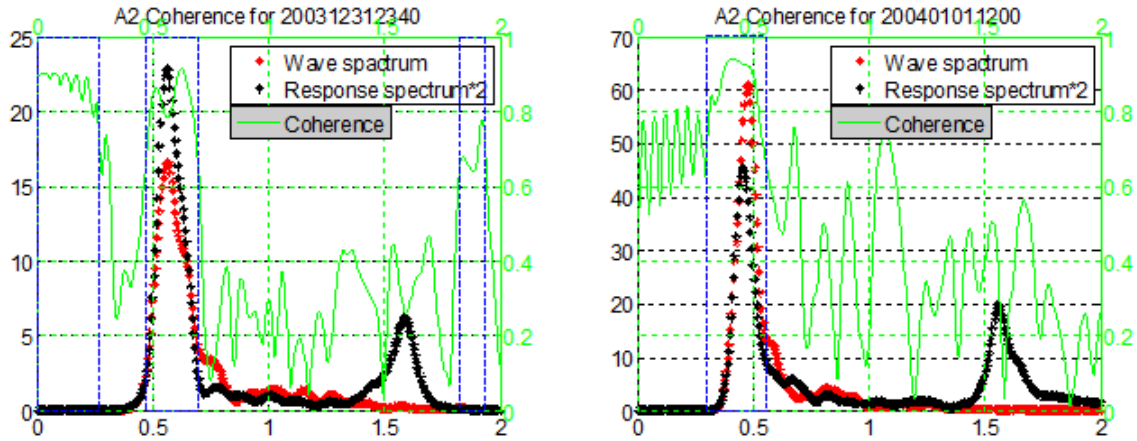

Figure 59: Coherence analysis during test.com 19 & 20 on leg A2

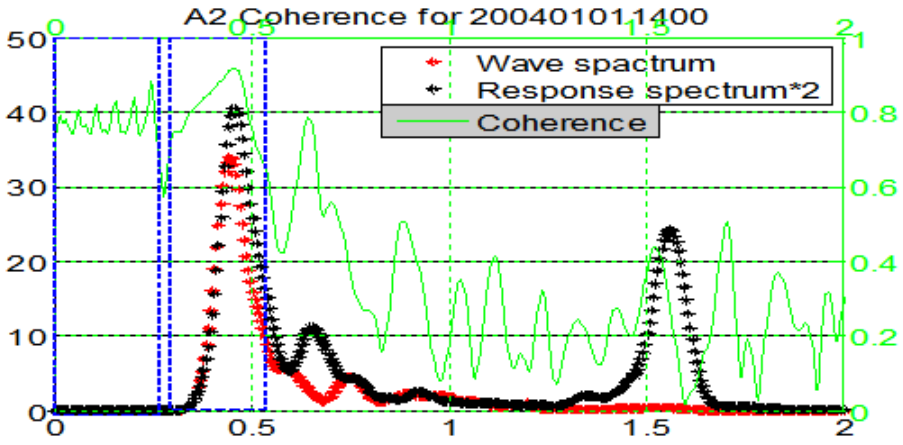

Figure 60: Coherence analysis during test.com 21 on leg A2

C-3: Possible Deviations of the Best Fit RAO at Different Frequency Ranges

1. ***At the Beginning of the Best Fit RAO [0-0.39]***

$$RAO(\omega) = \begin{cases} 1.28\omega, & \text{for } 0 \leq \omega \leq 0.39 \\ -5.34\omega^2 + 6.65\omega - 1.28, & \text{for } 0.39 \leq \omega \leq 0.85 \\ 0.50, & \text{for } 0.85 \leq \omega \leq 1.39 \\ 123.39\omega^2 - 345.50\omega + 242.35, & \text{for } 1.39 < \omega \leq 1.56 \\ 9181.18 * exp(-5.04\omega) & \text{for } \omega > 1.56 \end{cases} \quad (4)$$

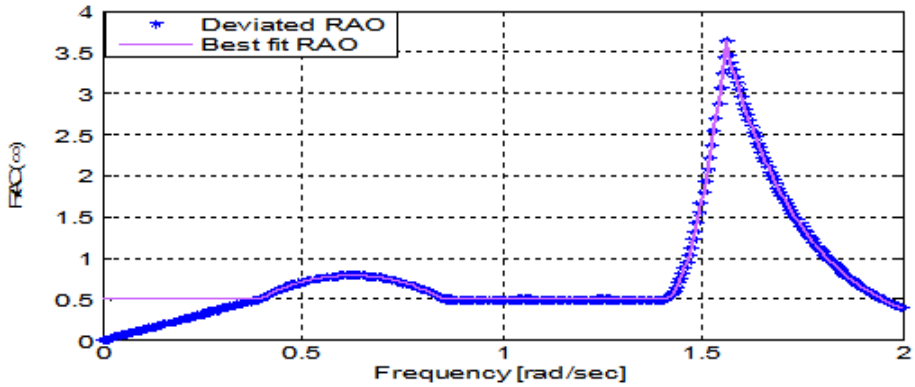

Figure 61: Possible deviation of the Best fit RAO at the beginning [0-0.39].

2. ***In the Major Wave Frequency Regime [0.39-0.85]***

a. 50% deviation above the best fit RAO in the frequency range [0.39-0.85]

$$RAO(\omega) = \begin{cases} 0.5, & \text{for } 0 \leq \omega \leq 0.39 \\ -7.99\omega^2 + 9.96\omega - 2.17, & \text{for } 0.39 \leq \omega \leq 0.85 \\ 0.50, & \text{for } 0.85 \leq \omega \leq 1.39 \\ 123.39\omega^2 - 345.50\omega + 242.35, & \text{for } 1.39 < \omega \leq 1.56 \\ 9181.18 * exp(-5.04\omega) & \text{for } \omega > 1.56 \end{cases} \quad (5)$$

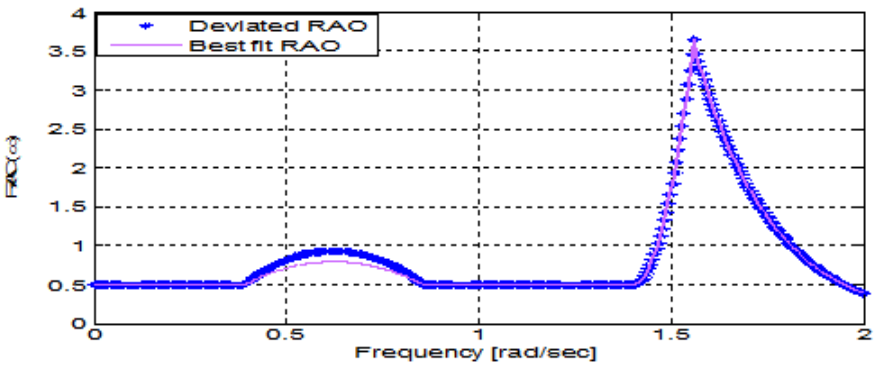

Figure 62: 50 % deviation above the best fit RAO in the major wave frequency regime at [0.39-0.85]

b. 50% below the estimated RAO in the frequency range [0.39-0.85]

$$RAO(\omega) = \begin{cases} 0.5, & \text{for } 0 \leq \omega \leq 0.39 \\ -2.68\omega^2 + 3.34\omega - 0.40, & \text{for } 0.39 \leq \omega \leq 0.85 \\ 0.50, & \text{for } 0.85 \leq \omega \leq 1.39 \\ 123.39\omega^2 - 345.50\omega + 242.35, & \text{for } 1.39 < \omega \leq 1.56 \\ 9181.18 * exp(-5.04\omega) & \text{for } \omega > 1.56 \end{cases} \quad (6)$$

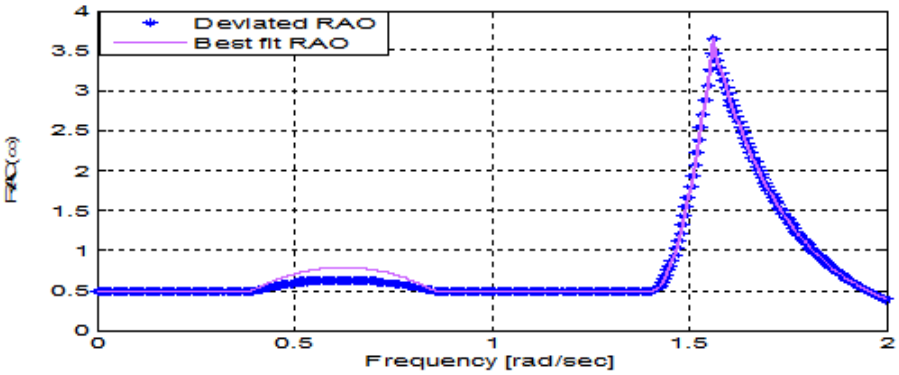

Figure 63: 50% deviation below the best fit RAO in the major wave frequency regime at [0.39-0.85]

3. ***Between the Major Wave Frequency Regime and Natural Frequency of the Structure [0.85-1.39]***

$$RAO(\omega) = \begin{cases} 0.5, & \text{for } 0 \leq \omega \leq 0.39 \\ -5.34\omega^2 + 6.65\omega - 1.28, & \text{for } 0.39 \leq \omega \leq 0.85 \\ 3.43\omega^2 - 7.68\omega + 4.55, & \text{for } 0.85 \leq \omega \leq 1.39 \\ 123.39\omega^2 - 345.50\omega + 242.35, & \text{for } 1.39 < \omega \leq 1.56 \\ 9181.18 * exp(-5.04\omega) & \text{for } \omega > 1.56 \end{cases} \tag{7}$$

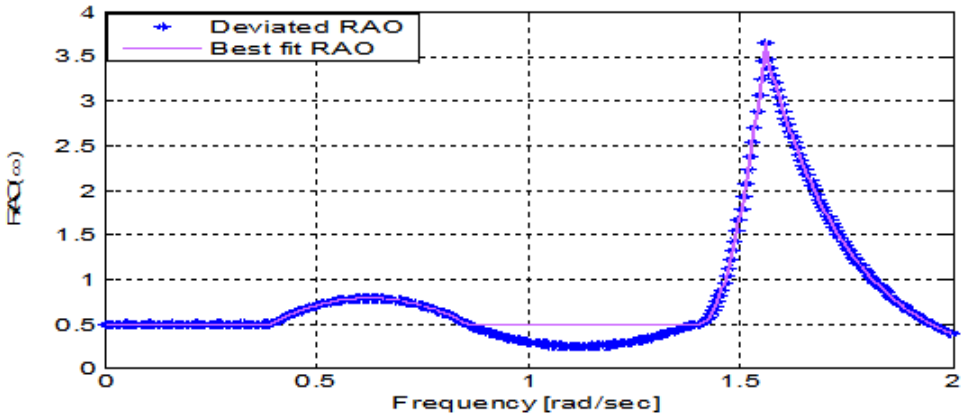

Figure 64: Possible deviation of the Best fit RAO at [0.85-1.39].

4. ***Around the Natural Frequency of the Jacket [1.56]***

   a. 50% deviation above the Best fit RAO around the natural frequency [1.56]

$$RAO(\omega) = \begin{cases} 0.5, & \text{for } 0 \leq \omega \leq 0.39 \\ -5.34\omega^2 + 6.65\omega - 1.28, & \text{for } 0.39 \leq \omega \leq 0.85 \\ 0.5, & \text{for } 0.85 \leq \omega \leq 1.39 \\ 172.90\omega^2 - 480.66\omega + 334.54, & \text{for } 1.39 < \omega \leq 1.56 \\ 76862.54 * exp(-6.12\omega) & \text{for } \omega > 1.56 \end{cases} \tag{8}$$

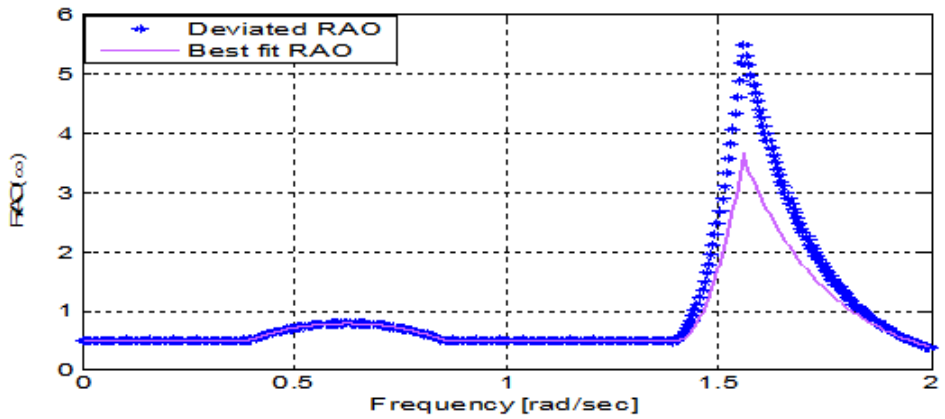

Figure 65: 50% deviation above the best fit RAO around the natural frequency of the jacket, around [1.56]

b. 50% deviation below the Best fit RAO around the natural frequency [1.56]

$$RAO(\omega) = \begin{cases} 0.5, & \text{for } 0 \leq \omega \leq 0.39 \\ -5.34\omega^2 + 6.65\omega - 1.28, & \text{for } 0.39 \leq \omega \leq 0.85 \\ 0.5, & \text{for } 0.85 \leq \omega \leq 1.39 \\ 46.06\omega^2 - 128.04\omega + 89.485, & \text{for } 1.39 < \omega \leq 1.56 \\ 256.62 * exp(- - 3.17\omega) & \text{for } \omega > 1.56 \end{cases} \quad (9)$$

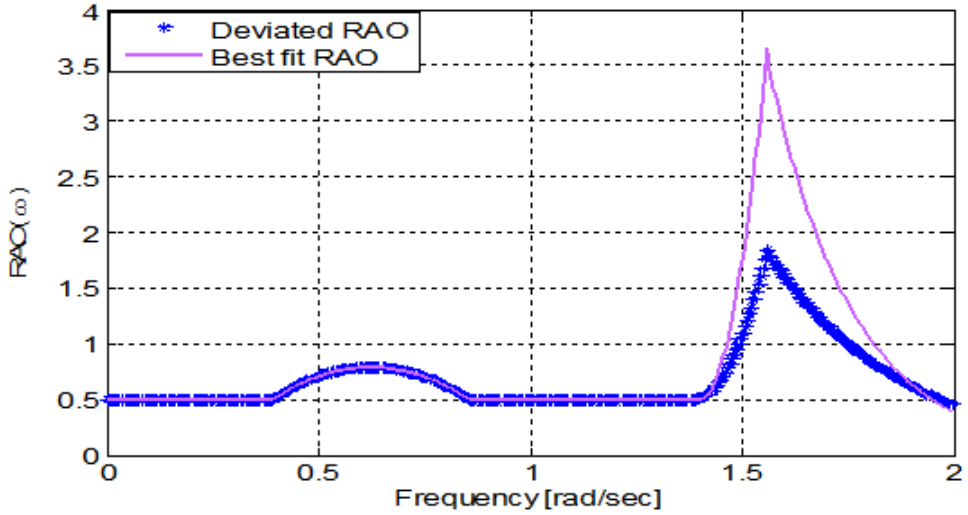

Figure 66: 50% deviation below the best fit RAO around the natural frequency of the jacket, around [1.56]

D: Fatigue Damage

D-1: Numerical Calculation for the Base/Primary Study Case

To calculate the fatigue damage on a given structural detail, generally the procedures presented in section 8.6.2 are followed. To show these steps numerically, fatigue damage for one sea state will be presented in this section while for the others are done in MATLAB with the same procedures. For this example let's take a sea state with a significant wave height of 8 meter and 10 second wave spectral peak period for 3-hour duration.

Step 1. For estimation of wave spectrum from time series wave records see chapter 4.

Step 2. For estimation of response spectrum from time series response record see chapter 5.

Steps 3-4. For estimation of the best fit RAO by performing coherence analysis between the incoming waves and responses of the jacket see chapter 6.Then from these steps, equation 6.7 has been taken as the best fit RAO of the structure and it is given below as:

$$RAO(\omega) = \begin{cases} 0.5\omega, & \text{for } 0 \leq \omega \leq 0.39 \\ -5.34\omega^2 + 6.65\omega - 1.28, & \text{for } 0.39 \leq \omega \leq 0.85 \\ 0.50, & \text{for } 0.85 \leq \omega \leq 1.39 \\ 123.39\omega^2 - 345.50\omega + 242.35, & \text{for } 1.39 < \omega \leq 1.56 \\ 9181.18 * exp(-5.04\omega) & \text{for } \omega > 1.56 \end{cases} \tag{10}$$

Step 5. In this step, the wave spectrum for the given sea state has to be determined using the Pierson-Moskowitz spectrum formula (8.1) and substituting the given wave parameters of H_s and T_p yields as:

$$S_{PM,\Xi\Xi}(\omega|8,10) = 3.12 * \omega^{-5} * exp(-0.1948 * \omega^{-4}) \tag{11}$$

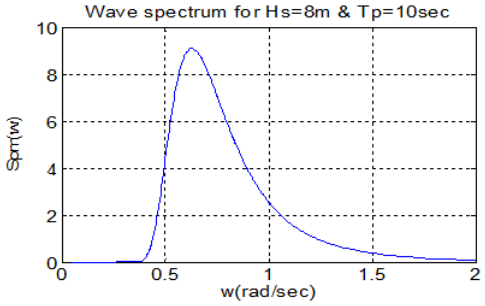

Figure 67: Pierson-Moskowitz wave spectrum for H_s=8m and T_p=10sec

Step 6. From steps 4 and 5 determine the response spectrum using the spectral relation equation 8.8, as a result the response of the jacket for the given sea state is represented as:

$$S_{\Gamma\Gamma}(\omega|8,10)$$

$$= \begin{cases} 0.78 * \omega^{-5} * exp(-0.1948\omega^{(-4)}), & \text{for } 0 \leq \omega \leq 0.39 \\ |-5.34\omega^2 + 6.65\omega - 1.28|^2 * 3.18 * \omega^{-5} * exp(-0.195\omega^{(-4)}), & \text{for } 0.39 \leq \omega \leq 0.85 \\ 0.78 * \omega^{-5} * exp(-0.195\omega^{(-4)}), & \text{for } 0.85 \leq \omega \leq 1.39 \\ |123.40\omega^2 - 345.50\omega + 242.35|^2 * 3.18 * \omega^{-5} * exp(-0.195\omega^{(-4)}), & \text{for } 1.39 < \omega \leq 1.56 \\ |9181.18 * exp(-5.04\omega)|^2 * 3.18 * \omega^{-5} * exp(-0.195\omega^{(-4)}), & \text{for } \omega > 1.56 \end{cases} \tag{12}$$

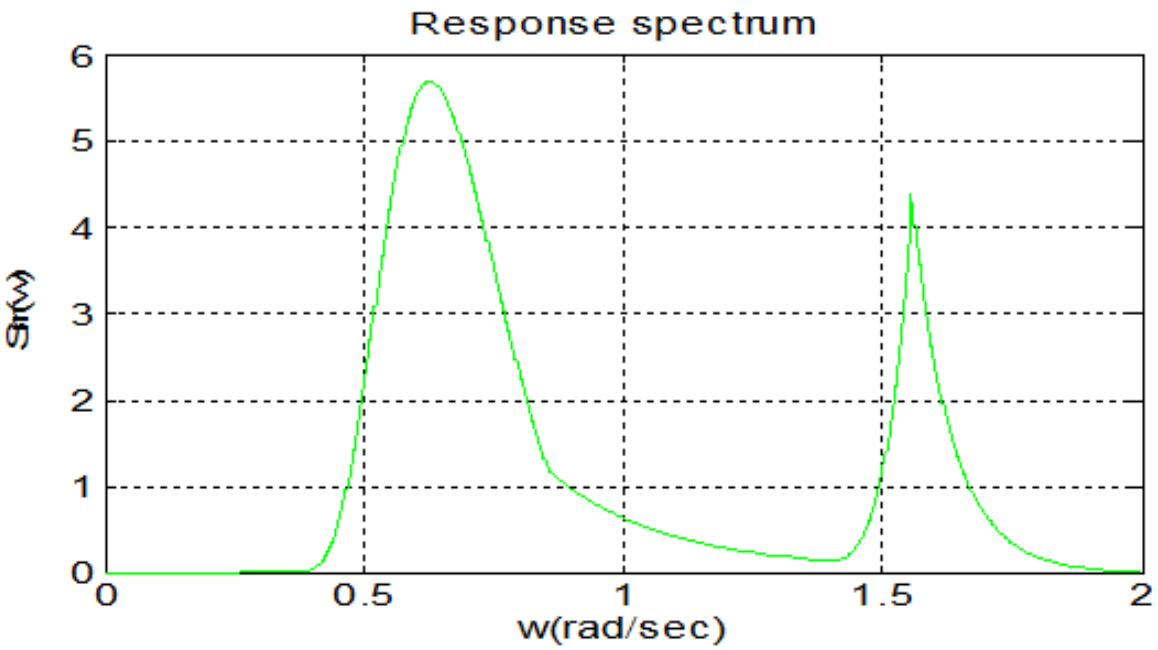

Figure 68: Response spectrum of the jacket for a sea state of H_s=8m and T_p=10sec

Step 7. Once the response spectrum for the given sea state is developed; its spectral moments can be calculated using equation 8.9. The zero order, $m_{0,\Gamma\Gamma}(8,10)$, and second order, $m_{2,\Gamma\Gamma}(8,10)$, spectral moments for the give response spectrum, $S_{\Gamma\Gamma}(\omega|8,10)$, are determined as below:

$$m_{0,\Gamma\Gamma}(8,10) = \int_0^\infty S_{\Gamma\Gamma}(\omega|8,10) * d\omega = \sum_0^\infty S_{\Gamma\Gamma}(\omega|8,10) * \Delta\omega \tag{13}$$

$$m_{0,\Gamma\Gamma}(8,10) = \begin{cases} \sum_{0}^{0.39} 0.78 * \omega^{-5} * exp\{-0.1948 * \omega^{-4}\} * \Delta\omega + \\ \sum_{0.39}^{0.85} |-5.34\omega^2 + 6.65\omega - 1.28|^2 * 3.12 * \omega^{-5} * exp\{-0.1948 * \omega^{-4}\} * \Delta\omega + \\ \sum_{0.85}^{1.39} 0.78 * \omega^{-5} * exp\{-0.1948 * \omega^{-4}\} * \Delta\omega + \\ \sum_{1.39}^{1.56} |123.40\omega^2 - 345.51\omega + 242.35|^2 * 3.12 * \omega^{-5} * exp\{-0.1948 * \omega^{-4}\} * \Delta\omega + \\ \sum_{1.56}^{\infty} |9181.18 * \exp(-5.04\omega)|^2 * 3.12 * \omega^{-5} * exp\{-0.1948 * \omega^{-4}\} * \Delta\omega \end{cases}$$

Assuming a frequency increment, $\Delta\omega$, to be 0.0052, the zero order response spectral moment for the given sea state, which is equal to the variance of the response process, $\sigma^2_{\Gamma\Gamma}(8,10)$, has been solved and found to be:

$$m_{0,\Gamma\Gamma}(8,10) = \sigma^2_{\Gamma\Gamma}(8,10) = 2.24 \tag{14}$$

Therefore, the standard deviation, $\sigma_{\Gamma\Gamma}(8,10)$, for this response process is estimated to be 1.197.
And second order response spectral moment, $m_{2,\Gamma\Gamma}(8,10)$, can be calculated as:

$$m_{2,\Gamma\Gamma}(8,10) = \int_0^{\infty} \omega^2 * S_{\Gamma\Gamma}(\omega|8,10) * d\omega = \sum_{0}^{\infty} \omega^2 S_{\Gamma\Gamma}(\omega|8,10) * \Delta\omega \tag{15}$$

$$m_{2,\Gamma\Gamma}(8,10) = \begin{cases} \sum_{0}^{0.39} \omega^2 * 0.78 * \omega^{-5} * exp\{-0.1948 * \omega^{-4}\} * \Delta\omega + \\ \sum_{0.39}^{0.85} \omega^2 * |-5.34\omega^2 + 6.65\omega - 1.28|^2 * 3.12 * \omega^{-5} * exp\{-0.1948 * \omega^{-4}\} * \Delta\omega + \\ \sum_{0.85}^{1.39} \omega^2 * 0.7793 * \omega^{-5} * exp\{-0.1948 * \omega^{-4}\} * \Delta\omega + \\ \sum_{1.39}^{1.56} \omega^2 * |123.40\omega^2 - 345.51\omega + 242.35|^2 * 3.12 * \omega^{-5} * exp\{-0.1948 * \omega^{-4}\} * \Delta\omega + \\ \sum_{1.56}^{\infty} \omega^2 * |9181.18 * \exp(-5.04\omega)|^2 * 3.12 * \omega^{-5} * exp\{-0.1948 * \omega^{-4}\} * \Delta\omega \end{cases}$$

Assuming a frequency increment, $\Delta\omega$, to be 0.0052, the second order response spectral moment for the given sea state has been solved and found to be 2.206.

From these two response spectral moments, the number of response cycles, $n_{0,\Gamma\Gamma}(8,10)$, for the given duration is determined using equation 8.13 and it is found to be around 1706 cycle. This mean the structure is subjected for around 1706 stress cycles within 3-hours.

Step 8. As described in section 8.5, for linear structures their stress range distribution can be modeled with a Rayleigh probability function for short term duration. The scaling parameter of the Rayleigh distribution is determined from the standard deviation of the response process in step 7. Therefore, the Rayleigh probability function given in equation 8.22 will reduced as below for the given sea state.

$$f(\Delta\sigma|8,10) = 0.112 * \Delta * exp(-(0.295\Delta\sigma)^2) \tag{16}$$

Step 9. From the function given in step 8 and number of response cycles in step 7, determine the number of stress cycles, $n_i(H_s,T_p)$, within a given stress block i of the distribution using equation 8.15. For the given sea state the number of cycles, $n_i(8,8)$, within a given stress block is determined as follows:

$$n_i(8,10) = 191.07 * \Delta\sigma_i * exp(-(0.295\Delta\sigma_i)^2) \tag{17}$$

Steps 10-11. As mentioned, all tubular structural details are classified as "T" class and their S-N curve constant parameters are given in table 8-2 and Figure 8-5. For this type of S-N curve, the number of stress cycles to failure at a constant $\Delta\sigma_i$ stress range within the stress block i is estimated as:

$$N_i(\Delta\sigma_i) = \begin{cases} 5.8076x10^11 * \Delta\sigma_i^{-3}, & \text{for } \Delta\sigma_i \leq 83.4 \\ 4.0364x10^15 * \Delta\sigma_i^{-5}, & \text{for } \Delta\sigma_i{>}83.4 \end{cases} \tag{18}$$

Steps 12. Once the number of cycles, $n_i(H_s,T_p)$, within the given stress block and the number of cycles to failure at a constant $\Delta\sigma_i$ stress range, $N_i(\Delta\sigma_i)$,are determined, the fatigue damage is their ratio and it is given as:

$$D_i(8,10) = \begin{cases} 32.9x10^{-11} * \Delta\sigma_i^4 * exp(-(0.295\Delta\sigma_i)^2), & \text{for } \Delta\sigma_i \leq 83.4 \\ 47.34x10^{-15} * \Delta\sigma_i^6 * exp(-(0.295\Delta\sigma_i)^2), & \text{for } \Delta\sigma_i{>}83.4 \end{cases} \tag{19}$$

Having calculated the fatigue damage for each stress block in the distribution and summing up all yields the cummulative fatigue damage due to the given sea state as bellow:

$$D_i(8,10) = \begin{cases} 32.9x10^{-11} \sum_{i=0}^{\infty} \Delta\sigma_i^4 * exp(-(0.295\Delta\sigma_i)^2), & \text{for } \Delta\sigma_i \leq 83.4 \\ 47.34x10^{-15} \sum_{i=0}^{\infty} \Delta\sigma_i^6 * exp(-(0.295\Delta\sigma_i)^2), & \text{for } \Delta\sigma_i{>}83.4 \end{cases} \tag{20}$$

By modeling this equation in MATLAB separately, the incurred fatigue damage due to the specified sea state, i.e. significant wave height of 8 meter and spectral peak period of 10 seconds for the 3-hour duration, was found to be $2.49x10^{-7}$.

Step 13. For other new sea states go back to step 5 and repeat steps 5 to 12.

In this thesis, these procedures are written in the MATLAB script and fatigue damage ratio for all the sea states given in table 8.1 (163133 sea states) are analyzed and the result is presented in section 8.6.4. The procedures given above are for the base case study only, but by customizing steps 4 and 11, the secondary study case, deviated Best Fit RAO, and third study cases, single slope S-N cure, are performed.

MATLAB Script for Accumulated Fatigue Damage vs. H_s

Accumulated Fatigue Damage vs. Significant Wave Height

```
clc
clear all
close all
%%  Given Sea states
Sea_state='sea state data.xlsx';
Hs1=xlsread(Sea_state,1,'B2:B163134');   % Given significant wave heights
Tp1=xlsread(Sea_state,1,'C2:C163134');   % Given Peak wave periods
%% Grouping the given sea states as in Table 8.1
Hs_Le_0=[];
Tp_Le_0=[];
Hs_Bn_0_1=[];
Tp_Bn_0_1=[];
Hs_Bn_1_2=[];
Tp_Bn_1_2=[];
Hs_Bn_2_3=[];
Tp_Bn_2_3=[];
Hs_Bn_3_4=[];
Tp_Bn_3_4=[];
Hs_Bn_4_5=[];
Tp_Bn_4_5=[];
Hs_Bn_5_6=[];
Tp_Bn_5_6=[];
Hs_Bn_6_7=[];
Tp_Bn_6_7=[];
Hs_Bn_7_8=[];
Tp_Bn_7_8=[];
Hs_Bn_8_9=[];
Tp_Bn_8_9=[];
Hs_Bn_9_10=[];
Tp_Bn_9_10=[];
Hs_Bn_10_11=[];
Tp_Bn_10_11=[];
Hs_Bn_11_12=[];
Tp_Bn_11_12=[];
Hs_Bn_12_13=[];
Tp_Bn_12_13=[];
Hs_Bn_13_14=[];
Tp_Bn_13_14=[];
Hs_Bn_14_15=[];
Tp_Bn_14_15=[];
Hs_Bn_15_16=[];
Tp_Bn_15_16=[];
Hs_Gr_16=[];
Tp_Gr_16=[];
countLe_0=1;
countBn_0_1=1;
countBn_1_2=1;
countBn_2_3=1;
countBn_3_4=1;
countBn_4_5=1;
countBn_5_6=1;
countBn_6_7=1;
countBn_7_8=1;
countBn_8_9=1;
countBn_9_10=1;
countBn_10_11=1;
countBn_11_12=1;
countBn_12_13=1;
countBn_13_14=1;
countBn_14_15=1;
countBn_15_16=1;
```

```
countGr_16=1;
for i=1:length(Hs1);
   %fprintf('Hs1:%d\n',Hs1(i))
   if 0<=Hs1(i)&&Hs1(i)<=0.2
      Hs_Le_0(countLe_0)=Hs1(i);
      Tp_Le_0(countLe_0)=Tp1(i);
      %fprintf( 'Less than 0: %d %d\n ' , Hs1(i),countLe_0)
      countLe_0=countLe_0+1;
      disp(Hs_Le_0)
   elseif 0.2<Hs1(i)&&Hs1(i)<=1
      Hs_Bn_0_1(countBn_0_1)=Hs1(i);
      Tp_Bn_0_1(countBn_0_1)=Tp1(i);
      %fprintf( 'between 0.2 and 1: %d %d\n ' , Hs1(i),countBn_0_1)
      countBn_0_1=countBn_0_1+1;
   elseif 1<Hs1(i)&&Hs1(i)<=2
      Hs_Bn_1_2(countBn_1_2)=Hs1(i);
      Tp_Bn_1_2(countBn_1_2)=Tp1(i);
      %fprintf( 'between 1 and 2: %d\n' , Hs1(i))
      countBn_1_2=countBn_1_2+1;
   elseif 2<Hs1(i)&&Hs1(i)<=3
      Hs_Bn_2_3(countBn_2_3)=Hs1(i);
      Tp_Bn_2_3(countBn_2_3)=Tp1(i);
      %fprintf( 'between 2 and 3:%d\n' , Hs1(i))
      countBn_2_3=countBn_2_3+1;
   elseif 3<Hs1(i)&&Hs1(i)<=4
      Hs_Bn_3_4(countBn_3_4)=Hs1(i);
      Tp_Bn_3_4(countBn_3_4)=Tp1(i);
      %fprintf( 'between 3 and 4:%d\n' , Hs1(i))
      countBn_3_4=countBn_3_4+1;
   elseif 4<Hs1(i)&&Hs1(i)<=5
      Hs_Bn_4_5(countBn_4_5)=Hs1(i);
      Tp_Bn_4_5(countBn_4_5)=Tp1(i);
      %fprintf( 'between 4 and 5:%d\n' , Hs1(i))
      countBn_4_5=countBn_4_5+1;
  elseif 5<Hs1(i)&&Hs1(i)<=6
      Hs_Bn_5_6(countBn_5_6)=Hs1(i);
      Tp_Bn_5_6(countBn_5_6)=Tp1(i);
      %fprintf( 'between 5 and 6:%d\n' , Hs1(i))
      countBn_5_6=countBn_5_6+1;
   elseif 6<Hs1(i)&&Hs1(i)<=7
      Hs_Bn_6_7(countBn_6_7)=Hs1(i);
      Tp_Bn_6_7(countBn_6_7)=Tp1(i);
      %fprintf( 'between 6 and 7:%d\n' , Hs1(i))
      countBn_6_7=countBn_6_7+1;
  elseif 7<Hs1(i)&&Hs1(i)<=8
      Hs_Bn_7_8(countBn_7_8)=Hs1(i);
      Tp_Bn_7_8(countBn_7_8)=Tp1(i);
      %fprintf( 'between 7 and 8:%d\n' , Hs1(i))
      countBn_7_8=countBn_7_8+1;

  elseif 8<Hs1(i)&&Hs1(i)<=9
      Hs_Bn_8_9(countBn_8_9)=Hs1(i);
      Tp_Bn_8_9(countBn_8_9)=Tp1(i);
      %fprintf( 'between 8 and 9:%d\n' , Hs1(i))
      countBn_8_9=countBn_8_9+1;
  elseif 9<Hs1(i)&&Hs1(i)<=10
      Hs_Bn_9_10(countBn_9_10)=Hs1(i);
      Tp_Bn_9_10(countBn_9_10)=Tp1(i);
      %fprintf( 'between 8 and 9:%d\n' , Hs1(i))
      countBn_9_10=countBn_9_10+1;

   elseif 10<Hs1(i)&&Hs1(i)<=11
```

```
        Hs_Bn_10_11(countBn_10_11)=Hs1(i);
        Tp_Bn_10_11(countBn_10_11)=Tp1(i);
        %fprintf( 'between 10 and 11:%d\n' , Hs1(i))
        countBn_10_11=countBn_10_11+1;
    elseif  11<Hs1(i)&&Hs1(i)<=12
        Hs_Bn_11_12(countBn_11_12)=Hs1(i);
        Tp_Bn_11_12(countBn_11_12)=Tp1(i);
        %fprintf( 'between 11 and 12:%d\n' , Hs1(i))
        countBn_11_12=countBn_11_12+1;
    elseif  12<Hs1(i)&&Hs1(i)<=13
        Hs_Bn_12_13(countBn_12_13)=Hs1(i);
        Tp_Bn_12_13(countBn_12_13)=Tp1(i);
        %fprintf( 'between 12 and 13:%d\n' , Hs1(i))
        countBn_12_13=countBn_12_13+1;

    elseif  13<Hs1(i)&&Hs1(i)<=14
        Hs_Bn_13_14(countBn_13_14)=Hs1(i);
        Tp_Bn_13_14(countBn_13_14)=Tp1(i);
        %fprintf( 'between 13 and 14:%d\n' , Hs1(i))
        countBn_13_14=countBn_13_14+1;
    elseif  14<Hs1(i)&&Hs1(i)<=15
        Hs_Bn_14_15(countBn_14_15)=Hs1(i);
        Tp_Bn_14_15(countBn_14_15)=Tp1(i);
        %fprintf( 'between 14 and 15:%d\n' , Hs1(i))
        countBn_14_15=countBn_14_15+1;
    elseif  15<Hs1(i)&&Hs1(i)<=16
        Hs_Bn_15_16(countBn_15_16)=Hs1(i);
        Tp_Bn_15_16(countBn_15_16)=Tp1(i);
        %fprintf( 'between 15 and 16:%d\n' , Hs1(i))
        countBn_15_16=countBn_15_16+1;
    else %12<Hs1(i)&&Hs1(i)<=20;
       Hs_Gr_16(countGr_16)=Hs1(i);
        Tp_Gr_16(countGr_16)=Tp1(i);
    %fprintf( 'Greater than 16:%d\n' , Hs1(i))
        countGr_16=countGr_16+1;
    end
end

median=[0,0.5,1.5,2.5,3.5,4.5,5.5,6.5,...
    7.5,8.5,9.5,10.5,11.5,12.5,13.5,14.5,15.5,16.5];

 mat_Hs=[Hs_Le_0,Hs_Bn_0_1,Hs_Bn_1_2,Hs_Bn_2_3,Hs_Bn_3_4,Hs_Bn_4_5,...
     Hs_Bn_5_6,Hs_Bn_6_7,Hs_Bn_7_8,Hs_Bn_8_9,Hs_Bn_9_10,Hs_Bn_10_11,...
     Hs_Bn_11_12,Hs_Bn_12_13,Hs_Bn_13_14,Hs_Bn_14_15,...
     Hs_Bn_15_16,Hs_Gr_16];
 mat_Tp=[Tp_Le_0,Tp_Bn_0_1,Tp_Bn_1_2,Tp_Bn_2_3,Tp_Bn_3_4,Tp_Bn_4_5,...
     Tp_Bn_5_6,Tp_Bn_6_7,Tp_Bn_7_8,Tp_Bn_8_9,Tp_Bn_9_10,Tp_Bn_10_11,...
     Tp_Bn_11_12,Tp_Bn_12_13,Tp_Bn_13_14,Tp_Bn_14_15,...
     Tp_Bn_15_16,Tp_Gr_16];

 range_len=[length(Hs_Le_0),length(Hs_Bn_0_1),length(Hs_Bn_1_2),...
     length(Hs_Bn_2_3),length(Hs_Bn_3_4),length(Hs_Bn_4_5),...
     length(Hs_Bn_5_6),length(Hs_Bn_6_7),length(Hs_Bn_7_8),...
     length(Hs_Bn_8_9),length(Hs_Bn_9_10),length(Hs_Bn_10_11),...
     length(Hs_Bn_11_12),length(Hs_Bn_12_13),length(Hs_Bn_13_14),...
     length(Hs_Bn_14_15),length(Hs_Bn_15_16),length(Hs_Gr_16)];
 Mat=[];
 h=1.2:0.2:2;     % Weibull shape parameter
 %h=2;
 for b=1:length(h);
  fprintf('When the Weibull shape parameter "beta" is:%d\n',h(b))
 w=0.01:0.0052:4;
```

```
num_ranges=18;
 r=1;
 Dr=0;
DT=0;
Dcum=0;
Fa=[];
Fa_cum=[];
count=1;

 while count<=num_ranges
    toindex = r+range_len(count)-1;
    %fprintf('fatigue damage due to range:%d\n',count)
    Hs=mat_Hs(r:toindex);
    Tp=mat_Tp(r:toindex);
     fprintf('Number of waves in this range> :%d\n',length(Hs))
     fprintf('Thier accumulated fatigue damage is\n')
for k=1:length(Hs);
   Wp(k)=pi*2/Tp(k); % Peak angular frequancy
   var(k)=0;        % Initial value for variance
   mor(k)=0;    % Initial value for zero order response spectral moment
   m2r(k)=0;    % Initial value for second order response spectral moment
   moe(k)=0;    % Initial value for zero order wave spectral moment
   m2e(k)=0;    % Initial value for second order wave spectral moment
   D(k)=0;      % Initial value for accumulated fatigue damage
for i=1:length(w);
   % Wave spectrum for each sea state
   Spm(i)=5/16*Hs(k)^2*Wp(k)^4*w(i)^-5*exp(-5/4*(w(i)/Wp(k))^-4);

    % Response Amplitude Operator for base case and deviated RAOs
    if (0<=w(i))&&(w(i)<=0.39);
       H(i)=0.5;                        % Base case
       %H(i)=1.2821*w(i);                % Deviated RAO [0-0.39]
   elseif (0.39<w(i))&&(w(i)<=0.8536);
       H(i)=-5.3384*w(i)^2+6.6538*w(i)-1.2834; % Base case
       %H(i)=-7.99*w(i)^2+9.96*w(i)-2.17;     % 50% up RAO [0.39-0.85]
       %H(i)=-2.68*w(i)^2+3.34*w(i)-0.40;     % 50% down RAO [0.39-0.85]
   elseif (0.8536<w(i))&&(w(i)<1.3929);
       H(i)=0.5;                        % Base case
       %H(i)=3.43*w(i)^2+-7.68*w(i)+4.55;     % Deviated RAO [0.85-1.39]
   elseif (1.3929<w(i))&&(w(i)<=1.5605);
       H(i)=123.3953*w(i)^2-345.507*w(i)+242.35; % Base case
       %H(i)=172.899*w(i)^2-480.66*w(i)+334.54;  % 50% up RAO  [1.57]
       %H(i)=46.06*w(i)^2-128.04*w(i)+89.49;     % 50% down RAO  [1.57]
   elseif w(i)>1.5605
    H(i)=9181.18*exp(-5.0351*w(i));             % Base case
    %H(i)=76862.536*exp(-6.121*w(i));           % 50% up RAO  [1.57]
    %H(i)=256.62*exp(-3.17*w(i));               % 50% down RAO  [1.57]
    end

    % Response spectrum for the given sea state
   Sm(i)=Spm(i)*H(i)*H(i);

   % Response spectral moments
   mor(k)=mor(k)+Sm(i)*0.0052;
   m2r(k)=m2r(k)+w(i)*w(i)*Sm(i)*0.0052;

   % Wave spectral moments
   moe(k)=moe(k)+Spm(i)*0.0052;
   m2e(k)=m2e(k)+w(i)*w(i)*Spm(i)*0.0052;

end
% Expected zero-up crossing response period
```

```
Tzr(k)=2*pi*sqrt(mor(k)/m2r(k));

% Expected zero-up crossing wave period for each state
Tze(k)=2*pi*sqrt(moe(k)/m2e(k));

% Number of stress range cycles within 3hrs duration
nor(k)=3*60*60/(Tzr(k));

% Number of wave cycles within 3hrs duration
noe(k)=3*60*60/(Tze(k));

% S-N curve details
s=0:0.2:100;                % Stress ranges
   for j=1:length(s)
  if s(j)<=83.4;
% Lower segment of the S-N curve
      m=5;
      A=4.0364*10^15;
  else
% Upper segment of the S-N curve
   m=3;
   A=5.8076*10^11;
 end

 % Accumulated fatigue damage
   d(j)=(nor(k)/A*s(j)^(m)*h(b)/(2*sqrt(2)*sqrt(mor(k))))*...
      (s(j)/(2*sqrt(2)*sqrt(mor(k))))^(h(b)-1)*...
      exp(-(s(j)/(2*sqrt(2)*sqrt(mor(k))))^2))*0.2*100;
   D(k)=D(k)+d(j);
    end

 Dr=Dr+D(k);
 Dcum=Dcum+D(k);

end
DT=DT+Dr;
 disp(Dr)
 Fa(count)=Dr;
 Fa_cum(count)=Dcum;
 Dr=0;
Wp=[];
Tzr=[];
Tze=[];
moe=[];
mor=[];
m2e=[];
m2r=[];
noe=[];
nor=[];
D=[];
r=r+range_len(count);
count=count+1;
 end
 Mat(b,:)=Fa;
 end
   figure
   plot(Mat(1,:),median,Mat(2,:),median,Mat(3,:),median,Mat(4,:)...
      ,median,Mat(5,:),median);set(gca,'fontsize',14); grid on;
   legend('beta=1.20','beta=1.40','beta=1.60','beta=1.80',...
      'beta=2.00')
   ylabel('Hs[m]')
  xlabel('Fatigue damage ratio [D]')
```

```
    % Wave spectral moments
    moe(k)=moe(k)+Spm(l)*0.0052;
    m2e(k)=m2e(k)+w(l)*w(l)*Spm(l)*0.0052;

end
% Expected zero-up crossing response period
Tzr(k)=2*pi*sqrt(mor(k)/m2r(k));

% Expected zero-up crossing wave period for each state
Tze(k)=2*pi*sqrt(moe(k)/m2e(k));

% Number of stress range cycles within 3hrs duration
nor(k)=3*60*60/(Tzr(k));

% Number of wave cycles within 3hrs duration
noe(k)=3*60*60/(Tze(k));

% S-N curve details
s=0:0.2:100;                % Stress ranges
    for j=1:length(s)
   if s(j)<=83.4;
% Lower segment of the S-N curve
        m=5;
        A=4.0364*10^15;
   else
% Upper segment of the S-N curve
    m=3;
    A=5.8076*10^11;
  end

 % Accumulated fatigue damage
    d(j)=(nor(k)/A*s(j)^(m)*h(b)/(2*sqrt(2)*sqrt(mor(k)))*...
        (s(j)/(2*sqrt(2)*sqrt(mor(k))))^(h(b)-1)*...
        exp(-(s(j)/(2*sqrt(2)*sqrt(mor(k))))^2))*0.2*100;
    D(k)=D(k)+d(j);

    end

 Dr=Dr+D(k);
 Dcum=Dcum+D(k);

end
DT=DT+Dr;
 disp(Dr)
 Fa(count)=Dr;
 Fa_cum(count)=Dcum;
 Dr=0;
Wp=[];
Tzr=[];
Tze=[];
moe=[];
mor=[];
m2e=[];
m2r=[];
noe=[];
nor=[];
D=[];
r=r+range_len(count);
count=count+1;
 end
 Mat(b,:)=Fa;
 end
```

D-2: Accumulated Fatigue Damage Results In Tabular Form

- ***A - Fatigue Damage Result For The Base/Primary Study Case***
  - Option 1 - Fatigue damage accumulation versus significant wave heights H_s for the base case study

Table 1: Fatigue accumulation vs. H_s for the base/primary case study

H_s ranges	No. of sea states	Accumulated fatigue (10^{-5})	Accumulated %	Cumulative %
0-1	14780	0.0197	0.02	0.02
1-2	54483	0.8989	0.92	0.94
2-3	41364	3.9594	4.07	5.01
3-4	24894	8.6379	8.89	13.9
4-5	14139	14.1790	14.59	28.49
5-6	7177	16.9880	17.48	45.97
6-7	3549	17.1710	17.67	63.64
7-8	1612	13.8600	14.26	77.9
8-9	714	9.9692	10.26	88.16
9-10	278	6.0298	6.20	94.36
10-11	101	3.1843	3.28	97.64
11-12	28	1.1371	1.17	98.81
12-13	7	0.4514	0.46	99.27
13-14	5	0.4904	0.50	99.77
14-15	1	0.1021	0.11	99.88
15-16	1	0.1090	0.11	100.00
>16	0	0.0000	0.00	100.00
Total	**163133**	**97.1872**	100.00	

  - Option 2 - Fatigue damage accumulation versus storm events for the base case study

Table 2: Fatigue accumulation vs. storm events for the base/primary case study

Year	Sea states	Frequency of occurrence %	Fatigue accumulated	Accumulated%
1957	974	0.60	0.4587	0.47
1958	2920	1.79	1.2969	1.33
1959	2920	1.79	1.6741	1.72
1960	2928	1.79	1.4034	1.44
1961	2920	1.79	1.618	1.66
1962	2920	1.79	1.2406	1.28
1963	2920	1.79	1.2399	1.28
1964	2928	1.79	1.1018	1.13
1965	2920	1.79	0.9765	1.00
1966	2920	1.79	1.0142	1.04
1967	2920	1.79	2.0638	2.12
1968	2928	1.79	1.1887	1.22
1969	2920	1.79	1.6729	1.72
1970	2920	1.79	1.5865	1.63
1971	2920	1.79	1.263	1.30
1972	2928	1.79	2.1427	2.20
1973	2920	1.79	1.3947	1.44
1974	2920	1.79	1.8152	1.87

1975	2920	1.79	2.0176	2.08
1976	2928	1.79	2.0847	2.15
1977	2920	1.79	1.5739	1.62
1978	2920	1.79	1.3919	1.43
1979	2920	1.79	1.6528	1.70
1980	2928	1.79	1.7223	1.77
1981	2920	1.79	2.0542	2.11
1982	2920	1.79	1.9773	2.03
1983	2920	1.79	2.2695	2.34
1984	2928	1.79	1.5042	1.55
1985	2920	1.79	1.2078	1.24
1986	2920	1.79	1.5955	1.64
1987	2920	1.79	1.0889	1.12
1988	2928	1.79	1.9317	1.99
1989	2920	1.79	2.0067	2.06
1990	2920	1.79	2.9349	3.02
1991	2920	1.79	1.962	2.02
1992	2928	1.79	1.8554	1.91
1993	2920	1.79	3.1372	3.23
1994	2920	1.79	2.0516	2.11
1995	2920	1.79	2.3484	2.42
1996	2928	1.79	1.4387	1.48
1997	2920	1.79	2.4979	2.57
1998	2920	1.79	1.8065	1.86
1999	2920	1.79	2.004	2.06
2000	2928	1.79	1.9923	2.05
2001	2920	1.79	1.2478	1.28
2002	2920	1.79	1.3812	1.42
2003	2920	1.79	1.5329	1.58
2004	2928	1.79	1.8017	1.85
2005	2921	1.79	1.9016	1.96
2006	2919	1.79	1.8239	1.88
2007	2920	1.79	1.7228	1.77
2008	2928	1.79	2.439	2.51
2009	2920	1.79	1.8505	1.90
2010	2920	1.79	1.2321	1.27
2011	2920	1.79	2.4623	2.53
2012	2928	1.79	1.9096	1.96
2013	1448	0.89	0.6227	0.64
Sum	163134	100	97.1876	100

- ***B - Fatigue Damage Result For The Secondary Study Case (Possible Deviations of The Best Fit RAO)***

1. Deviation of the Best fit RAO at the beginning [0-0.39]

Table 3: Fatigue accumulation for the secondary study case where the Best fit RAO deviated at [0-0.39].

H, ranges	*No. of sea states*	*Accumulatedfatigue (10^{-3})*	*Accumulated %*	*Cumulative %*
0-1	14780	0.01971	0.0205	0.02
1-2	54483	0.8986	0.9323	0.95
2-3	41364	3.9556	4.1041	5.06
3-4	24894	8.6192	8.9429	14.00
4-5	14139	14.1360	14.6668	28.67
5-6	7177	16.9200	17.5554	46.22
6-7	3549	17.0800	17.7214	63.94
7-8	1612	13.7460	14.2622	78.21
8-9	714	9.8376	10.2070	88.41
9-10	278	5.9085	6.1304	94.54
10-11	101	3.0917	3.2078	97.76
11-12	28	1.0757	1.1161	98.87
12-13	7	0.4299	0.4460	99.31
13-14	5	0.4705	0.4882	99.80
14-15	1	0.0958	0.0994	99.90
15-16	1	0.0960	0.0996	100.00
>16	0	0.0000	0.0000	100.00
Total	**163133**	**96.3808**	100.00	

2. Deviation of the Best fit RAO around the spectral peak [0.39-0.85]
   a. 50% deviation above the Best fit RAO in the frequency range [0.39-0.85]

Table 4: Fatigue accumulation for the secondary study case, where the Best fit RAO deviated 50% up at [0.39-0.85]

H, ranges	*No. of sea states*	*Accumulatedfatigue (10^{-3})*	*Accumulated %*	*Cumulative %*
0-1	14780	0.0211	0.0135	0.01
1-2	54483	1.0388	0.6643	0.68
2-3	41364	5.1238	3.2767	3.95
3-4	24894	12.3720	7.9119	11.87
4-5	14139	21.7910	13.9354	25.80
5-6	7177	27.4870	17.5780	43.38
6-7	3549	28.6740	18.3370	61.72
7-8	1612	23.5040	15.0308	76.75
8-9	714	16.9780	10.8574	87.61
9-10	278	10.2420	6.5498	94.15
10-11	101	5.3654	3.4312	97.59
11-12	28	1.8757	1.1995	98.79
12-13	7	0.7483	0.4785	99.26
13-14	5	0.8155	0.5215	99.79
14-15	1	0.1661	0.1062	99.89
15-16	1	0.1693	0.1083	100.00
>16	0	0.0000	0.0000	100.00
Total	**163133**	**156.372**	**100.00**	

b. 50% deviation below the Best fit RAO in the frequency range [0.39-0.85]

Table 5: Fatigue accumulation for the secondary study case, where the Best fit RAO deviated 50% down at [0.39-0.85].

H_s ranges	No. of sea states	Accumulated fatigue (10^{-5})	Accumulated %	Cumulative %
0-1	14780	0.0187	0.0320	0.03
1-2	54483	0.7980	1.3670	1.40
2-3	41364	3.1359	5.3719	6.77
3-4	24894	6.0481	10.3606	17.13
4-5	14139	9.0279	15.4651	32.60
5-6	7177	10.0630	17.2383	49.83
6-7	3549	9.7220	16.6541	66.49
7-8	1612	7.6701	13.1392	79.63
8-9	714	5.4789	9.3856	89.01
9-10	278	3.3241	5.6943	94.71
10-11	101	1.7747	3.0401	97.75
11-12	28	0.6523	1.1174	98.87
12-13	7	0.2573	0.4408	99.31
13-14	5	0.2779	0.4761	99.78
14-15	1	0.05955	0.1020	99.88
15-16	1	0.06743	0.1155	100.00
>16	0	0.0000	0.0000	100.00
Total	**163133**	**58.3759**	**100.00**	

3. Deviation between the major wave frequency regime and natural frequency of the Jacket [0.85-1.39]

Table 6: Fatigue accumulation for the secondary study case, where the Best fit RAO deviated at [0.85-1.39].

H_s ranges	No. of sea states	Accumulated fatigue (10^{-5})	Accumulated %	Cumulative %
0-1	14780	0.01683	0.0195	0.02
1-2	54483	0.7421	0.8595	0.88
2-3	41364	3.2291	3.7401	4.62
3-4	24894	7.2110	8.3521	12.97
4-5	14139	12.1690	14.0946	27.07
5-6	7177	14.9560	17.3226	44.39
6-7	3549	15.4240	17.8647	62.25
7-8	1612	12.6410	14.6413	76.89
8-9	714	9.1958	10.6510	87.55
9-10	278	5.6103	6.4981	94.04
10-11	101	2.9780	3.4492	97.49
11-12	28	1.0741	1.2441	98.74
12-13	7	0.4252	0.4925	99.23
13-14	5	0.4637	0.5371	99.77
14-15	1	0.0972	0.1126	99.88
15-16	1	0.1045	0.1210	100.00
>16	0	0.0000	0.0000	100.00
Total	**163133**	**86.3378**	**100.00**	

4. Deviation around the natural frequency of the Jacket [1.56]
    a. When the Best fit RAO is deviated up by 50% around the natural frequency

Table 7: Fatigue accumulation for the secondary study case, where the Best fit RAO deviated 50% up around natural frequency the jacket at [1.56].

H_s ranges	No. of sea states	Accumulatedfatigue (10^{-5})	Accumulated %	Cumulative %
0-1	14780	0.0869	0.05	0.05
1-2	54483	3.3174	2.05	2.10
2-3	41364	11.0030	6.79	8.89
3-4	24894	18.6950	11.54	20.43
4-5	14139	26.1170	16.12	36.55
5-6	7177	27.9120	17.23	53.78
6-7	3549	26.0880	16.10	69.88
7-8	1612	19.9040	12.29	82.17
8-9	714	13.7440	8.48	90.65
9-10	278	8.0606	4.98	95.63
10-11	101	4.1821	2.58	98.21
11-12	28	1.4411	0.89	99.10
12-13	7	0.5781	0.36	99.46
13-14	5	0.6196	0.38	99.84
14-15	1	0.1261	0.08	99.92
15-16	1	0.1308	0.08	100.00
>16	0	0.0000	0.00	100.00
Total	**163133**	**86.3378**	**100.00**	

    b. When the Best fit RAO is deviated down by 50% around the natural frequency

Table 8: Fatigue accumulation for the secondary study case, where the Best fit RAO deviated 50% down around natural frequency the jacket at [1.56].

H_s ranges	No. of sea states	Accumulatedfatigue (10^{-5})	Accumulated %	Cumulative %
0-1	14780	0.0037	0.01	0.01
1-2	54483	0.2412	0.38	0.38
2-3	41364	1.5407	2.42	2.80
3-4	24894	4.3110	6.77	9.57
4-5	14139	8.1783	12.84	22.41
5-6	7177	10.8750	17.07	39.49
6-7	3549	11.8350	18.58	58.07
7-8	1612	10.0800	15.83	73.89
8-9	714	7.5365	11.83	85.72
9-10	278	4.6931	7.37	93.09
10-11	101	2.5212	3.96	97.05
11-12	28	0.9307	1.46	98.51
12-13	7	0.3661	0.57	99.09
13-14	5	0.4023	0.63	99.72
14-15	1	0.0856	0.13	99.85
15-16	1	0.09371	0.15	100.00
>16	0	0.0000	0.00	100.00
Total	**163133**	**86.3378**	**100.00**	

- ***C - Fatigue Damage Result For The Third Study Case (Single Slope S-N Curve)***

1. With a straight "T" S-N curve with slope m=3.

Table 9: Fatigue accumulation for the third study case with straight S-N curve with slope m=3

H_s ranges	*No. of sea states*	*Accumulatedfatigue (10^{-3})*	*Accumulated %*	*Cumulative %*
0-1	14780	140.0000	0.3853	0.39
1-2	54483	2220.0000	6.1100	6.50
2-3	41364	5040.0000	13.8714	20.37
3-4	24894	6520.0000	17.9448	38.31
4-5	14139	6880.0000	18.9356	57.25
5-6	7177	5720.0000	15.7430	72.99
6-7	3549	4260.0000	11.7246	84.71
7-8	1612	2670.0000	7.3485	92.06
8-9	714	1560.0000	4.2935	96.36
9-10	278	780.0000	2.1468	98.50
10-11	101	350.0000	0.9633	99.47
11-12	28	110.0000	0.3027	99.77
12-13	7	36.1990	0.0996	99.87
13-14	5	33.7980	0.0930	99.96
14-15	1	6.8230	0.0188	99.98
15-16	1	6.8990	0.0190	100.00
>16	0	0.0000	0.0000	100.00
Total	**163133**	**36333.70**	100.00	

2. With a straight "T" S-N curve with slope m=5.

Table 10: Fatigue accumulation for the third study case with straight S-N curve with slope m=5

Hs ranges	*No. of sea states*	*Accumulatedfatigue (10^{-3})*	*Accumulated %*	*Cumulative %*
0-1	14780	0.0197	0.02	0.02
1-2	54483	0.8989	0.92	0.94
2-3	41364	3.9594	4.07	5.01
3-4	24894	8.6379	8.89	13.90
4-5	14139	14.1790	14.59	28.49
5-6	7177	16.9880	17.48	45.97
6-7	3549	17.1710	17.67	63.64
7-8	1612	13.8600	14.26	77.90
8-9	714	9.9692	10.26	88.16
9-10	278	6.0298	6.20	94.36
10-11	101	3.1843	3.28	97.64
11-12	28	1.1371	1.17	98.81
12-13	7	0.4514	0.46	99.27
13-14	5	0.4904	0.50	99.77
14-15	1	0.1021	0.11	99.88
15-16	1	0.1090	0.11	100.00
>16	0	0.0000	0.00	100.00
Total	**163133**	**97.1872**	100.00	